SYSTEM RELIABILITY MODEL FOR LONG SPAN ARCH BRIDGES

by

Marek K. Kolodziejczyk

A dissertation submitted to the Graduate Faculty of
Auburn University
in partial fulfillment of the
requirements for the Degree of
Doctor of Philosophy

Auburn, Alabama
August 4, 2018

Keywords: Reliability, Long-Span Bridges, System Reliability, Reliability Analysis, Arch Bridges

Approved by

Andrzej S. Nowak, Chair and Professor of Civil Engineering
J. Michael Stallings, Professor of Civil Engineering
James S. Davidson, Professor of Civil Engineering
Justin D. Marshall, Associate Professor of Civil Engineering
Jorge Valenzuela, Chair and Professor of Industrial and Systems Engineering

ABSTRACT

Every structural system consists of elements with certain dependencies between each other. Current design codes do not account for these interactions and they provide provisions only for particular components. Thus, the design and evaluation procedures do not include additional redundancy and ductility, which can have significant influence on the safety of the whole structure.

In this dissertation, the reliability of the 800-ft long span, steel arch bridge is evaluated. The steel arches made of built-up box sections with different properties along the length of the span are the primary components of the structure. Monte Carlo simulation technique is used to determine the reliability indices for all sections of the arch. Additionally, the system reliability is determined for different levels of correlation between segments of the arch.

To conduct the reliability analysis, load and resistance models were developed and limit state functions were formulated. Traffic data collected from the Weigh-In-Motion station located near the considered bridge serves the purpose of development for the live load model. Using these records, a uniformly distributed load for critical situation (traffic jam on the bridge) was calculated. In addition to the traffic load case with collected Weigh-In-Motion data, live load cases in accordance with AASHTO Standard Specifications for Highway Bridges and AASHTO LRFD Bridge Design Specifications were implemented in the analysis. Beam-column interaction equations served as a basis for limit state

function. In order to obtain values of axial forces and bending moment for segments of the arch, the Finite Element Model of the considered bridge was created. Three types of analyses were used: linear, nonlinear and buckling analysis.

DEDICATION

To my Wife - Magdalena and my Parents – Ewa and Wojciech.

ACKNOWLEDGMENTS

During my time at Auburn I encountered many people who supported, helped, guided and encouraged me to work hard and finalize my research.

Firstly, I want to thank my research advisor – Professor Andrzej S. Nowak, who extended the offer to come to Auburn and work for him. He involved me in incredibly interesting research projects, directed my work and always provided valuable comments and advice. Additionally, Professor Nowak created a notable research environment, and provided the opportunities to participate in many conferences and workshops. He always made himself available to me, and I could always rely on him (not only in professional circumstances).

Secondly, I extend my gratitude to Professor J. Michael Stallings. I am grateful for everything that he taught me during course work, his extremely valuable comments to my dissertation, and the immeasurable support. Since Professor Stallings' office was next to mine, he was one of the first people I asked when I had an engineering problem, and he always knew the right answer. I feel I have learned a lot from him, not only about structural engineering, but also about work ethics, interpersonal relations and culture in the United States (especially in Alabama).

Thirdly, I would like to express my gratitude to Professor James S. Davidson and Professor Justin D. Marshall for all that I have learned during their courses and for serving as my doctoral committee members. They were always able to answer my questions and supported me during my research. In addition, I offer my thanks to Professor Jorge Valenzuela for being the outside reader of my dissertation and reviewing my work.

I am grateful to all Auburn University Professors and Administrative Staff for their professionalism and creating a wonderful atmosphere. Everyone made me feel very comfortable and welcomed. I never had a bad experience while at Auburn, and I will always remember my four years in Auburn as a great time.

I would like to mention Professor Wojciech Radomski for creating the opportunity to meet Professor Nowak, and together with Professor Renata Kotynia, they were continuously supportive and assured me that everything is possible. They were right.

I am most grateful to my parents, Ewa and Wojciech Kolodziejczyk, and brother, Krzysztof Kolodziejczyk, for their love and continuous, unconditional support on both good and bad days. Similarly, I am truly thankful to my parents-in-law Dorota and Michal Biernat, grandparents Miroslawa and Henryk Kolodziejczyk, Stanislawa Lysik, Krystyna and Tadeusz Kornat, brother-in-law Maciej Biernat and his wife Ola Biernat for countless calls, emails, messages and keeping their fingers crossed which motivated and encouraged me throughout the time of my studies.

I would like to mention my Friends from Poland – Maciej Szumacher, Lukasz Kowalski, Bartlomiej Steidel, Michal Wozniak, Marcin Michalski, Mateusz Piera, Adam Turant, Rafal Wolski, Michal Kunikowski and their better halves for taking care of our relations, being interested in my progress and staying in touch regardless of the distance and the time passing by.

During my studies at Auburn, I had not only the best office mate ever, but also a great research partner and overall a very good friend - Anjan Mogali Ramesh Babu. We had numerous interesting conversations related to our research projects, culture of our home countries as well as about emotional intelligence and interpersonal relations.

I would like to acknowledge our research group members: Victor Aguilar Vidal, Olga Iatsko, Pavlo Voitenko, Haofan Zhao and Patryk Wolert for their cooperation during research projects, valuable comments and teamwork. Additionally, the great Polish Community in Auburn and other Friends which I met in here: Timothy Deimler, Yalin Liu, Aravind Tankasala, Eric Gross and Dave Mante who were supportive, reliable and always made the time spent together wonderful, especially during football seasons.

Finally and most importantly, I have a few words to my wife:

Madziu, Misiuniu, you are my love, my best friend, my Everything.

Without you, nothing would be possible. We did it together!

Thank you so much! I will always love you!

TABLE OF CONTENTS

LIST OF TABLES

LIST OF FIGURES

LIST OF ABBREVIATIONS

AASHTO	American Association of State Highway and Transportation Officials
AISC	American Institute of Steel Construction
CDF	Cumulative Distribution Function
DL	Dead Load
DLC	Dead Load of Concrete
DLS	Dead Load of Steel
FEM	Finite Element Model
FHWA	Federal Highway Administration
FLS	Fatigue Limit State
FORM	First-Order Reliability Method
GVW	Gross Vehicle Weight
LRFD	Load and Resistance Factor Design
LL	Traffic Live Load
NCHRP	National Cooperative Highway Research Program
NDT	Non-Destructive Testing
PDF	Probability Density Function
PMF	Probability Mass Function
SLS	Serviceability Limit State

UDL	Uniformly Distributed Load
ULS	Ultimate Limit State
WIM	Weigh-In-Motion

LIST OF SYMBOLS

A_s area of the steel section

F_{cr} buckling stress

F_e the Euler Buckling stress in the plane of bending

F_y specified minimum yield point of steel

M_n flexural resistance

M_p full plastic moment of the section

M_r factored flexural resistance

M_u maximum bending moment including second order effects

P_{fsys} probability of failure of the structural system

P_n compressive resistance

P_r factored axial resistance

P_u compressive force

C equivalent moment factor

I impact fraction

L span length

Q load effect

R resistance

β reliability index

β_e element reliability index

β_{sys}	system reliability index
$p_X(x)$	Probability Mass Function
$F_X(x)$	Cumulative Distribution Function
$f_X(x)$	Probability Density Function
μ	mean value
${\sigma_X}^2$	variance
σ	standard deviation
CoV	coefficient of variation
P_f	probability of failure
Φ^{-1}	the inverse of the standard normal cumulative distribution function
λ	bias factor
ρ	coefficient of correlation

CHAPTER 1 INTRODUCTION

1.1. STATEMENT OF THE PROBLEM

The application of reliability theory to assess structural behavior became the main trend in the development of the design specification of bridges in the last few decades. The first implementations of partial safety factors based on load and resistance uncertainties in the design codes took place in North America in the late 70s and early 80s (Galambos and Ravindra, 1978, Ellingwood, 1980, Nowak and Lind, 1979, Galambos, 1981). Since that time, the reliability theory, serving as a basis for better design with regard to safety, serviceability and durability, is widely used in current design codes. Examples of these *"new generation bridge design codes based on probabilistic methods"* (Nowak, 1999) are the American Association of State Highway and Transportation Officials (AASHTO) Load and Resistance Factor Design (LRFD) Bridge Design Specifications (2004), Eurocode (1994), or American Institute of Steel Construction (AISC) Load and Resistance Factor Design Specification (AISC 1998). In the documents mentioned above, not only loads, but also resistances are treated as random variables with specific statistical parameters. The main objective of implementing reliability theory in the design codes is to achieve the uniform component reliability.

A convenient way to determine the reliability of a structural element or a whole system is to measure it in terms of the reliability index, β. It includes both the margin of safety determined by the given design code and the uncertainties involved in the proper estimation of member's carrying capacity and applied loads. Moreover, the reliability index can be directly related to the probability of failure (Nowak and Collins, 2013).

Czarnecki and Nowak in 2006 stated that *"The traditional element-based approach to bridge design and evaluation does not allow for consideration of interaction between the components that form a structural system and, therefore, it can be conservative".* Meaning the redundancy (load sharing) and ductility of the structural system have significant influence on a structure's safety. Every bridge consists of a large number of structural elements which together work as a structural system (Liu, Moses, 1991). In most cases, the determination of reliability of a single element is not very difficult, but for the whole system it is much more convoluted, if not impossible. Usually, the probability of failure for the bridge is vastly different from probability of failure of its components like girders, decks or bracings. Typically, for a given bridge there are many potential failure modes and each may mean the failure of the component or the whole bridge. Total resistance of the bridge is influenced by the load magnitude, load configuration, redundancy of the elements, properties of materials and geometry of the cross sections (Nowak, 2004). Despite the fact that structural components do not behave independently, current design codes ignore this for the most part and provide provisions for the design of individual components. This approach does not account for the dependencies between elements and overall behavior of the structure. Therefore, it's necessary to develop system reliability methods to direct the design procedure from component-based more towards system-based.

Since the 1990s the Load and Resistance Factor (LRFD) design became the most widely used approach for girder bridges. For many types of long span bridges there is still a need for development of new LRFD code provisions. In the United States, there are 83 steel arch bridges with span lengths of 400 ft or longer (National Bridge Inventory Database, 2018). The average year of opening is 1970, average span length is 612 ft (Figure 1.1) and sufficiency rating is 69% (Figure 1.2).

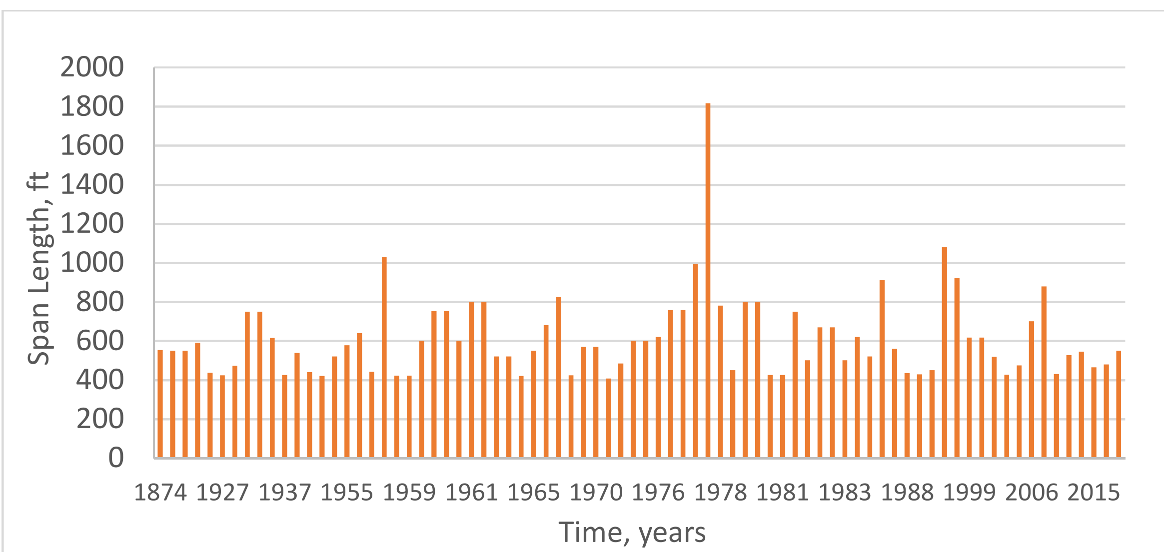

Figure 1.1: Span length of long span steel arch bridges in USA.

Bridge sufficiency rating is a method used to evaluate highway bridges by calculating four separate factors to obtain a percentage value which indicates the bridge sufficiency to remain in service (National Bridge Inventory Database, 2018). 100 percent represents an entirely sufficient bridge and 0 percent means that the structure is entirely insufficient.

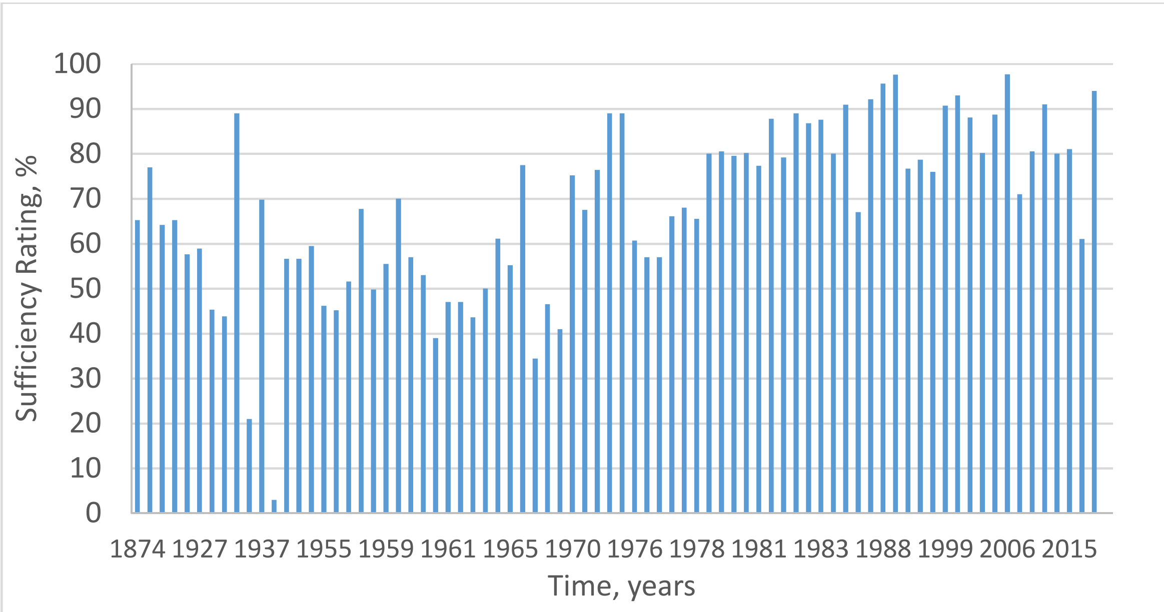

Figure 1.2: Sufficiency rating of long span steel arch bridges in USA.

The LRFD code provisions for long span arch bridges need to be verified. The improvement of rational design requirements for these structures involves the development of loads (mainly live loads) and resistance (load carrying capacity). Reliability analysis procedures reached a level of maturity that can be used for the calibration of design codes for bridges other than girder bridges. Therefore, the main objective of this dissertation is to verify the validity of existing procedures.

1.2. OBJECTIVES AND BENEFITS OF THE STUDY

The main objective of this study is to develop a reliability model for long span arch bridges, and to verify the design provisions in AASHTO Standard Specifications for Highway Bridges (2002) and AASHTO LRFD Bridge Design Specifications (2012). The reliability analysis procedure was developed in conjunction with calibration of the AASHTO LRFD code; however, that procedure was applied to girder bridges with spans up to 200 ft. In this study, the reliability analysis is performed for a steel arch with span of 800 ft. There are significant differences between load and resistance parameters for a girder bridge and for a steel arch bridge. The research involves development of a load model, in particular, live loads for long spans and resistance models for segments of the arch. The significant portion of the work is formulation of the limit state functions.

Reliability analysis is performed for a selected, representative steel arch bridge. The resulting values of reliability indices are compared for two design codes – AASHTO Standard Specifications for Highway Bridges and AASHTO LRFD Bridge Design Specifications.

The structural analysis was not generic and required the development of a special procedure due to the uniqueness of the considered arch. The arch bridge was considered as a series system, therefore its reliability is lower than that of individual components. Almost every long span bridge is different and requires a specific approach, especially for traffic load. As mentioned in the statement of the problem, there are not many long span bridges in the United States, but all of them play an important role in the transportation system (Wu, 2010). Thus, the proper design of their structural elements is critical.

The general idea of this dissertation is to calculate the reliability indices for different segments of the arch and using these values to determine the system reliability of the whole arch. In this case, it is a series system and there were considered various coefficients of correlation between its segments.

It is assumed the behavior of steel components is linear elastic.

1.3. ORGANIZATION OF THE DISSERTATION

Chapter 1 of this dissertation provides an introduction to the research conducted. It includes the statement of the problem, objectives and benefits of the study. Additionally, it presents the scope of the study and review of prior investigations regarding the topic.

Chapter 2 reviews the fundamental and basic concepts of the reliability theory. Definitions of standard variables, probability distributions, reliability index and limit state functions are introduced. Main methods for the calculation of reliability index, use of normal probability paper and simulation techniques are described and explained.

Chapter 3 presents basic information about Weigh-In-Motion technology, study of traffic data, and classification of vehicles. Moreover, this chapter includes information about the location of the Weigh-In-Motion station considered in this research and the algorithm for the development of uniformly distributed live load. Values of equivalent Uniformly Distributed Load calculated for the considered span lengths and statistical parameters are provided.

Chapter 4 provides the procedure for the development of the resistance model and includes interaction equations and curves for different design approaches. Furthermore, each segment of the arch is checked to verify it has sufficient load carrying capacity in accordance with the considered design codes.

Chapter 5 describes the Finite Element Model of the arch bridge selected for this research. The main components of the structure are presented, as well as the modeling approach and analytical procedure are explained.

Chapter 6 studies the reliability analysis of the particular sections of the arch. The formulation of limit state functions and load and resistance models are presented. Reliability indices for each segment of the arch are calculated using Monte Carlo simulation technique and compared to each other.

Chapter 7 presents the system reliability analysis of the whole structure using reliability indices for particular sections of the arch calculated in Chapter 6. Upper and lower bounds for system reliability are determined. Additionally, system reliability indices for different coefficient of correlation values are calculated and shown on the graphs.

Chapter 8 includes the summary of research done for the scope of this dissertation.

Chapter 9 concludes the work and presents the main findings.

Chapter 10 provides general recommendations and suggestions for future research.

1.4. Prior Investigations

Structural system reliability is a field of science investigated by numerous researchers. There are several valuable publications available in which different approaches and theories are presented, for example Thorf-Christtensen and Baker (1982), Ang and Tang (1984), Thorf-Christtensen and Murotsu (1986), Nowak and Zhou (1989), Bruneau (1992), Ayyub and McCuen (1997), Wolinski and Wrobel (2001), Nowak and Collins (2013). First implementations of these theories for design codes were done by Galambos and Ravindra (1978) – for buildings, and Nowak and Lind (1979) – for bridges. Incremental load approach for an identification of the collapse modes for ductile and brittle elements were proposed by Moses (1982) and Rashedi and Moses (1988). In addition to that, Moses and Verma (1987) developed a load and resistance reliability-based approach to evaluate the strength of bridge elements. Nowak and Tharmabala in 1988 applied reliability models to the bridge evaluation.

Several live load models were developed over the past few decades. Nowak and Szerszen (2000) stated that *"The development of a live load model is essential for a rational bridge design and/or evaluation code"*. They also concluded that the basic combination for highway bridges is a simultaneous occurrence of dead load and traffic load (including dynamic effects). The analysis of combinations of other loads like wind or collision forces would require a specific approach, which would take into account "*a reduced probability of a simultaneous occurrence of extreme values of several independent loads"*. Nowak and Hong (1991) developed the live load model for highway bridges based on traffic data from Ontario. They were extrapolating distributions to obtain the maximum load effects for a wide range of periods (from 1 day to 75 years). Using these extrapolated loads, researchers formulated a procedure to calculate maximum moments and shears for different time periods. In 1997, Kim, Sokolik and Nowak were analyzing WIM traffic records on bridges in the Detroit area. They found that the truck loads are very site specific and the weight of many vehicles is much higher than legal limits. Similar findings were achieved by Gindy and Nassif (2006) who did research on WIM data from the New Jersey area.

The contribution of Peter G. Buckland (1978, 1980 and 1991) to the development of live loading on long span bridges is invaluable. One of his main conclusions was that the traditional representation of the traffic on long span bridges by the set of uniform and concentrated loads is accurate. His other findings were that the uniform load increases as the loaded length decreases, and the concentrated load increases as the loaded length increases. These findings were different than the results of the other researchers. He made observations of live load distribution among the traffic lanes and developed the loading curves as traffic loads for long span bridges, which were recommended by the ASCE Committee in 1981. However, they have never been published as an official provision in the design codes. Additionally, Peter G. Buckland's research included the calculation of equivalent uniformly distributed live load and use of it to check equivalent shear force and bending moments for simply supported spans. Nevertheless, since none of the long span bridges have simply supported span in longitudinal direction, this procedure may serve only as a good method of comparison between design approaches from different design codes.

The development of the live load model for long span bridges was conducted by Lutomirska in 2009. She used WIM data from different locations in the United States, and calculated values of equivalent uniformly distributed load for spans between 600 and 5000 ft. She concluded that for most of the bridges, current live load provisions from AASHTO LRFD are appropriate, but for some specific bridges with high Average Daily Truck Traffic (ADTT) special attention and increase of the design load is recommended.

Not many studies have been conducted on the reliability of long span arch bridges in the past. Nevertheless, numerous researchers focus on the important components of the structural analysis of these structures.

Combined axial and bending moment behavior

A comprehensive study on the behavior of beam-columns (elements which are subjected to the combined axial and bending moment) is provided by Galambos (1998) and

Ziemian (2010). In the fifth and sixth editions of the *"Guide to Stability Design Criteria for Metal Structures",* these researchers presented the procedures for evaluation of beam-columns both for uniaxial and biaxial bending. Ziemian in 2010 identified three classes of problems for non-sway elements with doubly symmetric cross sections. They are as follows:

1. *Members subjected to major axis bending and braced against minor axis flexure (or subjected to minor axis bending), which will collapse by excessive in-plane bending deflections. This case corresponds to the interaction between column flexural buckling and simple uniaxial beam bending.*

2. *Unbraced members subjected to major axis bending, which will collapse by an interaction between column flexural buckling, beam lateral–torsional buckling, and uniaxial beam bending.*

3. *Unbraced members subjected to biaxial bending, which will collapse by an interaction between column flexural buckling, beam lateral–torsional buckling, and biaxial beam bending. Clearly, this constitutes the most general case—the previous ones corresponding to special cases of this one.*

The schematic drawings of these three classes are presented in the.

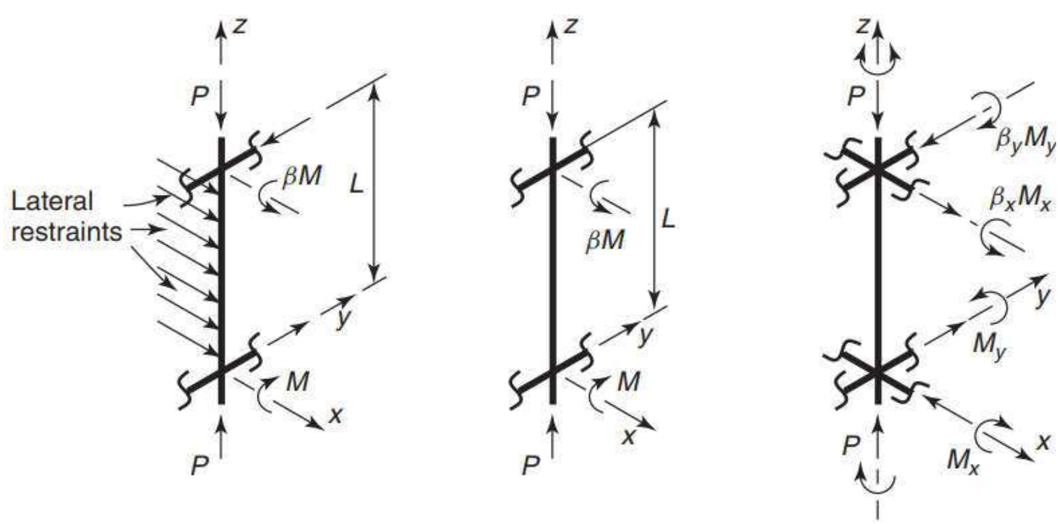

Figure 1.3: Classes of beam-column behavior (Ziemian, 2010).

In the same publication, three categories of factors having influence on the load-carrying capacity were provided. They are load related, member related and imperfection related factors. The first is useful when interaction diagrams are implemented in the design or evaluation because it allows the combination of the axial load and bending moments on the interaction diagram to be displayed. To construct this diagram, member related factors are required to determine the strength, unbraced length or end-support conditions for a given element. The third category of factors is related to phenomena including lack of straightness in either plane, residual stresses or variation of material strength. These "imperfections" influence not only the component strengths but also the shape of the interaction curve or surface.

$$f\left(\frac{P}{P_u}, \frac{M_x}{M_{ux}}, \frac{M_y}{M_{uy}}\right) \leq 1.0 \tag{1.1}$$

There are two categories of the design methods for beam-columns. First, using charts or tables to provide safe combinations of the internal forces and bending moments generated by the applied loads. Second, using interaction formulas, such as Equation (1.1), which only lead to accurate beam-column evaluation if the endpoints are precisely defined. Even though there are available methods to calculate exact solutions, they always require the implementation of the numerical procedures to include inelastic behavior in the calculation of the "true" maximum strength. Therefore, these methods cannot be directly used for the development process of the design equations. Instead, the modified formulas derived from elastic analysis or wholly empirical approach has to be implemented. In addition to that, numerous modern design codes allow the use of finite element-based, advanced analysis methods in the determination of the maximum strengths of beam-column elements.

For biaxial bending of short beam-columns, an important case for this study, Ziemian (2010) stated: *"failure is likely to be governed by full yielding of the most heavily stressed cross section (assuming that the individual component plates are not susceptible to local buckling)".* Further investigation of the bridge considered in this dissertation confirmed this statement.

Stability and Reliability assessment of the arch bridges

Many researchers investigated the stability behavior of the arch bridges. For example, in 2017, Rønnquist and Naess conducted the *"Global Buckling Reliability Analysis of Slender Network Arch Bridges"*. They utilized the Monte Carlo Simulation Technique for their analysis and confirmed that this method is convenient for this kind of structural system reliability assessment. Additionally, in 2013 Tang, Hu and Xie published the paper about the stability behavior of thin-walled steel box arch bridges. The authors evaluated two structures (arch bridges with 130 m and 90.8 m spans). They created the Finite Element Models of them and found that the structures considered by them have strong stability and that *"the occurrence of local buckling will accelerate the arrival of overall instability"*.

A majority of research topics related to the reliability of arch bridges focus on wind effects. In 2009, Cheng and Li published a paper about the reliability assessment of long span arch bridges against wind-induced stability failure. (Li et al., 2018) conducted the research about the *"Reliability Evaluation of Vortex-Induced Vibration for a Long-Span Arch Bridge"*. Based on different reliability calculation approaches, they checked and compared the influences of various parameters related to wind–bridge interactions on the Vortex-Induced-Vibration. Chen, Nakamura and Nishikawa in 2012, estimated the reliability of a concrete-filled steel, tubular arch bridge, according to Chinese code, by analysis and comparison of the results from static load tests with those from the Finite Element Models. Nowak and Cho in 2007 proposed the prediction method for the combination of failure modes of an arch bridge. Additionally, they suggested the way to compare risk assessment with the conventional system reliability analysis method. The researchers calculated and compared the upper and lower probabilities of failure for the structural system for all possible combination failure modes.

CHAPTER 2 STRUCTURAL RELIABILITY FUNDAMENTALS

2.1. INTRODUCTION

Structural reliability is a field of science that helps society answer the following questions:

1) *How to measure the safety of the structure?*

2) *How safe is safe enough?*

3) *How should the designer implement the optimum safety level?*

Finding answers to these questions helps to understand "what is a proper and safe design for the structure", as well as, "how to optimize the whole process to make it more efficient".

Structural reliability concepts may be applied in the rational design and evaluation of new structures. Knowledge about reliability fundamentals lead to more economical design and evaluation of new objects. Additionally, the development of all actual design codes are based on reliability concepts.

2.2. UNCERTAINTIES

The reason for dealing with reliability of structures are uncertainties in the building process. There are two groups of them:

1) *Natural causes:*

- *Wind, snow, very low or very high temperatures, temperature changes, excessive rain, earthquake*

- *Material properties (strength, modulus of elasticity, cross-section geometry)*

2) *Human causes:*

- *Approximation in the methods of analysis, design and construction*

- *Human errors*

Natural causes must be accepted by society. It is important to understand there is uncertainty about them, and their time of occurrence and scale cannot be clearly predicted. The material properties must be regarded as an additional source of uncertainty. In reality, it is not possible to have different elements made of the same material, with the exact same properties. That is why control of the production is a vital part of the building process.

Human causes are often much more difficult to assess than natural. Approximate methods are being implemented in design and construction of every structure to simplify the whole process. Nevertheless, the most important and responsible reason for around 90% of the problems are human error (Nowak and Collins, 2013). Usually, errors are caused by oversight of something or a mistake in the calculation, but sometimes they are made on purpose which, of course, is against the law.

The primary consequences of the existence of uncertainties are facts that:

1) *Deterministic analysis and design methods are insufficient.*

2) *The probability of failure is NEVER zero.*

3) *All design codes must include a rational safety reserve.*

4) *The reliability methods measure the structural performance in an efficient way.*

The deterministic analyses have many limitations. This is why it is so critical to implement the reliability concepts in the design process. Instead of asking “Does the given structure work well or not?” it is better to ask, “How reliable is the structure?” To answer this question, the quantification method is needed, so the measure of structural performance is required.

There are three main types of uncertainties:

1) *Physical uncertainties (due to the natural variation of load and resistance)*

2) *Statistical uncertainty (due to the limitation in sample size)*

3) *Model uncertainty (due to the simplifications and assumptions in the modeling process)*

Physical uncertainty is the phenomenon that exists, but there is limited amount of information about, for example, wind velocity. Statistical uncertainty is based on the amount and size of the samples. Model uncertainty occurs when the statistical parameters are being implemented into the model of the structure.

2.3. RANDOM VARIABLES

The random variable (Figure 2.1) is a function that maps events into intervals on the axis of real numbers. Random variables are divided into two groups:

1) *Discrete random variables (which take the finite number of possible outcomes of the experiment).*

2) *Continuous random variables (which take the infinite number of possible outcomes of the experiment – interval on the axis of real numbers).*

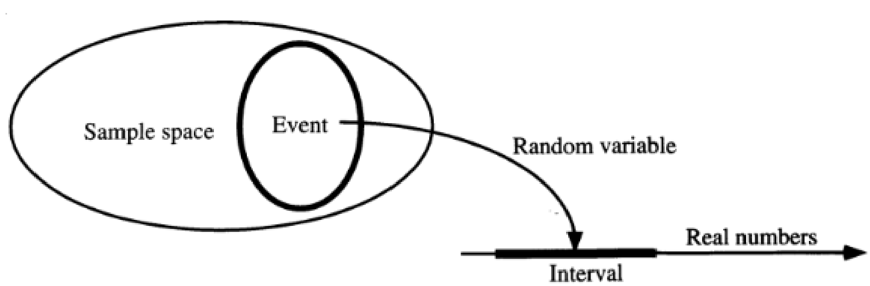

Figure 2.1: Random Variable (Nowak and Collins 2013).

There are three important functions of random variables:

1) *Probability Mass Function (PMF), $p_X(x)$ – defined only for discrete random variables.*

2) *Cumulative Distribution Function (CDF), $F_X(x)$ – defined both for discrete and continuous random variables.*

3) *Probability Density Function (PDF), $f_X(x)$ – defined only for continuous random variables.*

The Probability Mass Function ($p_X(x)$) is defined as the probability that a discrete random variable X is equal to a specific value x, where x is a real number:

$$p_X(x) = P(X = x) \tag{2.1}$$

The Cumulative Distribution Function ($F_X(x)$) (Figure 2.2) is defined as the probability that the random variable X is less or equal to x:

$$F_X(x) = P(X \le x) \tag{2.2}$$

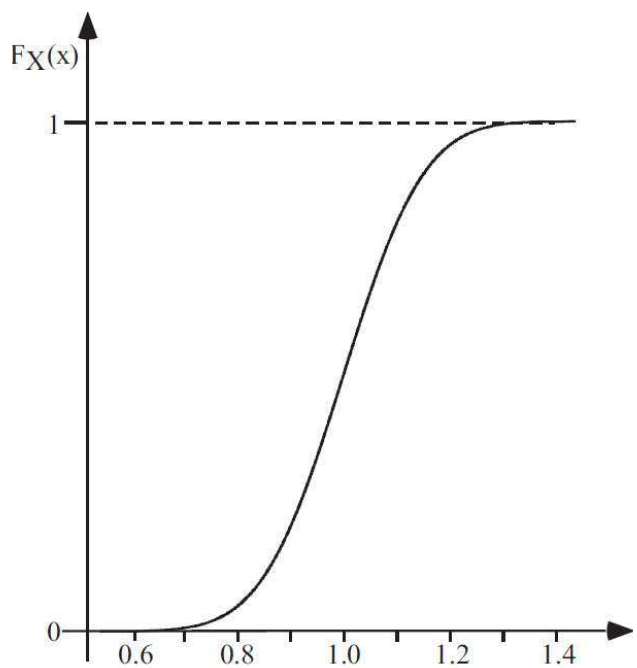

Figure 2.2: Example of CDF (Nowak and Collins 2013).

Since the CDF is a probability, it always has to be between 0 and 1. CDF is not decreasing, for $x = -\infty$ equals *0* and $x = \infty$ equals *1.0*. For continuous random variables there is a relationship as follows:

$$P(a \leq x \leq b) = F_X(b) - F_X(a) = \int_a^b f_X(\xi)d\xi \tag{2.3}$$

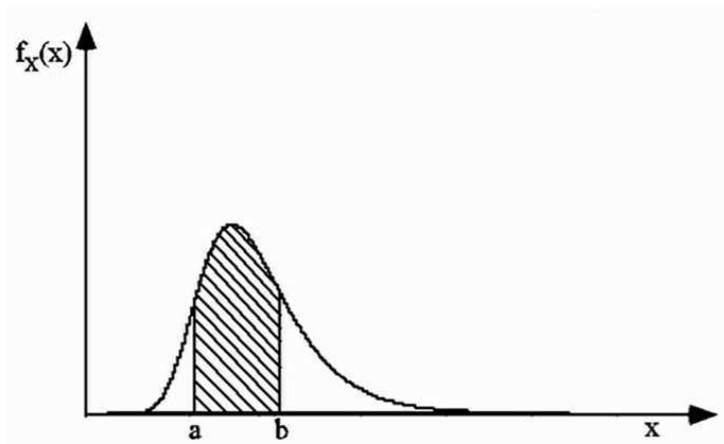

Figure 2.3: Graphical interpretation of Equation (2.3) (Nowak and Collins 2013).

The Probability Density Function ($f_X(x)$) (Figure 2.4) is defined as the first derivative of the cumulative distribution function:

$$f_X(x) = \frac{d}{dx}F_X(x) \tag{2.4}$$

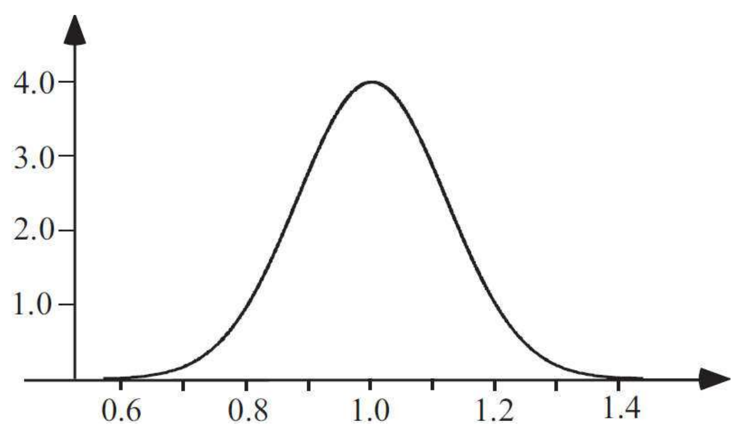

Figure 2.4: Example of PDF (Nowak and Collins 2013).

Mean value, variance and standard deviation are the three key parameters of a random variable.

Mean value

The mean (also called the expected value) is represented by a weighted average value of all collected results.

For the discrete random variables, to calculate the mean (μ), the following formula can be used:

$$\mu_X = \sum_{all\ x_i} x_i \cdot p_X(x_i) \tag{2.5}$$

For the set of results with equal weights, the alternative equation to calculate mean value is:

$$\bar{X} = \frac{1}{n}\sum_{i=1}^{j} x_i \tag{2.6}$$

For the continuous random variables, to calculate the mean (μ), the following formula can be used:

$$\mu_X = \int_{-\infty}^{\infty} x \cdot f_X(x) dx \tag{2.7}$$

Variance

Variance is defined as the second moment about the mean value. It is denoted by σ^2 for population and by S^2 for the sample.

For the discrete random variable, the variance can be computed as:

$$\sigma_X{}^2 = \sum_{all\ x_i} (x_i - \mu)^2 \cdot p_X(x_i) \tag{2.8}$$

For the continuous random variable, the equation is as follows:

$$\sigma_X{}^2 = \int_{-\infty}^{\infty} (x-\mu)^2 \cdot f_X(x)dx \tag{2.9}$$

For the case when n results in equal weight, the variance can be calculated using the following equation:

$$S^2 = \frac{1}{n-1}\sum_{i=1}^{n}(x_i - \bar{X})^2 \tag{2.10}$$

Standard deviation

For given probability distribution, the standard deviation (σ) is defined as the square root of the variance. Standard deviation has the same unit as the mean value.

Coefficient of variation

The coefficient of variation (CoV) is a dimensionless quantity represented by the following equation:

$$CoV = \frac{\sigma}{\mu} \tag{2.11}$$

This measure is usually denoted as a fraction or percentage.

2.4. Types of Random Variables

The function may be considered as a probability distribution of random variable when it satisfies the axioms of probability. There are two main types of probability distributions:

1) *Discrete probability distribution*

2) *Continuous probability distribution*

The variables of the discrete distribution can only use discrete values. Common types of discrete probability distribution are Binomial Distribution, Bernoulli Distribution, Geometric Distribution, Poisson Distribution, Multinomial Distribution and more. Some play an important role in civil engineering applications while others are useful in different fields of science.

The continuous probability distribution is a type of statistical distribution, where variables can take on a continuous range of values. Significant types of continuous probability distribution include uniform, normal, lognormal, gamma, beta, Weilbull and others. Some of these distributions are very useful for civil engineering as well as in other science disciplines.

The normal and lognormal distributions are considered in the analysis of this dissertation. That is why they are only presented in this chapter. The detailed information about other types of distributions can be found, for example, in Nowak and Collins (2013).

Normal Distribution

The normal distribution, also known as the Gaussian Distribution (Figure 2.5), is probably the most well-known and widely used type of probability distribution. The probability density function for this type of distribution is given by:

$$f_X(x) = \frac{1}{\sigma \cdot \sqrt{2 \cdot \pi}} exp\left[-\frac{1}{2}\left(\frac{x-\mu}{\sigma}\right)^2\right] \quad for \quad -\infty < x < \infty \tag{2.12}$$

where μ and σ are the parameters of the distribution.

The graphical interpretation is as follows:

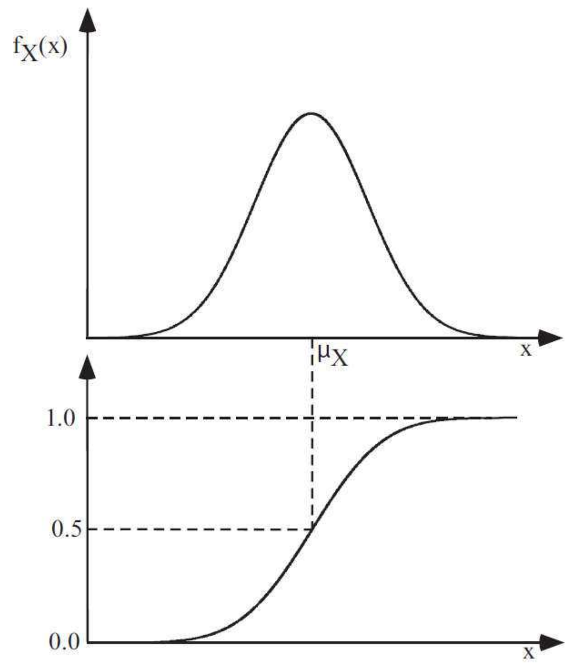

Figure 2.5: PDF and CDF of a normal random variable (Nowak and Collins 2013).

The special case of normal (Gaussian) distribution is the standard normal distribution. It has specific parameters. The mean value (μ) equals 0 and standard deviation (σ) equals 1. There is specific notation to indicate this kind of distribution: *N*(0,1). The evaluation of cumulative distribution function (CDF) can only be done by numerical methods, but in practice, the standardized curve is used for this evaluation. This curve is determined by the following transformation of the variate X and Z:

$$Z = \frac{X - \mu}{\sigma} \tag{2.13}$$

Using this transformation, the probability density function (PDF) and cumulative density function (CDF) of the standard normal distribution can be determined as follows:

$$\phi(z) = \frac{1}{\sqrt{2 \cdot \pi}} exp\left(-\frac{1}{2}z^2\right) \tag{2.14}$$

$$\Phi(z) = \int_{-\infty}^{z} \frac{1}{\sqrt{2 \cdot \pi}} exp\left(-\frac{1}{2}z^2\right) dz \tag{2.15}$$

where $\phi(z)$ and $\Phi(z)$ are special notations of PDF and CDF of the standard normal variable, respectively. To save time and effort, the results of integral $\Phi(z)$ usually are calculated and tabulated in most statistics-related textbooks. To obtain the negative values of z, the symmetry property of the normal distribution can be used:

$$\Phi(-z) = 1 - \Phi(z) \tag{2.16}$$

There are few significant properties of the normal distribution. Usually, in the reliability analysis there is a substantial need to use them. The most important properties are described by central limit theorem.

Central Limit Theorem states the **summation/sum** of large numbers of the independent observations, if none tend to dominate the sum and are under specific general conditions, approaches an approximate normal distribution. The more observations involved, the more accurate the analysis is. The sum of random variables (approximated to be normal variables) are often used in modeling the overall load applied to the given structure. The Central Limit Theorem is considered one of the most significant fundamentals of the probability theory.

Using mathematical notation, it can be stated that the sum of n normally distributed random variables X_1, X_2,..., X_n constitutes a normal distribution being:

$$Y = X_1 + X_2 + \cdots + X_n \tag{2.17}$$

with the mean of Y as follows:

$$\mu_Y = \mu_{X_1} + \mu_{X_2} + \cdots + \mu_{X_n} \tag{2.18}$$

and the variance of Y as follows:

$$\sigma_Y{}^2 = \sigma_{X_1}{}^2 + \sigma_{X_2}{}^2 + \cdots + \sigma_{X_n}{}^2 \tag{2.19}$$

Normal Probability Paper

To conveniently determine whether a set of data (cumulative distribution function) follows a particular distribution is probability paper. The most commercially and common available type is probability paper for the normal distribution. The CDF for normal distribution has an S-shape. The fundamental idea of using normal probability paper is to redefine the vertical scale, so the normal CDF will plot as a straight line instead. This operation allows a simple evaluation of the most important statistical parameters like standard deviation and distribution type (Nowak and Collins 2013). The basic variable is presented on the horizontal axis, while the vertical is representing the standard normal variable with distances from the mean value in terms of standard deviations. There is a relationship between the probability and the standard normal variable as presented in Table 2.1:

Table 2.1: Relationship between the probability and the standard normal variable on the vertical scale of Normal Probability Paper

Probability	Corresponding distance from the mean value in terms of standard deviations
0.99865	3
0.9772	2
0.841	1
0.5	0
0.159	-1
0.0228	-2
0.00135	-3

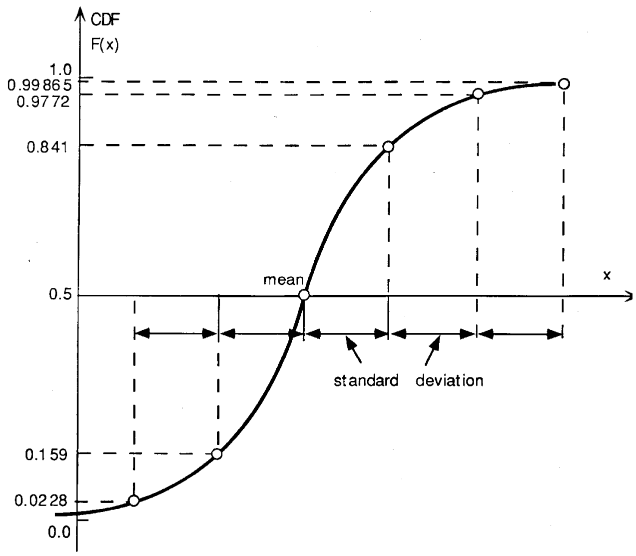

Figure 2.6: Normal Distribution Function on the Normal Probability Paper (Reliability of Structures - Course Slides, Nowak 2014)

The curve, which is presented in the Figure 2.6, represents the CDF and allows for the study of the experimental data plotted on the probability paper.

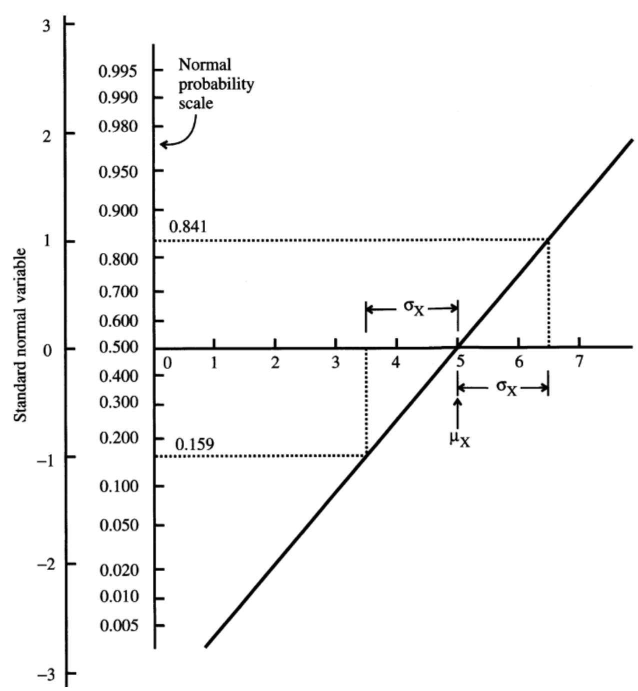

Figure 2.7: Interpretation of a straight-line plot on normal probability paper in terms of the mean and standard deviation of the normal random variable (Nowak and Collins 2013).

The most important and useful properties of normal probability paper are as follows:

1) *The intersection of the normal cumulative distribution function and horizontal axis represents the mean value of given set of data.*

2) *The straight line is a representation of the normal distribution function.*

3) *Both mean value and standard deviation can be read directly from the plot.*

Lognormal Distribution

The lognormal distribution is widely used in structural reliability analyses. It is especially useful for cycles-to-failure analysis in fatigue, material strengths as well as loading variables in probabilistic design. The random variable *X* is lognormally distributed if *Y=ln(X)* (logarithm of the random variable) is normally distributed. Because of the fact that the logarithms of the lognormally distributed random variable are normally distributed, the equation for lognormal distribution is as follows:

$$f_X(x) = \frac{1}{x \cdot \sigma_Y \cdot \sqrt{2 \cdot \pi}} exp\left[-\frac{1}{2}\left(\frac{lnx - \mu_Y}{\sigma_Y}\right)^2\right] \quad for \quad 0 < x < \infty \qquad (2.20)$$

where μ_Y and σ_Y are the mean and standard deviation of the lognormal distribution respectively.

The general shape of the probability density function for a lognormal variable is presented in the Figure 2.8:

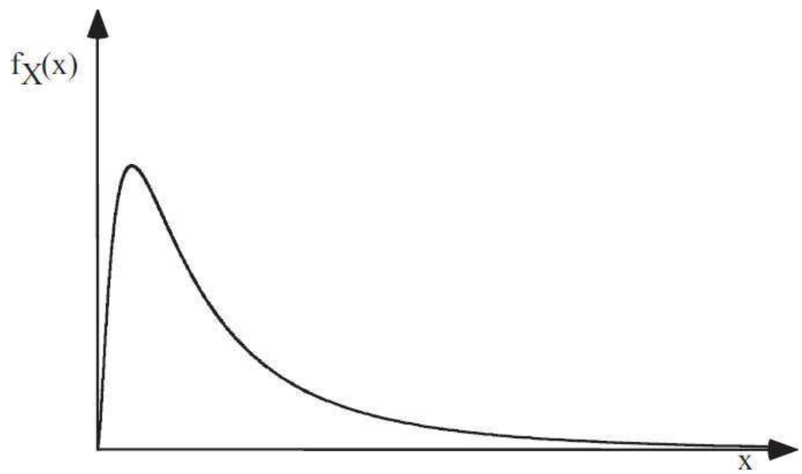

Figure 2.8: PDF of a lognormal random variable (Nowak and Collins 2013).

The corresponding parameters of the distribution - mean (μ_Y) and variance (${\sigma_Y}^2$), can be calculated as follows:

$$ {\sigma_Y}^2 = ln\left[1 + \left(\frac{\sigma_X}{\mu_X}\right)^2\right] \tag{2.21} $$

$$ \mu_Y = ln(\mu_X) - \frac{1}{2} \cdot {\sigma_Y}^2 \tag{2.22} $$

The cumulative distribution function for the lognormal distribution can be calculated using the relationship with the normal distribution. Similar to the normal distribution, the following transformation is used to evaluate cumulative distribution function of lognormal distribution:

$$ Z = \frac{lnX - \mu_Y}{\sigma_Y} \tag{2.23} $$

Central limit theorem states that the multiplication of large numbers of the independent observations, if none of them tend to dominate the sum and under specific general conditions, approaches an approximate lognormal distribution.

Using mathematical notation, it can be stated that the multiplication of n normally distributed random variables X_1, X_2,..., X_n constitutes a lognormal distribution being:

$$W = X_1 \cdot X_2 \cdot \ldots \cdot X_n \tag{2.24}$$

with the mean of W (first moment of W) as follows:

$$\mu_W = \mu_{Y_1} + \mu_{Y_2} + \cdots + \mu_{Y_n} \tag{2.25}$$

and the variance of W (second moment of W) as follows:

$$\sigma_W{}^2 = \sigma_{Y_1}{}^2 + \sigma_{Y_2}{}^2 + \cdots + \sigma_{Y_n}{}^2 \tag{2.26}$$

2.5. LIMIT STATE FUNCTIONS

Most of the modern design codes are based on the concept of limit states (Estes and Frangopol, 2001). All structures are designed to survive the loads that will be placed on them. The priority for the designer is to ensure that a given structure will perform as intended and in a safe manner. To fulfill this requirement, the resistance of a given element has to exceed the total demand of the load which is applied to this element. In most cases, there is an uncertainty associated with both resistance (*R*) and the load (*L*). Since the characteristics of the resistance and load are known, this uncertainty can be quantified, evaluated and quite accurately assumed. Therefore, the probability density function can be properly determined.

There are many definitions of Limit States. Two the most common are:

1) *Limit state is the boundary between desired and undesired performance of the particular element or the entire structure.*

2) *Limit state is the condition under which the given element or the entire structure is not able to perform the functions that it was designed for.*

The three most important types of limit states for reliability analysis of structures are:

1) *Ultimate Limit States (ULSs)*

2) *Serviceability Limit States (SLSs)*

3) *Fatigue Limit States (FLSs)*

Ultimate Limit States are related to the loss of carrying capacity (structural stiffness, strength). This may occur when elements of the structure exceed the moment carrying capacity, there is buckling or plastic hinges are forming.

Serviceability Limit States represents the gradual deterioration of functionality. This kind of limit state may or may not be directly related to structural integrity. The examples of SLSs can be: exceeded deflections and vibrations, permanent deformations or cracking.

Fatigue Limit States are associated with reduction of the strength of the structural component due to repeated loading. This leads to the accumulation of the damage and eventual failure under the repeated load, which is lower that the ultimate load. FLSs allows to design structures for an adequate fatigue life. This limit state typically occurs in steel components and reinforcement bars which are in tension. Failures due to fatigue were also reported in pre-stressing strands of post-tensioning bridges. Magnitude, frequency of the load and stress range are the most important factors in any fatigue analysis.

To perform any reliability analysis, the proper formulation of the limit states also known as performance functions is required. To do this, all loads have to be incorporated into one variable (Q) and the resistance of the structure has to be incorporated into one variable (R). Then, the limit state (performance function) can be formulated as:

$$g(R, Q) = R - Q \tag{2.27}$$

where g is the safety margin of the structure.

If $g(R, Q) = R - Q$ and R and Q are independent random variables, the probability of failure can be calculated as follows:

$$P_f = \int_{-\infty}^{\infty} f_Q(x) \cdot F_R(x)\, dx \qquad (2.28)$$

where f_Q represents the probability density function of all load components and F_R is the cumulative density function of resistance.

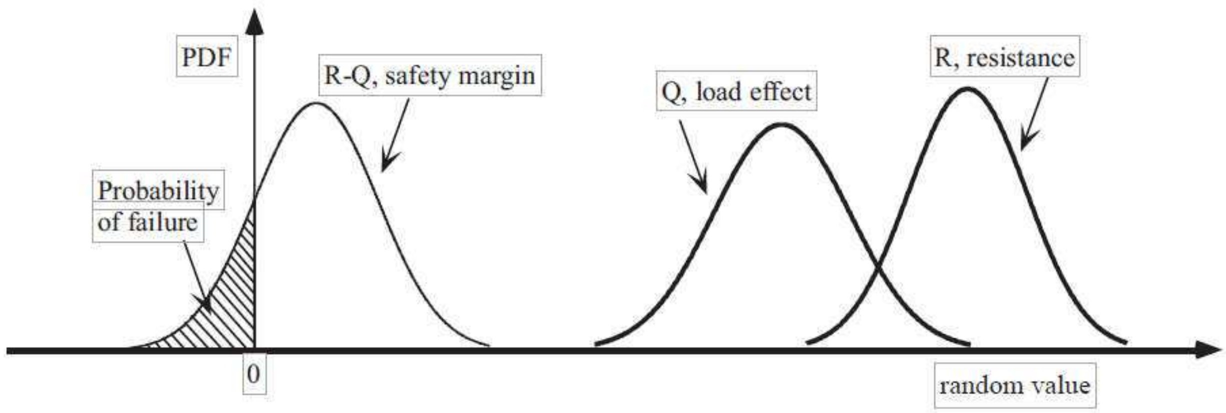

Figure 2.9: PDF's of load, resistance and safety margin (Nowak and Collins 2013).

In real design there is usually more than one variable for capacity and demand, so in a more general sense the limit state can be described as follows:

$$g(X) = g(\, X_1, X_2, \dots, X_n) \qquad (2.29)$$

where X_i represents the set of parameters with different, diverse uncertainties and probability distributions. Hence, $g(X)$ is a function with distribution determined by statistical characteristic of input parameters. In general, this function can take any form, provided that $g(X) \leq 0$ corresponds to a failure state and $g(X) > 0$ to a safe state (acceptable performance). Therefore, the limit state can be defined as $g(X) = 0$, also called failure surface. To calculate the corresponding probability of failure, the joint density function of the variables over the negative domain of $g(X)$ has to be integrated as follows (Thoft-Christensen and Baker 1982):

$$P_f = \int_{X_1}\int_{X_2}\cdots\int_{X_n} f_X(x_1, x_2, \ldots, x_n)\, dx_1 dx_2 \ldots dx_n \tag{2.30}$$

where f_X represents the probability density function of $X_1, X_2, \ldots, X_n$. The region of integration is defined by negative values of $g(X)$.

The Equation (2.30) is very difficult to evaluate because there is almost never sufficient data to define joint probability density function for all basic variables. Usually there is barely enough information to be confident about the distribution and the covariance. The other problem is that it is extremely time consuming, and requires a lot of computational power to evaluate the multi-dimensional integrals. The direct calculation of the probability of failure is impractical and inefficient. Therefore, to measure structural safety, it is much more convenient to use indirect procedures which involves terms such as reliability index.

2.6. Reliability Index

The reliability index, also known as the safety index, has been officially identified in UK in the mid-1950s as:

$$\beta = \frac{\bar{R} - \bar{Q}}{\sqrt{{\sigma_R}^2 + {\sigma_Q}^2}} \tag{2.31}$$

where:

β = reliability index,

$\bar{R}$ = resistance,

$\bar{Q}$ = total load effect,

σ_R = standard deviation of resistance,

σ_Q = standard deviation of the load.

Equation (2.31) incorporates the four key factors and includes uncertainties of the load and resistance parameters. Additionally, Cornell (1967) also formulated the approximate relationship between the probability of failure and reliability index. This is given by following equation:

$$P_f = \Phi(-\beta) \quad \text{or} \quad \beta = -\Phi^{-1}(P_f) \tag{2.32}$$

where Φ represents the standard normal distribution function.

First-Order Reliability Method

First-Order Reliability Method (FORM) for the assessment of structural safety has been developed due to difficulties involved in this evaluation using direct methods. The main concept of this method is to approximate the limit state function with a first-order polynomial at the point of failure boundary. Usually, this point is closest to the origin in a transformed standard normal space and referred to as the design point.

The combined means, μ_{X_i}, and standard deviations, σ_{X_i} or coefficients of variation CoV_{X_i} of the basic random variables, X_i, are used to approximate statistical parameters of limit state function. Additionally, to get first order mean and variance, the Taylor series expansion is implemented in this method. Hence, FORM involves the following equations for mean value and variance of $g(X)$:

$$\mu_g \cong g\left(\mu_{X_1}, \mu_{X_2}, \dots, \mu_{X_n}\right) \tag{2.33}$$

$$\sigma_g{}^2 \cong \sum_{i=1}^{n}\sum_{j=1}^{n}\left(\frac{\partial g}{\partial X_i}\right)_{\mu}\left(\frac{\partial g}{\partial X_j}\right)_{\mu} CoV(X_i, X_j) \tag{2.34}$$

where ∂g is evaluated about the mean value of the given random variable.

For the case with all statistically uncorrelated random, the Equation (2.34) can be written as:

$$\sigma_g{}^2 \cong \sum_{i=1}^{n} \left(\frac{\partial g}{\partial X_i}\right)_{\mu}^{2} \sigma_{X_i}{}^2 \tag{2.35}$$

Using the above equations, the definition of the reliability index can be presented as:

$$\beta = \frac{\mu_g}{\sigma_g} \tag{2.36}$$

Assuming normal distribution for all the statistical parameters and limit state function as $g(R, Q) = R - Q$, the probability of failure is given as:

$$P_f = \Phi\left(\frac{0 - \mu_g}{\sigma_g}\right) = \Phi(-\beta) = \Phi\left(-\frac{\mu_R - \mu_Q}{\sqrt{\sigma_R{}^2 + \sigma_Q{}^2}}\right) \tag{2.37}$$

The reliability index in the equation above is:

$$\beta = \frac{\mu_R - \mu_Q}{\sqrt{\sigma_R{}^2 + \sigma_Q{}^2}} \tag{2.38}$$

For lognormally distributed statistical parameters, the limit state function is as follows:

$$g(R, Q) = \frac{R}{Q} \tag{2.39}$$

For this situation, the probability of failure, P_f, can be calculated as:

$$P_f = P(g < 1) \tag{2.40}$$

Implementing the properties of lognormal distribution presented in Section 2.4.2, the probability of failure can be formulated as:

$$P_f = \Phi(-\beta) = \Phi\left(- \frac{ln\left(\frac{\mu_R}{\mu_Q} \cdot \sqrt{\frac{{CoV_Q}^2 + 1}{{CoV_R}^2 + 1}}\right)}{\sqrt{ln\left(\left({CoV_R}^2 + 1\right) \cdot \left({CoV_Q}^2 + 1\right)\right)}} \right) \tag{2.41}$$

So for this case, the equation for reliability index is:

$$\beta = \frac{ln\left(\frac{\mu_R}{\mu_Q} \cdot \sqrt{\frac{{CoV_Q}^2 + 1}{{CoV_R}^2 + 1}}\right)}{\sqrt{ln\left(\left({CoV_R}^2 + 1\right) \cdot \left({CoV_Q}^2 + 1\right)\right)}} \tag{2.42}$$

The first-order reliability method is commonly used in various practical engineering analyses because it is easy, and does not require knowledge about the distribution of the random variable. On the other hand, since FORM assumes linearized characteristic of $g(X)$, a significant error can occur in the situation when limit state function is nonlinear. Therefore, this simplified method of analysis can be effectively and accurately implemented only for analyses with normally distributed variables and linear limit state function $g(X)$.

Second-Moment Method

In the Equation (2.38), the reliability index depends only on the means and standard deviations of the random variables, it is called *second-moment* measure of structural safety. This method does not require the knowledge about the probability distributions of the random variables, but if these distributions are known, β may be calculated using equivalent normal distributions. For random variables with normal distribution, Equation (2.32) provides the exact solution. For other situations, it is only an approximation.

The reduced variables $X'_1, X'_2, \ldots, X'_n$ serve as an expression for random variables $X_1, X_2, \ldots, X_n$ in second-moment method. The transformation is given by:

$$X'_i = \frac{X_i - \mu_{X_i}}{\sigma_{X_i}} \tag{2.43}$$

where μ_{X_i} and σ_{X_i} are the mean and standard deviation of X_i, respectively. For fundamental problem, where limit state function is given by:

$$g(R, Q) = R - Q \tag{2.44}$$

the result is as follows:

$$g(R', Q') = (\mu_R - \mu_Q) + R' \cdot \sigma_R - Q' \cdot \sigma_Q \tag{2.45}$$

For any explicit values of $g(R', Q')$, the Equation (2.45) is represented by a straight line. This line divides the space of random variables and separates it into two: safe space and failure space. In 1974, Hasofer and Lind introduced the definition of the reliability index as the shortest distance from the origin of the reduced variables coordinates system to the line $g(R', Q') = 0$. The graphical representation of this approach is presented in the Figure 2.10:

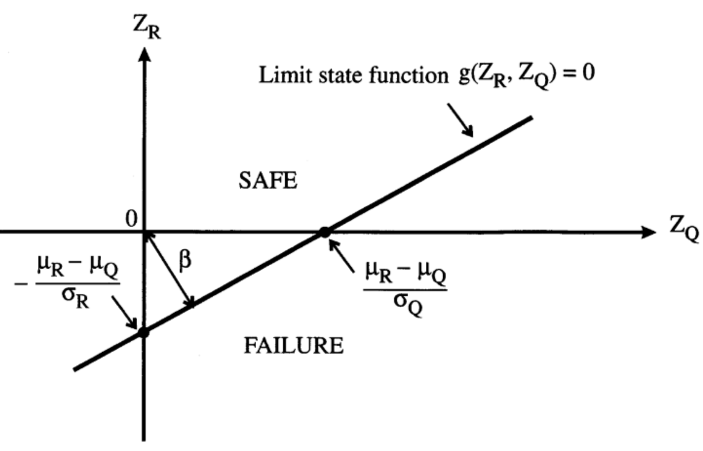

Figure 2.10: Reliability Index defined as the shortest distance in the space of reduced variables (Nowak and Collins 2013).

The formula to calculate the value of reliability index, using geometry, is given by:

$$\beta = \frac{\mu_R - \mu_Q}{\sqrt{{\sigma_R}^2 + {\sigma_Q}^2}} \tag{2.46}$$

In Equation ((2.46), β is the inverse of the coefficient of variation of the function $g(R, Q) = R - Q$ assuming that R and Q are uncorrelated.

The methods presented above are useful, but it is imperative to remember that in real analyses and real design there are many random variables involved. For these situations, the performance function becomes very complex: $g(X) = g(X_1, X_2, \dots, X_n)$, so the calculation of the reliability index is much more complicated.

<u>Reliability index for correlated variables with normal distribution</u>

The engineering applications for which random variables are correlated have specific reliability analysis procedures, which is not an uncommon situation and has significant influence on the final level of structural safety. When the limit state function is determined by correlated random variables, the reliability index may be calculated using the formula proposed by Ang and Tang in 1984. The equation is as follows:

$$\beta = \frac{\mu_g}{\sigma_g} = \frac{a_0 + \sum_{i=1}^{n} a_i \cdot \mu_{X_i}}{\sqrt{\sum_{i=1}^{n} \sum_{j=1}^{n} a_i \cdot a_j \cdot \rho_{ij} \cdot \sigma_{X_i} \cdot \sigma_{X_j}}} \tag{2.47}$$

where ρ_{ij} if the coefficient of correlation between random variables X_i and X_j.

2.7. Simulation Techniques

Simulation techniques serve as useful tools for solving complicated engineering and science problems. They are being commonly implemented in the reliability analyses to find out the performance of a given element or the whole structural system. From an engineering standpoint, one of the most popular is the Monte Carlo method (Thoft-

Christensen and Baker 1979). Point Estimate Methods (Rosenblueth 1975, 1981 and Gorman 1979) and Latin Hypercube Sampling (McKay et al. 1979) are other interesting simulation techniques. However, since the Monte Carlo Simulation is probably the most popular, only that method is described in detail in this dissertation.

Monte Carlo Simulation

The Monte Carlo Simulation Method is one of the methods used to predict the performance of structural elements without testing them. To perform this simulation, a large number of random variables have to be generated in accordance with the corresponding probability distributions. The more variables generated, the more efficient the simulation is. This is especially valuable for the problems involving rare events, in which physical testing would be very expensive or sometimes even impossible to perform. Since there is a similarity between simulated values and values for physical samples, the results from the Monte Carlo Simulation can be treated statistically. For nonlinear limit state functions with random variables of distributions known in advance, this method is especially efficient and provides accurate results.

Below are the following steps to perform the Monte Carlo Simulation:

1) *Generation of the uniformly distributed random variables between 0 and 1 ($u_1, u_2, \dots, u_n$). This can be done by a built-in computer option or manually.*

2) *Calculation of the standard normal values using generated numbers and information about the distributions and other statistical parameters like the mean or standard deviation of each design variable. To calculate the standard normal random numbers, the following equation is utilized:*

$$z_i = \Phi^{-1}(u_i) \tag{2.48}$$

where $\Phi^{-1}$is the inverse of the standard normal cumulative distribution function.

3) *Generation of the sample random numbers for the random normal variable* x *using mean value and standard deviation:*

$$x_i = \mu_x + z_i \cdot \sigma_x \tag{2.49}$$

where x_i, μ_x, z_i *and* σ_x *are the sample random numbers for the random normal variable, mean, standard normal random numbers and standard deviation respectively*

4) *Simulation of the efficient number of sets. This is to avoid the situation when an insufficient number of simulations would have an influence on the final results.*

5) *The following general equation is used for calculation of the probability of failure:*

$$\bar{P_f} = \frac{n}{N} \tag{2.50}$$

where $g(\bar{X})$ *is the performance function with the limit* $g(\bar{X}) = 0$, n *is the total number of simulations when* $g(\bar{X}) < 0$ $(failure)$ *and* N *total number of simulations of* $g(\bar{X})$.

The Monte Carlo Simulation Method is useful not only for studying structural performance for a certain set of statistical parameters, but also for the measurement of the sensitivity of the system due to changes in some of the parameters. Thus, this method serves as beneficial tool for the optimization of the structural design.

2.8. LOAD MODELS

Dead Load

Dead load is the gravity load due to the self-weight of the structural and nonstructural components permanently connected to the structure. From bridge design perspective it will be the weight of factory-made elements (steel, precast concrete members) as well as cast-in-place concrete elements.

All components of dead load are typically treated as normal random variables. Usually it is assumed that the total dead load, *D*, remains constant throughout the life of the structure.

The most important statistical parameters for dead load are:

1) *Bias factor, λ, is the ratio of mean to nominal values*

2) *Coefficient of Variation, CoV, is standard deviation divided by the mean value*

<u>Live Load</u>

For bridge design, the live load covers a range of forces produced by vehicles moving on the bridge. The effect of live load on the bridge depends on many parameters such as span length, truck weight, axle loads, axle configuration, position of the vehicle on the bridge (transverse and longitudinal), number of vehicles on the bridge (multiple presence), girder spacing, and stiffness of structural members (slab and girders). For Long Span Bridges, if local WIM data is available, Equivalent Uniformly Distributed Load can be calculated. For the purposes of this study, WIM data was collected and processed. Results served as live load applied to the Finite Element of the Arch Bridge.

2.9. Resistance Models

The load-carrying capacity of every structure depends on the resistance of the elements of which it is made and connections between them. The resistance of each component consists of material properties (strength), geometry of the cross section and dimensions. In real-life design, these parameters are treated as deterministic, but for the purposes of reliability analysis there is an uncertainty associated with each of these factors. Thus, the resistance, *R*, is a random variable. There are three categories for the sources of uncertainty:

1) *Material properties (strength of material, modulus of elasticity, cracking stresses, chemical composition etc…)*

2) *Fabrication (geometry of the cross section and overall dimensions of the element which can affect the properties like moment of inertia, section modulus, area of the cross section)*

3) *Analysis (usage of approximate methods of analysis, idealization of the stress/strain models, assumptions which were made)*

Using the tests results, observations of existing structures and engineering judgement, the variability of the resistance can mostly be quantified. For the basic structural elements, the majority of this information is widely available. However, if there is limited information for specific components, it is necessary to develop the resistance model using the available material test data and simulation techniques.

In the reliability analysis, it is popular and convenient to consider resistance as a product of the nominal resistance and parameters, which depend on the three sources of uncertainty described above. Therefore, the equation for the resistance model is as follows:

$$R = R_n MFP \tag{2.51}$$

where:

R_n = nominal resistance specified by the code

M = variation in the strength of the material

F = uncertainties in fabrication (dimensions)

P = analysis (professional) factor which stands for the uncertainties caused by used methods of analysis.

The material and fabrication factors are actual to nominal ratios of material and cross-sectional properties, respectively. The professional factor is representing the ratio of test capacity (in situ performance) and predicted capacity (used in model).

The mean value of the resistance, μ_R, is given by:

$$\mu_R = R_n \mu_M \mu_F \mu_P \tag{2.52}$$

where μ_M, μ_F and μ_P are mean values of M, F and P, respectively.

Additionally, the bias factor, λ_R, and coefficient of variation of R, CoV_R, are as follows:

$$\lambda_R = \lambda_M \lambda_F \lambda_P \tag{2.53}$$

$$CoV_R = \sqrt{{CoV_M}^2 + {CoV_F}^2 + {CoV_P}^2} \tag{2.54}$$

where:

λ_M, λ_F and λ_P = bias factors

$CoV_M, CoV_F\ and\ CoV_P$ = coefficients of variation of M, F and P, respectively.

The statistical parameters of material properties, fabrication and analysis factors, including bias factors, mean values and coefficients of variation can be found in the literature. Ellingwood et al. (1980, 1982) and Galambos et al. (1982) presented a comprehensive summary of the statistical parameters for different components of building structures. For different components of the bridge structures, useful sources of information about these parameters are provided by Tabsh and Nowak (1991) and Nowak, Yamani and Tabsh, (1994).

2.10. System Reliability Models

Each structure is a system of interconnected elements. In general, failure of a single component does not mean failure of the whole structure. The failure is usually reaching the limit state (e.g. ultimate load carrying capacity). There are two extreme types of elements:

1) *Brittle Elements – a component is perfectly brittle if it becomes ineffective after failure.*

2) *Ductile Elements – a component is perfectly ductile if it maintains its load carrying capacity after failure.*

The typical load-displacement curves are presented in the Figure 2.11:

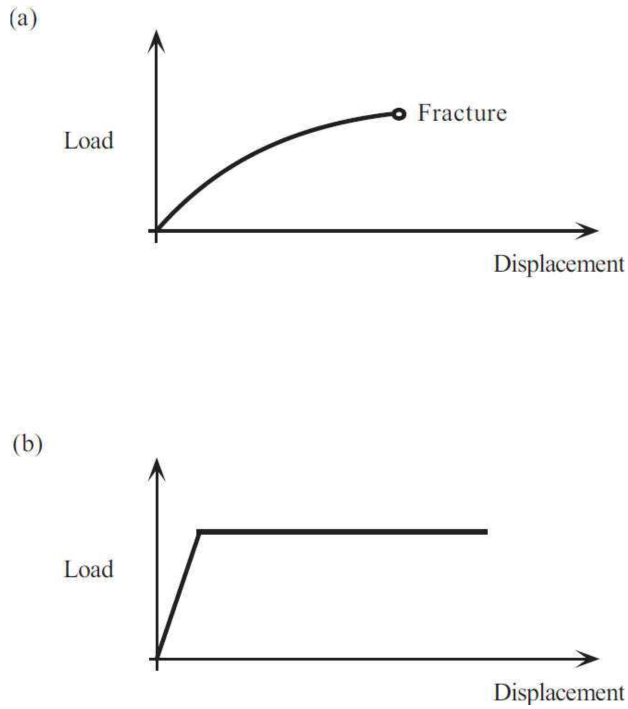

Figure 2.11: Load-displacement curves for (a) brittle and (b) ductile elements (Nowak and Collins 2013).

Since the system reliability analysis is usually a convoluted process, it is convenient to draw a scheme using specific symbols for different types of elements. For brittle and ductile elements, they are as follows:

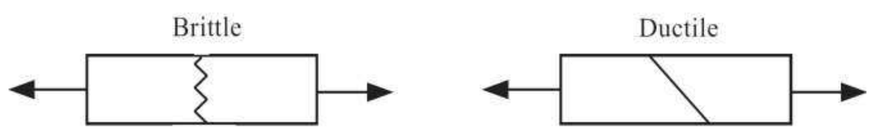

Figure 2.12: Symbols used in literature to distinguish brittle and ductile elements (Nowak and Collins 2013).

Another important characteristic of the structural system is its configuration. There are two main categories of structural systems:

1) *Series System – is in a state of failure whenever any of its elements fails. Also called a weakest-link system.*

2) *Parallel System – a system in which failure of all components is required for the overall system to fail.*

Both types of systems can consist of ductile or brittle elements. Moreover, in practice, a structure is a combination of both series and parallel as well as hybrid systems. The graphical representations of series and parallel systems are presented in the Figure 2.13:

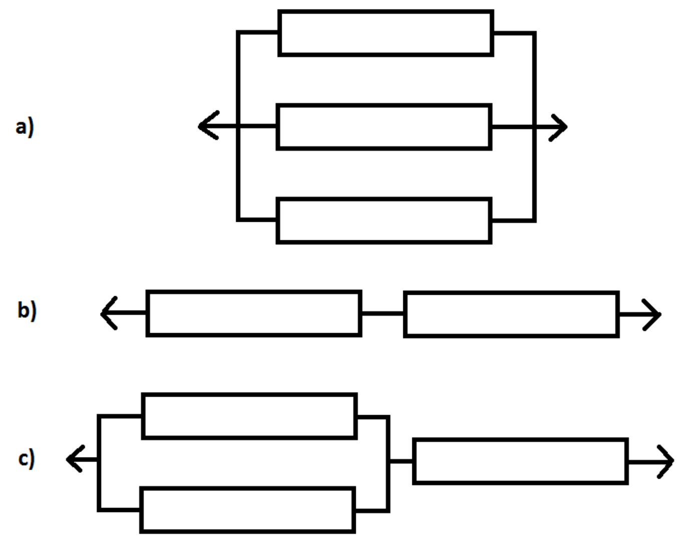

Figure 2.13: Examples of different structural systems (a) parallel, (b) series and (c) hybrid.

<u>Series systems.</u>

For the series system, the failure of any element means the failure of the structural system. That is why it is referred to as a weakest link system. In other words, to provide success for the whole system, each of the elements must succeed. Therefore, the probability of failure of this kind of system is equivalent to the probability that any of the elements will fail.

For structural systems made up of elements where the strength properties are statistically independent, the probability of failure of the system, P_f, is given by the equation derived by Ang and Tang (1984) and Thoft-Christensen Baker (1982):

$$P_f = 1 - \prod_{i=1}^{n} \left(1 - P_{f_i}\right) \tag{2.55}$$

where P_{f_i} means the probability of failure of the element.

For structural systems in which the strength properties of elements are perfectly correlated, the probability of failure of the system, P_f, is given by the following equation:

$$P_f = \max_i \left(P_{f_i}\right) \tag{2.56}$$

If the series system has positive correlation between the elements, simple bounds of the probability of failure can be derived. This approach applies only for the correlation coefficient, ρ_{ij}, greater than or equal to zero.

By combining Equation (2.55) and Equation (2.56), it is clear that the probability of failure must satisfy the Equation (2.57), known as Cornell's bounds:

$$\max_i \left(P_{f_i}\right) \leq P_f \leq 1 - \prod_{i=1}^{n} \left(1 - P_{f_i}\right) \tag{2.57}$$

In this equation, the lower bound corresponds to the system with full correlation, while the upper bound represents the system of statistically independent components.

When the correlation between the components is unknown, the exact calculation of the probability of failure is complicated, if not impossible. Nevertheless, there are methods and equations to estimate the probability of failure for these situations.

For series systems with equally correlated elements, in 1958, Stuart proposed the following equation:

$$P_f(\rho) = 1 - \int_{-\infty}^{\infty} \left[\Phi\left(\frac{\beta_e + \sqrt{\rho}\, t}{\sqrt{1-\rho}}\right)\right]^n \varphi(t)dt \tag{2.58}$$

where Φ and φ denote the distribution and density function for standard normal variable, β_e is a reliability index of the element, n is a number of elements,

The correlation coefficient between the elements in the real structure are not normally equal. In this case, Thoft-Christensen and Sorensen proposed, in 1982, the equation for the average correlation coefficient, as follows:

$$\bar{\rho} = \frac{1}{n(n-1)} \sum_{i,j=1\ i\neq j}^{n} \rho_{ij} \tag{2.59}$$

Additionally, the average correlation coefficient calculated in Equation (2.59) may be inserted into Equation (2.58), instead of ρ, to get an estimation for the probability of failure. This approach is conservative, for that reason, it is justified to use for structure reliability analysis.

<u>Parallel systems.</u>

For parallel systems to provide success of the whole system, at least one of the elements must succeed. Therefore, the probability of failure for this kind of system is equivalent to the probability that all of the elements fail.

For structural systems made up of elements where the strength properties are statistically independent, the probability of failure of the system, P_f, is given by the following equation:

$$P_f = \prod_{i=1}^{n} P_{f_i} \tag{2.60}$$

where P_{f_i} means the probability of failure of the element.

For structural systems in which the strength properties of elements are perfectly correlated, the probability of failure of the system, P_f, is given by the following equation:

$$P_f = \min_i \left(P_{f_i}\right) \tag{2.61}$$

If the parallel system has positive correlation between the elements, simple bounds of the probability of failure can be derived. This approach applies only for the correlation coefficient, ρ_{ij}, greater than or equal to zero.

By combining Equation (2.60) and Equation (2.61), it is clear that the probability of failure must satisfy the Equation (2.62), known as Cornell's bounds:

$$\prod_{i=1}^{n} P_{f_i} \leq P_f \leq \min_i \left(P_{f_i}\right) \tag{2.62}$$

In this equation, the lower bound corresponds to the system with statistically independent components when the upper bound represents system with full correlation.

When the correlation between the components is unknown, the exact calculation of the probability of failure is very complicated, if not impossible. Nevertheless, there are methods and equations to estimate the probability of failure for these situations.

For parallel systems with equally correlated elements, Grigoriou and Turkstra, in 1979, proposed the following equation for system reliability index (β_s):

$$\beta_s = \beta_e \cdot \sqrt{\frac{n}{1 + \rho(n-1)}} \tag{2.63}$$

where:

ρ = coefficient of correlation

β_e = reliability index the same for all of the elements and

n = a number of elements.

Similar to the series system, the average correlation coefficient calculated in Equation (2.59) may be inserted into Equation (2.63), instead of ρ, to get an estimation for the system reliability index.

CHAPTER 3 DEVELOPMENT OF LIVE LOAD MODEL

3.1. TRAFFIC DATA – WEIGH-IN-MOTION

Weigh-In-Motion (WIM) is *"the process of measuring the dynamic tire forces of a moving vehicle and estimating the corresponding tire loads of the static vehicle"* (ASTM E1318-09). First efforts to develop this system date back to the early 1950s. Preliminary systems consisted of strain gage load cells which supported concrete floating platforms embedded in the roadway. The measurements were obtained by observing the traces with an oscilloscope and taking pictures of them. In addition, other types of WIM systems, like steel bending plates with strain gages and strip sensors, were being developed. The most important obstacles at that time were limitations in signal conditioning, sensing and inaccessibility of data acquisition systems. In contrast, modern WIM systems are highly advanced and very effective. In addition to the weight and length of the whole vehicle, they can also provide different kind of information like vehicle's type (class), speed, number of axles, each axle's weight, spacing etc… (LTBP, 2016). These systems are able to process all records mentioned above in real time for vehicles passing with regular highway speed. Incredibly effective hardware and software is being employed in order for WIM to collect the vast amounts of data necessary for analyzing, sorting, classification and transmission. Common WIM stations involve the following types of sensors: polymeric, ceramic, and quartz piezoelectric systems; bending plates; and load cells. (Norman, O.K. and Hopkins, R.C., 1952)

Table 3.1: WIM sensors comparison. (Zhang, L., 2007)

Characteristic		Bending Plate	Single Load Cell	Piezoelectric Sensor	Quartz Piezoelectric Sensor
Cost	Initial installation cost per lane (USD)	Medium (~$20,000)	High (~$50,000)	Low (~$9,000)	Medium (~$20,000)
	Annual maintenance and operation costs (USD)	Medium (~$6,000)	High (~$8,000)	Low (~$5,000)	High
Accuracy (GVW 95-percent confidence)		±10 percent	±6 percent	±15 percent	±10 percent
Sensitivity		Medium	Medium	High	None to temperature, but high to roughness
Expected life (years)		6	12	4	Expected > 15
Reliability		Medium	High	Low	Medium

The WIM sensors take measurements through signals recorded by devices such as voltage, strain and resistance. The most popular type of sensor is the bending plate and inductive loops embedded in the roadway surface (Figure 3.1). However, there are sensors which may be mounted under the bridge's girders and after proper calibration, by measuring strains, they provide WIM data. The accuracy of the whole system depends on the interaction between the vehicle and pavement (this is related to the roughness of pavement), vehicle's speed and suspension system. On the other hand, the system's accuracy is determined by proper installation, calibration and maintenance of the measuring devices.

Figure 3.1: WIM Station – bending plate and inductive loops. (Hallenbeck, M. and Weinblatt, H. 2004)

Each state has its own regulations about trucking activities and vehicle weight limits. These regulations usually are different for different types of roads and bridges. Most of the Federal rules have not changed since 1982, but some states achieved exceptions for Gross Vehicle Weight (GVW) and axle weight limits by Federal legislations. The following are the main limits included in the National Cooperative Highway Research Program (NCHRP) Synthesis 453 on the States' legal loads:

1) *A total of 36 of 50 states set limits for axle load at 20,000 lb., and 14 States set higher limits on axle load, with the highest being 24,000 lb.*

2) *A total of 33 of 50 states set limits for load on tandem axles equal to 34,000 lb.*

3) *A total of 17 states set higher limits for tandem-axle load. The highest limit is 48,000 lb.*

4) *A total of 32 states set limits for GVW equal to 80,000 lb., the limit set in Title 23 U.S. Code.(10)*

5) *A total of 9 states set GVW limits greater than 100,000 lb. The largest limit is 164,000 lb.*

States set limits on GVW in relation to axle count and wheelbase using the Federal Bridge Formula or using State-specific bridge formulas.

Some states have seasonal provisions for exemption of legal loads. Vehicles may be exempt for specific uses, specific commodities, or specific owners. For example, in North Dakota, agriculture-related loads receive a 10 percent increase over legal loads during harvest time.

In addition, current Federal law provides the dimension limits as follows (Federal size regulations for commercial motor vehicles):

1) *Maximum vehicle width: 102 in.*

2) *Minimum vehicle length for a semi-trailer in a truck-tractor/semitrailer combination: 48 ft.*

3) *Minimum vehicle length for a semi-trailer or trailer operating in a truck-tractor/semi-trailer/trailer combination: 28 ft.*

3.2. TYPES AND CLASSES OF VEHICLES

The Federal Highway Administration (FHWA) classified vehicles into 13 categories (also called classes). Classes 1 to 3 are motorbikes, cars and small vehicles, 4 to 7 are single unit trucks and buses, 8 to 10 are combination trucks and 11 to 13 are multi-trailer trucks. In this study, to eliminate the lightest vehicles, only classes 3 to 13 are considered. The scheme with examples of vehicles for each class is presented in the Figure 3.2.

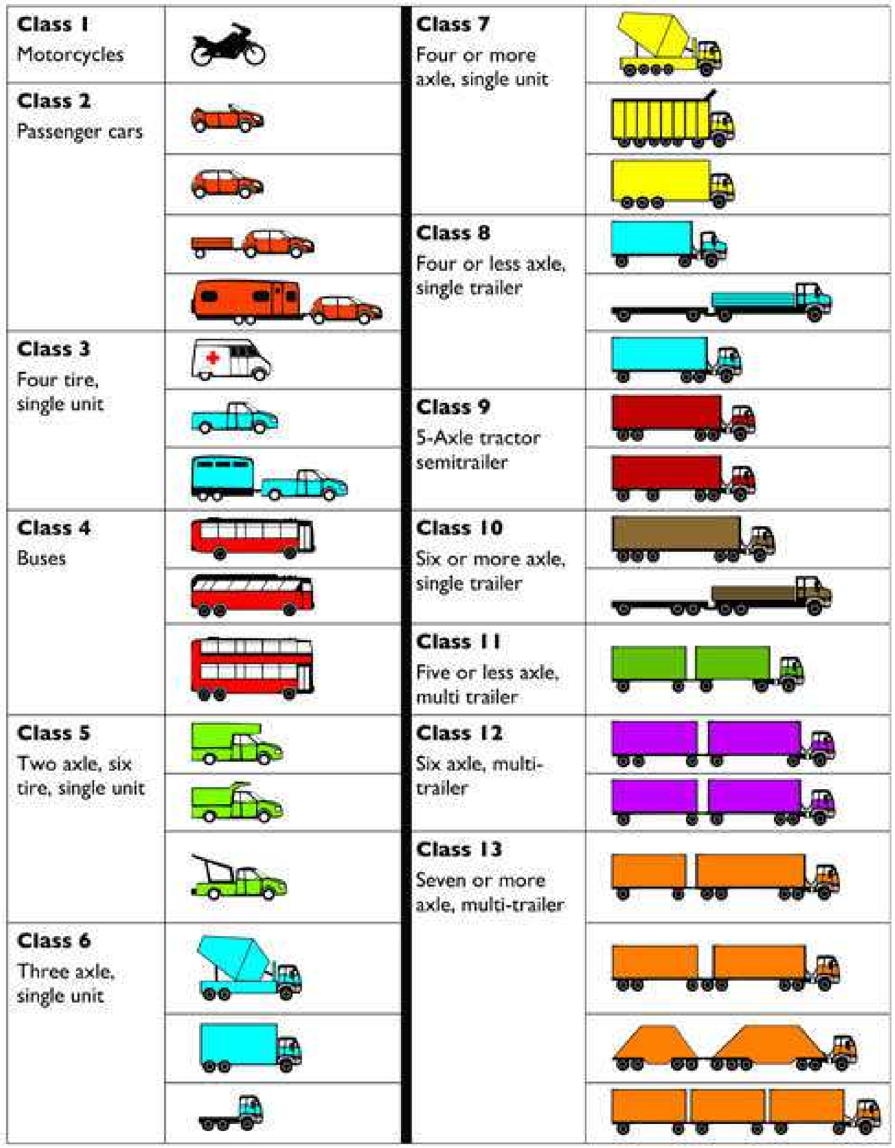

Figure 3.2: Classes of vehicles. (FHWA)

3.3. LOCATION AND DESCRIPTION OF THE CONSIDERED WIM STATION

The Weigh-In-Motion station considered in this study is WIM 961 in Alabama, located north-east of Mobile (exact coordinates are: 30°53'18.6"N 88°01'33.3"W). This station was chosen because it is on the same interstate highway (I-65) as the General W.K. Wilson Jr. Bridge, which is the focus of this dissertation. The distance from the station to the bridge is approximately 4 miles, so it is assumed that the traffic on the bridge is the same as measured by 961 WIM station. Exact location, distance between WIM station and the bridge and broader view are presented in the Figure 3.3 and Figure 3.4.

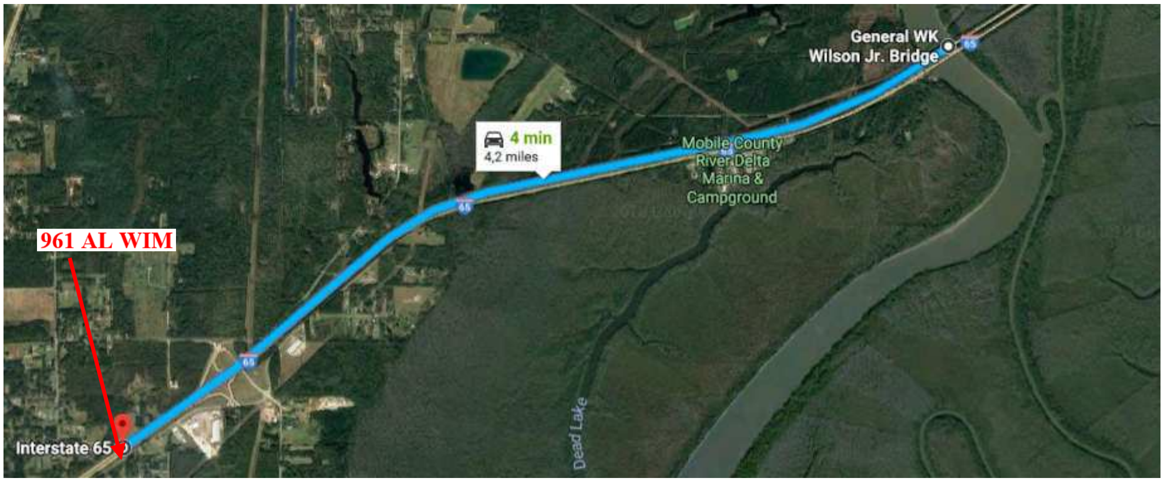

Figure 3.3: Location and distance between 961 Alabama WIM station and General W.K. Wilson Jr. Bridge. (Google Maps)

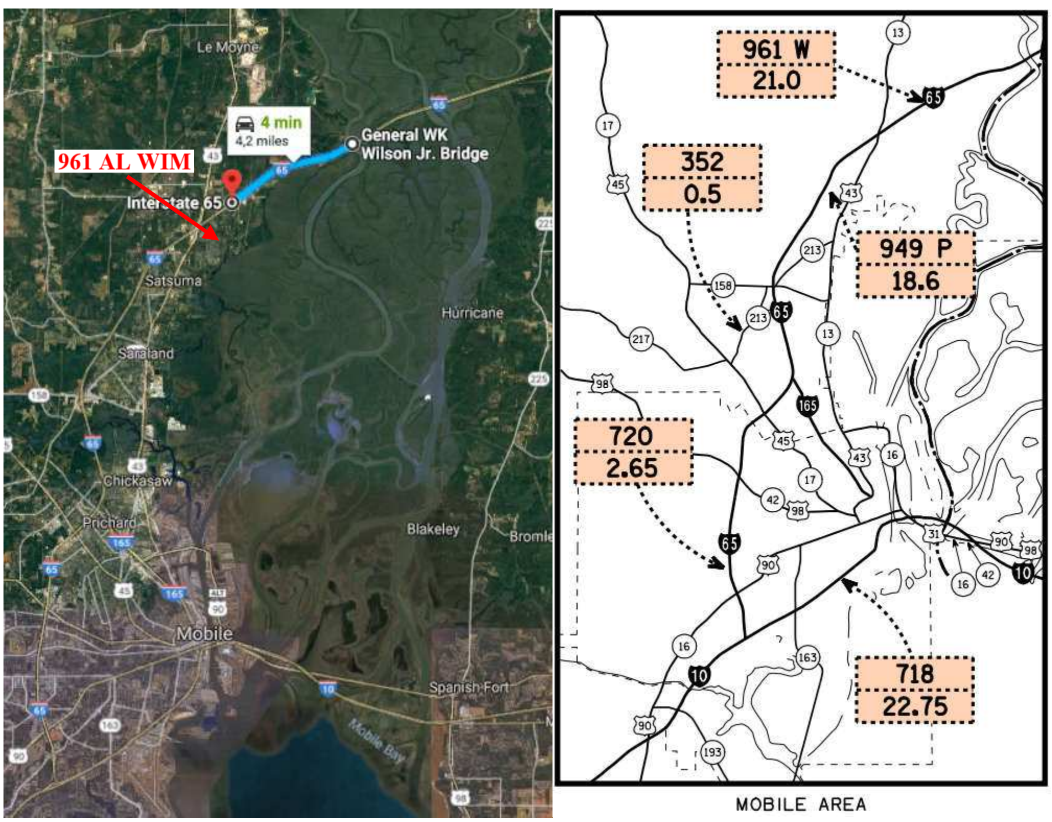

Figure 3.4: Broader view of the 961 WIM station and General W.K. Wilson Jr. Bridge.

(Google Maps and Alabama Permanent Traffic Recorders Map)

The considered 961 WIM station is made of bending plates and inductive loops (Figure 3.5). The main function of bending plates is measurement of the weight of each axle. Inductive loops mainly serve for detection of axles and vehicle count.

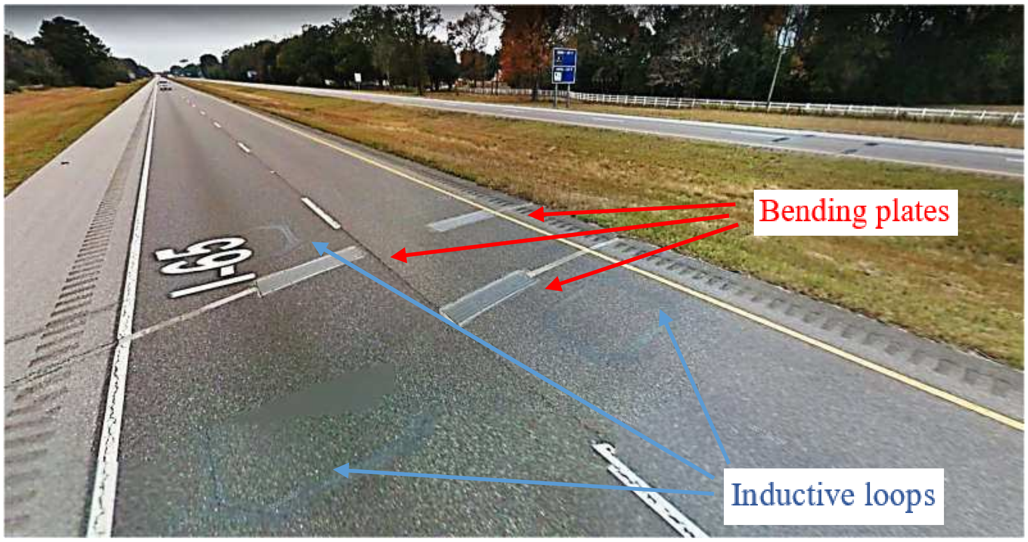

Figure 3.5: Steel bending plates and inductive loops at 961 WIM station. (Google Street view)

3.4. WIM DATA PROCESSING

The Weigh-In-Motion database was obtained from a previous Research Project conducted for Alabama Department of Transportation at Auburn University. The title of the ongoing project is: "Application of WIM and Permit Data" by Andrzej S. Nowak and J. Michael Stallings. The summary for the considered WIM data is presented in the Table 3.2.

Table 3.2: 961 WIM Station Database summary.

Year	Number of Months	Number of records before filtering
2014	10 (Jan-Oct)	2,136,008
2015	1 (Dec)	191,853
2016	11 (no Sept)	1,821,562

For the purpose of processing the collected WIM data, the specific filtering criteria was applied. The reasons for that were to eliminate corrupted records, measurement errors and vehicles with relatively low GVW. This elimination provided data for the simulation of most critical traffic jam situations (Caprani, OBrien, Lipari, 2016). Implemented filtering criteria are the same as for previous similar analyses and research projects. They are as follows:

Vehicle's records, which were filtered out from the database:

1) *GVW less than 20 kips.*
2) *Individual axle weight greater than 70 kips or less than 2.0 kips.*
3) *Total length greater than 120 ft.*
4) *Total length less than 7 ft.*
5) *First axle spacing less than 5 ft.*
6) *Individual axle spacing less than 3.4 ft.*
7) *GVW ±10% the sum of axle weights*
8) *Class of vehicle according to FHWA <4 or >13*
9) *Sum of axle's spacing is greater than the wheel base of truck by 1 ft. or more*

The amount of remaining data after the application of filtering criteria is presented in Table 3.3.

Table 3.3: 961 WIM Station Database summary – after filtering.

Year	Number of records remained after filtering (% of original data)
2014	818,700 (38.3%)
2015	106,959 (55.8%)
2016	1,083,203 (59.5%)

In addition to regular filtering, to obtain moderate values for traffic jam simulation, modified filtering criteria were used. Criteria 1, 2, 4 and 5 were not applied.

The amount of remaining data after applying the modified filtering criteria is presented in the Table 3.4.

Table 3.4: 961 WIM Station Database summary – after moderate filtering.

Year	Number of records remained after moderate filtering (% of original data)
2014	2,134,031 (99.9%)
2015	191,578 (99.9%)
2016	1,818,445 (99.8%)

For filtered data, statistical analysis was conducted. Cumulative Distribution Functions were calculated and presented on the probability paper. The analysis shows differences for the distribution of GVW depending on the applied filtering criteria. For example higher mean value and “cut-off” of GVW smaller than 20 kip are visible in the charts for regular filtering. Plots for different years and two different filtering criteria are shown in the Figure 3.6, Figure 3.7 and Figure 3.8. They are showing the distribution of the traffic for the considered location. The mean value is significantly different for both types of filtering. For regular filtering, it is around 50 kip, while for moderate filtering – around two times smaller.

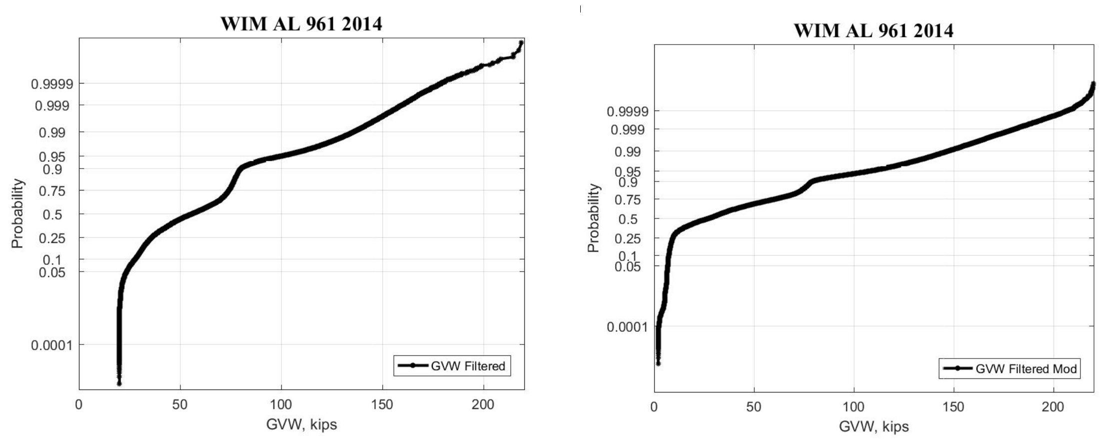

Figure 3.6: GVW – 961 WIM for year 2014.
Regular filtering – left, moderate filtering – right.

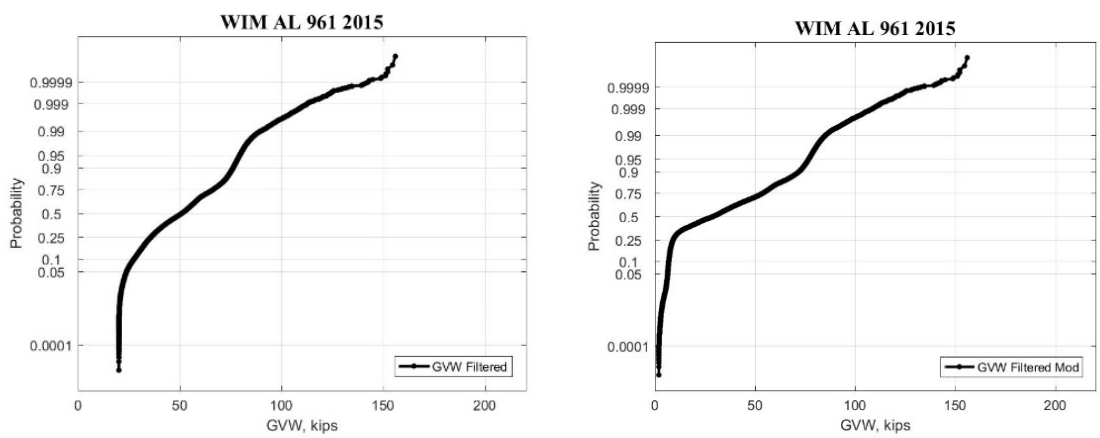

Figure 3.7: GVW – 961 WIM for year 2015.
Regular filtering – left, moderate filtering – right.

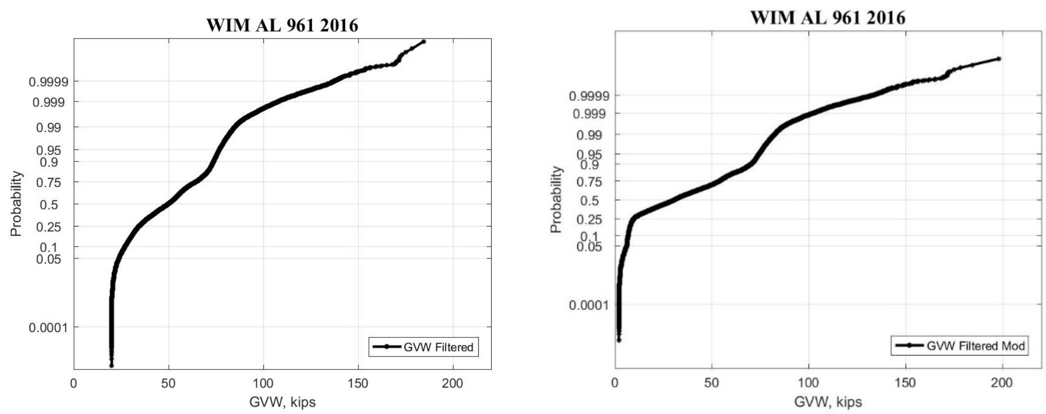

Figure 3.8: GVW – 961 WIM for year 2016.
Regular filtering – left, moderate filtering – right.

The 961 AL WIM station collects data for both directions of the traffic, so for four traffic lanes. The records for right lane for both directions were combined and in the analysis they are called “Lane1”. The same procedure was applied to left lane and these records are called “Lane 2”. The heavier traffic is expected to be on the right lane and collected data shown, that the number of records for right lane is much higher than for the left lane. Therefore, the results were split into two categories (Lane 1 - right lane, Lane 2 – left lane) and presented in the Figure 3.9, Figure 3.10 and Figure 3.11.

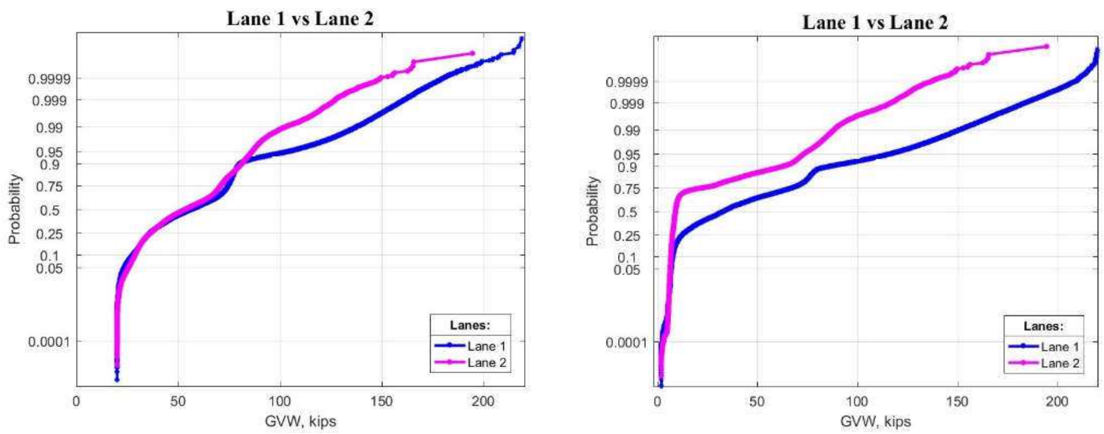

Figure 3.9: GVW per lane – 961 WIM for year 2014.
Regular filtering – left, moderate filtering – right.

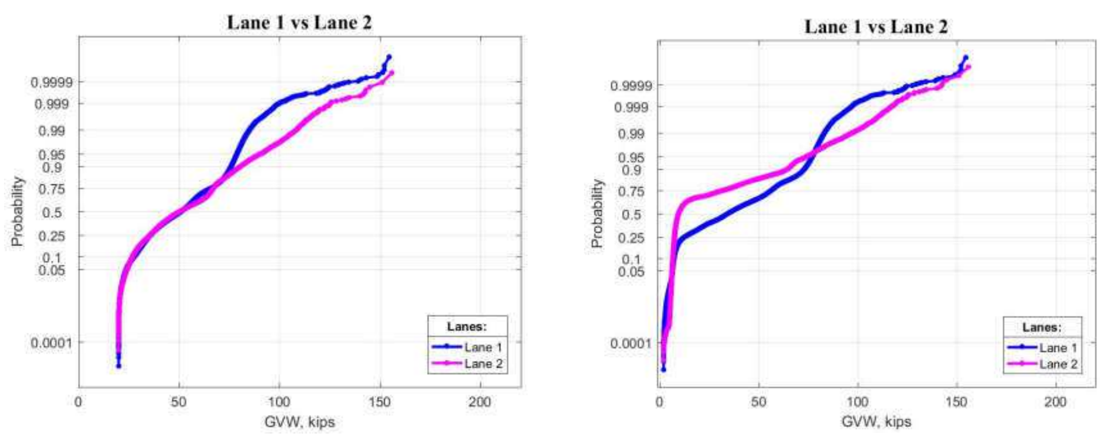

Figure 3.10: GVW – 961 WIM for year 2015.
Regular filtering – left, moderate filtering – right.

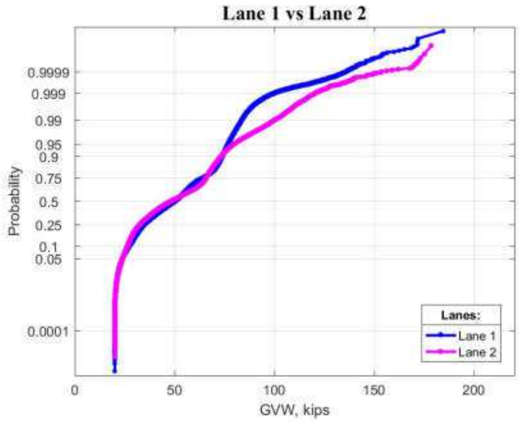

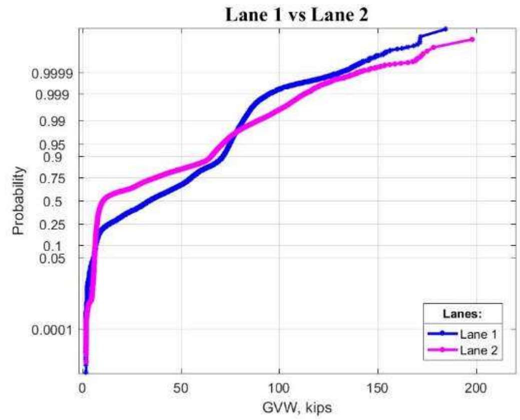

Figure 3.11: GVW – 961 WIM for year 2016.
Regular filtering – left, moderate filtering – right.

Table 3.5: Total number of vehicles per lane.

	Number of Vehicles			
	Regular Filtering		**Moderate Filtering**	
Year	Right Lane (1)	Left Lane (2)	Right Lane (1)	Left Lane (2)
2014	722,385	96,315	1,742,958	391,073
2015	94,020	12,939	148,595	42,983
2016	959,604	123,599	1,483,033	335,412

The distribution of different classes of vehicles have been checked and presented in the Figure 3.12, Figure 3.13 and Figure 3.14. It is clearly visible that each year, for a database with regular filtering criteria, class 9 vehicles are dominating; while for moderate filtering, most vehicles are classes 5 and 9.

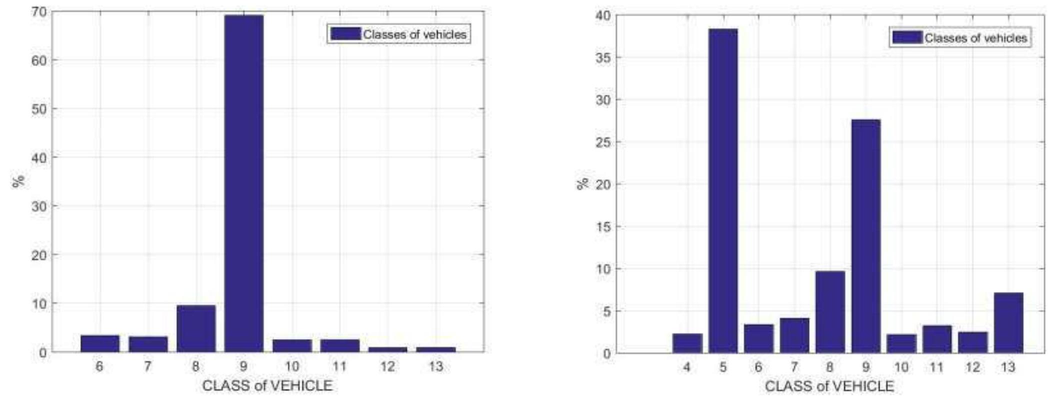

Figure 3.12: Classes of vehicles distribution – 961 WIM for year 2014. Regular filtering – left, moderate filtering – right.

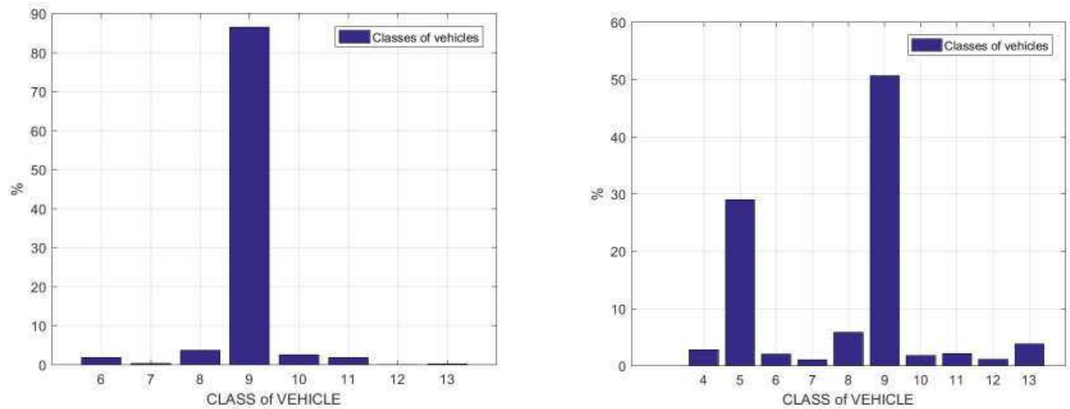

Figure 3.13: Classes of vehicles distribution – 961 WIM for year 2015. Regular filtering – left, moderate filtering – right.

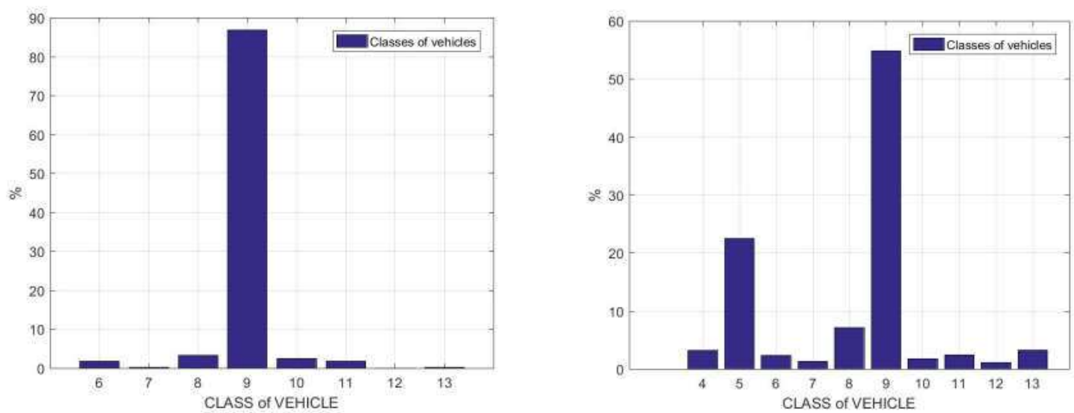

Figure 3.14: Classes of vehicles distribution – 961 WIM for year 2016. Regular filtering – left, moderate filtering – right.

Distributions of GVW for different classes of vehicles are presented in the Figure 3.15, Figure 3.16 and Figure 3.17.

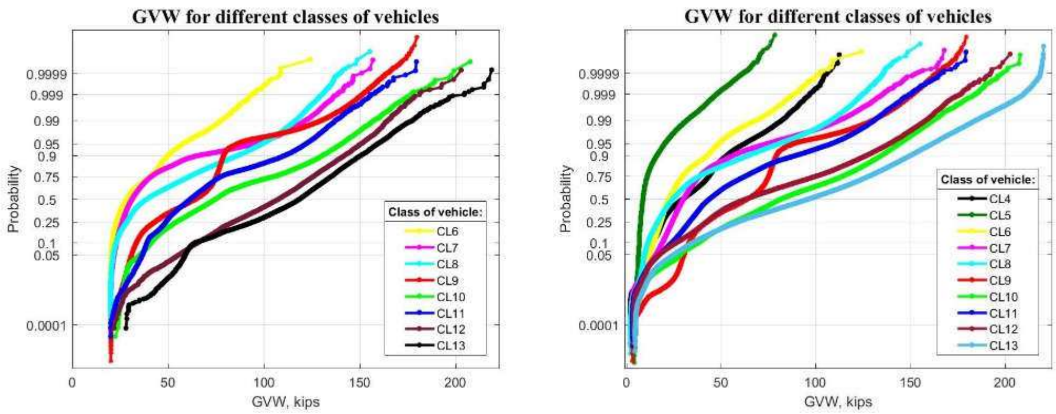

Figure 3.15: GVW for different classes of vehicles – 961 WIM for year 2014. Regular filtering – left, moderate filtering – right.

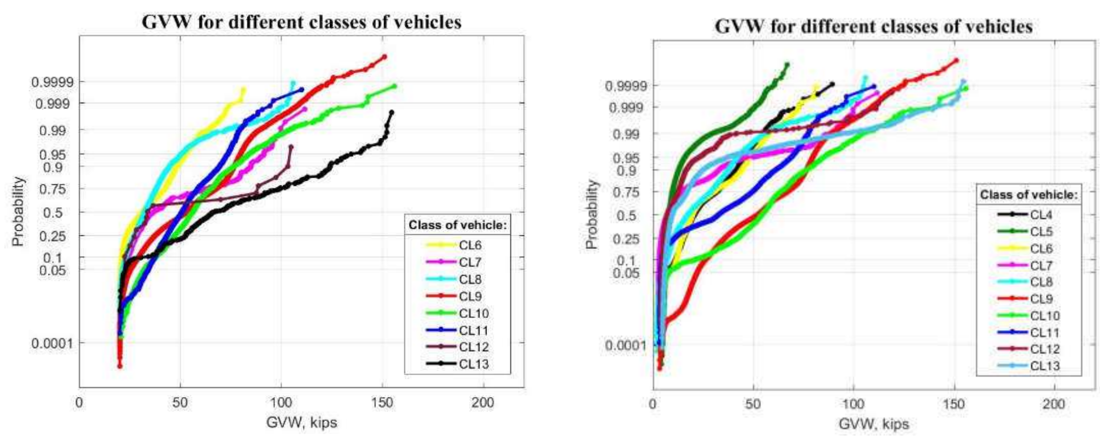

Figure 3.16: GVW for different classes of vehicles – 961 WIM for year 2015. Regular filtering – left, moderate filtering – right.

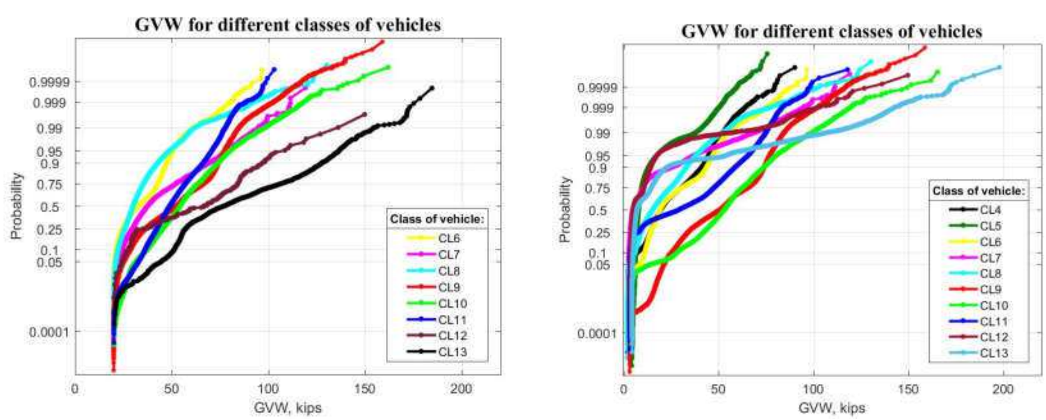

Figure 3.17: GVW for different classes of vehicles – 961 WIM for year 2016. Regular filtering – left, moderate filtering – right.

3.5. Development of the Uniformly Distributed Live Load

The analysis of the collected WIM data was conducted using Matlab Software. This program allows large databases to process in an efficient way, and provides numerous options for graphical representation of the results.

For the purpose of this study, the traffic jam situation on the bridge is considered as the most critical situation from a live load analysis perspective.

The simulation procedure is as follows:

Firstly, there is the line of trucks on the span. For the purpose of this project, spacing between the last axle of one truck and first axle of the following is assumed as 25 ft (Lutomirska 2009). Then the total load of the trucks on the span is divided by the length of the span and it gives a value of Uniformly Distributed Load (UDL). Next, the first truck in the line is deleted and one is added at the end of the line and the scheme is repeated for every record for WIM data for given location. The number of combinations for each year is shown in the Table 3.6. The whole process is repeated for different span lengths (from 500 ft. up to 1000 ft.). At the end, the mean value for each span length is calculated and uses these values. For this research the mean value or Uniformly Distributed Load (UDL, black trace on the plots), and UDL for maximum daily and weekly combinations of vehicles were presented (yellow and red traces in the Figure 3.18, Figure 3.19 and Figure 3.20).

Plots of UDL (mean, max daily and max weekly combinations) for different span lengths were created and they are presented in the Figure 3.18, Figure 3.19 and Figure 3.20.

Table 3.6: Number of combinations of trucks used to calculate UDL.

	Number of UDL combinations	
Year	Regular Filtering	Moderate Filtering
2014	1,444,767	3,485,895
2015	188,027	297,177
2016	1,919,196	2,966,051

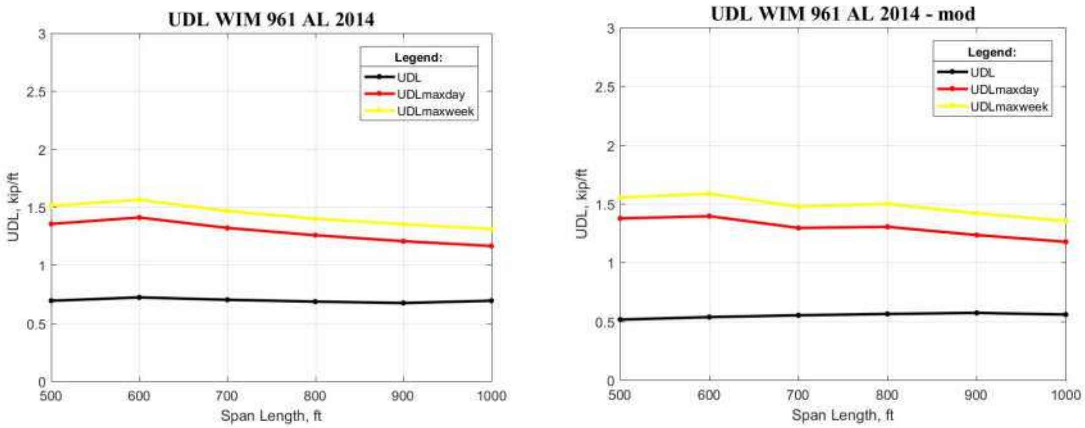

Figure 3.18: Equivalent Uniformly Distributed Load for different span lengths 961 WIM for year 2014.
Regular filtering – left, moderate filtering – right.

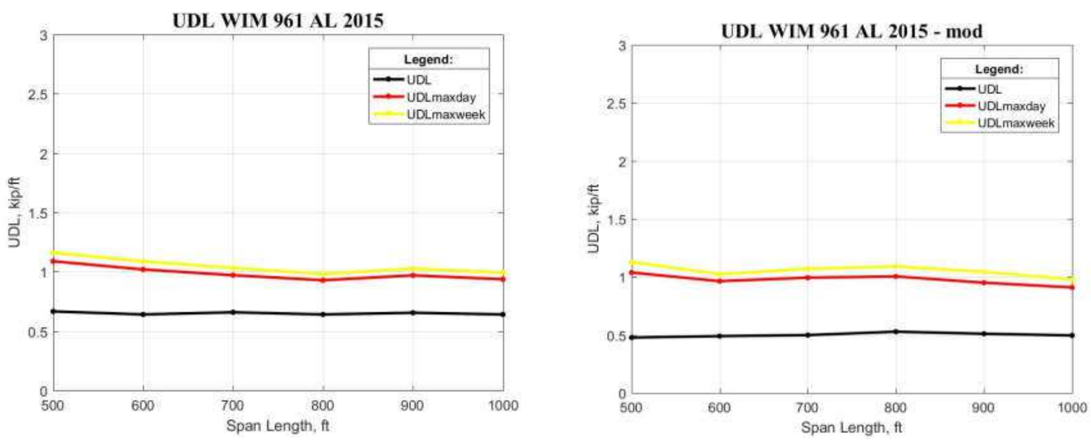

Figure 3.19: Equivalent Uniformly Distributed Load for different span lengths 961 WIM for year 2015.
Regular filtering – left, moderate filtering – right.

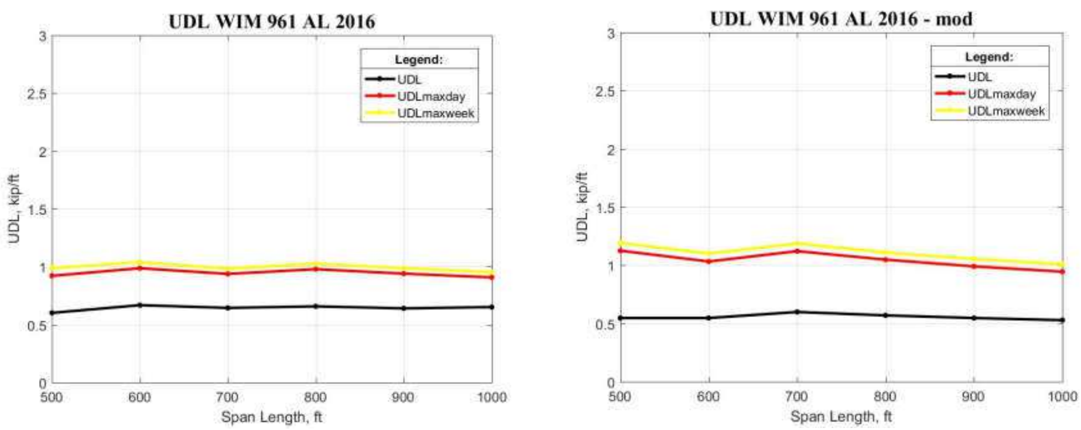

Figure 3.20: Equivalent Uniformly Distributed Load for different span lengths 961 WIM for year 2016.
Regular filtering – left, moderate filtering – right.

The arch bridge considered in this study has span 800-ft long. A detailed summary of Uniformly Distributed Load (UDL) for this structure is presented in the Table 3.7.

Table 3.7: Mean value of UDL for 800-ft long span.

	Mean value of UDL (kip/ft)	
Year	Regular Filtering	Moderate Filtering
2014	0.69 kip/ft	0.53 kip/ft
2015	0.64 kip/ft	0.53 kip/ft
2016	0.66 kip/ft	0.53 kip/ft

CHAPTER 4 DEVELOPMENT OF RESISTANCE MODEL

4.1. Interaction of Axial force – Bending Moment

The structural behavior of the arch ribs of the considered bridge can be idealized by the beam-column element. Both compressive axial force and bending moment (or moments) have significant influence on the performance of the structure. The most prevalent, effective way for designing or checking the capacity of these kinds of elements are application of interaction equations. The general form of the axial force – bending moment interaction equation is given by the Equation (4.1).

$$\frac{P_u}{P_n} + \frac{M_u}{M_n} \leq 1.0 \tag{4.1}$$

where P_u and M_u are maximum compressive force and bending moment, including amplification due to second order effects, P_n and M_n are axial and bending moment resistances, respectively.

In the current version of Specification for Structural Steel Buildings (2014) the interaction between axial force and bending moment is normalized and includes length effects. The equations are as follows:

$$\frac{P_u}{P_n} + \frac{8M_u}{9M_n} = 1.0 \quad for \quad \frac{P_u}{P_n} \geq 0.2 \tag{4.2}$$

$$\frac{P_u}{2P_n} + \frac{M_u}{M_n} = 1.0 \quad for \quad \frac{P_u}{P_n} < 0.2 \tag{4.3}$$

The graphical representation of interaction Equations (4.2) and (4.3) is presented in the Figure 4.1.

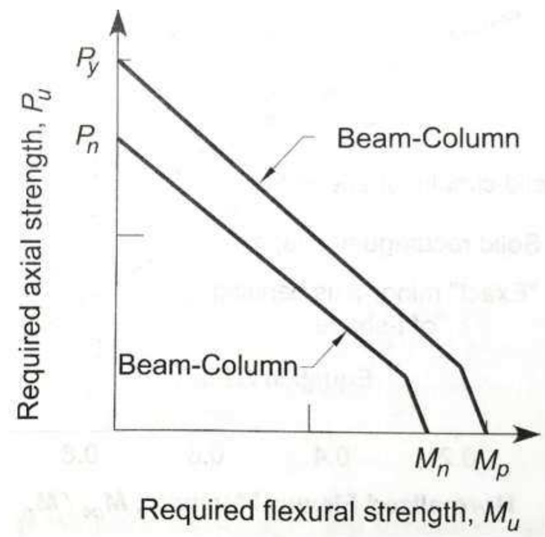

Figure 4.1: Interaction curve for beam-column (AISC Manual, 14th Edition).

4.1.1. Design according to AASHTO Standard Specifications.

For AASHTO Standard Spec., the structural elements with combined axial load and bending moment shall satisfy the following equations:

$$\frac{P}{0.85A_sF_{cr}} + \frac{MC}{M_u\left(1 - \frac{P}{A_sF_e}\right)} \leq 1.0 \tag{4.4}$$

$$\frac{P}{0.85A_sF_y} + \frac{M}{M_p} \leq 1.0 \tag{4.5}$$

where:

P = axial compression in the member

M = maximum bending moment

C = equivalent moment factor

A_s = area of the steel section

F_y = specified minimum yield point of steel

F_{cr} = buckling stress

M_u = maximum strength

F_e = the Euler Buckling stress in the plane of bending

M_p = full plastic moment of the section.

The Equations (4.4) and (4.5) were slightly modified by adding the second component, bending moment – bending about weak axis (out of plane of the arch). Using these equations and values obtained from analyses in the Midas Civil software (Chapter 5), four segments of the arch in the considered bridge were examined and their structural capacity was checked. The results of the calculations for load configurations maximizing compressive force in each segment of the arch are presented in the Figure 4.2. The results of the calculations for load configurations maximizing major bending moment in each segment of the arch are presented in the Figure 4.3.

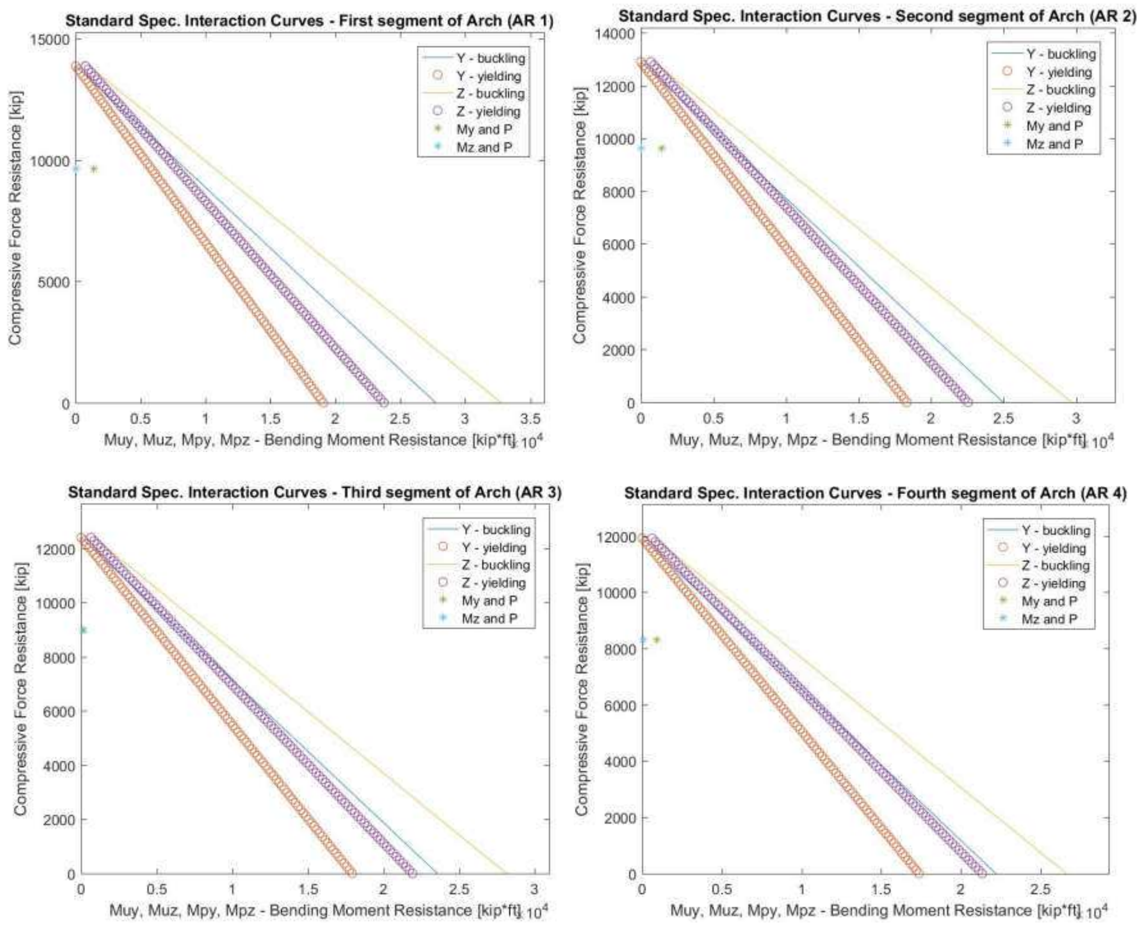

Figure 4.2: Interaction curves for beam-column according to AASHTO Standard Spec. procedure (maximum compressive force).

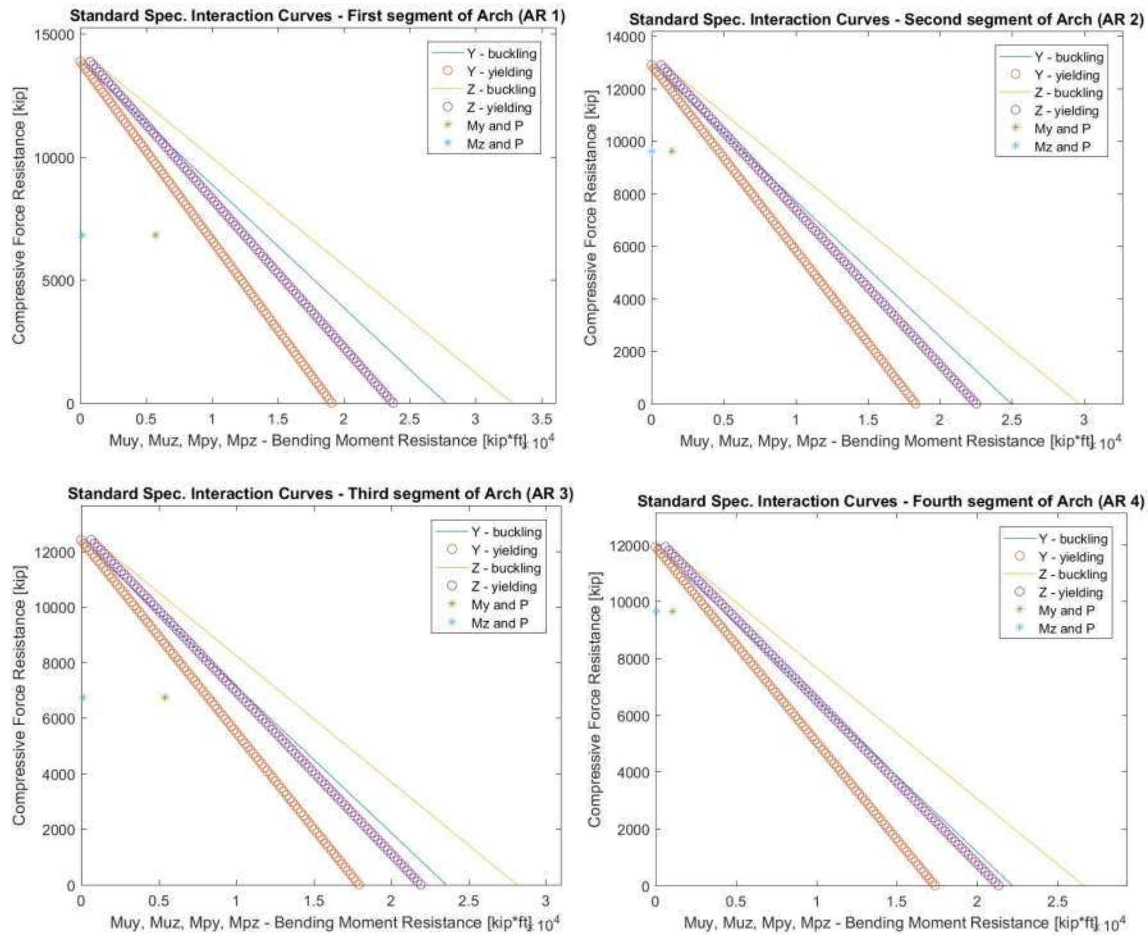

Figure 4.3: Interaction curves for beam-column according to AASHTO Standard Spec. procedure (maximum major bending moment).

Any point (representing a combination of compressive force and bending moment) inside the area limited by the interaction equation boundaries given by AASHTO Standard Spec. means that this combination of the load does not exceed the capacity of the component. The results shown in the Figure 4.2 and Figure 4.3 confirmed that all four segments of the arch rib met that requirement indicating, in accordance with this design code, they are safe.

4.1.2. Design according to AASHTO LRFD.

For AASHTO LRFD, similarly as in the AISC Manual, the structural elements with combined axial load and bending moment shall satisfy the following equations:

$$\frac{P_u}{P_r}+\frac{8}{9}\left(\frac{M_{ux}}{M_{rx}}+\frac{M_{uy}}{M_{ry}}\right)\leq 1.0 \quad for \quad \frac{P_u}{P_r}\geq 0.2 \tag{4.6}$$

$$\frac{P_u}{2P_r}+\left(\frac{M_{ux}}{M_{rx}}+\frac{M_{uy}}{M_{ry}}\right)\leq 1.0 \quad for \quad \frac{P_u}{P_n}< 0.2 \tag{4.7}$$

where:

P_r= factored compressive resistance

M_{rx}= factored flexural resistance about the x-axis taken equal to ϕ_f times the nominal flexural resistance about the x-axis

M_{ry}= factored flexural resistance about the y-axis taken equal to ϕ_f times the nominal flexural resistance about the y-axis

M_{ux}= factored flexural moment about the x-axis

M_{uy}= factored flexural moment about the y-axis

Using the equations presented above and values obtained from analyses in the Midas Civil software (Chapter 5), four segments of the arch in the considered bridge were examined and their structural capacity checked. The results of the calculations for load configurations maximizing compressive force in each segment of the arch are presented in the Figure 4.4. The results of the calculations for load configurations maximizing the major bending moment in each segment of the arch are presented in the Figure 4.5.

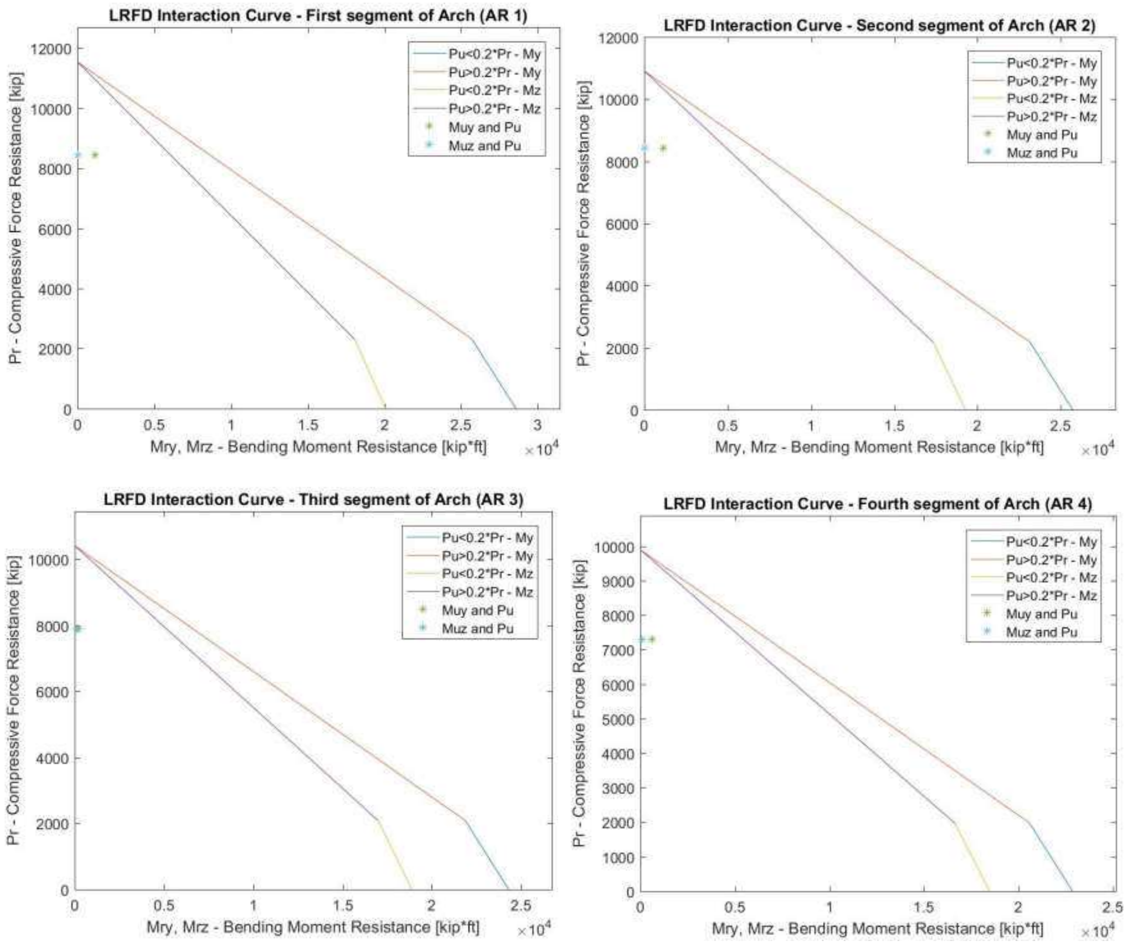

Figure 4.4: Interaction curves for beam-column according to AASHTO LRFD procedure (maximum compressive force).

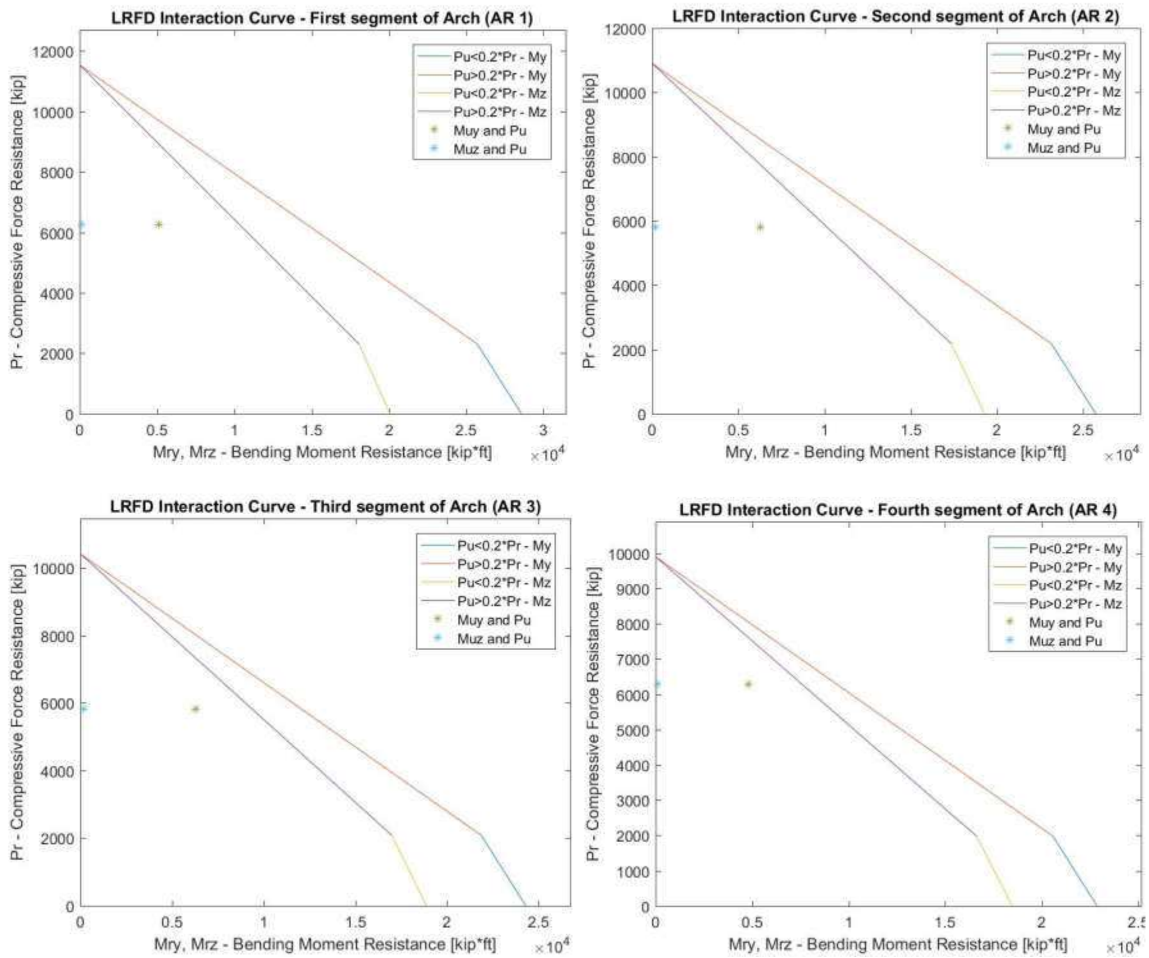

Figure 4.5: Interaction curves for beam-column according to AASHTO LRFD procedure (maximum major bending moment).

Any point (representing a combination of compressive force and bending moment) inside the area limited by the interaction equation boundaries given by AASHTO LRFD means that this combination of the load does not exceed the bearing capacity of the component. The results shown in the Figure 4.4 and Figure 4.5 confirmed that all four segments of the arch rib met that requirement indicating, in accordance with this design code, they are safe.

CHAPTER 5 FINITE ELEMENT MODEL OF THE CONSIDERED BRIDGE

5.1. INTRODUCTION

The General W.K. Wilson Jr. Bridge (Figure 5.1) was chosen as the case study structure for this study. The structure consists of dual parallel tied through arches. Because of its complexity, it reflects the specialized technological advances in design, materials and construction that evolved over the years. The author of this dissertation was granted access to the documentation of the bridge (I-65 over Mobile River Bridge Inspection Manual), which was a sufficient source of information to create the Finite Element model.

Figure 5.1: Overview of the General W.K. Wilson Jr. Bridge (https://www.youtube.com/watch?v=LjtkE5WLjys).

5.2. DESCRIPTION OF THE BRIDGE

The twin tied arch bridges carry I-65 across the Mobile River Delta above Mobile, AL in Baldwin and Mobile Counties as separate northbound and southbound structures. The HNTB Company designed these structures for the Alabama Highway Department (now Alabama Department of Transportation – ALDOT) in 1976. They were let to contract in February 1977 and construction was completed in December 1980. The entire project opened to traffic in October 1981.

Since opening these spans to traffic they appeared to perform in a satisfactory manner. The first and only major overhaul began in February 2015, lasted around a year and costed \$14.1 million. Main tasks were to replace deck's joints and improve drainage systems to keep water off the critical structural members. Additionally, cracks of concrete and steel components were repaired. According to National Bridge Inventory Data (2018), the actual sufficiency rating for this bridge is 80%.

The two spans are on tangent alignment, both are identical and symmetrical about the centerline of bridge and centerline of span; except for the reversal and cross slope, and related vertical dimensions from northbound to southbound roadways. The overview of the bridge from original drawings is shown in the Figure 5.2 and Figure 5.3. The listing of main dimensions obtained from the design plans is presented in Table 5.1. All this information and description of the particular components of the bridge were found in the "I-65 over Mobile River Bridge Inspection Manual".

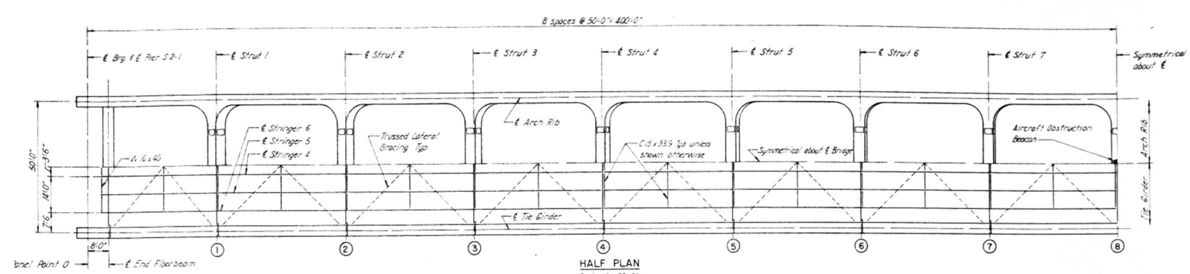

Figure 5.2: Original drawing – Half plan of the bridge (I-65 over Mobile River Bridge Inspection Manual).

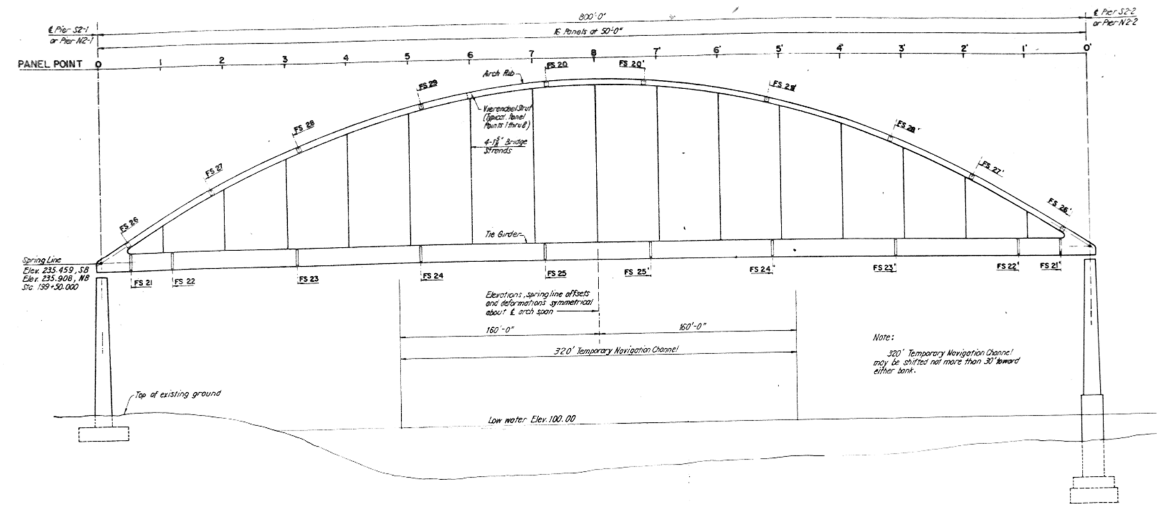

Figure 5.3: Original drawing – Arch elevation (I-65 over Mobile River Bridge Inspection Manual).

Table 5.1: General dimensions of the bridge.

Item	Length
Roadway width, face to face of concrete barrier	39'-3"
Span length, 16 panels @ 50'-0"	800'-0"
Horizontal distance center to center of ribs and tie girders	50'-0"
Stringer spacing, 5 spaces @ 7'-0"	35'-0"
Vertical distance centerline of rib to centerline of tie girder @ midspan, Panel 8, under full Dead Load	133'-8-3/16"
Vertical clearance above high water	125'-0"
Center to center of bridges	178'-9"

The structure was designed in accordance with the Standard Specification for Higway Bridges adopted by the American Association of State Highway and Transportation Officials (Eleventh Edition 1973), as amended by the Interim Specifications for 1974 and 1975. Working stress design method was used. The live load was HS-20-44 and alternate military loading.

Construction was performed in accordance with the Standard Specifications for Highway Construction of the State of Alabama Highway Department 1976 Edition, the special Provisions and the American Welding Society Structural Welding Code. The listing of materials used for different components of the bridge is presented in the Table 5.2.

Table 5.2: Material of different components of the bridge.

Component	Material
Steel structural elements	ASTM A-588 weathering steel
Superstructure concrete	Class E
Cables	Galvanized multiple wire bridge strand
Cable Anchorages	Galvanized alloy steel casting A148 grade 80-50 and galvanized 1” diameter bolts
Bolts	7/8”, 1” and 1-1/8” diameter A325 bolts

<u>Concrete deck</u>

The concrete deck slab is 6-1/2” thick between the stringer supports and is 8” thick where it rests on the stringers. The clear cover of the top reinforcing steel is 1-3/4” and the clear cover of the bottom reinforcing steel is 1”. The design of the slab did not include assumption about the integral wearing surface, but did include provisions for the addition of a future wearing surface with a weight of 15 pounds per square foot. Galvanized steel corrugated stay-in-place forms were used between stringers. The design strength of the concrete is 4,500 psi which has an allowable compressive stress of 1,800 psi. The reinforcing steel used in the deck slab is Grade 60, which has an allowable tensile stress of 24 ksi.

The essential function of the bridge deck is to provide a riding surface for traffic and to transmit wheel loads to the underlying supporting members. The bridge deck is subjected to the wearing action of the traffic, the deterioration caused by weather and chemical actions and corrosion of rebars.

Expansion joints are equipped on the arch spans at both ends to permit the bridge superstructure to expand and contract as the temperature varies. They are steel tooth (finger) type joints that has a gap of 6” when the steel has reached a temperature of 70 degrees Fahrenheit. These joints are fabricated from A-588 steel plates and are bolted to the upper flange of the steel stringers and transverse diaphragms.

Three intermediate transverse joints are provided in the deck at 200 foot intervals to prevent the deck slab from contributing to the stresses in steel arches. They are the common diaphragm type neoprene seal that provide a gap. The width of the gap is not directly related with the function of the change in steel temperature.

Vehicles induce large forces in the expansion joints while passing them. These forces usually cause cracks in the welds, damage joint material and also may detach the expansion joint from its supporting structure.

Stringers

Stringers are the structural steel components extending in the longitudinal direction of the bridge which support the concrete deck slab. Six stringers, spaced at seven foot centers, spanning approximately fifty feet between floorbeams, have been arranged under the deck slab of each structure. The stringers are rolled steel W30x99 I-beams.

Floorbeams

Floorbeams are the structural steel elements below the deck, transverse to the bridge. Intermediate trussed floorbeams are members fabricated from angles and rolled beam sections (top chords). The end floorbeams are fabricated from solid plates with the top flange being in the shape of a box.

Trussed Lateral Bracing

Lateral bracing is a system of trusses installed below the deck which extend diagonally between the panel points of the tie girders. The trussed lateral braces are elements consisting of rolled structural steel "T" shapes and plates. Their bracing members are bolted to gusset plates at the intersections of the floorbeams and tie girders.

Tie Girders

The tie girders are the structural steel elements extending between the spring lines of the arches, and due to lack of redundancy, are considered to be one of the most critical components of the superstructure. The tie girders are hollow box shaped members composed of welded steel plates, transverse and longitudinal stiffeners, diaphragms and are 4 feet wide by 14 feet deep. Access doors are provided near the ends of the tie girders which permit entry into the interior of the boxes.

Arch Ribs

The arch ribs are welded, structural steel components in the shape of a box that are four feet wide and five feet deep. Access to the interior of the arch ribs is provided through the hatches at each end of the tie girders and in the top of the upper strut at the peak of the arch.

Vierendeel Struts

The Vierendeel struts are the structural steel elements extending laterally between the arch ribs. The Vierendeel struts are hollow box shaped members composed of welded steel plates and are five feet deep and four feet wide. The struts are flared in width at their juncture with arch ribs. Access to the inside of Vierendeel struts is available from the interior of the arch ribs or from access holes in the top flange of the struts.

Cable Hangers

The galvanized cable hangers are made up of four 1-5/8” diameter multiple wire bridge strands. Each hanger strand has a minimum breaking strength of 155 tons when subjected to a direct tensile load. The cable hangers are provided at fifteen locations (every 50 feet) along each of the tied arches.

The typical section of the bridge is presented in the Figure 5.4.

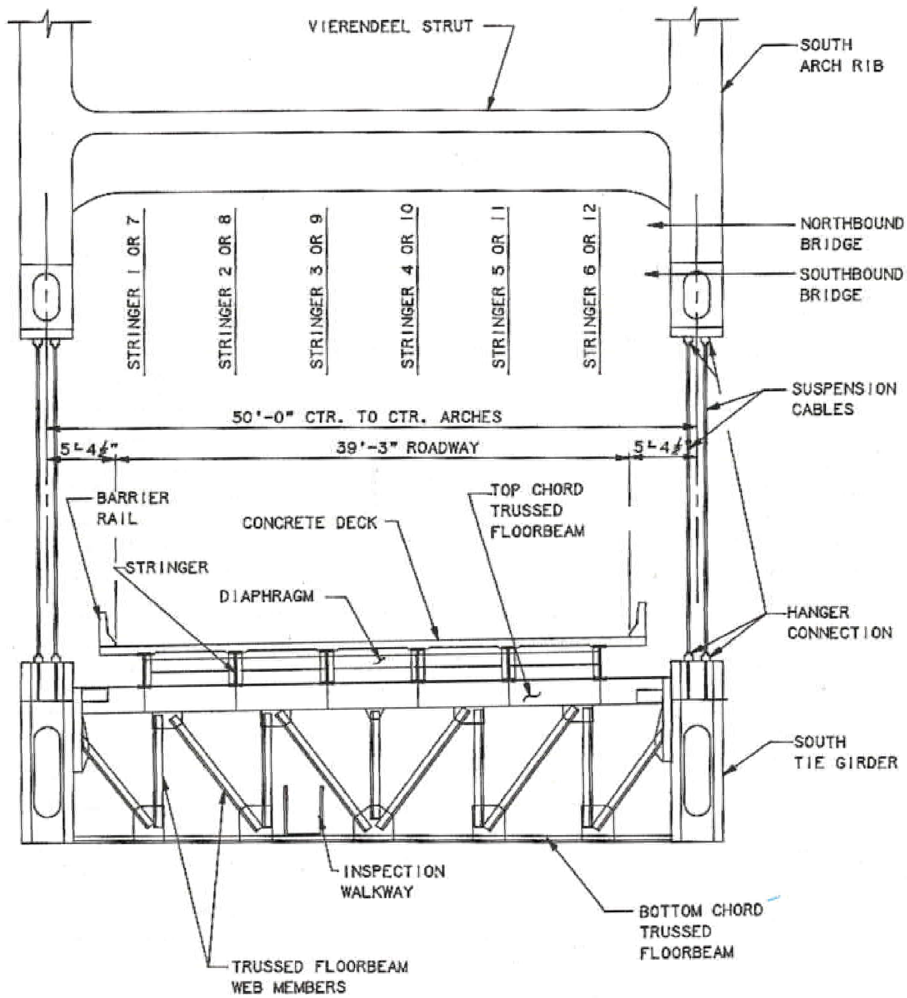

Figure 5.4: Typical section at trussed floorbeam
(I-65 over Mobile River Bridge Inspection Manual).

5.3. FINITE ELEMENT MODELING APPROACH

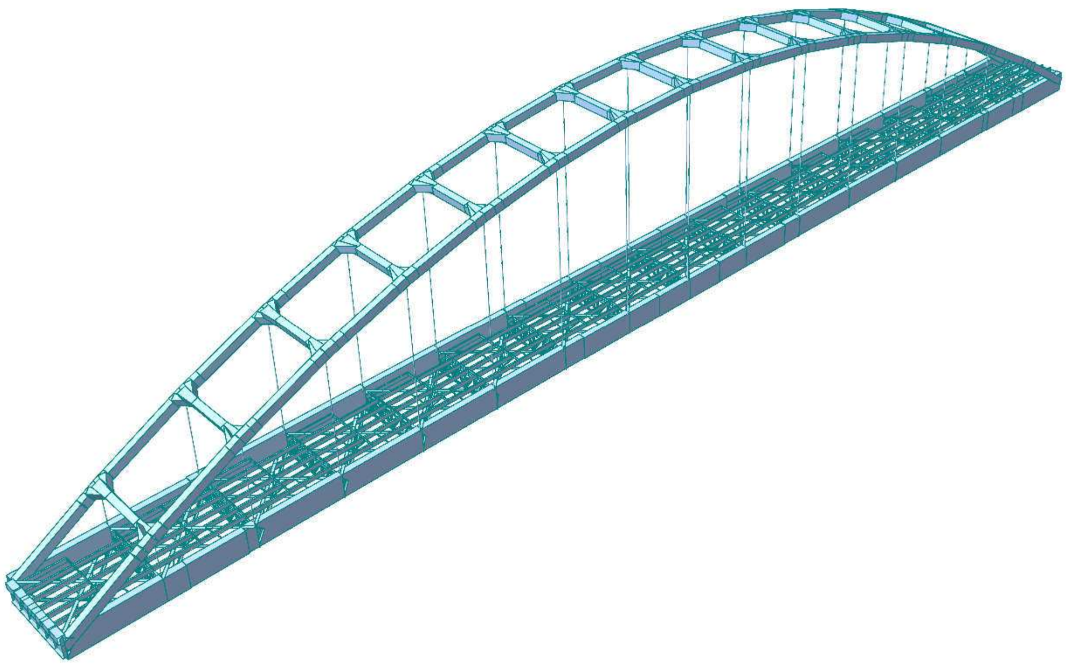

Figure 5.5: Overview of the Finite Element Model of the considered bridge.

5.3.1. Midas Civil software

For the purpose of creating the Finite Element Model of the considered bridge (Figure 5.5), Midas Civil software was utilized. It has a very user-friendly interface, optimal design solution functions and extremely efficient pre- and post-processor. Modeling in Midas Civil is intuitive and the software provides a variety of different analysis options (1st order, 2nd order, buckling, eigenvalue, staged construction and others).

5.3.2. Models of the structural components

Materials

All steel elements are modeled with ASTM A588-50 Steel. Mechanical properties given by the software are shown in the Figure 5.6. Material model for concrete is not used. Loads from the deck were calculated and distributed along the stringers and applied as line load.

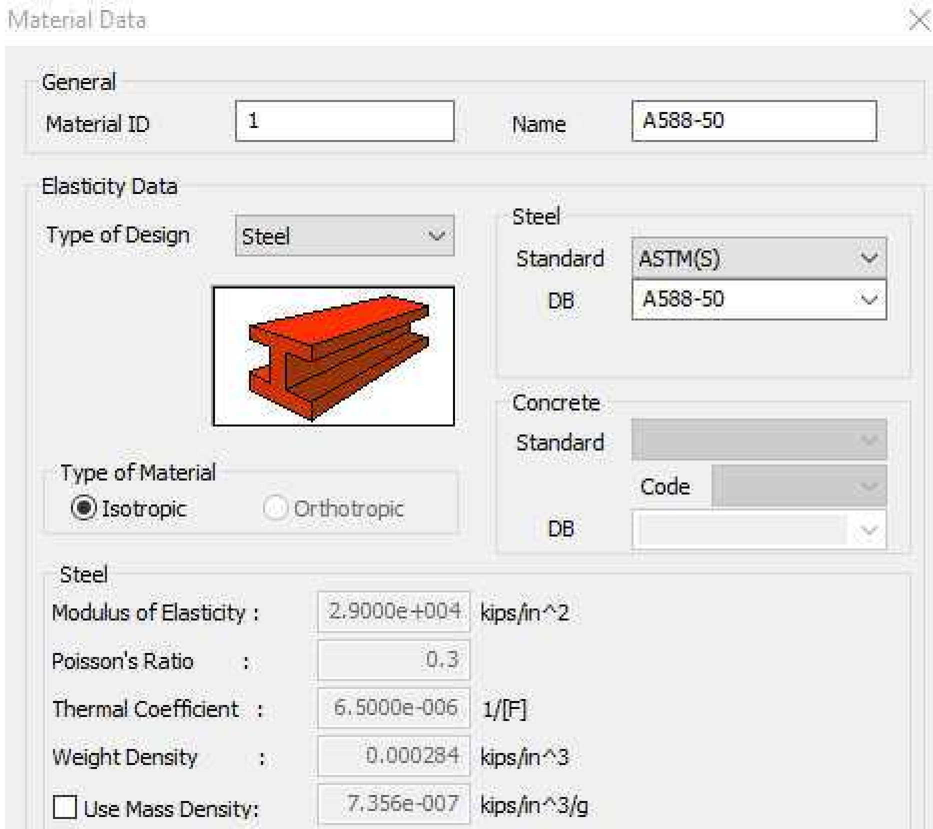

Figure 5.6: Material parameters – ASTM A588-50 Steel.

Cross sections

The cross sections of the arch ribs, tie girders and Vierendeel struts are built-up steel boxes. There are four types of arch ribs and three types of tie girders. Main dimensions are the same; the only difference is the thickness of the flanges. The cross sections for the arches and tie girders along with their locations are presented in the Table 5.3 and Table 5.4.

Vierendeel struts are modeled with built-up 4x5 feet steel box cross sections. Their geometry is simplified – in actuality there is a radial connection between struts and arch ribs. In the model it is represented by additional skew elements on both sides of the strut.

Table 5.3: Cross sections for different segments of Arch Ribs.

Location of the element with given cross section	Cross section description:
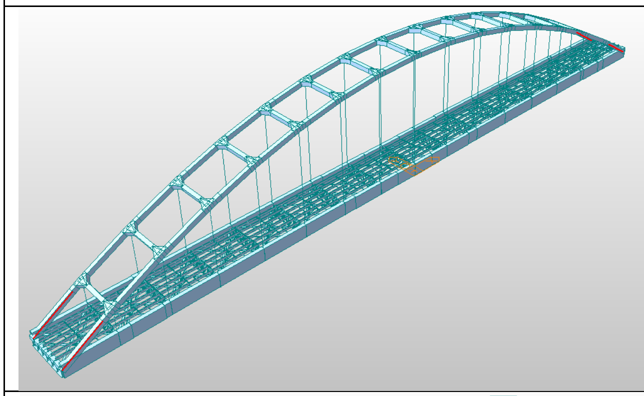	Built-up steel box. Height: 58” Width: 48” Webs thickness: 1.25” Flanges thickness: 2” Name of this segment of arch: **AR 1**
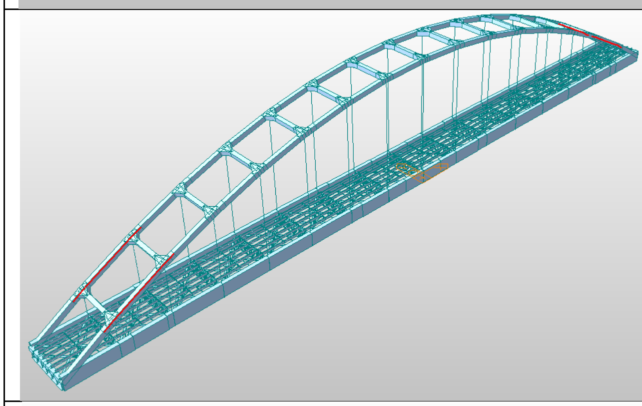	Built-up steel box. Height: 58” Width: 48” Webs thickness: 1.25” Flanges thickness: 1.75” Name of this segment of arch: **AR 2**
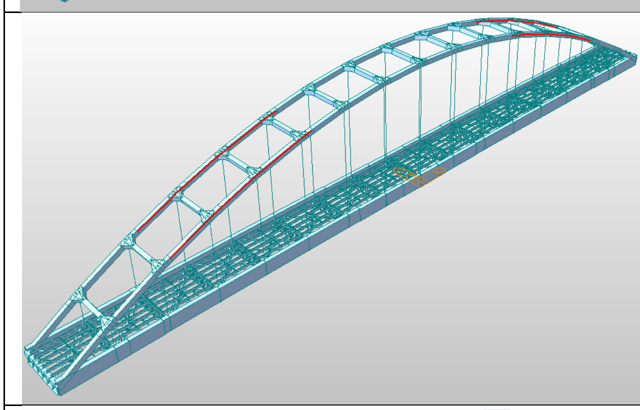	Built-up steel box. Height: 58” Width: 48” Webs thickness: 1.25” Flanges thickness: 1.625” Name of this segment of arch: **AR 3**
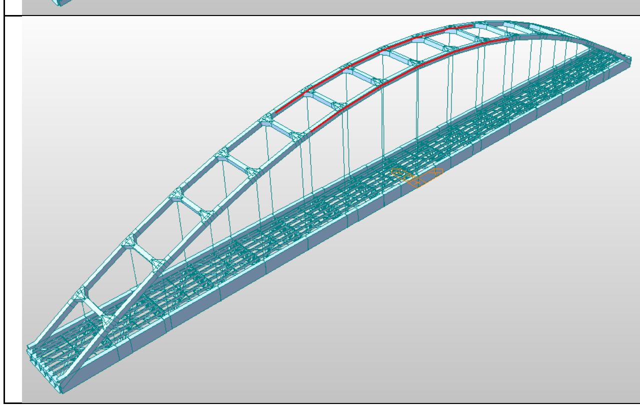	Built-up steel box. Height: 58” Width: 48” Webs thickness: 1.25” Flanges thickness: 1.5” Name of this segment of arch: **AR 4**

Table 5.4: Cross sections for different segments of Tie Girders.

Location of the element with given cross section	Cross section description:
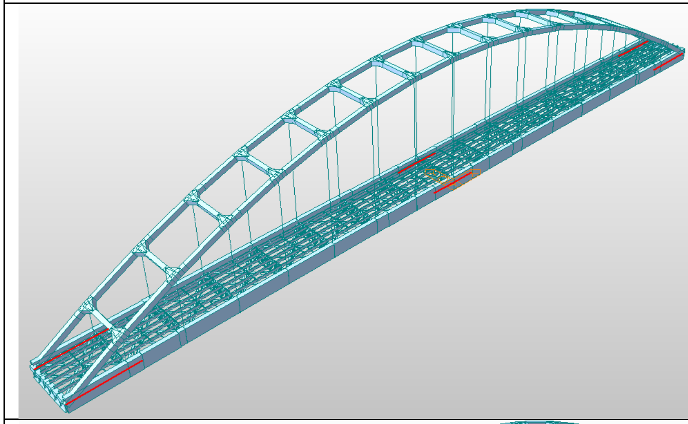	Built-up steel box. Height: 168” Width: 48” Webs thickness: 0.5” Top flange thickness: 1” Bottom flange thickness: 1”
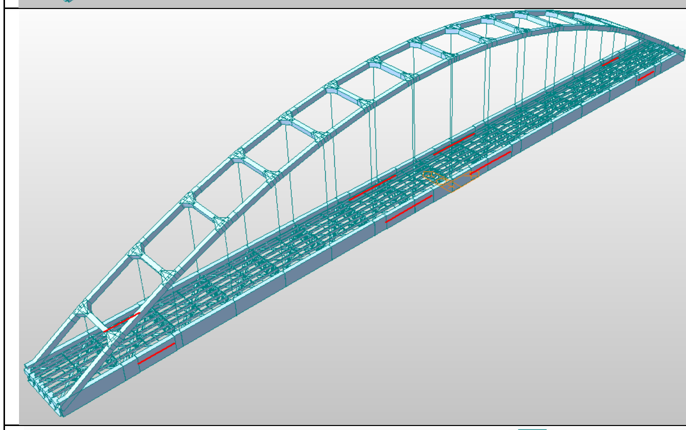	Built-up steel box. Height: 168” Width: 48” Webs thickness: 0.5” Top flange thickness: 1.25” Bottom flange thickness: 1”
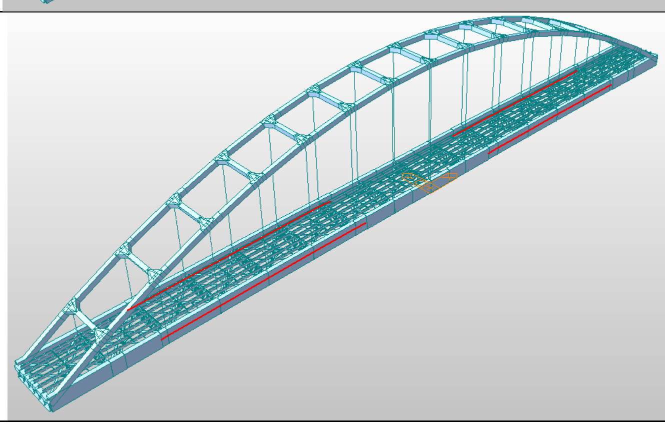	Built-up steel box. Height: 168” Width: 48” Webs thickness: 0.5” Top flange thickness: 1.75” Bottom flange thickness: 1”

Stringers are modeled with regular W30x99 I-beams, for diaphragms between them and C15-33.9 are used. For top chords of trussed floorbeams two types of cross sections are defined. For locations with extension joints, WT18x67.5 + MC18x42.7 combined shape is installed on the bridge, but due to the lack of WT18x67.5 shape in the software’s library, W18x78 was used. This cross section together with MC18x42.7 has similar geometric properties as WT18x67.5 + MC18x42.7. For other top chords of intermediate trussed floorbeams, W24x100 is installed on the bridge and defined in the software. End floorbeams consist of stiffened solid plates with a box-shaped top chord. For diagonals and bottom chords of trussed floor beams, and for elements of trussed lateral bracings, double angles and T-shapes are used. Cable hangers installed on the bridge are four 1-5/8" diameter multiple wire bridge strands per location. In the Finite Element Model, they are defined as one, 2.85" diameter circular solid element (it has the same area as four 1-5/8" strands). Details of the selected elements are presented in the Figure 5.7, Figure 5.8 and Figure 5.9.

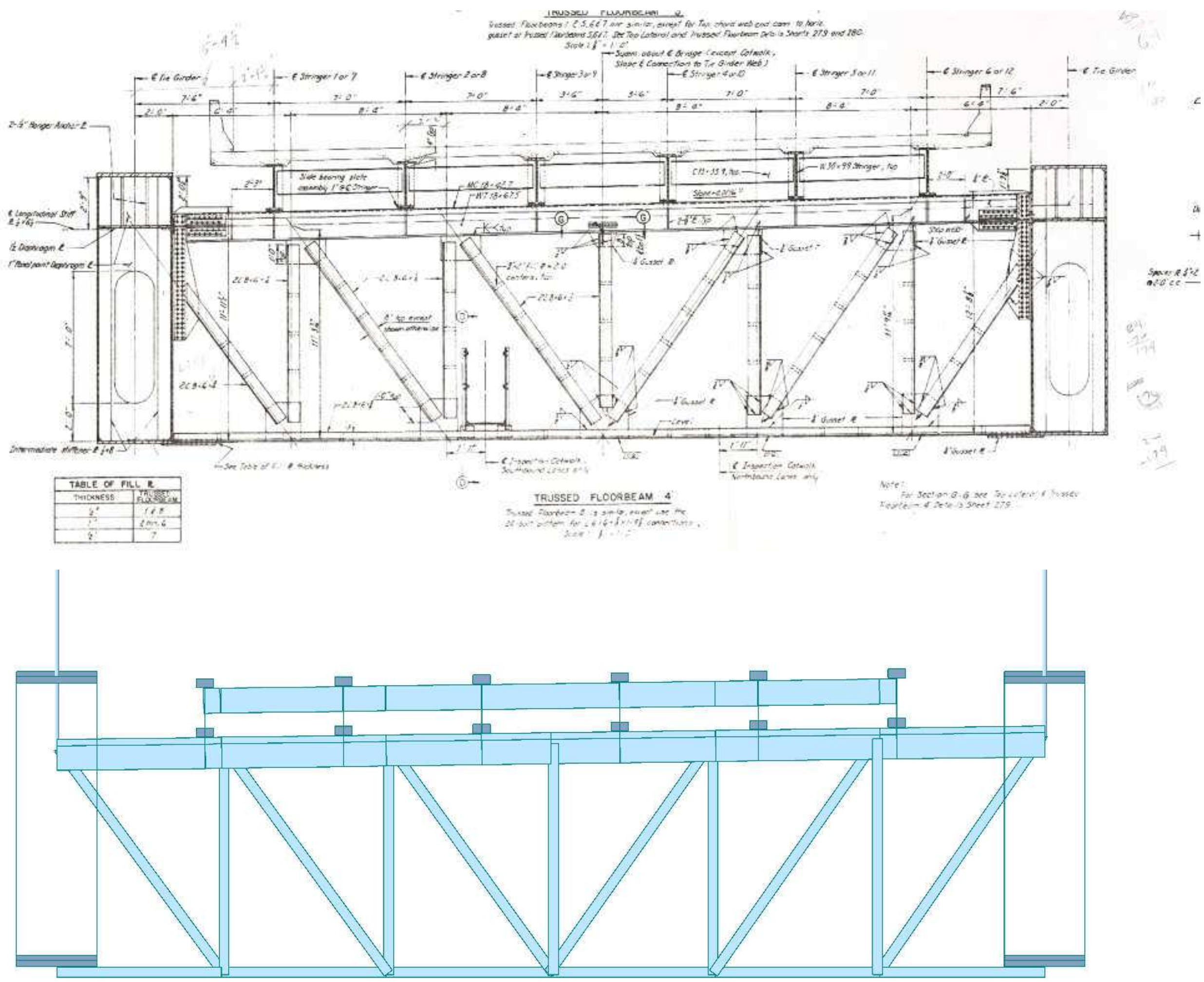

Figure 5.7: Typical cross section of the bridge (I-65 over Mobile River Bridge Inspection Manual – top, from Midas Civil model - bottom).

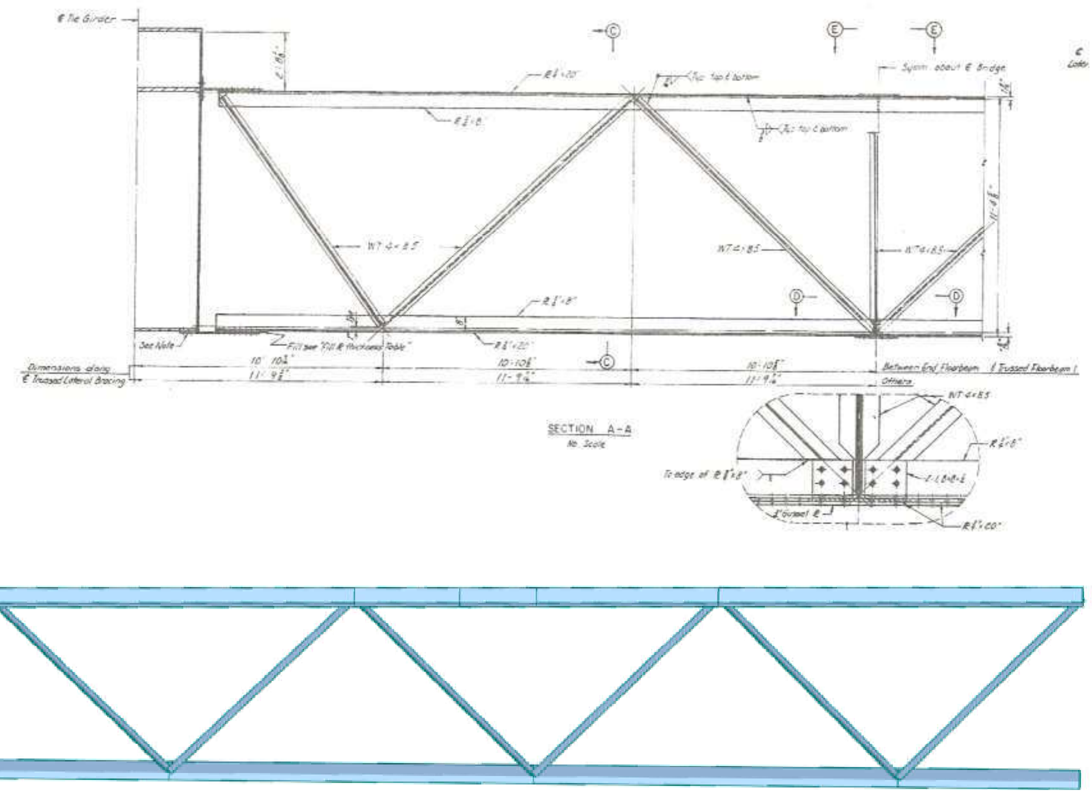

Figure 5.8: Trussed lateral bracing of the bridge (I-65 over Mobile River Bridge Inspection Manual – top, from Midas Civil model - bottom).

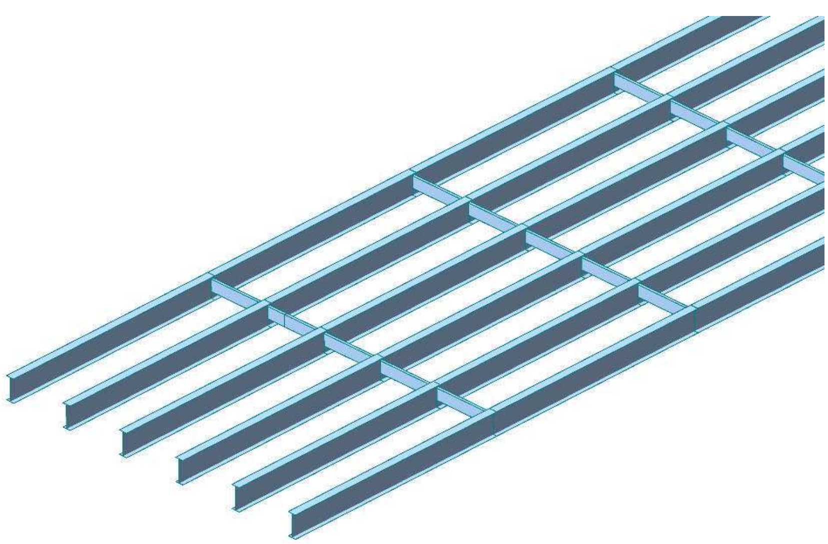

Figure 5.9: Stringers with diaphragms (Midas Civil model).

Types of elements

Three types of elements are used to model components of the structure – beam, truss and tension-only elements.

Beam Elements

Beam elements have six degrees of freedom per node. They are reflecting axial, shear, bending and torsional stiffness. According to Midas Civil User Manual, Timoshenko beam theory is used to formulate beam elements. It assumes that the plane section is initially normal to the neutral axis of the beam remains plane but is not necessarily normal to the neutral axis in the deformed state. This allows for the inclusion of shear deformations. In the software, beam and truss elements are idealized line elements, so their cross-sections are assumed to be dimensionless. This means that the cross-sectional properties of an element are concentrated at the neutral axis that connects the end nodes. This assumption leads to the fact that the effects of panel zones between members and the effects of non-alignment of neutral axes are not considered. To address this issue with nodal effects, the beam end offset option or geometric constraints are used. The tapered section is used when the section of a member is non-prismatic (in the considered bridge for end floorbeams). To model pin end connection, Beam End Releases are used.

Beam elements are used to model most of the components of the bridge. They are: arches, tie girders, stringers (including diaphragms between them), Vierendeel struts, top and bottom chords of the trussed floorbeams and truss lateral bracings.

Truss Elements

To model diagonal elements of the trussed floorbeams and truss lateral bracings (they are mostly steel angles) Truss Elements were used. The sign convention of internal forces is presented in Figure 5.10.

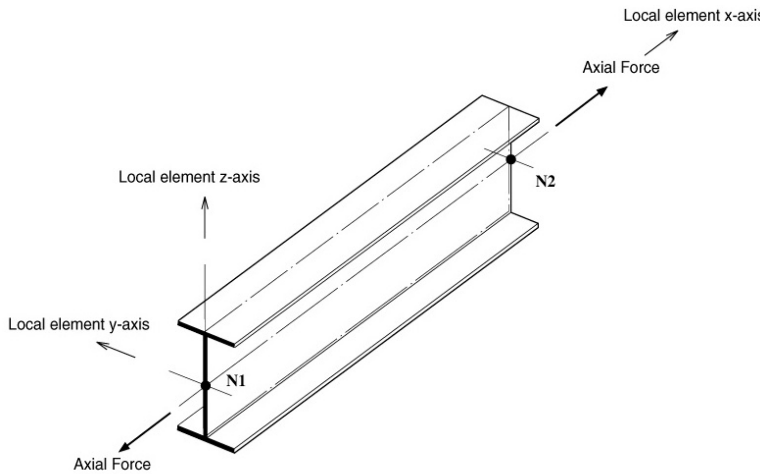

Figure 5.10: Sign convention of internal forces in the truss element's local coordinate system (Midas Civil User Manual).

Tension-only Truss Elements

Tension-only Truss Elements are used to model cables in the considered structure. For tension-only elements, the allowable compression is assumed as zero. The tension limit is generally checked off. When it is checked on, the element no longer resists forces exceeding the specified value of tension limit, so the excess forces are transferred to the neighboring elements.

5.3.3. Boundary conditions

There are bearings at each end of the arch span designed to prevent transverse and longitudinal movement of the superstructure. The bearings under the east end of the arch spans include a nest of six cylindrical rollers which were provided to permit proper positioning of the bearings after all the dead loads had been placed upon the structure. After those bearings were in proper position, the roller guide bars were welded in place and the voids between the rollers were filled with portland cement grout. Each bearing is attached both to the arch rib and to the pier with six 2-1/4” diameter bolts. To represent this connection in the Finite Element Model, pin connection is assumed for one end of the structure and roller for another. This is presented in the Figure 5.11.

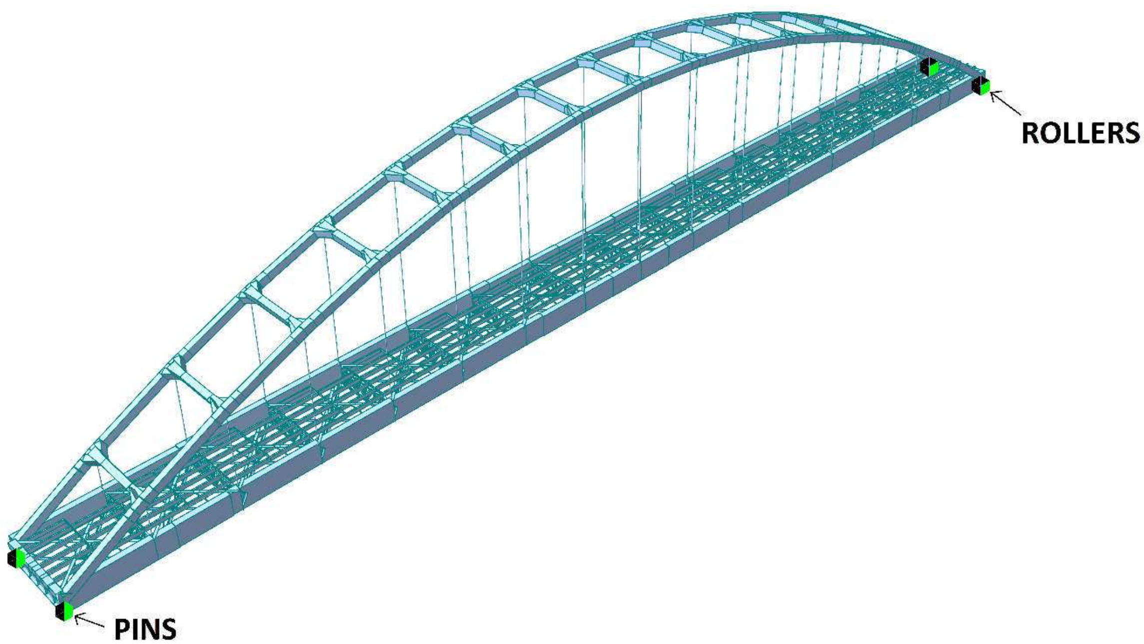

Figure 5.11: Boundary conditions.

Releases and Rigid Links

To achieve proper behavior of the structure, releases are applied to certain components of the bridge. For stringers, at the ends and quarter points of the length of the span, the bending moments are released. These are the locations of expansion joints and supports. For bottom chords of the trussed floorbeams, hinges are applied to represent the connection between them and tie girders. Releases are presented in the Figure 5.12.

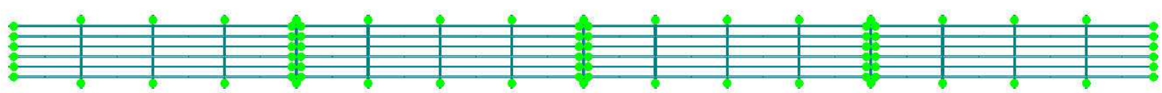

Figure 5.12: Moment releases applied to the structure.

For real structure, the concrete deck provides continuous bracing for the top flange of the stringers. To imitate this function, rigid links are used at quarter points of the span length. They virtually connect nodes at these locations and this is close to their real behavior. Rigid links are presented in the Figure 5.13.

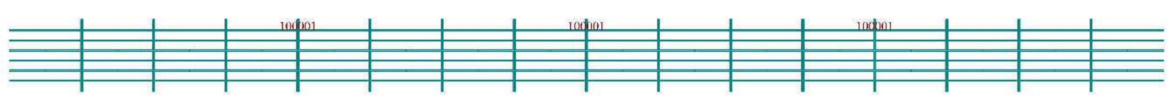

Figure 5.13: Rigid links applied to the structure.

5.3.4. Load for the considered structure

There are three main components of the load applied to the structure: Dead Load of Steel (DLS), Dead Load of Concrete (DLC) and traffic Live Load (LL). DLS is automatically applied to the structure due to defined material properties. DLC is calculated as total load of concrete distributed along the stringers as line load (Figure 5.14).

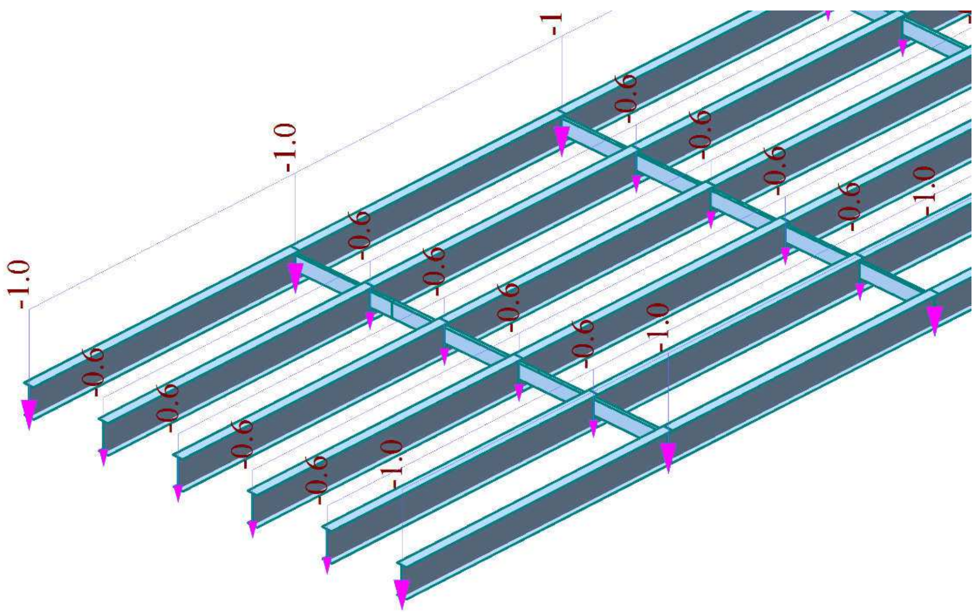

Figure 5.14: Concrete deck loads (DLC) applied to the stringers (kip/ft).

For Live Load, three separate situations are considered: Live Load case according to AASHTO Standard Specifications for Highway Bridges, Live Load case according to AASHTO LRFD Bridge Design Specifications and Live Load case created using collected and processed Weigh-In-Motion Data from the station located 4 miles from the bridge, on the same I-65 highway.

Live Load according to AASHTO Standard Specifications for Highway Bridges

The applied live load according to AASHTO Standard Specifications consists of design truck and lane load. The design truck is a tri-axle vehicle HS20-44. It has a gross vehicle weight of 72 kip and spacing between axles as presented in the Figure 5.15. In addition to the design truck live load case, alternate military load case is applied (2x24 kip spaced at 4 feet).

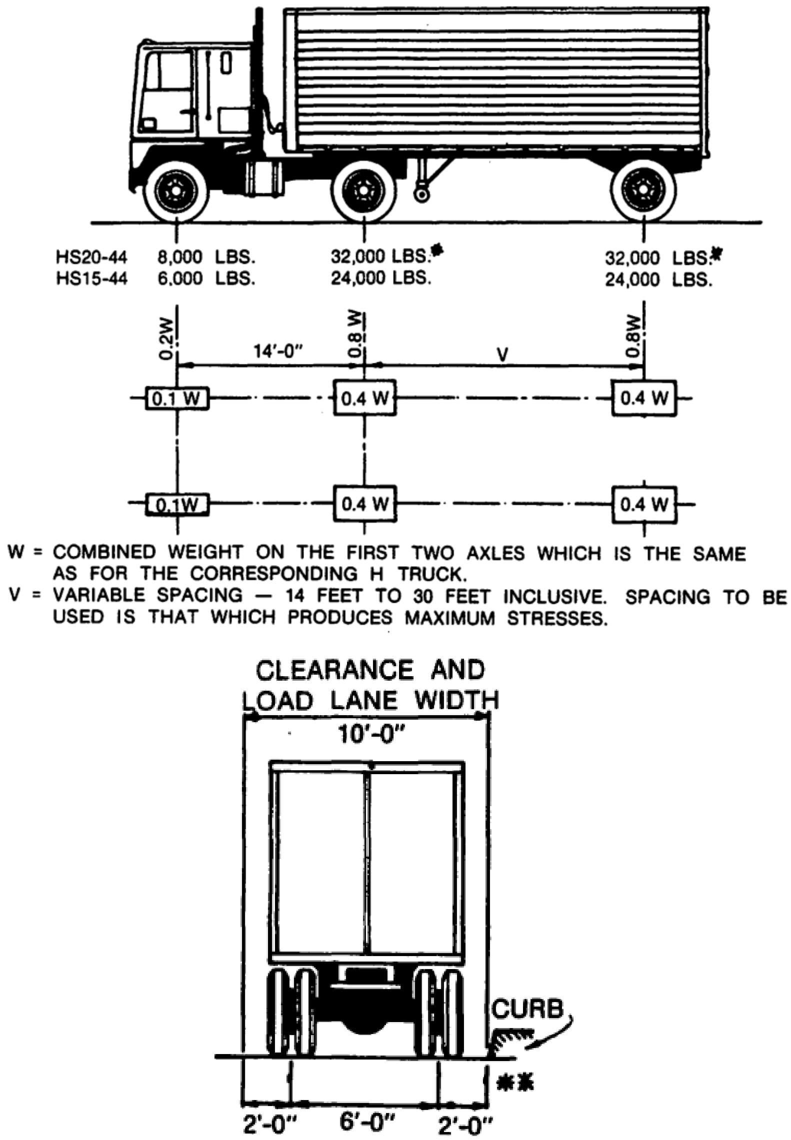

Figure 5.15: HS20-44 design truck (AASHTO Standard Spec).

For long spans, usually the most critical live load configuration is represented by uniform load. In FEM, live load case with 0.64 kip/ft uniformly distributed over a 10-ft width lane load is considered plus two types of trailing point loads (18 kip and 26 kip) are considered (Figure 5.16).

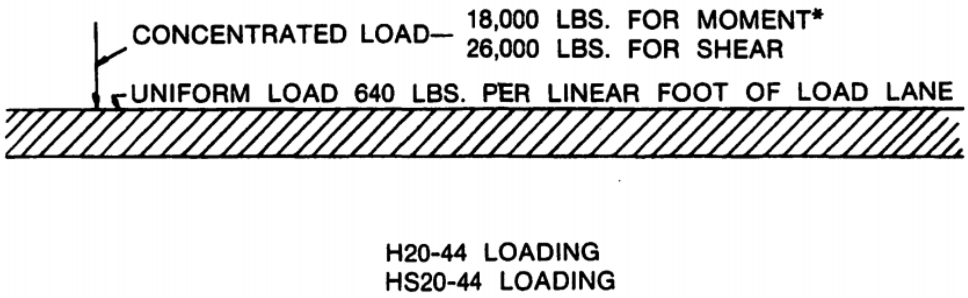

Figure 5.16: HS20-44 Lane loading (AASHTO Standard Spec).

The AASHTO Standard Spec. provides the formula to calculate the impact of the live load. This is expressed as a fraction of the live load stress and is determined by the following Equation (5.1):

$$I = \frac{50}{L - 125} \tag{5.1}$$

where:

I = impact fraction (maximum 30 percent)

L = span length.

For the considered bridge with span length of 800 ft, the impact (I) is calculated as 5.4%.

For the situations with more than one lane loaded simultaneously, there is reduction of load intensity specified in the code. The reason for using them is the improbability of coincident maximum loading. Values for different numbers of loaded lanes are presented in Table 5.5.

Table 5.5: AASHTO Standard Spec. reduction of load intensity.

Number of loaded lanes	Percent of the load
One or two lanes	100
Three lanes	90
Four lanes or more	75

Live Load according to AASHTO LRFD Bridge Design Specifications.

The vehicular live loading on the roadways of bridges or incidental structures according to AASHTO LRFD Bridge Design Specifications is called HL-93 and consists of the combination of design truck or design tandem, and design lane load. The design truck is a tri-axle vehicle with gross vehicle weight of 72 kip and spacing between axles as presented in the Figure 5.17. Moreover, alternate military load case is applied (2x25 kip spaced at 4 feet). In addition to design truck, in the FEM model, live load case with 0.64 kip/ft uniformly distributed over a 10-ft width lane load is considered.

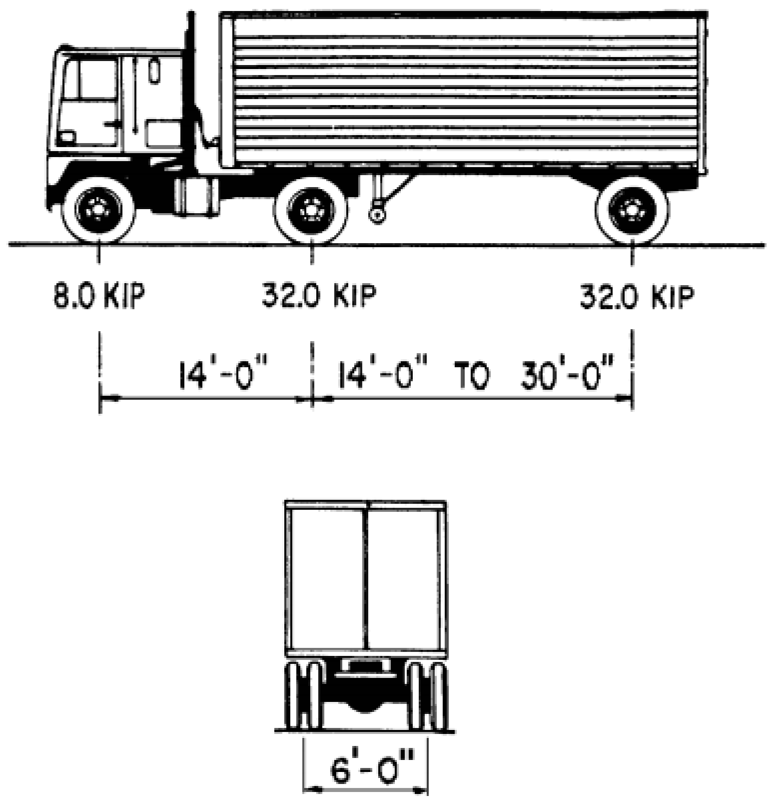

Figure 5.17: HL-93 design truck (AASHTO LRFD Bridge Design Spec.).

The AASHTO LRFD Bridge Design Spec. provides provisions related to dynamic load allowance. For the considered structure it is 33% of design truck or alternate military load. This fraction has to be added to the total live load before multiplying by load factor. Dynamic load allowance is not applied to the lane load.

Similar to the AASHTO Standard Spec., there are multiple presence factors specified in the AASHTO LRFD for situations with more than one lane loaded simultaneously. The reason for using them is the improbability of coincident maximum loading. Values for different number of loaded lanes are presented in the Table 5.6.

Table 5.6: AASHTO LRFD Bridge Design Spec. Multiple Presence Factors.

Number of loaded lanes	Multiple presence factors, m
One lane	1.20
Two lanes	1.00
Three lanes	0.85
More than three lanes	0.65

Live Load according to Weigh-In-Motion Data

The third live load case is based on collected traffic data from the WIM station located near the bridge. Processing of records and development of live load model was described in Chapter 3 of this dissertation. Since the values for year 2014 (Table 3.7) are the highest, they are used in the analysis. For the right lane there is an applied uniformly distributed load of 0.69 kip/ft, for the left lane 0.53 kip/ft and for the middle lane the average of these two – 0.61 kip/ft. These loads are distributed over a 10-ft width per lane. The idea of this live load pattern is based on observation of the real traffic described in previous research, Lutomirska (2009) and is presented in Figure 5.18. No multiple presence factors were used to simulate, theoretically, the most critical live load that can exist on a considered structure.

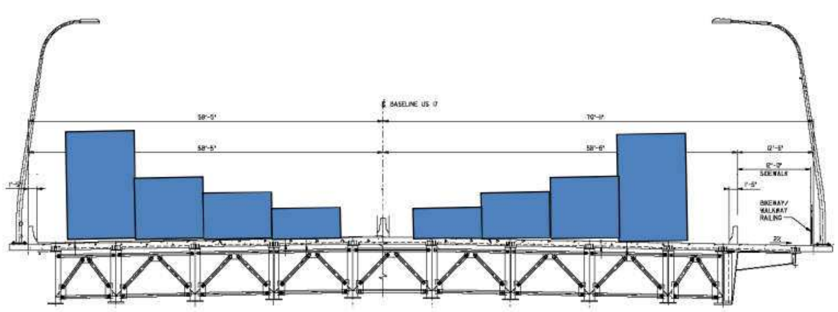

Figure 5.18: Multilane load in actual observation (Lutomirska M., 2009).

The configuration of the live load applied in this research is presented in Figure 5.19.

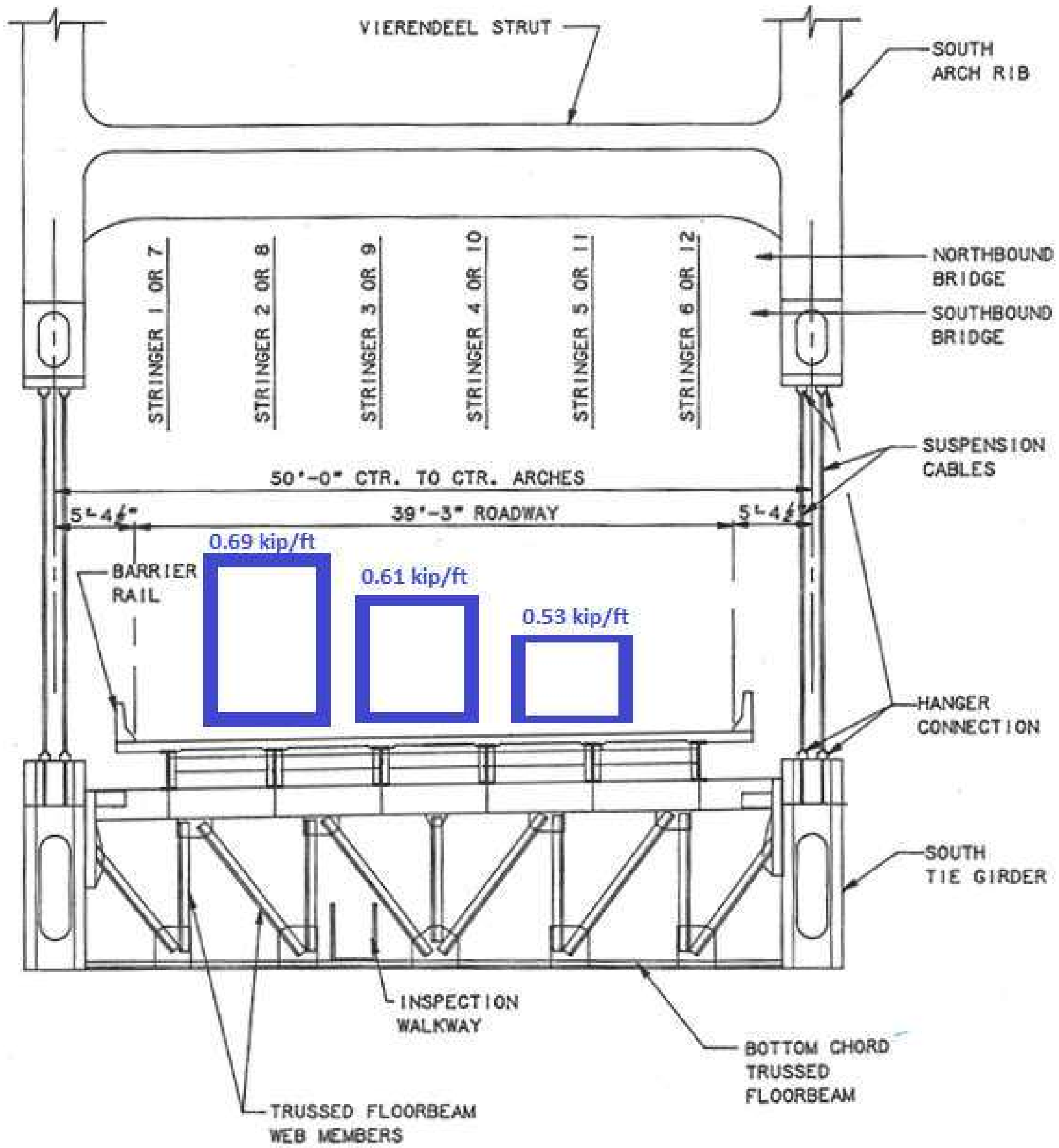

Figure 5.19: Scheme of live load configuration applied in the FEM model of the considered bridge.

Traffic Lanes

There are two traffic lanes on the existing structure. However, the gutter-to-gutter distance is 39'-3", allowing three 12-foot wide design traffic lanes to fit. The three lanes are created in the FEM model for moving load analysis purposes and placed so that they creates maximum effect of the live load (not symmetrically). The scheme of traffic lanes is presented in **the** Figure 5.20.

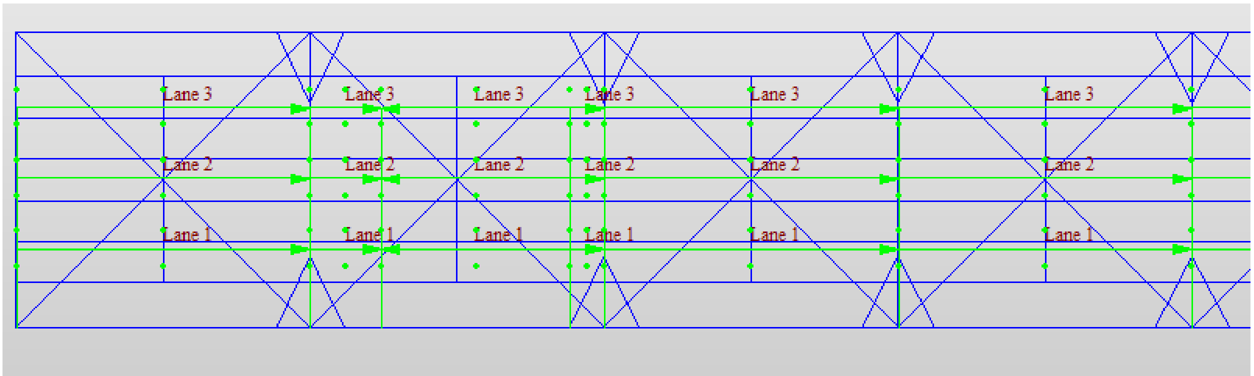

Figure 5.20: Scheme of the traffic lanes for moving load analysis in Midas Civil model.

<u>Considered limit states</u>

For analysis of the bridge according to AASHTO Standard Spec., there was Group I, Load Factor Design limit state considered. The load factors for this limit state are 1.30 for dead load and 2.17 (1.3x1.67) for live load plus impact.

For analysis of the bridge according to AASHTO LRFD, there was Strength I limit state considered. This limit state includes only dead load and live load. The implemented load factors are: 1.25 for dead load and 1.75 for live load plus impact.

For analysis of the bridge using WIM data, no load factors and resistance factors were used. Results from this analysis served as input values to the reliability analysis (Monte Carlo Simulation) of the considered arch.

Wind is not included in the analyses described above. The reason is because it is assumed that when there is strong wind, most very heavy vehicles will not be on the bridge. Trucks like semi-trailers are tall and they act like a sail, so it is recommended they not drive under windy conditions.

5.3.5. <u>Analytical procedure</u>

The geometry of the structure, material and cross-sectional properties, boundary conditions and releases were defined in the Midas Civil Software. In addition to that, dead load (steel + concrete) and live load (3 types of moving load) were applied and that was the starting point to the analyses.

General comment about nomenclature of Live Load cases in this dissertation

In all tables and figures where abbreviations “LRFD”, “STD”, “WIM”, “My” and “Fx” are used, their meaning is as follows:

LRFD – Load case including Live Load according to AASHTO LRFD Bridge Design Specifications (2012).

STD – Load case including Live Load according to AASHTO Standard Specifications for Highway Bridges (2002).

WIM – Load case including Live Load according to measured and processed Weigh-In-Motion data (explained in details in Chapter 3).

My – Load case resulting in maximum major bending moment for given segment of arch.

Fx – Load case resulting in maximum compressive force for given segment of arch.

<u>Linear (First Order) analysis</u>

Using the applied loads, load combinations for three situations were determined and linear analyses were run for them. The obtained results (Table 5.7) show the elements of four segments of the arch (AR 1, AR 2, AR 3 and AR 4) at their largest compressive forces and bending moments.

Table 5.7: Summary of the first order analysis results for all segments of arch rib. Force (kip), Moment (kip-ft).

	DL Steel			DL Concrete			LL		
Load	Axial	Moment y	Moment z	Axial	Moment y	Moment z	Axial	Moment y	Moment z
AR 1 My LRFD	-2383	442	-51	-1581	291	-12	-751	2372	-25
AR 1 Fx LRFD	-2384	436	16	-1581	289	-9	-1991	112	-4
AR 1 My STD	-2383	442	-51	-1581	291	-12	-775	2163	-20
AR 1 Fx STD	-2384	436	16	-1581	289	-9	-2062	200	-6
AR 1 My WIM	-2383	442	-51	-1581	291	-12	-735	2037	-13
AR 1 Fx WIM	-2380	431	-16	-1579	284	9	-2082	50	-21
	DL Steel			DL Concrete			LL		
Load	Axial	Moment y	Moment z	Axial	Moment y	Moment z	Axial	Moment y	Moment z
AR 2 My LRFD	-2243	269	-102	-1479	105	-79	-667	3298	19
AR 2 Fx LRFD	-2384	436	16	-1581	289	-9	-1991	112	-4
AR 2 My STD	-2243	269	-102	-1479	105	-79	-624	2977	-10
AR 2 Fx STD	-2384	436	16	-1581	289	-9	-2062	109	-75
AR 2 My WIM	-2243	269	-102	-1479	105	-79	-591	2825	-22
AR 2 Fx WIM	-2380	431	-16	-1579	284	9	-2082	50	-21
	DL Steel			DL Concrete			LL		
Load	Axial	Moment y	Moment z	Axial	Moment y	Moment z	Axial	Moment y	Moment z
AR 3 My LRFD	-2243	269	-102	-1479	105	-79	-667	3298	19
AR 3 Fx LRFD	-2244	264	49	-1480	104	43	-1850	-397	19
AR 3 My STD	-2243	269	-102	-1479	105	-79	-624	2977	-10
AR 3 Fx STD	-2244	264	49	-1480	104	43	-1915	-279	22
AR 3 My WIM	-2243	269	-102	-1479	105	-79	-591	2825	-22
AR 3 Fx WIM	-2240	263	-50	-1478	103	-44	-1942	-411	-11
	DL Steel			DL Concrete			LL		
Load	Axial	Moment y	Moment z	Axial	Moment y	Moment z	Axial	Moment y	Moment z
AR 4 My LRFD	-2027	-1	-39	-1341	110	-19	-1194	2662	-5
AR 4 Fx LRFD	-2073	190	34	-1370	112	24	-1712	-547	2
AR 4 My STD	-2027	-1	-39	-1341	110	-19	-1187	2479	-5
AR 4 Fx STD	-2073	190	34	-1370	112	24	-1772	-602	3
AR 4 My WIM	-2027	-1	-39	-1341	110	-19	-1128	2362	-9
AR 4 Fx WIM	-2070	190	-35	-1369	113	-24	-1789	-500	3

<u>Nonlinear (Second Order) Analysis</u>

The moving tracer option was used after the elements with the largest forces have been found. This option provides the configuration of the traffic load, which together with dead loads creates the maximum effect for a given element. These configurations are usually different for compressive force and bending moment. For each arch segment two critical configurations have been indicated – one for maximum compressive force and one for maximum major bending moment. These configurations of live load were saved and converted to the equivalent static load cases. The justification is that it is not possible to run nonlinear analysis for moving load. The example of live load configuration given by the moving tracer option (for segment AR 1), before conversion to static load case is presented in the Figure 5.21, Figure 5.22 and Figure 5.23.

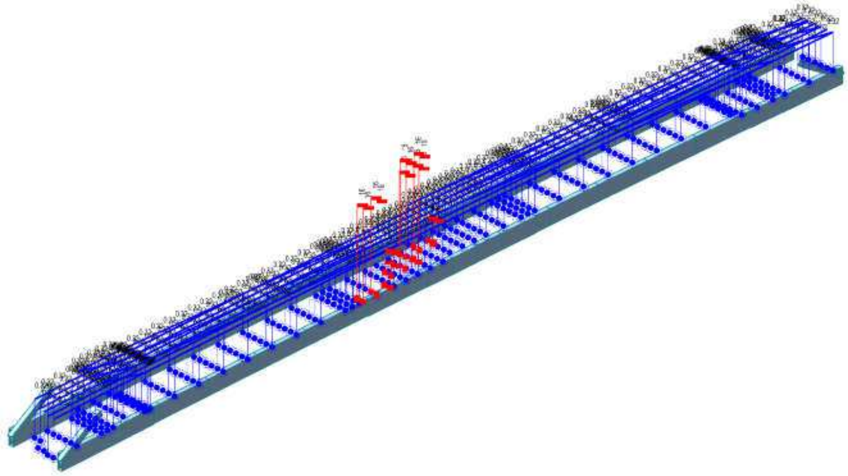

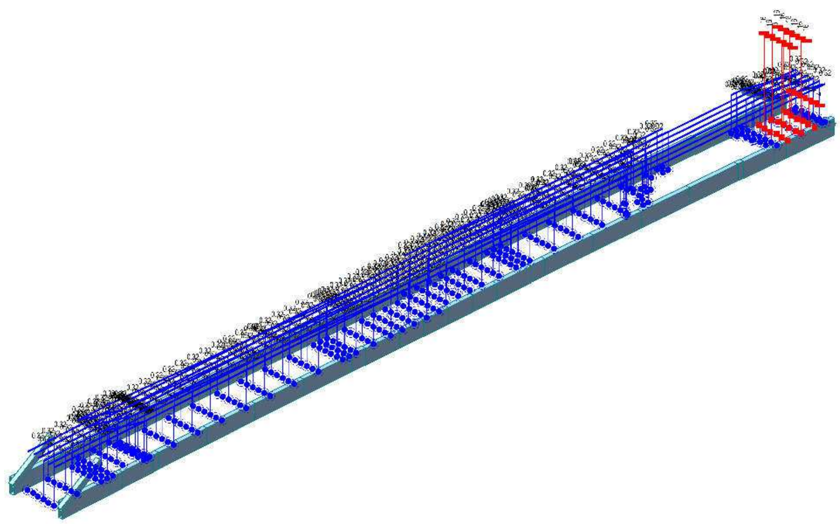

Figure 5.21: Configuration of AASHTO LRFD live load causing maximum compressive force (top) and maximum major bending moment (bottom) in AR 1.

Red and blue arrows in the Figure 5.21 indicate loads from design truck (or design tandem) and design lane load, respectively, for AASHTO LRFD.

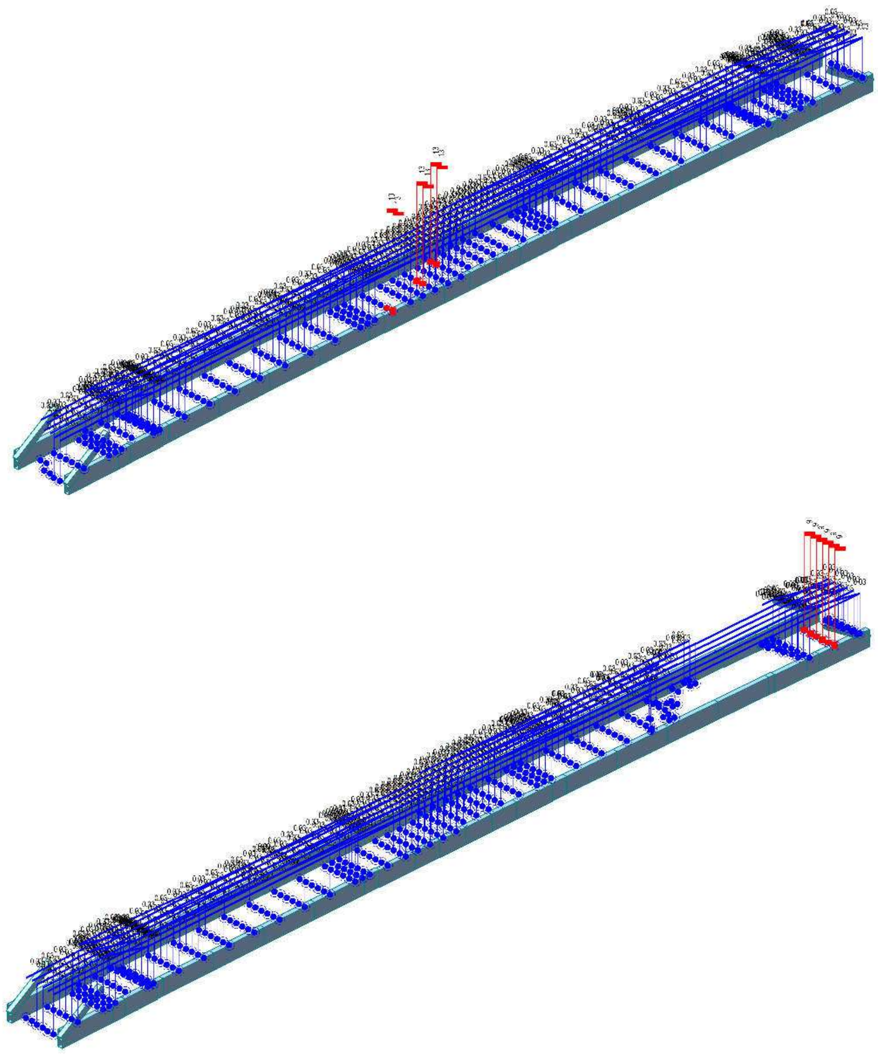

Figure 5.22: Configuration of AASHTO Standard Spec. live load causing maximum compressive force (top) and maximum major bending moment (bottom) in AR 1.

Red and blue arrows in the Figure 5.22 indicate loads from design truck (or design tandem) and design lane load, respectively, for AASHTO Standard Specifications.

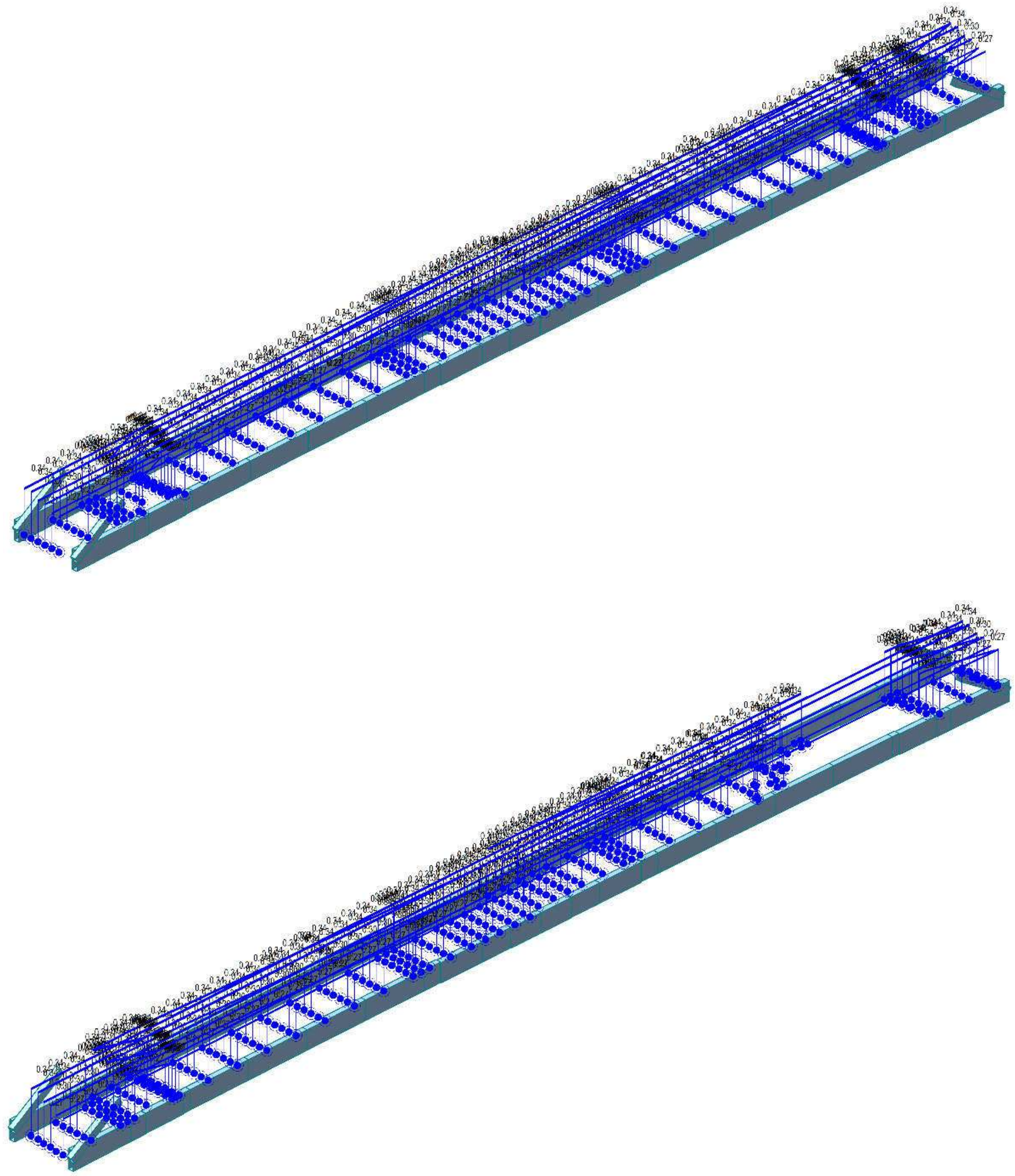

Figure 5.23: Configuration of measured WIM live load causing maximum compressive force (top) and maximum major bending moment (bottom) in AR 1.

Black arrows in the Figure 5.23 indicate equivalent uniformly distributed loads obtained from Weigh-In-Motion records processing.

Configurations of live load for the remaining segments of the arch (AR 2, AR3 and AR4) are presented in Appendix B.

The converted live load cases were combined with dead load, and second order analysis has been conducted. The assumed type of nonlinearity was geometric nonlinearity, and Newton-Raphson method was used.

Nonlinear analysis

The conventional process of the design or evaluation of the structure is based on the elastic behavior of the structural components. It is referred to as first order analysis. The two types of verifications must be followed – first, related to the strength capacity and guaranteeing the structural safety and second, the serviceability to ensure the proper performance during the working life. Because real structures are often very complex, the simplified methods are used to satisfy these two requirements. It is typically assumed that the behavior of the material is linear and elastic, and the structural deformations caused by the internal efforts may be neglected. This procedure is common and provides acceptable estimation of the structural behavior for most structures. Nevertheless, some of them require more detailed analysis to obtain the true results. To account for that, the linear first order analysis has to be supplemented with more advanced structural analysis methodology to include nonlinear material behavior and influence of the structural deformation during the load application procedure.

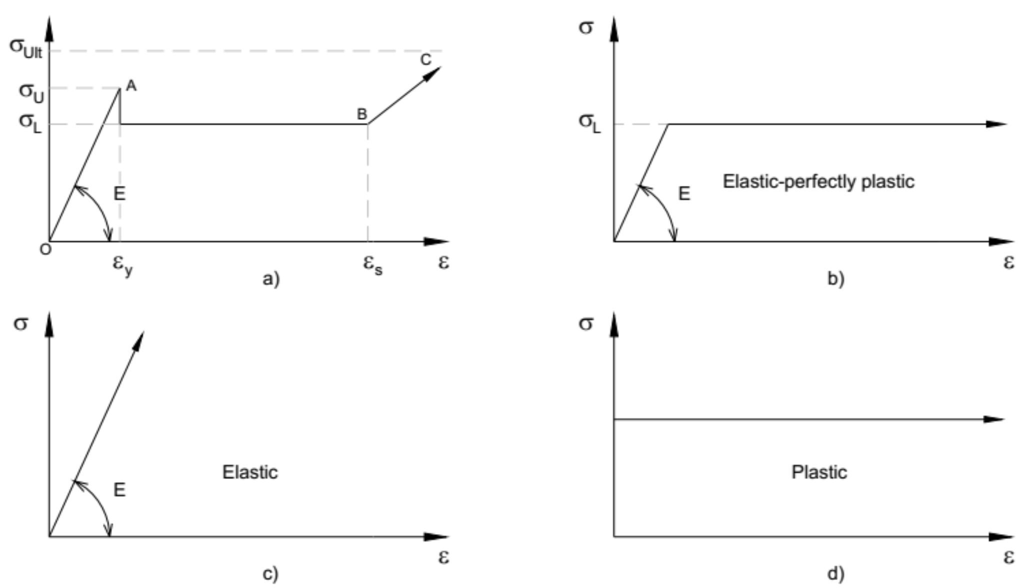

Figure 5.24: Simplified stress-strain constitutive laws (Gonçalves, Barros and Cesar, 2009).

It is possible to simplify the material behavior in order to obtain the desired constitutive law, according to the chosen analysis methodology. In the Figure 5.24, the example material models that may be obtained from a real constitutive law are presented. For design and evaluation of structures, elastic and plastic analyses are the most popular due to their simplicity. The main criterion for plastic analysis is collapse load, and it is found via the material strength in the plastic range. This assumption generally provides a significant economy, because the sizes of the cross sections determined using this method are smaller than those required by an elastic analysis.

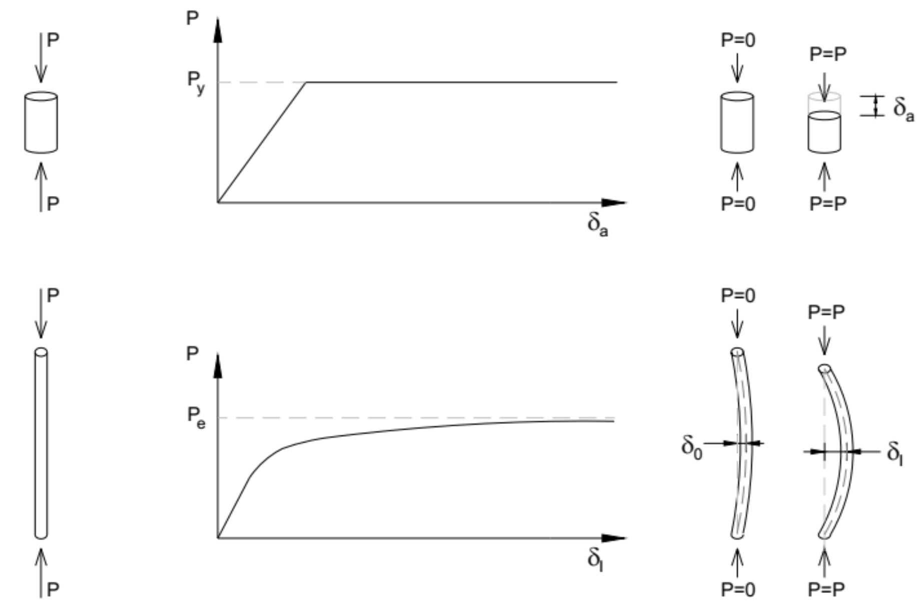

Figure 5.25: Nonlinear behavior of columns (Gonçalves, Barros and Cesar, 2009).

The material nonlinearity is usually the major source of the nonlinear structural behavior. Nevertheless, for many structures, the geometric nonlinear analysis cannot be omitted to properly estimate the effects of the applied loads. The example of a significant nonlinear response before reaching the resistant capacity for slender element is presented in the Figure 5.26.

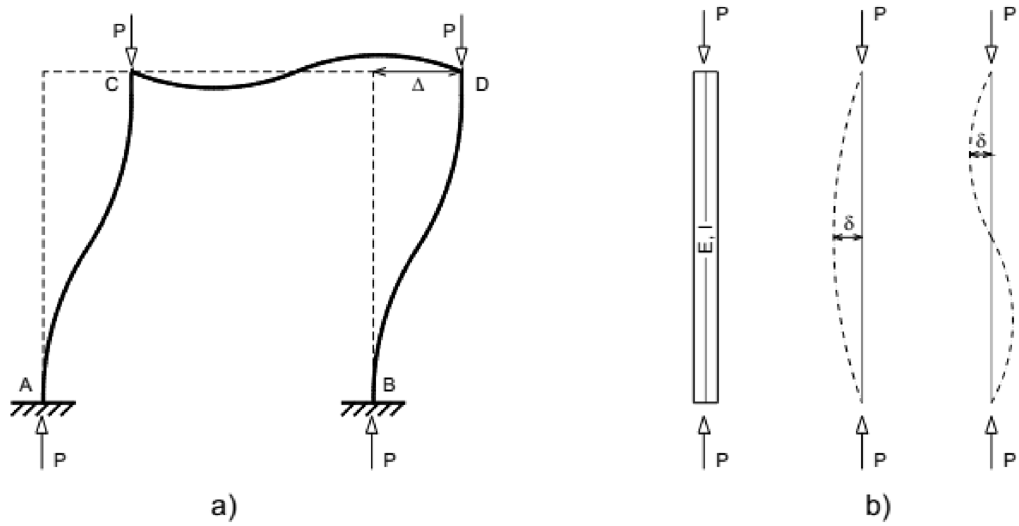

Figure 5.26: The two P-Delta effects: (a) P-Δ ; (b) P-δ (Gonçalves, Barros and Cesar, 2009).

When elastic behavior is expected for a large applied load (which is assumed for the arch considered in this study), the material nonlinearity can be excluded and only the nonlinear geometric analysis can be conducted. In this case, the global deformations of the structure (P-Δ effects), local deformations of structural members (P-δ effects) and initial imperfections are the main sources of the nonlinearity (Gonçalves, Barros and Cesar, 2009).

Newton-Raphson Method

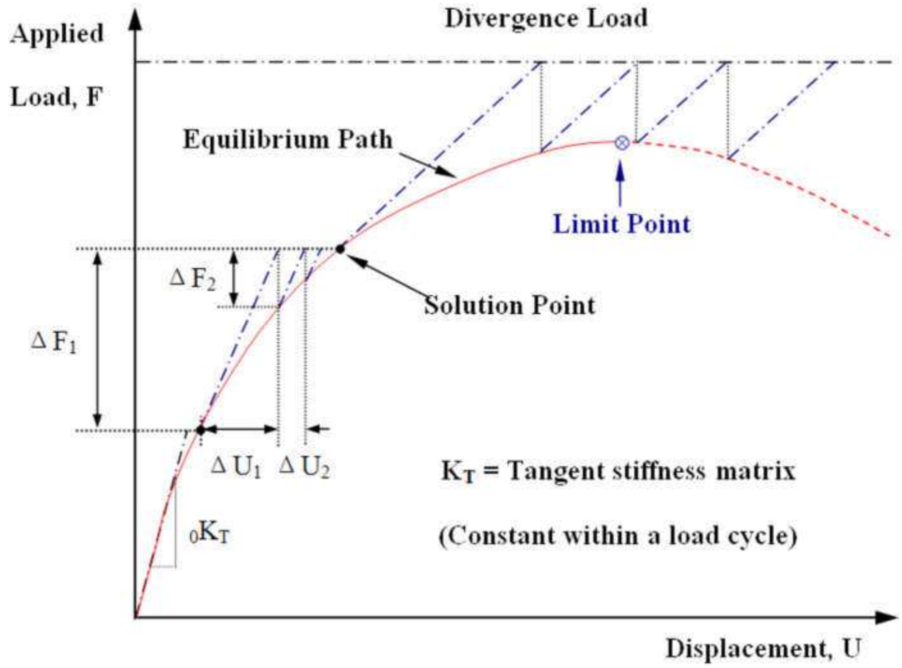

Figure 5.27: Newton-Raphson Method (http://www.nidaeurope.com/free-guides/38-numerical-methods-for-nonlinear-analysis).

In the Newton-Raphson Method (Figure 5.27), the tangent stiffness matrix of the structure is updated at every iteration. This iteration is activated to obtain equilibrium conditions between the internal structural resistance and the applied forces within a load step. In pure incremental method, no equilibrium check is performed. It is different for the Newton-Raphson Method, because the iterative procedure causes the dissipation of the unbalanced force, thus it can be eliminated. Additionally, due to the lack of drift error, the solution is more accurate and efficient from the standpoint of computational time. The Newton-Raphson Method provides a rapid rate of convergence in the stable equilibrium range. Disadvantages of this approach may be the large number of iterations required for the small increment when approaching the limit point at the load-deflection curve. No unloading paths can be traced in this method because the solution point is wanted at the specified applied load level.

5.3.6. Summary of the results

As mentioned above, two critical conditions were considered in nonlinear analysis. First with maximum compressive force and second with maximum bending moment. The results for all four segments of the arch are presented in Table 5.8. These results are used for further interaction equation checks and reliability analysis.

Table 5.8: Summary of the second order analysis results for all segments of arch rib. Force (kip), Moment (kip-ft).

	DL Steel			DL Concrete			LL		
Load	Axial	Moment y	Moment z	Axial	Moment y	Moment z	Axial	Moment y	Moment z
AR 1 My LRFD	-2381	456	-54	-1580	298	-13	-748	2389	-18
AR 1 Fx LRFD	-2381	450	20	-1580	298	-8	-1990	118	-1
AR 1 My STD	-2381	456	-54	-1580	298	-13	-773	2179	-14
AR 1 Fx STD	-2381	450	20	-1580	298	-8	-2061	207	-2
AR 1 My WIM	-2381	456	-54	-1580	298	-13	-732	2051	-7
AR 1 Fx WIM	-2377	445	-20	-1578	292	9	-2083	54	-24
	DL Steel			DL Concrete			LL		
Load	Axial	Moment y	Moment z	Axial	Moment y	Moment z	Axial	Moment y	Moment z
AR 2 My LRFD	-2242	278	-103	-1479	106	-80	-668	3325	19
AR 2 Fx LRFD	-2381	450	20	-1580	298	-8	-1990	118	-1
AR 2 My STD	-2242	278	-103	-1479	106	-80	-624	3001	-11
AR 2 Fx STD	-2381	450	20	-1580	298	-8	-2061	207	-2
AR 2 My WIM	-2242	278	-103	-1479	106	-80	-591	2847	-24
AR 2 Fx WIM	-2377	445	-20	-1578	292	9	-2083	54	-24
	DL Steel			DL Concrete			LL		
Load	Axial	Moment y	Moment z	Axial	Moment y	Moment z	Axial	Moment y	Moment z
AR 3 My LRFD	-2242	278	-103	-1479	106	-80	-668	3325	19
AR 3 Fx LRFD	-2243	273	50	-1479	107	44	-1848	-400	19
AR 3 My STD	-2242	278	-103	-1479	106	-80	-624	3001	-11
AR 3 Fx STD	-2243	273	50	-1479	107	44	-1913	-280	22
AR 3 My WIM	-2242	278	-103	-1479	106	-80	-590	2847	-23
AR 3 Fx WIM	-2239	272	-51	-1478	106	-44	-1942	-417	-7
	DL Steel			DL Concrete			LL		
Load	Axial	Moment y	Moment z	Axial	Moment y	Moment z	Axial	Moment y	Moment z
AR 4 My LRFD	-2027	-7	-40	-1341	108	-20	-1193	2681	-6
AR 4 Fx LRFD	-2074	190	34	-1370	112	24	-1709	-558	2
AR 4 My STD	-2027	-7	-40	-1341	108	-20	-1186	2497	-7
AR 4 Fx STD	-2074	190	34	-1370	112	24	-1769	-614	4
AR 4 My WIM	-2027	-7	-40	-1341	108	-20	-1128	2377	-11
AR 4 Fx WIM	-2070	190	-35	-1369	113	-24	-1787	-513	5

The obtained values of compressive force and bending moment for first order (linear) and second order (nonlinear) analyses were compared. Detailed summary is presented in the Table 5.9 and Figure 5.28.

Table 5.9: Percentage differences between values of the major bending moment obtained for first and second order analyses of the considered arch.

		% Difference - Moment y			
		DL Steel	DL Concrete	Live Load	My Total
AR 1	AR 1 My LRFD	3.1%	2.2%	0.7%	1.2%
	AR 1 My STD	3.1%	2.2%	0.7%	1.2%
	AR 1 My WIM	3.1%	2.2%	0.7%	1.2%
AR 2	AR 2 My LRFD	3.2%	1.8%	0.8%	1.0%
	AR 2 My STD	3.2%	1.8%	0.8%	1.0%
	AR 2 My WIM	3.2%	1.8%	0.8%	1.0%
AR 3	AR 3 My LRFD	3.2%	1.8%	0.8%	1.0%
	AR 3 My STD	3.2%	1.8%	0.8%	1.0%
	AR 3 My WIM	3.2%	1.8%	0.8%	1.0%
AR 4	AR 4 My LRFD	86.4%	-2.0%	0.7%	0.4%
	AR 4 My STD	86.4%	-2.0%	0.7%	0.4%
	AR 4 My WIM	86.4%	-2.0%	0.7%	0.3%

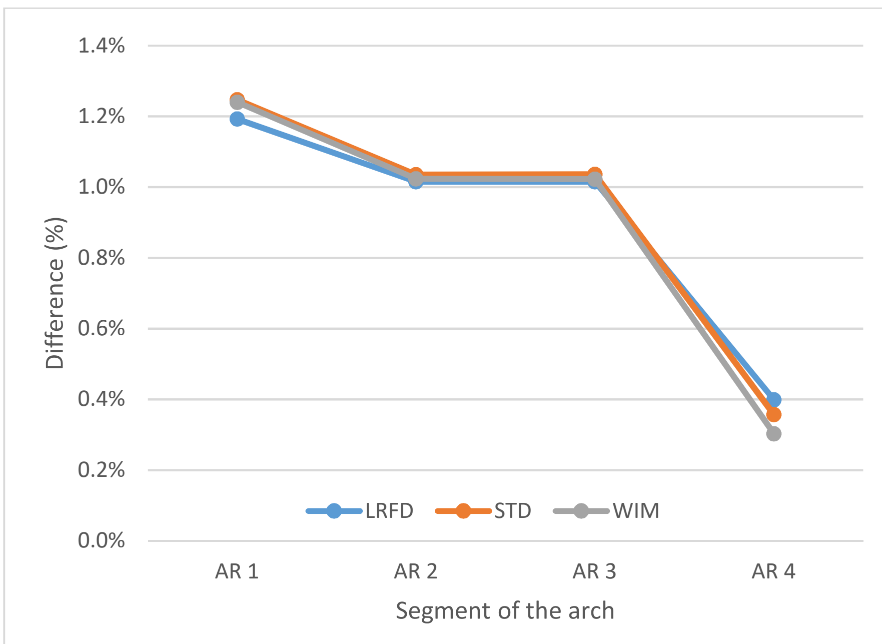

Figure 5.28: Graphical representation of percentage differences from Table 5.9.

<u>Fractions of Dead Load of Steel (DLS), Dead Load of Concrete (DLC) and Live Load (LL) for axial force and major bending moment</u>

For the considered arch, results from Finite Element Analysis have been processed and summarized. The portions of each kind of load were determined for load cases with maximum compressive force and maximum major bending moment and for all three types of live load (WIM – measured, according to AASHTO Standard Spec. and according to AASHTO LRFD). These fractions for the axial force in the arch are presented in Figure 5.29.

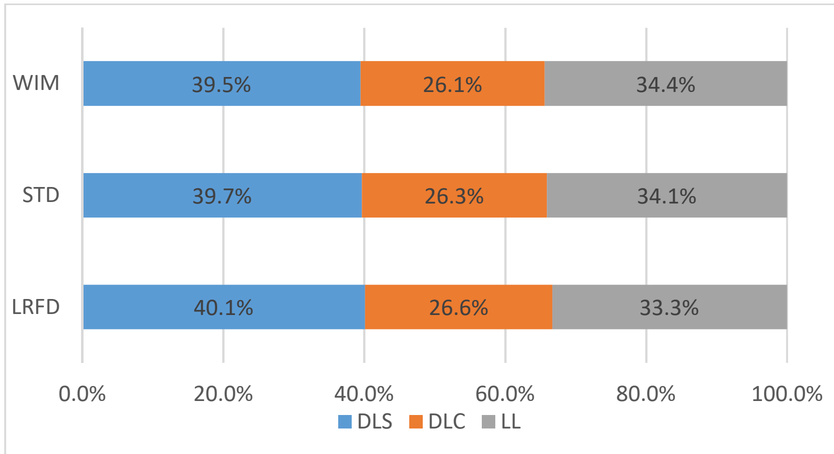

Figure 5.29: Fractions of dead load of steel (DLS), dead load of concrete (DLC) and Live load (LL) for Axial Force, for load cases with maximum compressive force.

Similar results were obtained for major bending moment in the load cases with maximum compressive force and they are shown in Figure 5.30.

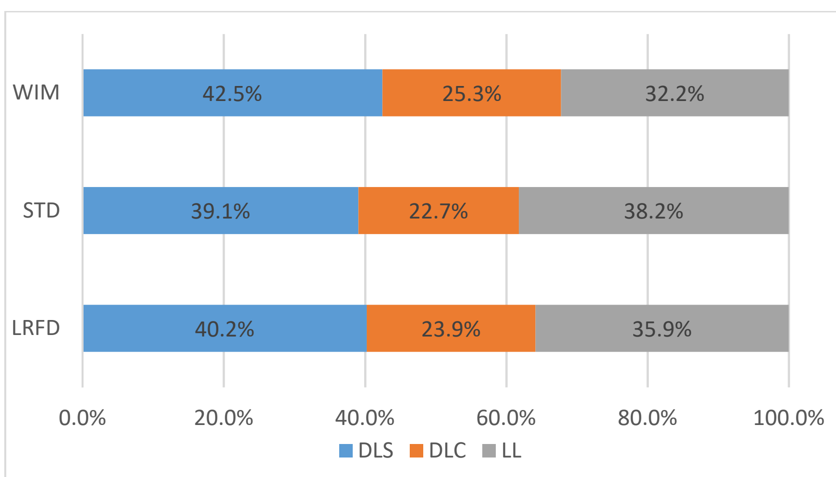

Figure 5.30: Fractions of dead load of steel (DLS), dead load of concrete (DLC) and Live load (LL) for Major Bending moment, for load cases with maximum compressive force.

The fractions of DLS, DLC and LL for the axial force in the arch and for the load case with maximum bending moment are similar to those for maximum compressive force and are presented in the Figure 5.31.

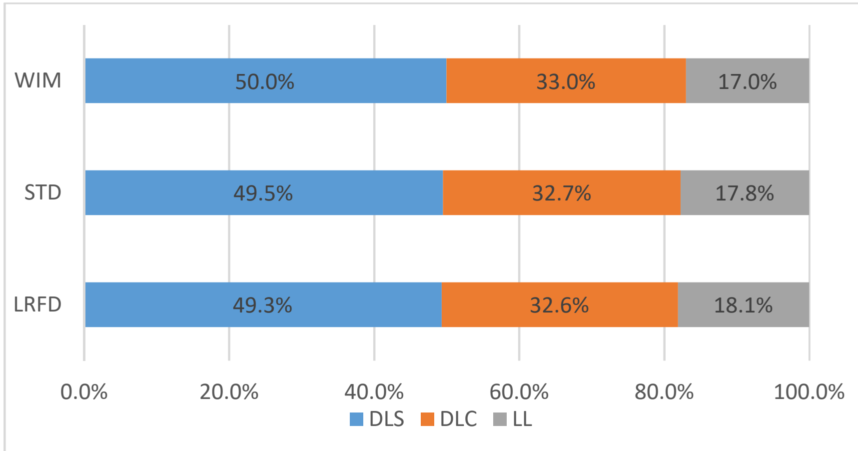

Figure 5.31: Fractions of dead load of steel (DLS), dead load of concrete (DLC) and Live load (LL) for Axial Force, for load cases with maximum major bending moment.

Only the portions of DLS, DLC and LL for major bending moment in the load cases with maximum major bending moment are more diverse than from previous. These cases are shown in the Figure 5.32 and the live load part for them is much more significant (almost 90%).

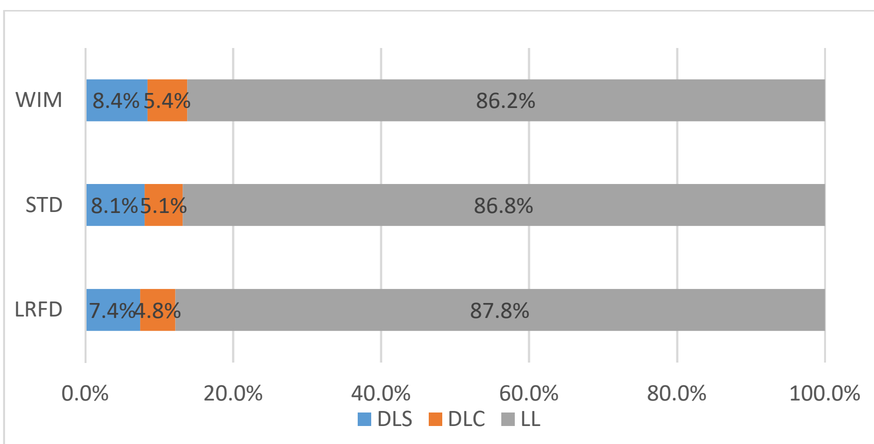

Figure 5.32: Fractions of dead load of steel (DLS), dead load of concrete (DLC) and Live load (LL) for Major Bending moment, for load cases with maximum major bending moment.

A more detailed summary of the obtained results of portions of different kinds of load is presented in Appendix B.

<u>Comparison of obtained values of axial force and major bending moment</u>

The maximum total axial forces obtained from FEM model were compared and shown in Figure 5.41. There are no significant differences between the values for three different load cases. For the first two segments of the arch (AR 1 and AR 2) axial force is around 800 kip higher than for segment AR 4 which includes the crown of the arch.

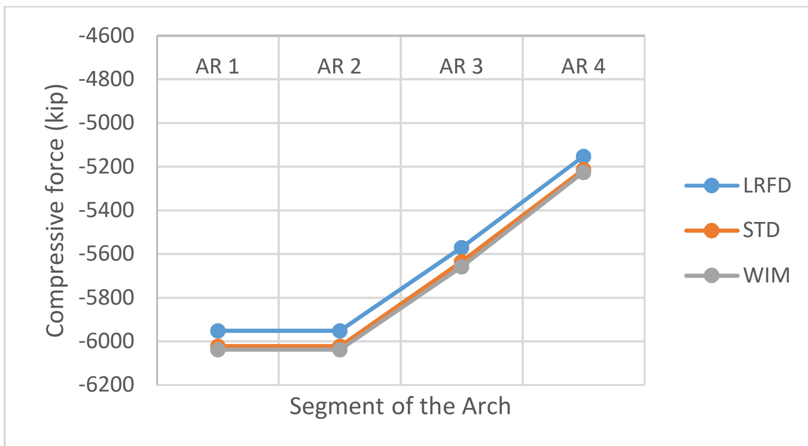

Figure 5.33: Comparison of the maximum total axial force for each segment of the arch.

The compared values of axial force caused by live load only are also very similar. The difference between AR 1 and AR 4 is around 300 kip for all load cases (Figure 5.34).

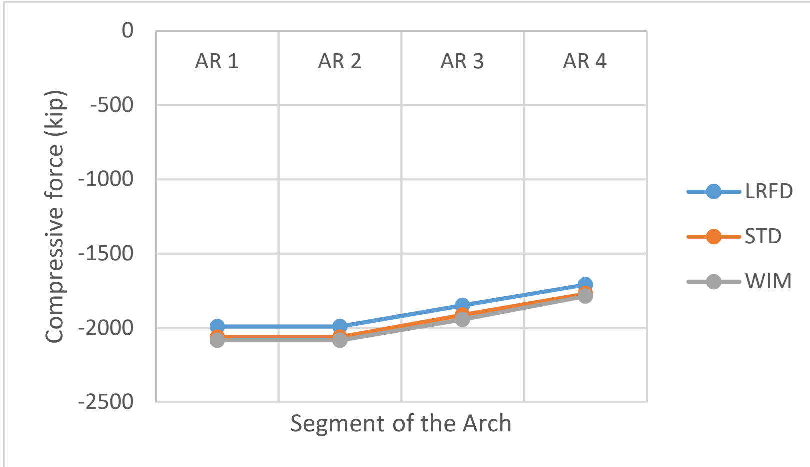

Figure 5.34: Comparison of the maximum live load component of the axial force for each segment of the arch.

The maximum total major bending moments obtained from FEM model were compared and shown in the Figure 5.35. Values for AASHTO LRFD approach are slightly (around 10%) higher than for other two (WIM and AASHTO Standard Spec.). For first and middle segment of the arch (AR 1 and AR 4) bending moments are smaller than for segments AR 2 and AR 3.

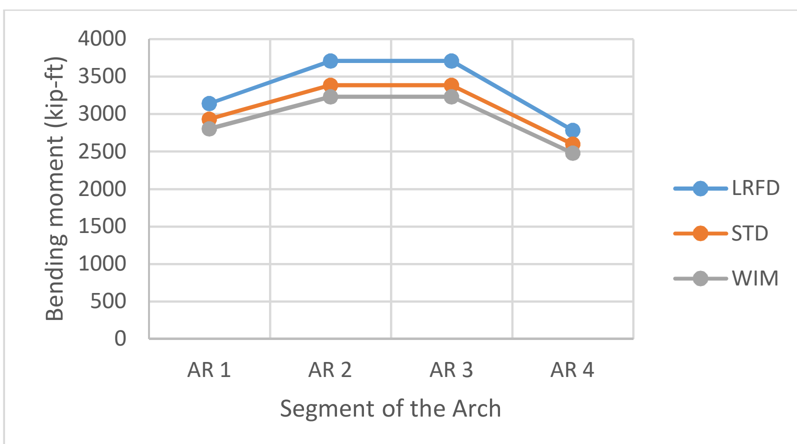

Figure 5.35: Comparison of the maximum total major bending moment for each segment of the arch.

For bending moment caused by live load only, there is a similar trend as for total load – configuration of vehicles according to AASHTO LRFD creates maximum flexure in the arch. Also, values obtained at the beginning and at the crown of the arch are smaller than for other segments.

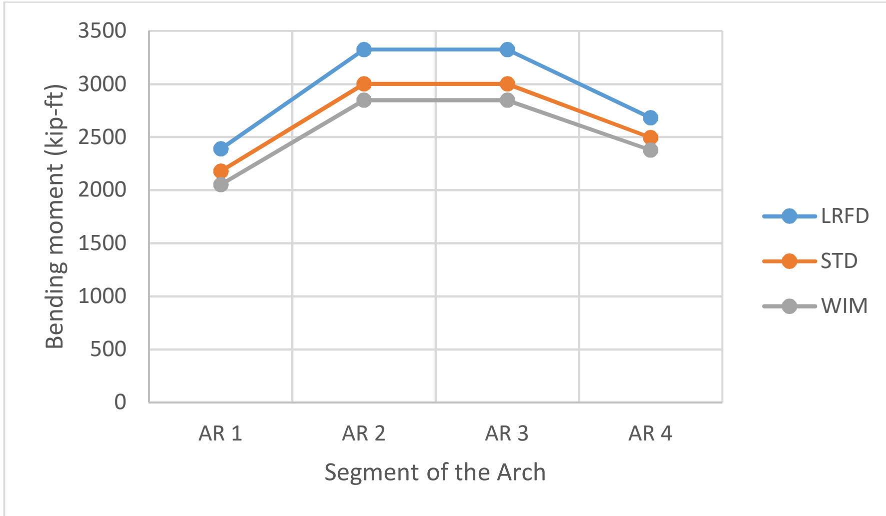

Figure 5.36: Comparison of the maximum live load component of the major bending moment for each segment of the arch.

Buckling Analysis

Due to the unclear unbraced length of the specific type of bracing (Vierendeel Struts) and the geometry of the arch, the buckling analysis was conducted in order to obtain the critical buckling forces for each segment. The sum of unfactored dead and live loads was used. The result of this analysis was a multiplier of the applied load which was obtained for first buckling mode. The summary of these multipliers is provided in the Table 5.10.

Table 5.10: Load multipliers obtained from buckling analyses.

Segment of the arch	Load multiplier		
	WIM	LRFD	STD
AR 1	4.67	4.31	4.37
AR 2	4.67	4.31	4.37
AR 3	4.66	4.30	4.39
AR 4	4.63	4.25	4.39

The multipliers shown above were used to create load cases for each arch segment for three calculation situations. Then, for these load cases, second order analysis was conducted to calculate compressive forces, which were elastic buckling forces. The summary of these forces in presented in the Table 5.11. and in the Figure 5.28.

Table 5.11: Elastic buckling forces for each segment of the arch obtained from second order analysis using multipliers of the load from buckling analysis.

Segment of the arch	Buckling Force (kip)		
	WIM	LRFD	STD
AR 1	28,265	25,782	26,520
AR 2	28,123	25,650	26,387
AR 3	26,256	23,951	24,841
AR 4	24,133	22,153	22,941

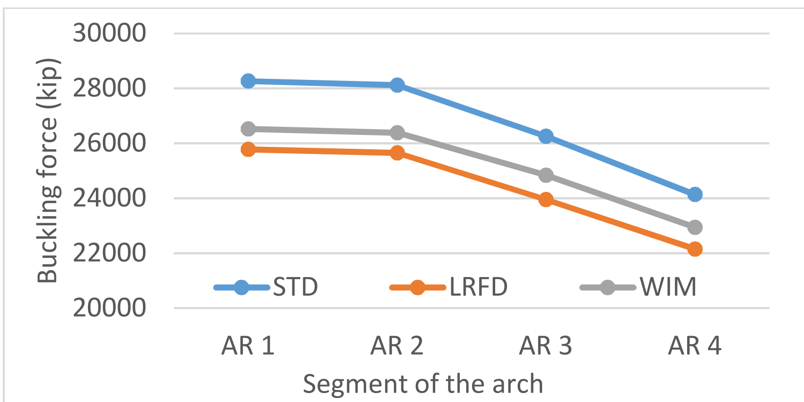

Figure 5.37: Buckling forces comparison.

In addition to the values of buckling forces for the considered arch, general shape of first buckling mode is presented in the Figure 5.38.

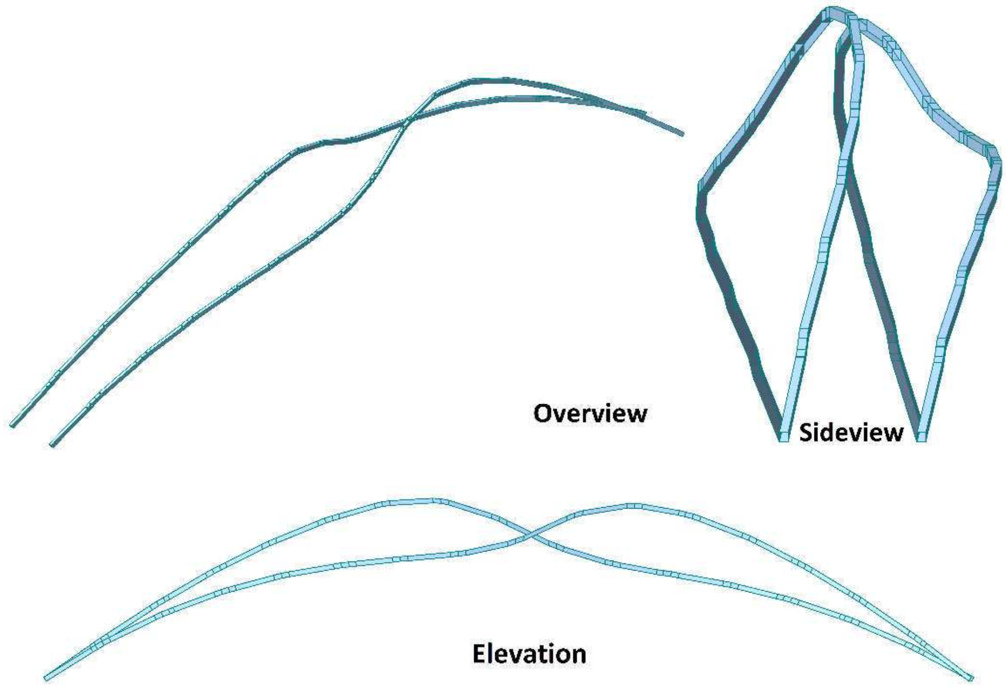

Figure 5.38: General shape for first buckling mode.

<u>Validation of the model</u>

The software indicated no errors or singularities for the conducted analyses in Midas Civil software. To validate the FEM model of the structure, the overall behavior, deflections, redistribution of forces and moments as well as load paths were examined. The following comparisons can serve as an example of convergence between FEM model behavior and performance of the real structure (planned by the designer).

Deformed Shape

In the Figure 5.39 and Figure 5.40 there are deflected shapes presented for dead load of concrete deck only and total dead load, respectively. The maximum deflection for concrete deck obtained from second order analysis is 0.466 ft and for total dead load: 0.988 ft. It is crucial to mention that in the FEM model, stiffeners, gusset plates, cable sockets and other secondary steel elements are not included, making the total weight of the structural steel smaller.

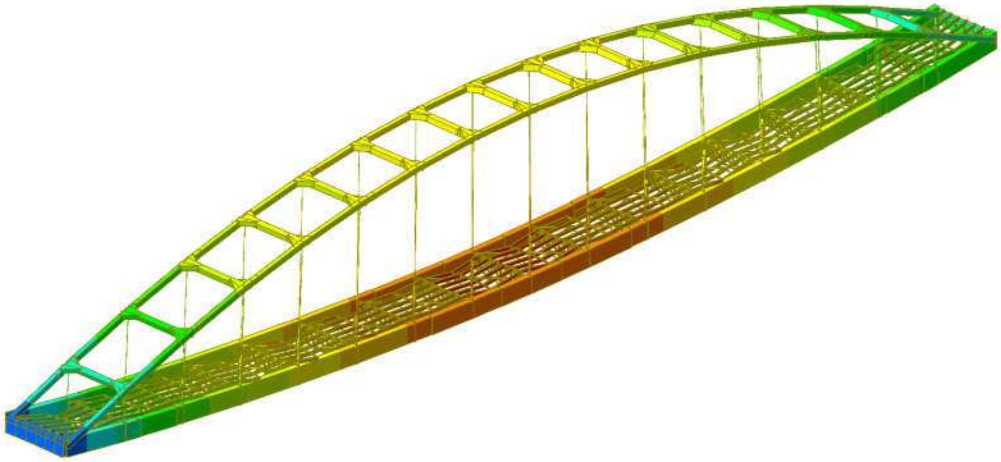

Figure 5.39: Deformed shape of the model for concrete deck load only.

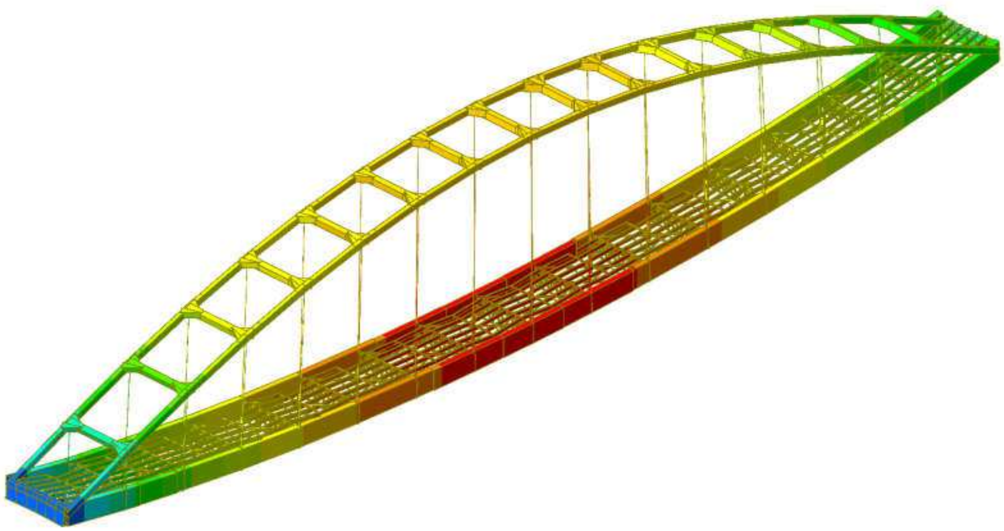

Figure 5.40: Deformed shape of the model for total dead load.

Forces in cables

In the Figure 5.41 and Figure 5.42 there are cable forces presented for dead load of concrete deck only and total dead load, respectively. The maximum cable force for concrete deck obtained from second order analysis is 114.1 kip and for total dead load: 205.2 kip. The designer predicted 109.1 kip and 214.7 kip, respectively.

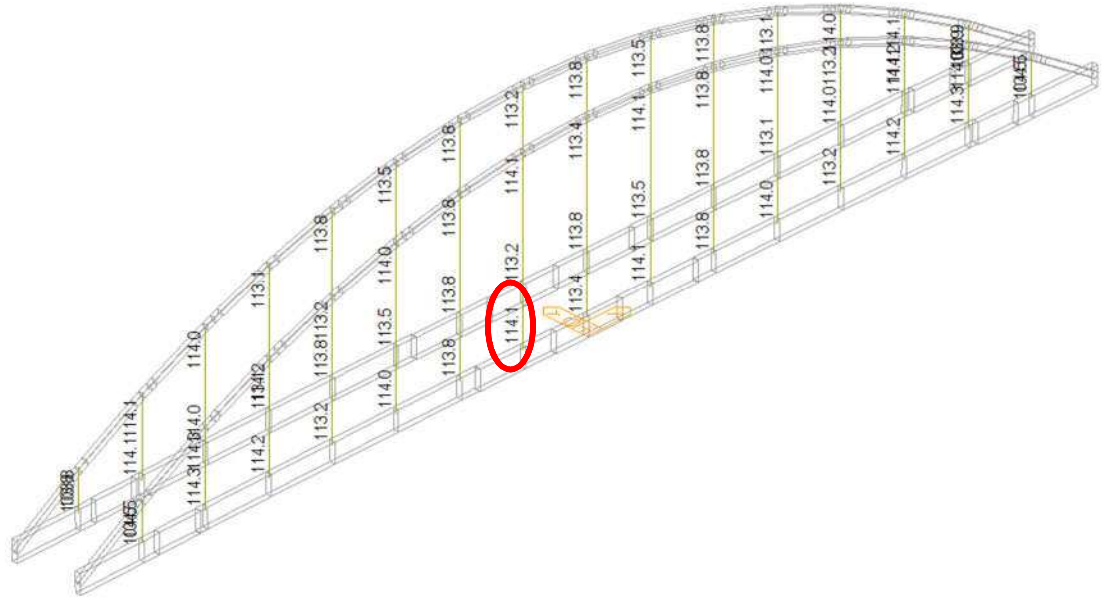

Figure 5.41: Forces in cables for deck dead load only (kip).

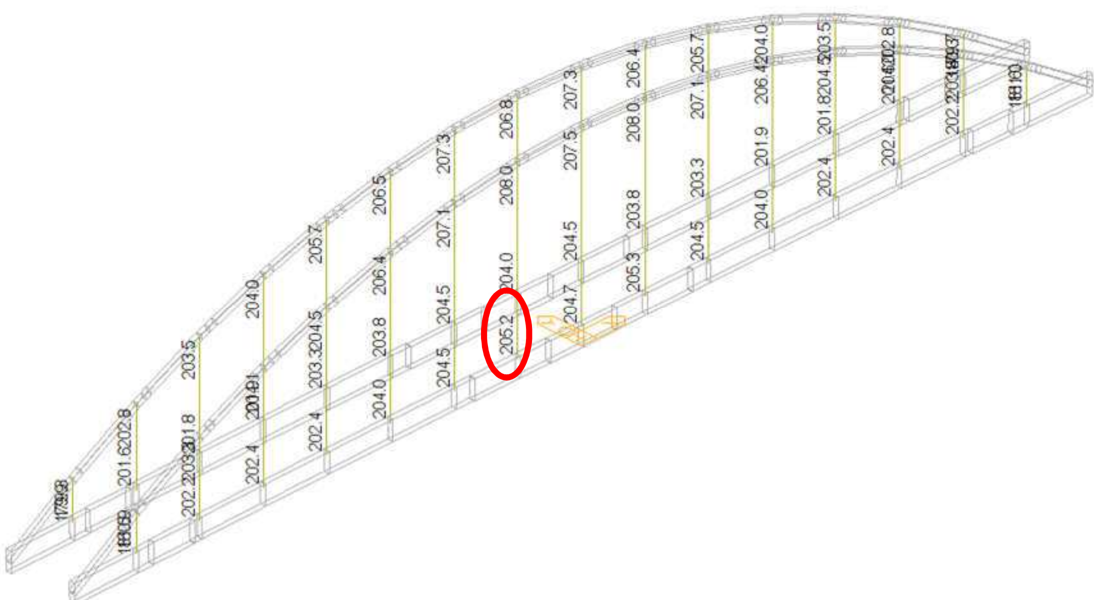

Figure 5.42: Forces in cables for total dead load (kip).

Figure 5.43 is a scan from the original project with predicted deflections and forces in cables.

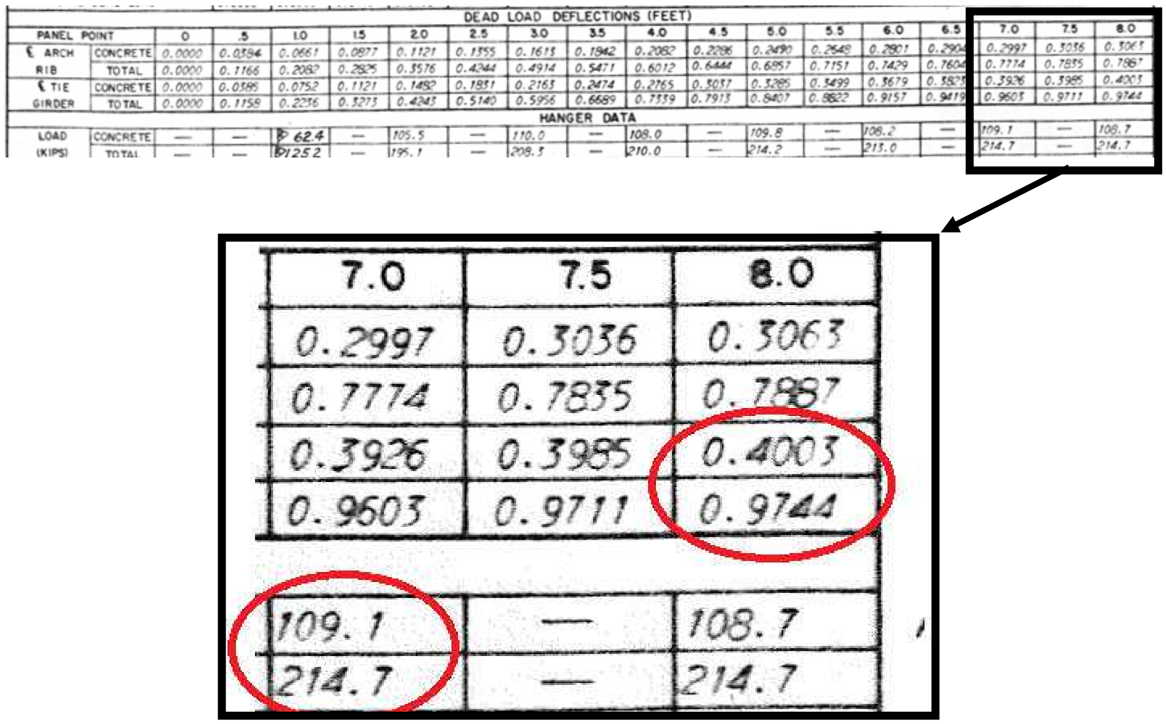

DEAD LOAD DEFLECTIONS (FEET)																		
PANEL POINT		0	.5	1.0	1.5	2.0	2.5	3.0	3.5	4.0	4.5	5.0	5.5	6.0	6.5	7.0	7.5	8.0
℄ ARCH RIB	CONCRETE	0.0000	0.0384	0.0661	0.0877	0.1121	0.1355	0.1613	0.1942	0.2082	0.2286	0.2490	0.2648	0.2801	0.2904	0.2997	0.3036	0.3063
	TOTAL	0.0000	0.1166	0.2082	0.2825	0.3576	0.4244	0.4914	0.5471	0.6012	0.6444	0.6857	0.7151	0.7429	0.7604	0.7774	0.7835	0.7887
℄ TIE GIRDER	CONCRETE	0.0000	0.0385	0.0752	0.1121	0.1482	0.1831	0.2163	0.2474	0.2765	0.3037	0.3285	0.3499	0.3679	0.3825	0.3926	0.3985	0.4003
	TOTAL	0.0000	0.1158	0.2236	0.3273	0.4243	0.5140	0.5956	0.6689	0.7339	0.7913	0.8407	0.8822	0.9157	0.9419	0.9603	0.9711	0.9744
HANGER DATA																		
LOAD (KIPS)	CONCRETE	—	—	62.4	—	105.5	—	110.0	—	108.0	—	109.8	—	108.2	—	109.1	—	108.7
	TOTAL	—	—	125.2	—	195.1	—	208.3	—	210.0	—	214.2	—	213.0	—	214.7	—	214.7

Figure 5.43: Deflections and forces in cables calculated by the designer of the bridge (I-65 over Mobile River Bridge Inspection Manual).

The values given by the model and predicted by the designer are very similar. The difference for maximum deflection is around 1% and for maximum force in the cable is around 5%. This confirms that the FEM model is a valuable source of information needed for the purposes of this study.

CHAPTER 6 RELIABILITY ANALYSIS FOR COMPONENTS OF THE BRIDGE

6.1. RELIABILITY ANALYSIS PROCEDURE

The reliability analysis procedure was performed for the different segments of the arch of the bridge. The main purpose of this analysis was to calculate reliability indices for each segment of the arch and use these values in further system reliability analysis. Three approaches were implemented:

1) *Calculation of reliability indices using Monte Carlo Simulation for existing cross sections of the arch using unfactored loads and resistances, total dead load (steel + concrete) and WIM live load data.*

2) *Calculation of reliability indices using Monte Carlo Simulation for cross sections of the arch determined according to AASHTO Standard Specifications (assuming the interaction equation equals to 1.0)*

3) *Calculation of reliability indices using Monte Carlo Simulation for cross sections of the arch determined according to AASHTO LRFD (assuming the interaction equation equals to 1.0)*

Additionally, for each approach, two situations were considered. First with maximum axial force and corresponding bending moments in a given element and second with maximum major bending moment and corresponding axial force and minor bending moment in a given element.

The steps for reliability analysis procedure are presented in the following subsections.

6.1.1. Selection of the representative arch bridge

The General W.K. Wilson Jr. Bridge was the chosen representative structure for examining arches. The detailed description of the bridge and Finite Element Modeling approach were presented in Chapter 5 of this study.

Dead load to live load ratio is much higher for long span bridges than for short and medium, so weight of the components is definitely the most critical load for structures like the selected. Arch ribs were chosen as one of the most important components and at the same time vulnerable to the live load effects, especially for flexure.

6.1.2. Formulation of the limit state function

Since the performance of steel arch is similar to beam-column structural behavior, the limit state function was formulated using basic axial load – bending moment interaction equation. The failure is assumed when the sum of quotients of loads and resistances exceed the unity. General form of the limit state function is presented in Equation (6.1).

$$g = 1.0 - \left(\frac{P_u}{P_n} + \frac{M_{uy}}{M_{ny}} + \frac{M_{uz}}{M_{nz}}\right) \tag{6.1}$$

where:

P_u = axial load

M_{uy} = major bending moment

M_{uz} = minor bending moment

P_n = compressive resistance

M_{ny} = flexural resistance (major axis)

M_{nz} = flexural resistance (minor axis)

6.1.3. Resistance model

The resistance model was described in Chapter 4. In addition to that, the statistical parameters of resistance for steel beam-columns needed to be determined. Nowak and Collins (2013), Ellingwood, Galambos, MacGregor and Cornell (1980) provided the statistical parameters for steel beam-columns. They are shown in Table 6.1.

Table 6.1: Statistical resistance parameters for beam-columns.

Element type	μ_P	CoV_P	μ_M	CoV_M	μ_F	CoV_F	λ_R	CoV_R
Beam columns	1.02	0.10	1.05	0.10	1.00	0.05	1.07	0.15

6.1.4. Load model

The load combinations considered for this study contain dead load and live load only. Dead load is represented by weight of the steel and weight of the concrete. The statistical parameters for dead load are shown in Table 6.2. Normal distribution is assumed for dead load random variables.

Table 6.2: Recommended statistical parameters of dead load for bridges.

Element type:	λ_D	CoV_D
Factory made steel and precast concrete	1.03	0.08
Cast in place concrete	1.05	0.10

Lognormal distribution is assumed for live load random variables. The comparison between obtained in WIM processing data and ideal lognormal distribution is shown in Figure 6.1.

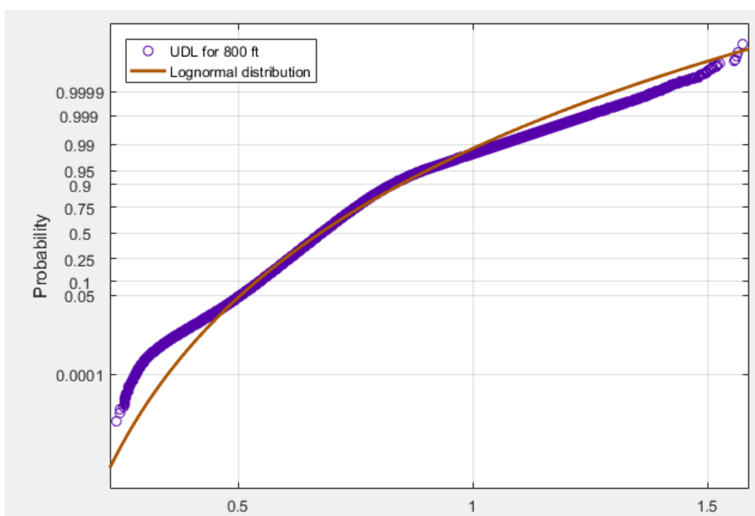

Figure 6.1: Distribution of UDL (kip/ft) values for 800-ft span length.

6.1.5. Calculation of reliability indices for existing cross sections of the arch

Monte Carlo simulation method was used to calculate reliability indices for each segment of the arch. Section 2.7 contains the list of steps for this simulation technique. To conduct calculations of reliability indices efficiently, the code in Matlab software has been developed. Each component of the Equation (6.1) has been simulated 1,000,000 times using specific distributions and statistical parameters. Furthermore, the load components ($\bar{P}_u$, $\bar{M}_{uy}$ and $\bar{M}_{uz}$) consisted of three subcomponents related to dead load of steel (DLS), dead load of concrete (DLC) and live load (LL). Each of these subcomponents has its own statistical parameters and type of distribution and also has been simulated 1,000,000 times.

The distributions of the simulated values for the considered limit state function (g) for first approach (existing cross section) are presented in Figure 6.2 (for load cases with maximum major bending moment) and Figure 6.3 (for maximum compressive force). Every point below zero on the horizontal axis mean failure of given segment of the arch.

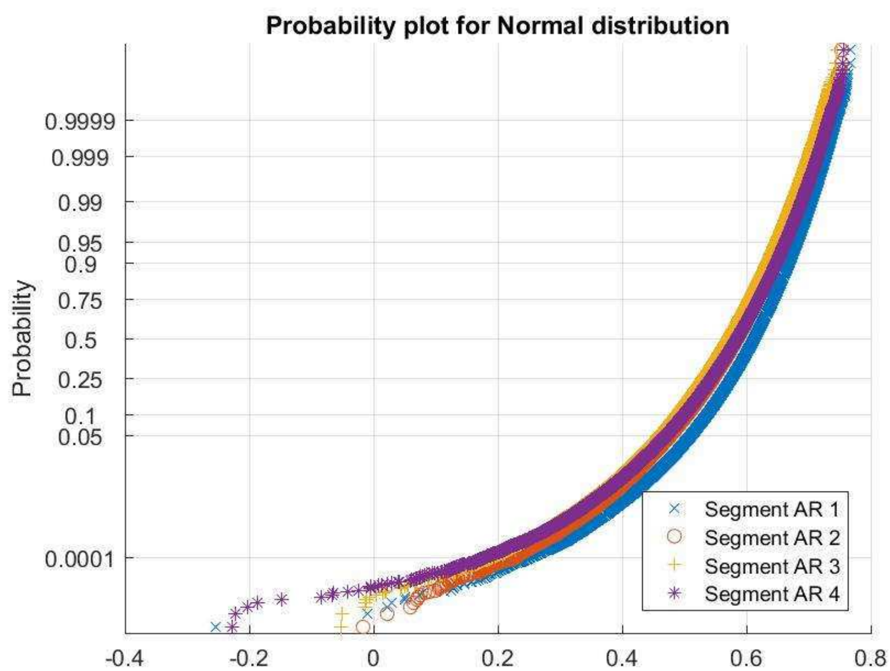

Figure 6.2: Probability plot for normal distribution of *g* values for existing cross section properties (load case with maximum bending moment).

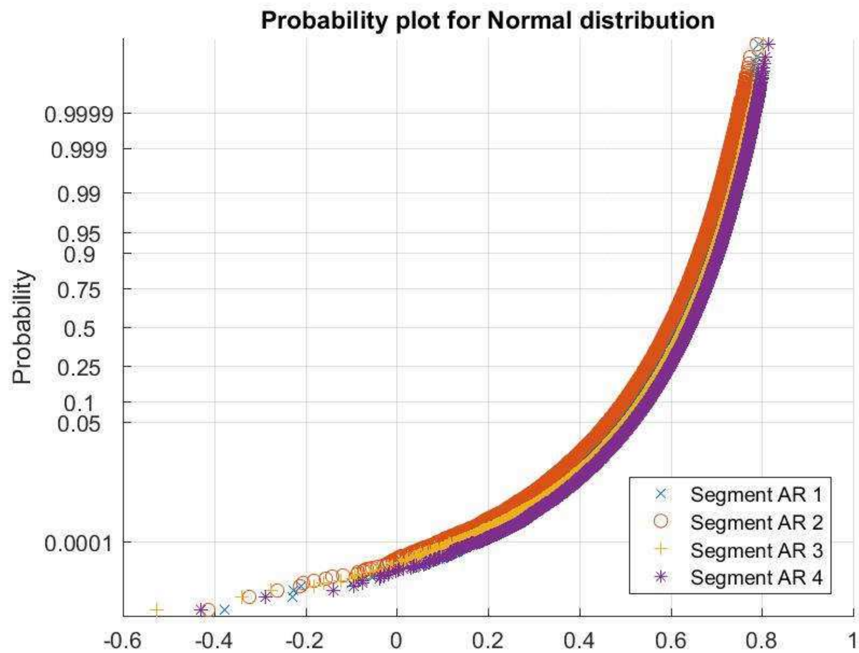

Figure 6.3: Probability plot for normal distribution of *g* for existing cross section properties (load case with maximum compressive force).

The portions related to the following components: axial force $\left(\frac{\bar{P}_u}{\bar{P}_n}\right)$, major bending moment $\left(\frac{\bar{M}_{uy}}{\bar{M}_{ny}}\right)$ and minor bending moment $\left(\frac{\bar{M}_{uz}}{\bar{M}_{nz}}\right)$ were determined for the simulated values of limit state function. These fractions for load cases with maximum compressive force are shown in Figure 6.4, and for maximum major bending moment in Figure 6.5.

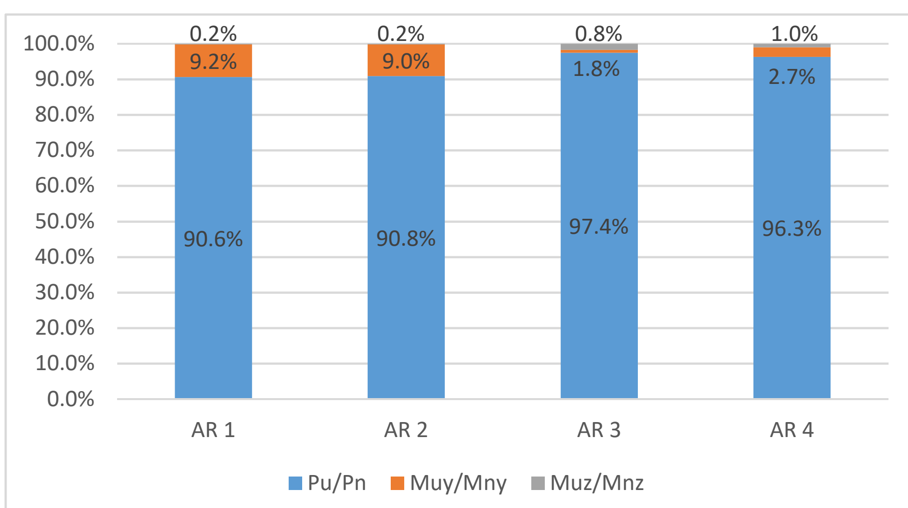

Figure 6.4: Averaged fractions of mean values of the components of limit state function – load cases with maximum compressive force.

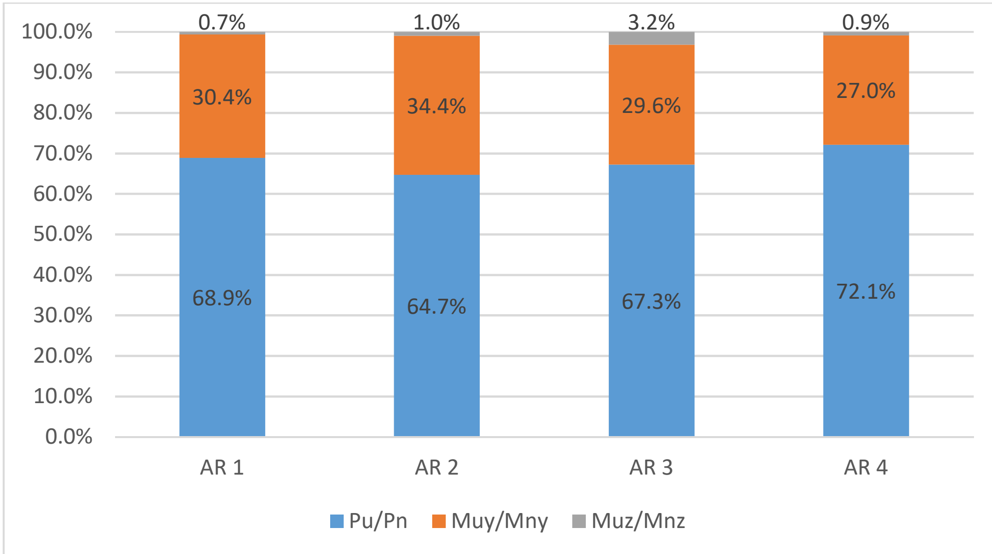

Figure 6.5: Averaged fractions of mean values of the components of limit state function – load cases with maximum major bending moment.

For the load cases with maximum axial force, the average value of the limit state function component $\left(\frac{\bar{P}_u}{\bar{P}_n}\right)$ is around 91% for segments AR 1 and AR 2 and around 97% for segments AR 3 and AR 4, which means that this is definitely the critical portion from the design point of view.

Similarly, for the load cases with maximum bending moment, a fraction of axial force component of the limit state equation $\left(\frac{\bar{P}_u}{\bar{P}_n}\right)$ is also significant (65-72%). In addition, the major bending moment portion $\left(\frac{\bar{M}_{uy}}{\bar{M}_{ny}}\right)$ is an important part of the equation (27-34%) and has to be properly determined to achieve realistic results.

<u>Reliability analysis for the cross sections of the arch determined according to AASHTO Standard Specifications and AASHTO LRFD</u>

To conduct the reliability analysis, the dimensions of the arch cross sections have to be determined according to a specific design code. For the considered steel arch, the structural behavior is idealized by beam-column interaction equations. These equations for AASHTO Standard Spec. and AASHTO LRFD were presented in Section 4.1.1. and Section 4.1.2. of this dissertation, respectively. Each segment of the arch with existing cross section properties was checked to verify if it has sufficient load carrying capacity. Results were plotted and show that every arch segment is safe in accordance with both considered design codes and both load cases (maximum axial force and maximum bending moment). The applied loads and existing cross section dimensions provided the results of interaction equations, which were not equal, but smaller than unity. This difference is called "additional redundancy" by the author of this dissertation. Calculations and plots show that for AASHTO Standard Spec. and AASHTO LRFD, the existing cross sections for each arch segment have 26%-30% and 17%-29% additional redundancy, respectively. To find out what the cross sections would be for each arch segment when the results of interaction equations equal to 1.0, back-calculations have been performed. The summary of the cross section geometry for each design code and comparison with the existing dimensions is presented in Table 6.3. The detailed calculation process of these values is shown in Appendix C.

Table 6.3: Cross section geometry – summary and comparison.

Segment of the arch	Cross section dimension (in)											
	Width of the flanges			Total height			Thickness of the flanges			Thickness of the webs		
	Existing	STD	LRFD	Existing	STD	LRFD	Existing	STD	LRFD	Existing	STD	LRFD
AR 1	58.00	46.00	44.00	62.00	51.5	53.25	2.000	1.75	1.625	1.25	1.00	1.00
AR 2	58.00	46.00	44.00	61.50	51.5	53.25	1.750	1.75	1.625	1.25	1.00	1.00
AR 3	58.00	46.00	44.00	61.25	58.0	55.00	1.625	1.50	1.500	1.25	1.00	1.00
AR 4	58.00	46.00	44.00	61.00	57.0	54.00	1.500	1.50	1.500	1.25	1.00	1.00

The determined cross sectional properties as well as the axial and flexural resistances were used for reliability analysis for two design codes.

The distributions of the simulated values for the considered limit state function (g) for cross section designed according to AASHTO Standard Spec are presented in Figure 6.6 (for load cases with maximum major bending moment) and Figure 6.7 (for maximum compressive force).

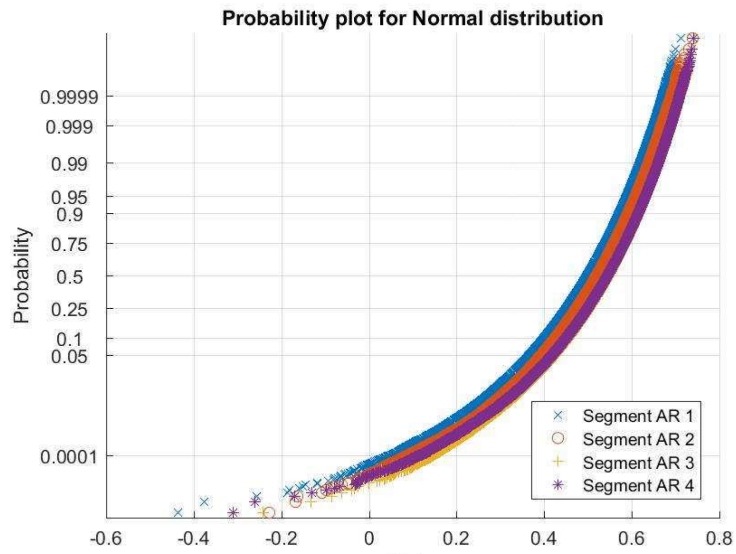

Figure 6.6: Probability plot of normal distribution of *g* values (load case with maximum bending moment) for cross section properties determined according to AASHTO Standard Spec.

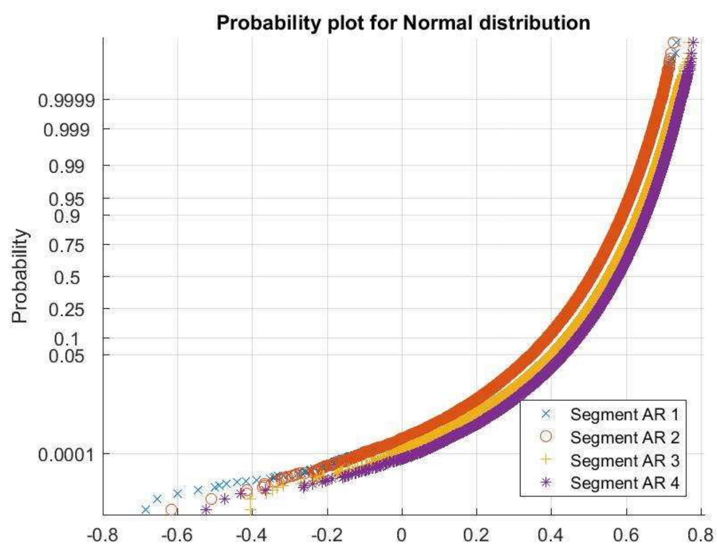

Figure 6.7: Probability plot of normal distribution of *g* values (load case with maximum compressive force) for cross section properties determined according to AASHTO Standard Spec.

The distributions of the simulated values for the considered limit state function (g) for cross section designed according to AASHTO LRFD are presented in Figure 6.8 (for load cases with maximum major bending moment) and Figure 6.9 (for maximum compressive force).

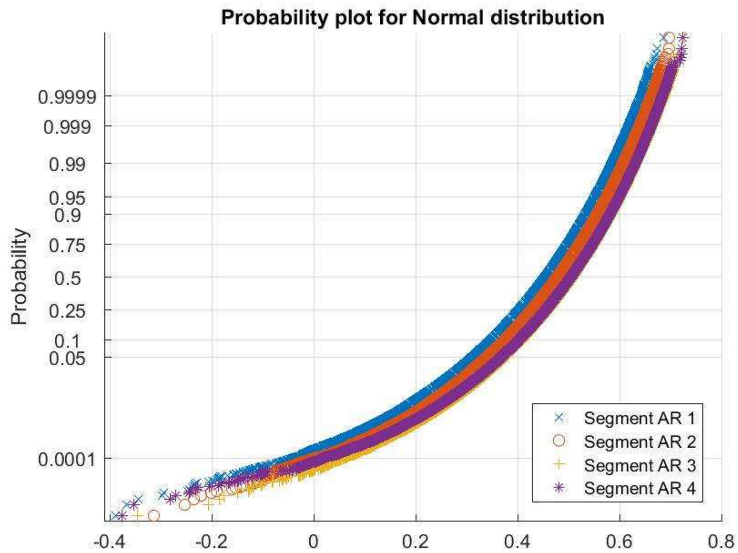

Figure 6.8: Probability plot of normal distribution of *g* values (load case with maximum bending moment) for cross section properties determined according to AASHTO LRFD.

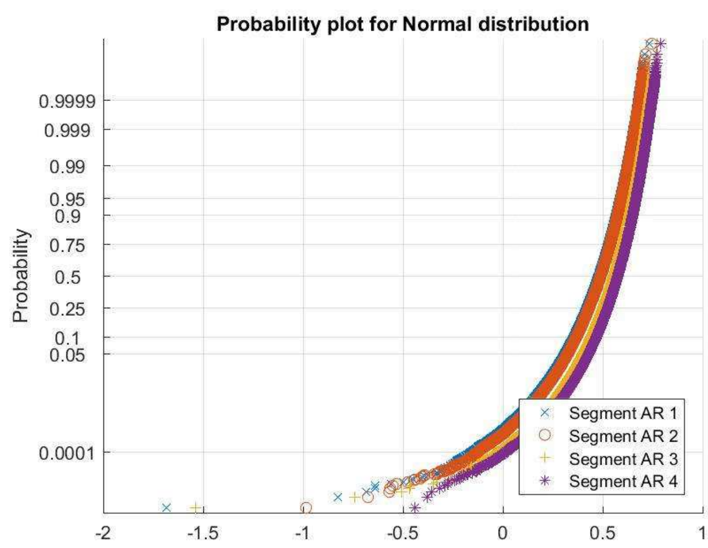

Figure 6.9: Probability plot of normal distribution of *g* values (load case with maximum compressive force) for cross section properties determined according to AASHTO LRFD.

The probability of failure of each segment of the arch was determined using the Monte Carlo simulation technique. The results are presented in Table 6.4.

Table 6.4: Probability of failure for each segment of the arch.

Segment of the arch	Probability of failure					
	Max compressive force			Max bending moment		
	Cross section properties			Cross section properties		
	Existing	STD	LRFD	Existing	STD	LRFD
AR 1	9.77×10^{-6}	2.7×10^{-4}	5.77×10^{-4}	2.56×10^{-6}	6.67×10^{-5}	1.31×10^{-4}
AR 2	2.79×10^{-5}	2.8×10^{-4}	5.57×10^{-4}	3.24×10^{-6}	4.07×10^{-5}	7.84×10^{-5}
AR 3	1.59×10^{-5}	1.47×10^{-4}	2.6×10^{-4}	4.94×10^{-6}	2.91×10^{-5}	5.91×10^{-5}
AR 4	8.54×10^{-6}	6.41×10^{-5}	9.57×10^{-5}	6.5×10^{-6}	2.67×10^{-5}	8.5×10^{-5}

The reliability indices for three approaches are summarized in Table 6.5.

Table 6.5: Reliability indices - summary.

Segment of the arch	Reliability index					
	Max compressive force			Max bending moment		
	Cross section properties			Cross section properties		
	Existing	STD	LRFD	Existing	STD	LRFD
AR 1	4.27	3.46	3.25	4.56	3.82	3.65
AR 2	4.03	3.45	3.26	4.51	3.94	3.78
AR 3	4.16	3.62	3.47	4.42	4.02	3.85
AR 4	4.30	3.83	3.73	4.36	4.04	3.76

The graphical representation of the results for load cases with maximum axial force and maximum bending moment are shown in Figure 6.10 and Figure 6.11, respectively.

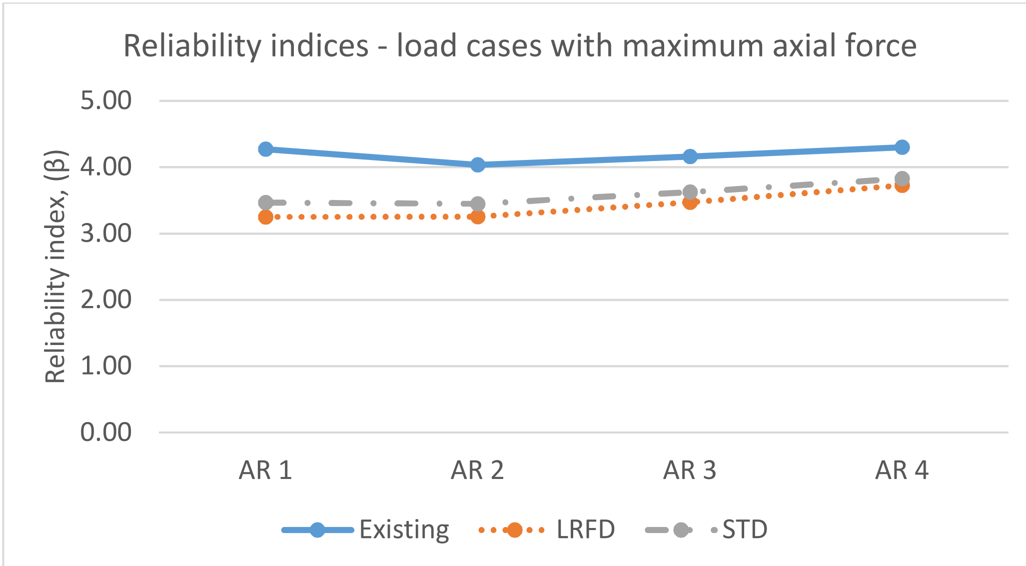

Figure 6.10: Graphical comparison of reliability indices – load cases with maximum axial force.

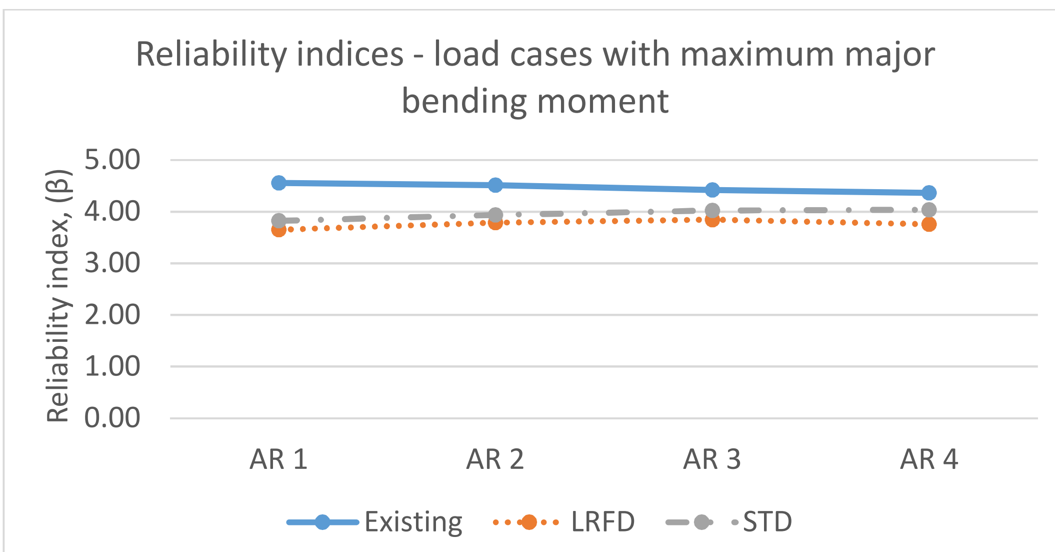

Figure 6.11: Graphical comparison of reliability indices – load cases with maximum major bending moment.

CHAPTER 7 SYSTEM RELIABILITY ANALYSIS OF THE BRIDGE

7.1. SYSTEM RELIABILITY MODELS FOR THE CONSIDERED STRUCTURE

The reliability indices calculated in previous chapter for three different approaches and for two different cases (with maximum compressive force and with maximum major bending moment) are used in system reliability analysis of the arch. Each arch consists of eight segments with four different cross sections. These segments constitute a series reliability system (Figure 7.1).

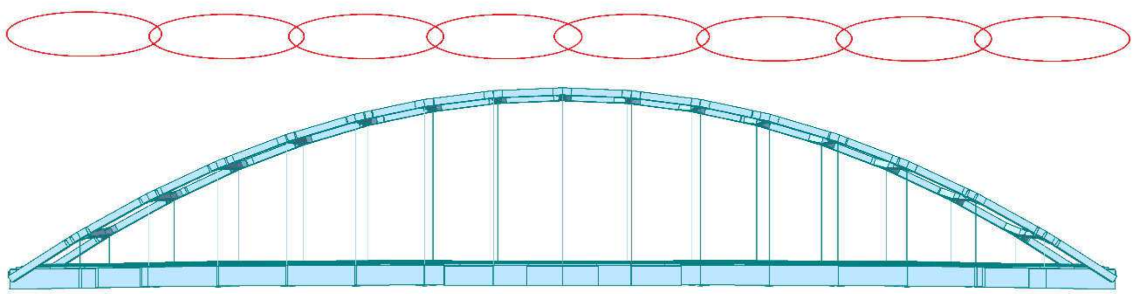

Figure 7.1: Arch bridge – series structural system as an analogy of a chain.

To determine the upper and lower bounds of the probability of failure of the whole system, Equations (2.51), (2.52) and (2.53) were used. The calculated values are presented in Table 7.1.

Table 7.1: Upper and lower bounds for probability of failure.

Probability of failure	Max compressive force			Max bending moment		
	Cross section properties			Cross section properties		
	Existing	STD	LRFD	Existing	STD	LRFD
Lower bound	2.8×10^{-5}	2.80×10^{-4}	5.80×10^{-4}	6.67×10^{-5}	6.50×10^{-6}	1.30×10^{-4}
Upper bound	1.24×10^{-4}	3.27×10^{-4}	2.98×10^{-3}	1.52×10^{-3}	3.45×10^{-5}	7.07×10^{-4}

7.2. EFFECT OF CORRELATION

There is a relationship between given sections of the arch, which in terms of reliability analysis is quantified by the coefficient of correlation (ρ). For structures, like the bridge considered in this research, where material and sections are fabricated by the same manufacturer; it is very likely that coefficient of correlation for section properties (material, geometry) will be close to one. For loads applied to each section, the prediction of value of the coefficient of correlation is difficult because of the randomness of the load (especially live load). For the purpose of this research, the probabilities of failure and reliability indices were calculated and compared for full range of coefficient of correlation (between 0.0 and 1.0) using Equation (7.1) proposed by Stuart (1958):

$$P_f = 1 - \int_{-\infty}^{\infty} \left\{ \Phi \left(\frac{\beta_e + t\sqrt{\rho}}{\sqrt{1-\rho}} \right) \right\}^n \phi(t) dt \tag{7.1}$$

where:

β_e = reliability index for each element,

Φ = standard normal CDF

ϕ = standard normal PDF,

ρ = coefficient of correlation

In Equation (7.1) it is assumed that the reliability indices for each element of the system is constant. For the arch studied in this dissertation, the reliability indices for different segments are very similar, the average value of reliability indices is used as β_e.

7.3. RESULTS OF SYSTEM RELIABILITY ANALYSIS

Using Equation (7.1), values of probability of failure and reliability indices for the whole system with existing cross sections were determined. These values are summarized in Table 7.2.

Table 7.2: System reliability results for different values of coefficient of correlation.

	Maximum compressive force		Maximum major bending moment	
Coefficient of correlation	**Probability of failure**	**Reliability Index**	**Probability of failure**	**Reliability Index**
0.0	$1.1x10^{-4}$	3.69	$3.2x10^{-5}$	3.99
0.2	$1.1x10^{-4}$	3.69	$3.2x10^{-5}$	3.99
0.4	$1.1x10^{-4}$	3.69	$3.2x10^{-5}$	4.00
0.6	$1.0x10^{-4}$	3.71	$3.1x10^{-5}$	4.01
0.8	$8.0x10^{-5}$	3.78	$2.4x10^{-5}$	4.06
1.0	$2.0x10^{-5}$	4.11	$5.2x10^{-6}$	4.41

In addition to the tabulated values, the same results are presented on the charts. On the horizontal axis there are values of coefficient of correlation (ρ), on the vertical axis there are probability of failure (P_{fsys}) and reliability index (β_{sys}) in Figure 7.2 and Figure 7.3, respectively. Subscript "P" means the case with maximum axial force, subscript "M" means the case with maximum major bending moment.

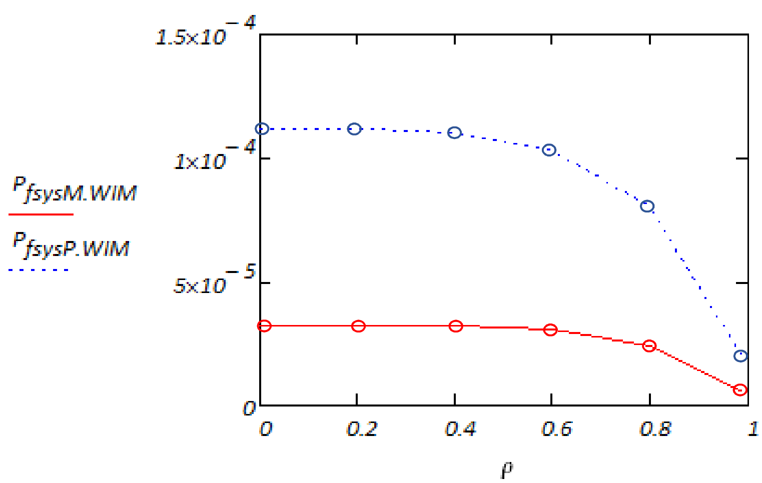

Figure 7.2: Probability of failure for series system with equally correlated elements based on Equation (7.1).

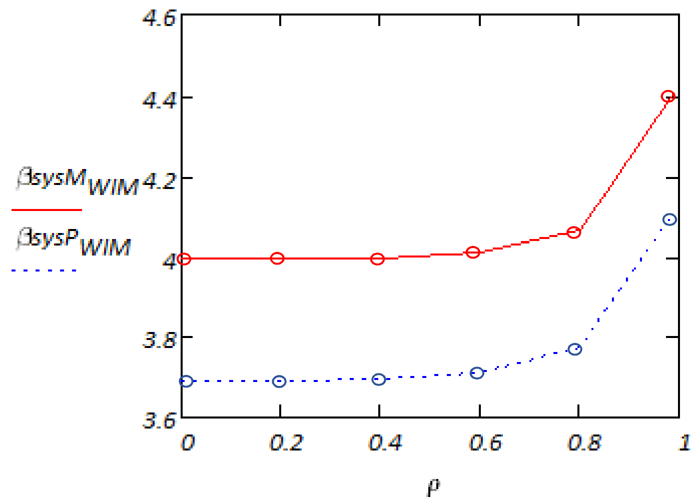

Figure 7.3: Reliability indices for series system with equally correlated elements.

Additionally, the calculated system reliability indices were divided by the average component reliability indices and plotted with respect to the coefficient of correlation. The results are presented in Figure 7.4.

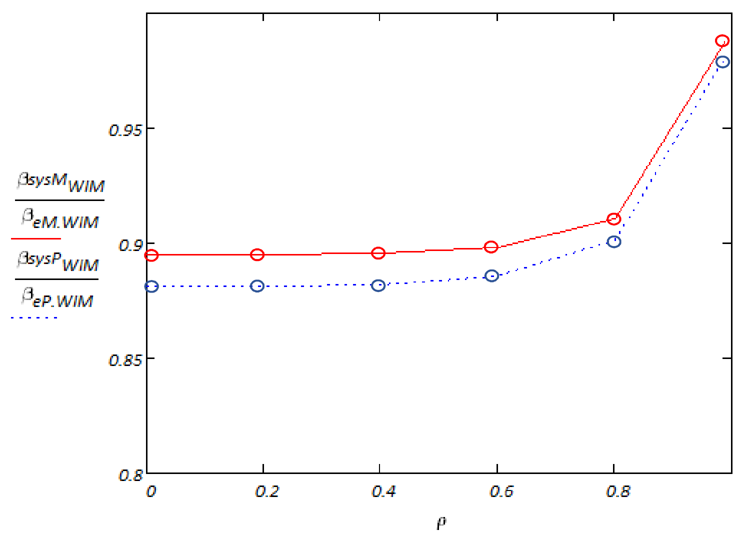

Figure 7.4: Ratio of system and component reliability indices for series system with equally correlated elements.

The same procedure as presented above was conducted for cross sections determined according to AASHTO Standard Spec. and AASHTO LRFD. The obtained results for both approaches are summarized in Table 7.3 and Table 7.4.

Table 7.3: System reliability results for different values of coefficient of correlation – arch designed in accordance with the AASHTO Standard Spec.

	Maximum compressive force		Maximum major bending moment	
Coefficient of correlation	**Probability of failure**	**Reliability Index**	**Probability of failure**	**Reliability Index**
0.0	1.32×10^{-3}	3.01	3.06×10^{-4}	3.43
0.2	1.31×10^{-3}	3.01	3.05×10^{-4}	3.43
0.4	1.27×10^{-3}	3.02	3.00×10^{-4}	3.43
0.6	1.13×10^{-3}	3.05	2.76×10^{-4}	3.46
0.8	8.38×10^{-4}	3.14	2.10×10^{-4}	3.53
1.0	2.72×10^{-4}	3.46	6.55×10^{-5}	3.82

Table 7.4: System reliability results for different values of coefficient of correlation – arch designed in accordance with the AASHTO LRFD.

	Maximum compressive force		Maximum major bending moment	
Coefficient of correlation	**Probability of failure**	**Reliability Index**	**Probability of failure**	**Reliability Index**
0.0	2.43×10^{-3}	2.82	6.80×10^{-4}	3.20
0.2	2.41×10^{-3}	2.82	6.77×10^{-4}	3.20
0.4	2.31×10^{-3}	2.83	6.59×10^{-4}	3.21
0.6	2.03×10^{-3}	2.87	5.97×10^{-4}	3.24
0.8	1.49×10^{-3}	2.97	4.47×10^{-4}	3.32
1.0	4.70×10^{-4}	3.31	1.20×10^{-4}	3.67

The graphical representations of results presented in Table 7.2, Table 7.3 and Table 7.4 are shown in Figure 7.5 and Figure 7.6 for probabilities of failure of the system and system reliability indices, respectively.

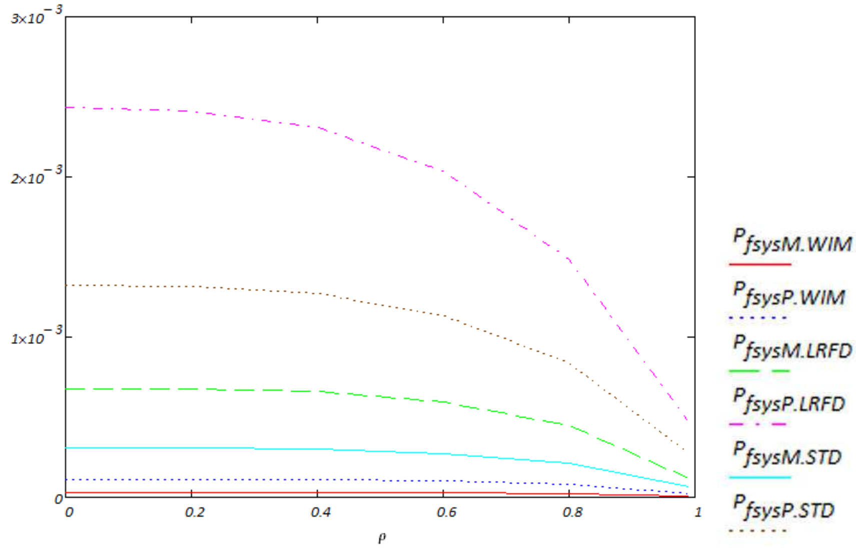

Figure 7.5: Comparison of probability of failure of the system calculated using the Equation (7.1) for existing cross sections and according to two design codes.

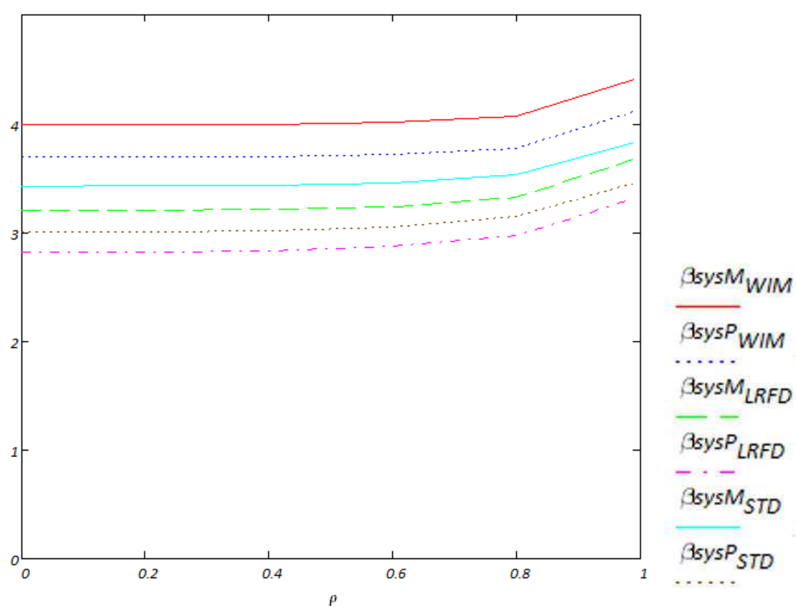

Figure 7.6: Comparison of system reliability indices calculated for existing cross sections and according to two design codes.

System reliability indices were divided by the average component reliability indices for all three calculation approaches are presented in Figure 7.7.

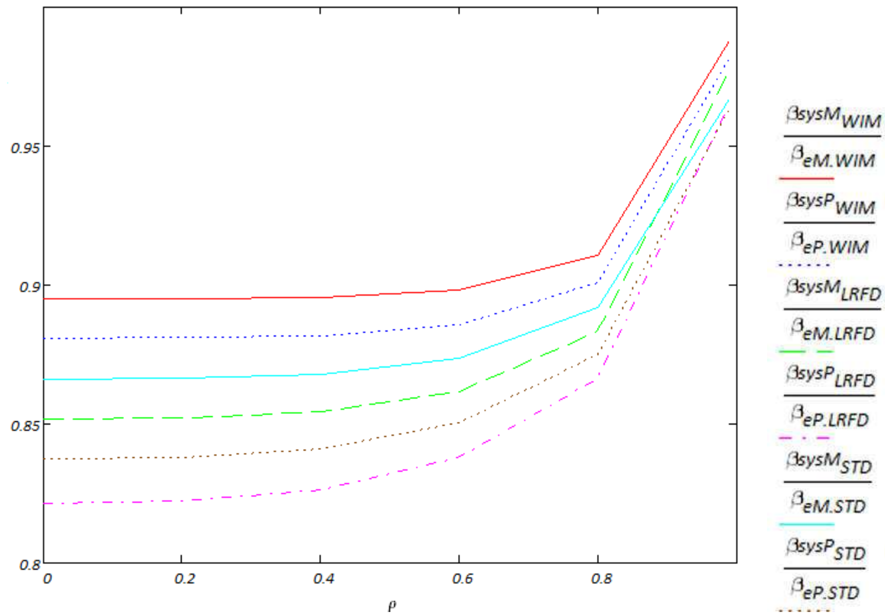

Figure 7.7: Comparison of the ratios of system and element reliability indices for series system with equally correlated elements.

CHAPTER 8 SUMMARY

Introduction.

In this study, the system reliability model for long span steel arch bridges was developed. A representative structure (800-ft long span steel arch bridge) was selected and the Finite Element Method model was created. Three types of analysis were utilized (linear, nonlinear and buckling) to determine maximum values of axial force and bending moment, as well as, buckling resistance of the components. To simulate real live load conditions, Weigh-In-Motion records were used and processed. Equivalent Uniformly Distributed Load for spans between 500 and 1000 ft and statistical parameters for live load model were determined. For comparison purposes, the reliability analysis was performed for two design codes – AASHTO Standard Specification and AASHTO LRFD. The safety of the structure was evaluated using beam-column interaction equations in accordance with provisions from the design codes. For each of three analysis approaches (using existing cross sections, cross sections determined according to AASHTO Standard and cross sections determined according to AASHTO LRFD) reliability analysis was conducted. The limit state functions were formulated and reliability indices were calculated for different segments of the arch using Monte Carlo simulation technique. Series system reliability analysis was performed and lower and upper bounds of probability of failure were defined. In addition, system reliability for different coefficients of correlation between segments of the bridge were determined and compared.

Determination of the equivalent Uniformly Distributed Load using WIM records

The Weigh-In-Motion records collected in 2014, 2015 and 2016 served as a source of data for calculation of the Uniformly Distributed Load (UDL) for the considered structure. Since the maximum UDL values were obtained for the records from 2014, they were used for FEM model and reliability analysis of the bridge. Traffic jam situation of the bridge was assumed with 25-ft distance between last axle of leading vehicle and first axle of following vehicle. Additionally, it was assumed that the right lane is occupied only by heavy trucks, left lane by mixed traffic and middle lane by average of adjacent lanes. Using these assumptions, the equivalent UDL for each lane was determined. For right, middle and left lane, the values of UDL from 2014, were 0.69 kip/ft, 0.61 kip/ft and 0.53 kip/ft respectively. These loads served as input data for one of the live load cases in the FEM model of the bridge. The developed code in Matlab software allows the calculation of equivalent UDL for any WIM station and any span length. Meaning the designer of the bridge, using data from the bridge's WIM station nearby, can determine the live load for real traffic. Then, the designer can create an additional live load case (for example, traffic jam or just regular traffic) in the software and compare values of the forces in the elements. If they are higher than the live load cases created according to design code provisions, then the dimensions of the cross sections should be changed accordingly. It is concluded, that long span bridges require additional site-specific check of local traffic load to make sure that its effects do not exceed the effects caused by live load according to design code provisions.

Finite Element Model of the considered structure.

The FEM model of the bridge was created using Midas Civil Software. Dead load of steel, dead load of concrete and three different live load approaches (using WIM data, according to AASHTO Standard Spec. and according to AASHTO LRFD) were included. The model has been successfully validated by comparing obtained deflections and forces in the cables with those predicted by the designer of the structure. The critical traffic load configurations found for each segment of the arch were converted to static load cases to get results for nonlinear analysis. The two types of results, both for linear and nonlinear analysis were obtained. First, with maximum axial force and corresponding major and minor bending moment. Second, with maximum major bending moment and corresponding axial force and minor bending moment. First and second order effects were compared for each segment of the arch. Differences of the values of major bending moment do not exceed 1.3%. In addition to that, for each segment of the arch, the buckling analysis using dead load of steel, dead load of concrete and critical live load configuration load cases were performed. The load multipliers given by the software for first buckling mode were applied, thus the buckling force for each segment of the arch was found. These forces, together with results of nonlinear analysis (axial forces and bending moments in two directions) were utilized in the interaction equations checks and reliability analysis. Using the output from the FEM model and provisions from two design codes (assuming interaction equations equal to 1.0), the dimensions of the cross sections were determined.

Reliability analysis of the segments of the arch.

For each segment of the arch, the reliability analysis was conducted. Two types of load cases were used (with maximum axial force and corresponding bending moments and with maximum major axis bending moment and corresponding axial force and minor axis bending moment). Dead load of steel, dead load of concrete and live load determined using WIM database together with their statistical parameters were implemented. For resistance model, statistical parameters for beam-columns were used. A combined axial force and bending moment interaction equation, without any load and resistance factors, served as limit state function. Firstly, the reliability analysis was conducted for the existing cross sections of each segment of the arch. The reliability indices were calculated using Monte Carlo simulation technique. Secondly, the reliability analysis was repeated for determined cross sections according to the design codes, using corresponding compressive and flexural resistances and the same loads as for existing cross sections. The obtained reliability indices for AASHTO Standard Spec. and AASHTO LRFD were compared with those for current cross sections.

The reliability analysis results are as follows:

1) *Existing cross sections:*

For load cases with maximum axial force, the calculated values of β_e are from 4.0 to 4.3, and for load cases with maximum major bending moment they are from 4.4 to 4.6.

2) *Cross sections determined according to AASHTO Standard Spec.:*

For load cases with maximum axial force, the calculated values of β_e are from 3.5 to 3.8, and for load cases with maximum major bending moment they are from 3.8 to 4.0.

3) *Cross sections determined according to AASHTO LRFD:*

For load cases with maximum axial force, the calculated values of β_e are from 3.3 to 3.7, and for load cases with maximum major bending moment they are from 3.7 to 3.9.

The results, summarized above, confirmed that each segment of the existing arch is safe from a structural point of view and even has additional redundancy. Furthermore, the reliability indices obtained for AASHTO Standard Spec. are slightly higher than those for AASHTO LRFD, meaning the considered arch is theoretically more reliable when designed according to the older design code. The values of reliability indices for segments of the arch were implemented in the system reliability analysis.

System reliability analysis.

The arch in the considered structure is symmetrical about the vertical axis at mid-span and consists of eight segments with four different cross sections. Using the reliability indices calculated for each and the fact that together they form a series system, the system reliability analysis was conducted. Upper and lower bounds of the probability of failure were calculated. Furthermore, the effect of correlation between segments of the arch was examined. The system reliability analysis conducted for two types of load cases (with maximum axial force and corresponding bending moments and with maximum major bending moment and corresponding axial force and minor bending moment) and repeated for existing cross sections and those determined by the design codes.

The system reliability analysis results are as follows:

1) *Existing cross sections:*

For load cases with maximum axial force, the calculated values of β_{sys} are from 3.7 to 4.1, and for load cases with maximum major bending moment they are from 4.0 to 4.4, depending on the coefficient of correlation.

2) *Cross sections determined according to AASHTO Standard Spec.:*

For load cases with maximum axial force, the calculated values of β_{sys} are from 3.0 to 3.5, and for load cases with maximum major bending moment they are from 3.4 to 3.8, depending on the coefficient of correlation.

3) *Cross sections determined according to AASHTO LRFD:*

For load cases with maximum axial force, the calculated values of β_{sys} are from 2.8 to 3.3, and for load cases with maximum major bending moment they are from 3.2 to 3.7, depending on the coefficient of correlation.

The system reliability analysis proved the structure is safe and provided additional comparable results of the safety margin for the two design codes. Since the elements of the existing arch were fabricated in the same factory and were erected by the same contractor, it is very possible that the coefficient of correlation for the considered bridge is closer to 1.0, than 0.0. This observation allows the reader to treat higher values of the obtained reliability indices as closer to actual values. However, even the results obtained for coefficient of correlation equal to zero, which are based on the extremely conservative assumption, provide sufficient level of the structural safety.

CHAPTER 9 CONCLUSIONS

The main findings and conclusions are as follows:

1. Reliability indices calculated for cross sections determined according to provisions from AASHTO Standard Spec. are on average 5% higher than those for AASHTO LRFD. It means that the design consistent with AASHTO Standard Spec. is theoretically safer than according to AASHTO LRFD.
2. The existing structure, depending on the load case and segment of the arch, has up to 30% larger carrying capacity than this required by the design codes.
3. For almost all segments and all load cases the reliability indices are larger than 3.5. This value is used as target reliability for the design, so it means that the considered structure would be structurally sufficient even with smaller cross sections.
4. For the first two segments of the arch with cross sections determined according to AASHTO LRFD, the values of reliability indices are about 3.3, with regards to load cases with maximum axial force and corresponding bending moments. It means that for these situations, code provisions do not provide target safety and should be additionally checked and possibly recalibrated.
5. In the system reliability analysis, the effect of correlation was negligible. Even for the values of coefficient of correlation close to zero, which is a conservative assumption, the system reliability index is above 4.0.
6. System reliability indices for the arch designed using AASHTO Standard Spec. and AASHTO LRFD are smaller than these calculated for the existing system. The average differences are 16% and 21%, respectively.
7. Live load effect for long span bridges is strongly site-specific. Therefore, it is necessary to collect local traffic data to include in the analysis and design of such structures.
8. The developed code to process the WIM data and determine equivalent uniformly distributed load can be used for any WIM dataset and any span length.
9. For the considered structure, axial forces for critical real traffic load cases were slightly higher than these obtained for live load cases according to code provisions.

10. For load cases with maximum axial force and corresponding bending moments, dead load is a dominating effect (up to 68% of total load).
11. For load cases with maximum major bending moment and corresponding axial force and minor bending moment, dead load is a dominating effect for compression (up to 83% of total load), but live load is a dominating effect for flexure (up to 88% of total load).
12. For the considered bridge, Dead Load to Live Load ratio is about 2.0 for the axial force. For bending moment this ratio is between 0.04 and 0.37.
13. The results obtained from the Finite Element Model of the bridge show small differences between first and second order effects (less than 1.3%).

CHAPTER 10 RECOMMENDATIONS AND FUTURE RESEARCH

1. It is recommended to verify the presented analytic results by Non-Destructive Methods. NDT can be a valuable source of data including material parameters and condition, actual deflections, stresses and strains of the structural elements. They can also provide information about the level of deterioration or corrosion, which is necessary for proper rating of the whole structure.
2. The statistical parameters of materials such as concrete or steel can be verified by lab testing.
3. It is recommended to extend the reliability analysis to cover other components including cables and tie girders.
4. The simulation of the traffic load on the long span bridge is a complex task. In this dissertation, traffic jam situation was considered as a critical live load configuration. Future research can help to verify the filtering criteria and site-specific multiple presence factors for the traffic.
5. The reliability-based methodology utilized in this dissertation can be applied to other similar structures.
6. This research will be continued to consider other long span arch bridges. Since not many similar analyses were conducted in the past, it would be valuable to examine such structures, calculate their system reliability and compare with results presented in this dissertation.

REFERENCES

1) 14^{th} Edition AISC Steel Construction Manual. (2013).
2) *A Guide to Important National Bridge Inventory Terms*, (2018) Retrieved January 15, 2018, from: http://nationalbridges.com/guide-to-ratings
3) AASHTO *LRFD Bridge Design Specifications.* (2012). American Association of StateHighway Transportation Officials, Washington, D.C.
4) AASHTO *Standard Specifications for Highway Bridges.* (2002). American Association of State Highway Transportation Officials, Washington, D.C.
5) Ang A. H-S. and Tang W.H. (1984). *Probability Concepts in Engineering Planning and Design.* Volume II: Decision, Risk, and Reliability, John Wiley & Sons, New York.
6) ASTM E1318-09. (2009). *Standard Specification for Highway Weigh-In-Motion (WIM) Systems with User Requirements and Test Methods*, ASTM International, West Conshohocken, PA.
7) Bruneau M. (1992). *Evaluation of system-reliability methods for cable-stayed bridge design* ASCE *is part of the* Journal of Structural Engineering, *Vol. 118, No. 4, April, 1992. ©ASCE, ISSN 0733-9445/92/0004-1106/$1.00 + $.15 per page. Paper No. 872.*
8) Caprani C. C., OBrien E. J., Lipari A. (2016). *Long-span bridge traffic loading based on multi-lane traffic micro-simulation,* Engineering Structures 115 207–219
9) Chen K., Nakamura S., Nishikawa T. and Wu Q. (2012). *Reliability estimation of an CFST arch bridge by static loading test according to Chinese code*, International Conference on Renewable Energy Research and Applications (ICRERA)*, Nagasaki, 2012, pp. 1-6.*
10) Cheng J. and Li Q.S. (2009). *Reliability analysis of long span steel arch bridges against wind-induced stability failure,* Journal of Wind Engineering and Industrial Aerodynamics 97 (2009) 132–139
11) Cornell C. A. (1967). *Bounds on the Reliability of Structural Systems,* Journal of the Structural Division, ASCE, 93 (ST1), 171-200,1967

12) Czarnecki A. A. (2006). *System Reliability Models for Evaluation of Corroded Steel Girder Bridges*.

13) Czarnecki A. A., Nowak A.S., Pandey M. et al (2006) *System reliability assessment of steel girder bridges* Advances in Engineering Structures, Mechanics & Construction, *699–710*.

14) Ditlevsen O. (1982). *System Reliability Bounding by Conditioning,* Journal of Engineering Mechanics Division, ASCE, Vol. 108.

15) Ditlevsen O. and Madsen H.O. (1986). *Structural Reliability Methods,* John Wiley & Sons Inc., New York.

16) Ellingwood B., Galambos T. V., MacGregor J. G. ,and Cornell C. A. (1980). *Development of a Probability-Based Load Criterion for American National Standard A58*, NBS Special Publication 577, National Bureau of Standards, Washington, DC

17) Ellingwood B., MacGregor J.G., Galambos T.V., and Cornell, C.A. (1982). *Probability Based Load Criteria: Load factors and Load Combinations,* Journal of Structural Engineering, ASCE, Vol. 108, No. ST5.

18) Estes A. C. and Frangopol D. M. (2001). *Bridge lifetime system reliability under multiple limit states*

19) Galambos T.V. (1981). *Load and Resistance Factor Design*, Engineering Journal / American Institute of Steel Construction, Third Quarter 1981.

20) Galambos T.V., and Ravindra M.K. (1978). *Load and Resistance Factor Design,* Journal of Structural Division, ASCE, ST9, Proc. Paper 14008, Sep. 1978.

21) Galambos T.V., and Ravindra M.K. (1978). *Load and Resistance Factor Design,* Journal of Structural Division, ASCE, ST9, Proc. Paper 14008, Sep. 1978

22) Ghosn M., and Moses F. (1984). *Bridge Load Modeling and Reliability Analysis,* Report No. R 84-1, Department of Civil Engineering, Case Western Reserve University.

23) Ghosn M., and Moses F. (1998). *Redundancy in Highway Bridge Superstructures,* NCHR Report 406. Transportation Research Board, Washington, D.C.

24) Gonçalves G., Barros R.C. and Cesar M.B. (2009). *Geometric and material nonlinear analyses of imperfect circular hollow section (CHS) columns: Steel tubes and concrete filled tubes.,* 3rd International Conference on Integrity, Reliability and Failure, Porto/Portugal, 20-24 July 2009.

25) Hallenbeck, M. and Weinblatt, H. (2004). *Equipment for Collecting Traffic Load Data*, Report 509, Transportation Research Board, National Cooperative Highway Research Program, Washington, DC.

http://en.midasuser.com/product/civil_overview.asp and http://manual.midasuser.com/EN_TW/Civil/830/whnjs.htm

http://www3.fi.mdp.edu.ar/quimicafisica/Manual%20Mathcad/Mathcad%20manual%202000i%20(st).pdf

https://www.mathworks.com/matlabcentral/

26) Li L., Wu T., He X., Hao J., Wang H. and Xu H. (2018). *Reliability Evaluation of Vortex-Induced Vibration for a Long-Span Arch Bridge,* Journal of Bridge Engineering, 2018, 23(5): 05018002.

27) Liu Y. and Moses F. (1991). *Bridge design with reserve and residual reliability constraints* Structural Safety, *11 (1991) 29-42*

28) LTBP Program's Literature Review on Weigh-in-Motion Systems, (2016, June). Publication No. FHWA-HRT-16-024

29) Lutomirska M. (2009). *Live Load Models for Long Span Bridges.*

30) *Major overhaul to begin on 35 year-old delta bridge* by Hal Scheurich, FOX10 News Reporter, (February 23, 2015), Retrieved January 15, 2018 from: http://www.fox10tv.com/story/28180795/major-overhaul-to-begin-on-35-year-old-delta-bridge

31) *Map of Alabama Permanent Traffic Recorders*, Retrieved January 20, 2018, from: http://www.dot.state.al.us/tpmpweb/dcdm/pdf/trafficMonitoring/ATRLocationMap32008.pdf

32) *Mathcad software user manual*, Retrieved January 15, 2018, from:

33) *Matlab software user manuals*, Retrieved January 15, 2018, from: https://www.mathworks.com/help/matlab/

34) *Midas Civil software user manuals*, Retrieved December 12, 2017, from:

35) Moses F. (1982). *System reliability developments in structural engineering*, Structural Safety, *1 (1982)3-13, Scientific Publishing Company, Amsterdam*

36) *National Bridge Inventory Data* (2018), Retrieved January 15, 2018, from: http://bridgereports.com/

37) Norman, O.K. and Hopkins, R.C. (1952). Weighing Vehicles in Motion, *Highway Research Board Bulletin, Issue 50, Highway Research Board*.

38) Nowak A. S., Collins K. R., (2013) *Reliability of Structures*, Second Edition, Taylor & Francis.

39) Nowak A. S., Szerszen M. M. (2000). *Structural reliability as applied to highway bridges*, *USA* Prog. Struct. Engng Mater.; *2*:218d224

40) Nowak A. S., Zhou J. (1990). *System reliability models for bridges.* Structural Safety*,* 7 (1990) 247-254.

41) Nowak A.S. (1999). *Calibration of LRFD Bridge Design Code,* NCHRP Report 368, Transportation Research Council, Washington, D.C.,

42) Nowak A.S. (2004). *System reliability models for bridge structures*. Bulletin of the Polish Academy of Technical Sciences, Vol. 52, No. 4, 2004

43) Nowak A.S. and Cho T. (2007). *Prediction of the combination of failure modes for an arch bridge system,* Journal of Constructional Steel Research 63 (2007). 1561–1569.

44) Nowak A.S. and Stallings J.M. (2018). *Application of WIM and Permit Data,* ongoing research project for the Alabama Department of Transportation, Montgomery, Alabama.

45) Nowak A.S. and Tharmabala T. (1998). *Bridge Reliability Evaluation using Load Tests,* Journal of Structural Engineering, ASCE, Vol. 114, No. 10, pp. 2268-2279, October 1988.

46) Nowak A.S., and Lind N.D. (1979). *Practical Bridge Code Calibration,* Journal of

Structural Division, ASCE, pp. 2497-2510, December 1979.

47) *Numerical Methods for Nonlinear Analysis*, Retrieved March 5, 2018 from: http://www.nidaeurope.com/free-guides/38-numerical-methods-for-nonlinear-analysis

48) Rackwitz R. (1976). *Practical Probabilistic Approach to Design,* Bulletin 112, Comite European du Beton, Paris, France.

49) Rønnquist A., Naess A. (2017). *Global Buckling Reliability Analysis of Slender Network Arch Bridges: An Application of Monte Carlo-Based Estimation by Optimized Fitting.* In: Gardoni P. (eds) Risk and Reliability Analysis: Theory and Applications. Springer Series in Reliability Engineering. Springer, Cham

50) Stuart A.J. (1958). *Equally correlated variates and the multinormal integral* Journal of the Royal Statistical SocietyVolume 20, Pages 373-378

51) Tabsh S.W. and Nowak A.S. (1991). *Reliability of Highway Girder Bridges,* Journal of Structural Engineering, ASCE, Vol. 117, No. 8, August 1991.

52) Tang Z., Hu X., Xie X. (2013). *The stability behavior of thin-walled steel box arch bridges,* Conference Paper.

53) *The General W.K. Wilson Jr. Bridge aka the Dolly Parton* Bridge – video Retrieved December 12, 2017, from: https://www.youtube.com/watch?v=LjtkE5WLjys

54) Thoft-Christensen, P. and Baker M.J. (1982). *Structural Reliability Theory and Its Applications,* Springer-Verlag, New York, New York.

55) Wu J. (2010). *Reliability-based lifetime performance analysis of long-span bridges*.

56) Zhang, L. (2007). *An Evaluation of the Technical and Economic Performance of Weigh-in-Motion Sensing Technology*, Master's Thesis, University of Waterloo, Ontario, Canada, 2007, obtained from: tps://uwspace.uwaterloo.ca/bitstream/handle/10012/3219/Thesis%20final.pdf?sequence=1, last accessed December 29, 2015.

57) Ziemian R.D. (2010). *Guide to Stability Design Criteria for Metal Structures, Sixth Edition, Copyright © 2010 John Wiley & Sons, Inc.*

APPENDIX A

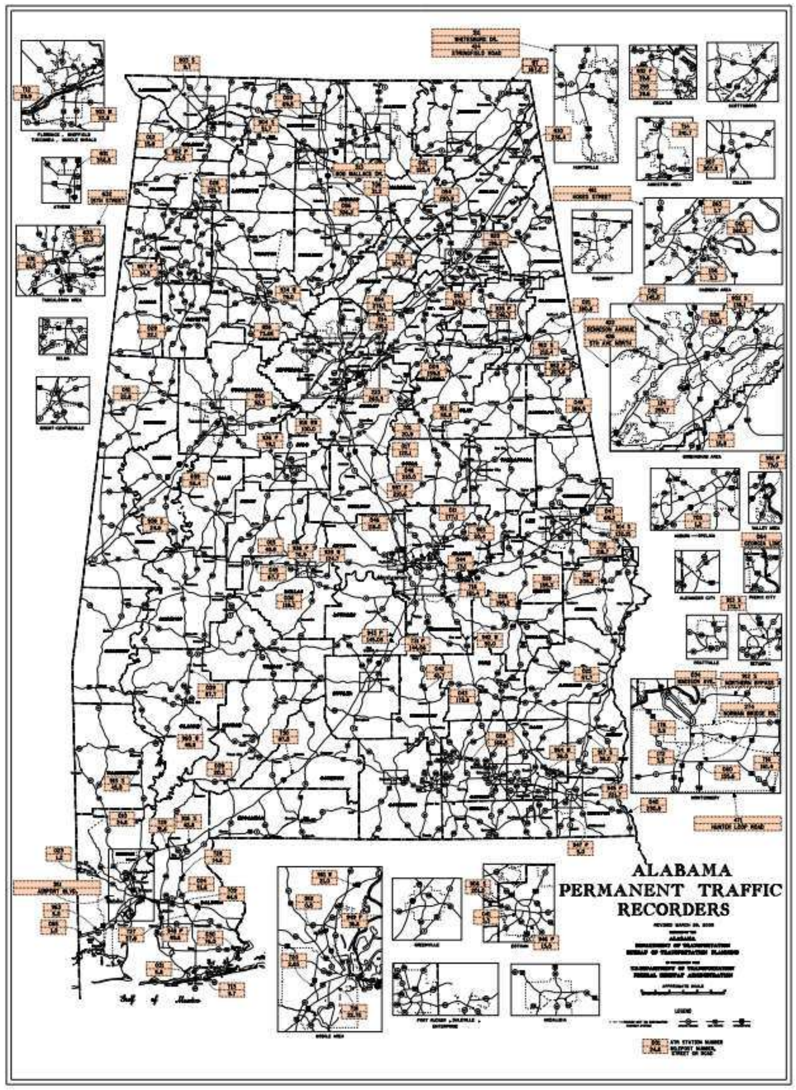

Figure A- 1. Map of Alabama Permanent Traffic Recorders.

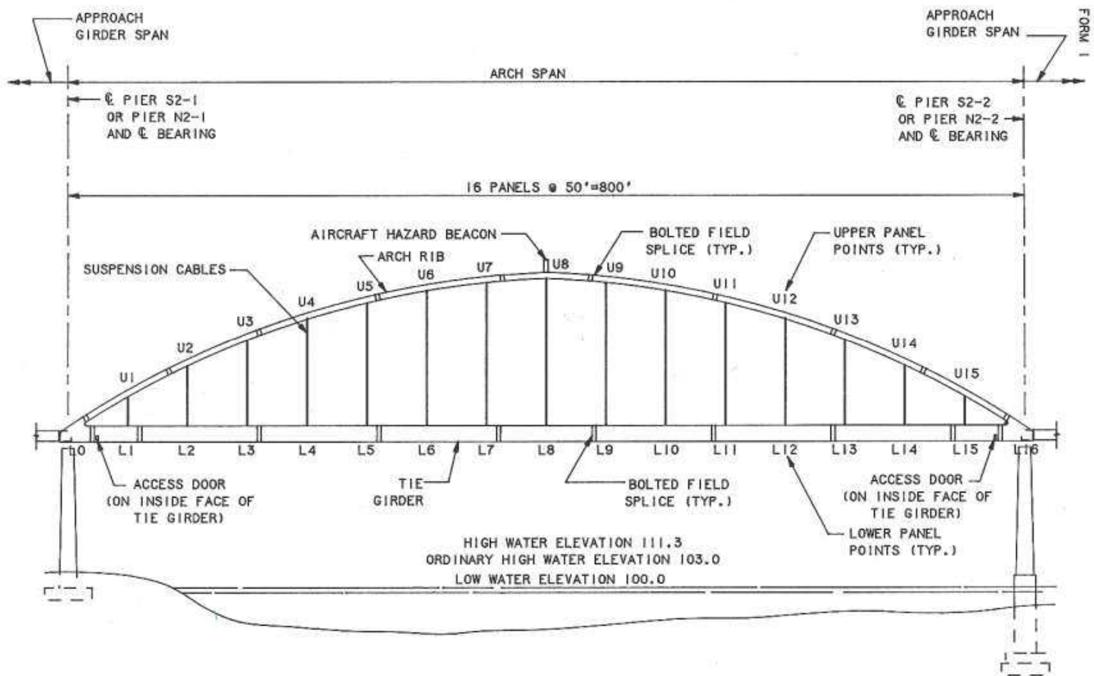

Figure A- 2. Elevation of the bridge - looking North (I-65 over Mobile River Bridge Inspection Manual).

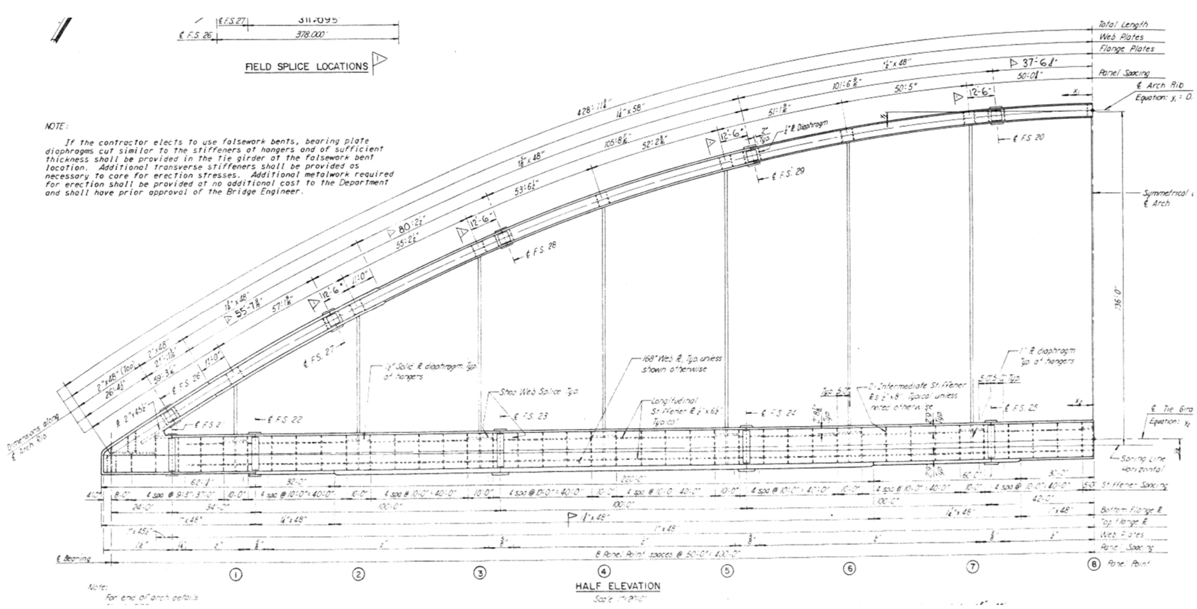

Figure A- 3. Half elevation (I-65 over Mobile River Bridge Inspection Manual).

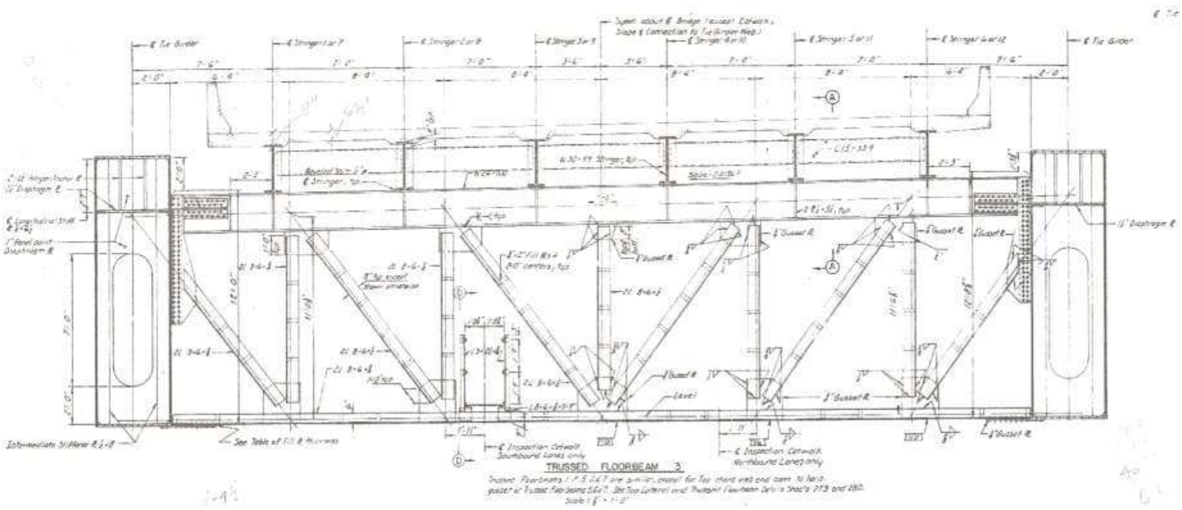

Figure A- 4. Typical trussed floorbeam (I-65 over Mobile River Bridge Inspection Manual).

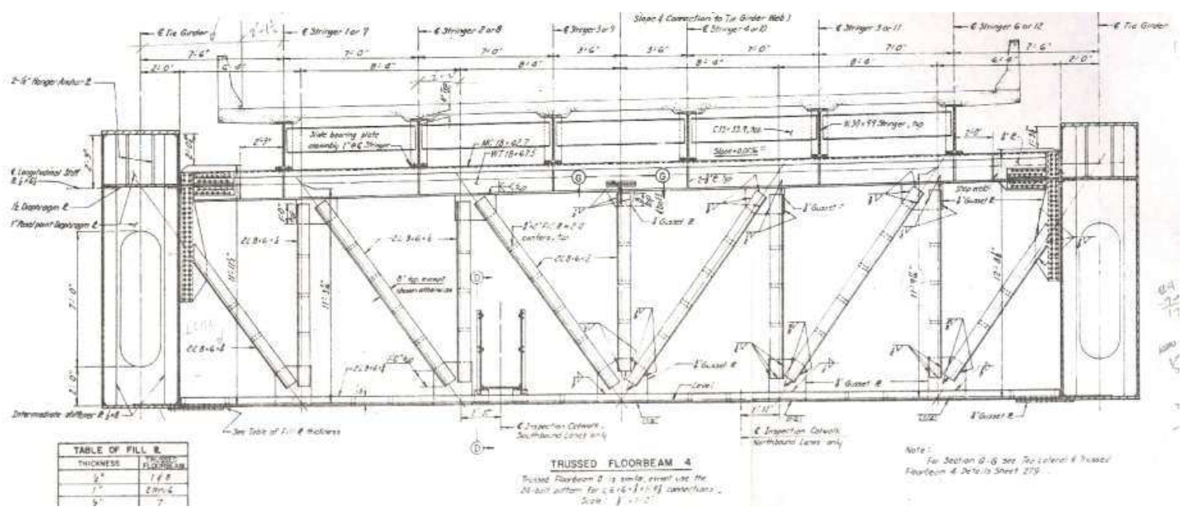

Figure A- 5. Trussed floorbeam at extension joints (I-65 over Mobile River Bridge Inspection Manual).

APPENDIX B

Table B - 1. Summary of linear analysis results – load cases with maximum axial force, (kip).

		Load cases with maximum axial force				
		DLS	DLC	LL	Total	DL/LL
AR 1	LRFD	-2384	-1581	-1991	-5956	199%
AR 1	STD	-2384	-1581	-2062	-6027	192%
AR 1	WIM	-2380	-1579	-2082	-6041	190%
AR 2	LRFD	-2384	-1581	-1991	-5956	199%
AR 2	STD	-2384	-1581	-2062	-6027	192%
AR 2	WIM	-2380	-1579	-2082	-6041	190%
AR 3	LRFD	-2244	-1480	-1850	-5573	201%
AR 3	STD	-2244	-1480	-1915	-5638	194%
AR 3	WIM	-2240	-1478	-1942	-5660	191%
AR 4	LRFD	-2073	-1370	-1712	-5155	201%
AR 4	STD	-2073	-1370	-1772	-5215	194%
AR 4	WIM	-2070	-1369	-1789	-5229	192%

Table B - 2. Summary of linear analysis results – load cases with maximum major bending moment (kip*ft).

		Load cases with maximum major bending moment				
		DLS	DLC	LL	Total	DL/LL
AR 1	LRFD	442	291	2372	3105	31%
AR 1	STD	442	291	2163	2896	34%
AR 1	WIM	442	291	2037	2770	36%
AR 2	LRFD	269	105	3298	3671	11%
AR 2	STD	269	105	2977	3350	13%
AR 2	WIM	269	105	2825	3198	13%
AR 3	LRFD	269	105	3298	3671	11%
AR 3	STD	269	105	2977	3350	13%
AR 3	WIM	269	105	2825	3198	13%
AR 4	LRFD	-1	110	2662	2771	4%
AR 4	STD	-1	110	2479	2589	4%
AR 4	WIM	-1	110	2362	2471	5%

Table B - 3. Summary of nonlinear analysis results – load cases with maximum axial force (kip).

		Load cases with maximum axial force				
		DLS	DLC	LL	Total	DL/LL
AR 1	LRFD	-2381	-1580	-1990	-5951	199%
AR 1	STD	-2381	-1580	-2061	-6022	192%
AR 1	WIM	-2377	-1578	-2083	-6038	190%
AR 2	LRFD	-2381	-1580	-1990	-5951	199%
AR 2	STD	-2381	-1580	-2061	-6022	192%
AR 2	WIM	-2377	-1578	-2083	-6038	190%
AR 3	LRFD	-2243	-1479	-1848	-5570	201%
AR 3	STD	-2243	-1479	-1913	-5634	195%
AR 3	WIM	-2239	-1478	-1942	-5659	191%
AR 4	LRFD	-2074	-1370	-1709	-5152	202%
AR 4	STD	-2074	-1370	-1769	-5212	195%
AR 4	WIM	-2070	-1369	-1787	-5226	192%

Table B - 4. Summary of nonlinear analysis results – load cases with maximum major bending moment (kip*ft).

		Load cases with maximum major bending moment				
		DLS	DLC	LL	Total	DL/LL
AR 1	LRFD	456	298	2389	3142	32%
AR 1	STD	456	298	2179	2933	35%
AR 1	WIM	456	298	2051	2805	37%
AR 2	LRFD	278	106	3325	3709	12%
AR 2	STD	278	106	3001	3385	13%
AR 2	WIM	278	106	2847	3231	13%
AR 3	LRFD	278	106	3325	3709	12%
AR 3	STD	278	106	3001	3385	13%
AR 3	WIM	278	106	2847	3231	13%
AR 4	LRFD	-7	108	2681	2782	4%
AR 4	STD	-7	108	2497	2598	4%
AR 4	WIM	-7	108	2377	2479	4%

Table B - 5. Summary fractions of DLS, DLC and LL for nonlinear analysis.

	Axial force			Major bending moment			Minor bending moment		
Load case and segment	DLS	DLC	LL	DLS	DLC	LL	DLS	DLC	LL
AR 1 My LRFD	50.6%	33.6%	15.9%	14.5%	9.5%	76.0%	63.9%	15.3%	20.8%
AR 1 Fx LRFD	40.0%	26.5%	33.4%	52.0%	34.4%	13.6%	67.1%	28.8%	4.1%
AR 1 My STD	50.3%	33.4%	16.3%	15.5%	10.2%	74.3%	67.1%	16.1%	16.8%
AR 1 Fx STD	39.5%	26.2%	34.2%	47.1%	31.2%	21.7%	64.5%	27.6%	7.9%
AR 1 My WIM	50.7%	33.7%	15.6%	16.2%	10.6%	73.1%	73.4%	17.6%	9.0%
AR 1 Fx WIM	39.4%	26.1%	34.5%	56.2%	37.0%	6.8%	37.7%	16.6%	45.7%
AR 2 My LRFD	51.1%	33.7%	15.2%	7.5%	2.9%	89.6%	51.2%	39.6%	9.2%
AR 2 Fx LRFD	40.0%	26.5%	33.4%	52.0%	34.4%	13.7%	67.2%	28.7%	4.2%
AR 2 My STD	51.6%	34.0%	14.4%	8.2%	3.1%	88.7%	53.2%	41.2%	5.6%
AR 2 Fx STD	39.5%	26.2%	34.2%	47.1%	31.2%	21.7%	64.6%	27.6%	7.9%
AR 2 My WIM	52.0%	34.3%	13.7%	8.6%	3.3%	88.1%	49.9%	38.6%	11.5%
AR 2 Fx WIM	39.4%	26.1%	34.5%	56.2%	37.0%	6.8%	37.8%	16.5%	45.6%
AR 3 My LRFD	51.1%	33.7%	15.2%	7.5%	2.9%	89.6%	51.1%	39.6%	9.3%
AR 3 Fx LRFD	40.3%	26.6%	33.2%	35.0%	13.8%	51.3%	44.0%	39.0%	17.0%
AR 3 My STD	51.6%	34.0%	14.4%	8.2%	3.1%	88.7%	53.3%	41.2%	5.5%
AR 3 Fx STD	39.8%	26.2%	33.9%	41.3%	16.2%	42.5%	42.8%	38.0%	19.2%
AR 3 My WIM	52.0%	34.3%	13.7%	8.6%	3.3%	88.1%	50.0%	38.7%	11.3%
AR 3 Fx WIM	39.6%	26.1%	34.3%	34.2%	13.4%	52.5%	49.7%	43.6%	6.6%
AR 4 My LRFD	44.4%	29.4%	26.2%	0.2%	3.9%	95.9%	60.7%	29.9%	9.4%
AR 4 Fx LRFD	40.2%	26.6%	33.2%	22.1%	13.1%	64.9%	56.8%	40.1%	3.1%
AR 4 My STD	44.5%	29.5%	26.0%	0.3%	4.1%	95.6%	60.3%	29.7%	10.0%
AR 4 Fx STD	39.8%	26.3%	33.9%	20.7%	12.3%	67.0%	55.1%	39.0%	5.9%
AR 4 My WIM	45.1%	29.8%	25.1%	0.3%	4.3%	95.4%	56.7%	27.9%	15.4%
AR 4 Fx WIM	39.6%	26.2%	34.2%	23.3%	13.8%	62.8%	54.1%	37.8%	8.1%

Table B - 6. Input values of the load for Monte Carlo simulation. Force (kip), Moment (kip*ft).

	DL Steel			DL Concrete			LL		
	Axial	Moment y	Moment z	Axial	Moment y	Moment z	Axial	Moment y	Moment z
AR 1 My WIM	-2381	456	-54	-1580	298	-13	-732	2051	-7
AR 2 My WIM	-2242	278	-103	-1479	106	-80	-591	2847	-24
AR 3 My WIM	-2242	278	-103	-1479	106	-80	-590	2847	-23
AR 4 My WIM	-2027	-7	-40	-1341	108	-20	-1128	2377	-11
AR 1 Fx WIM	-2377	445	-20	-1578	292	9	-2083	54	-24
AR 2 Fx WIM	-2377	445	-20	-1578	292	9	-2083	54	-24
AR 3 Fx WIM	-2239	272	-51	-1478	106	-44	-1942	-417	-7
AR 4 Fx WIM	-2070	190	-35	-1369	113	-24	-1787	-513	5

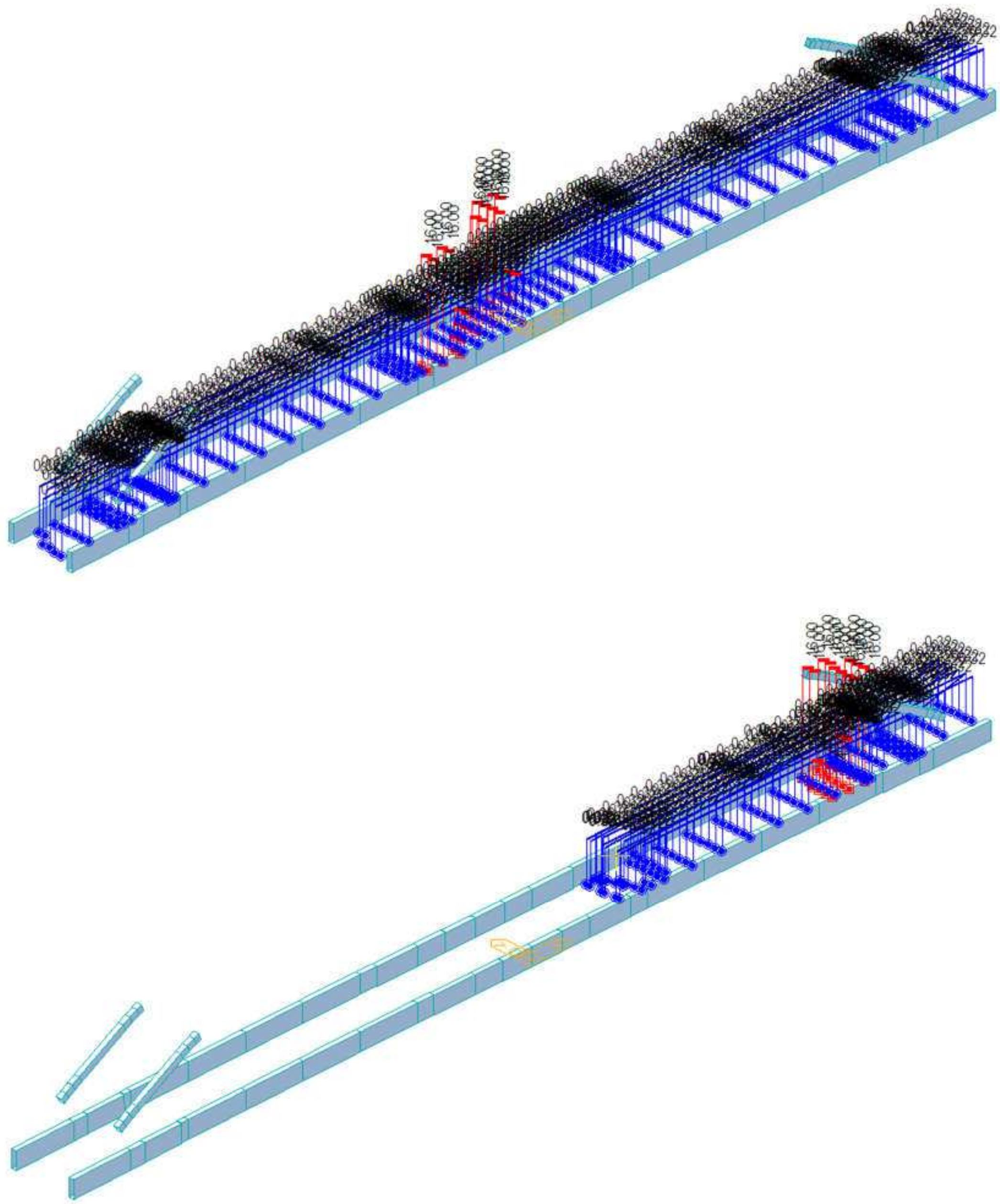

Figure B- 1. Configuration of AASHTO LRFD live load causing maximum compressive force (top) and maximum major bending moment (bottom) in AR 2.

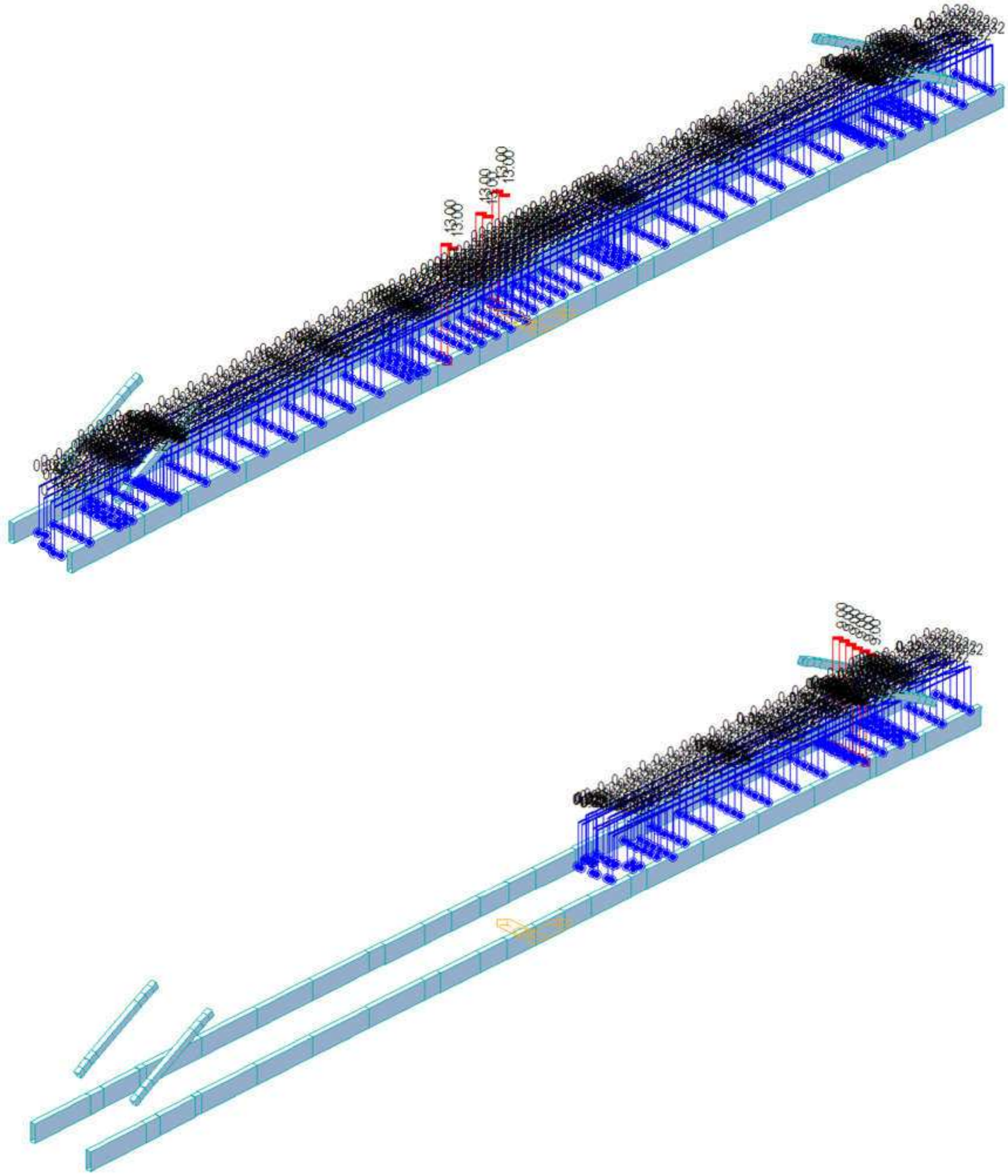

Figure B- 2. Configuration of AASHTO Standard Spec. live load causing maximum compressive force (top) and maximum major bending moment (bottom) in AR 2.

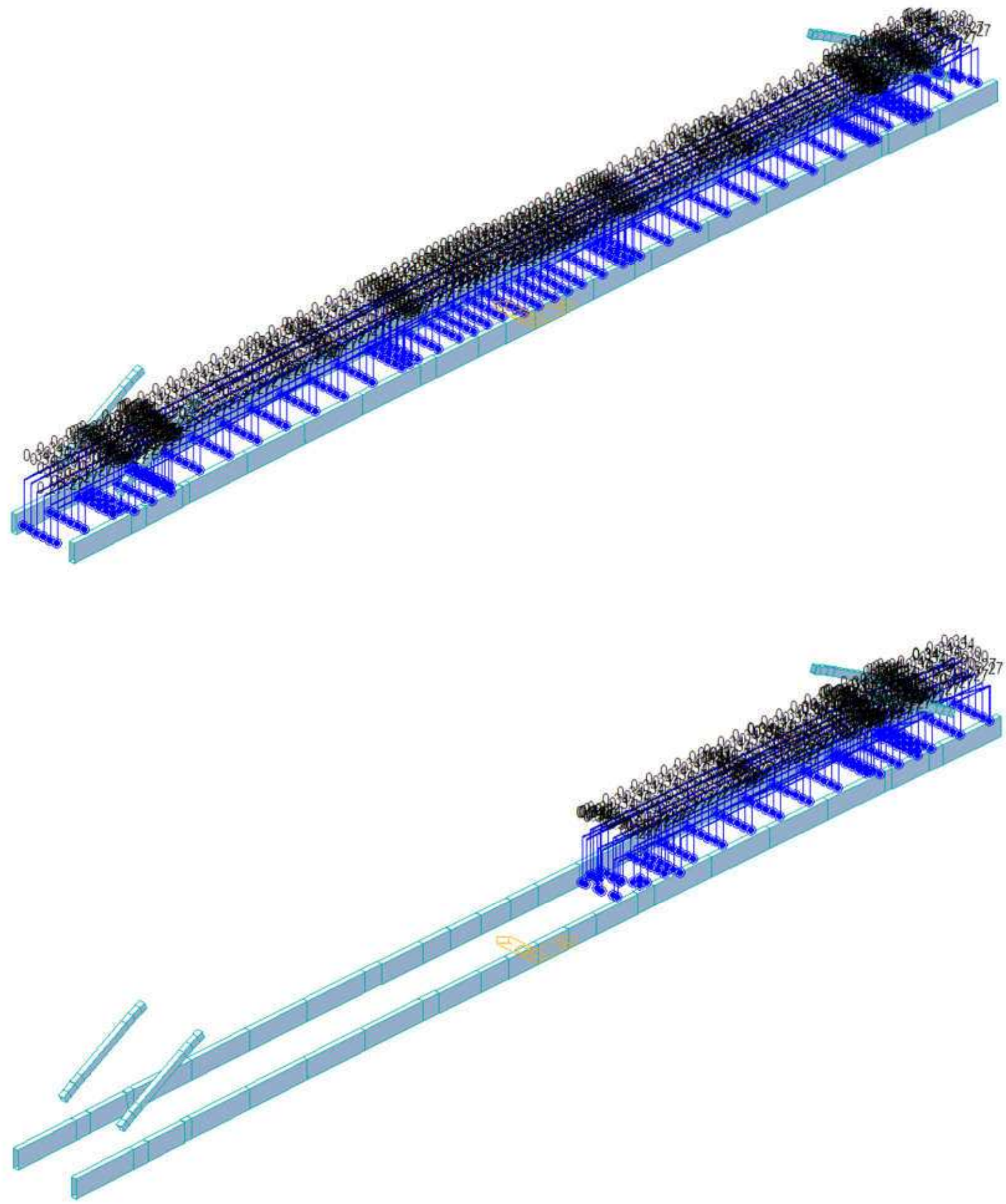

Figure B- 3. Configuration of measured WIM live load causing maximum compressive force (top) and maximum major bending moment (bottom) in AR 2.

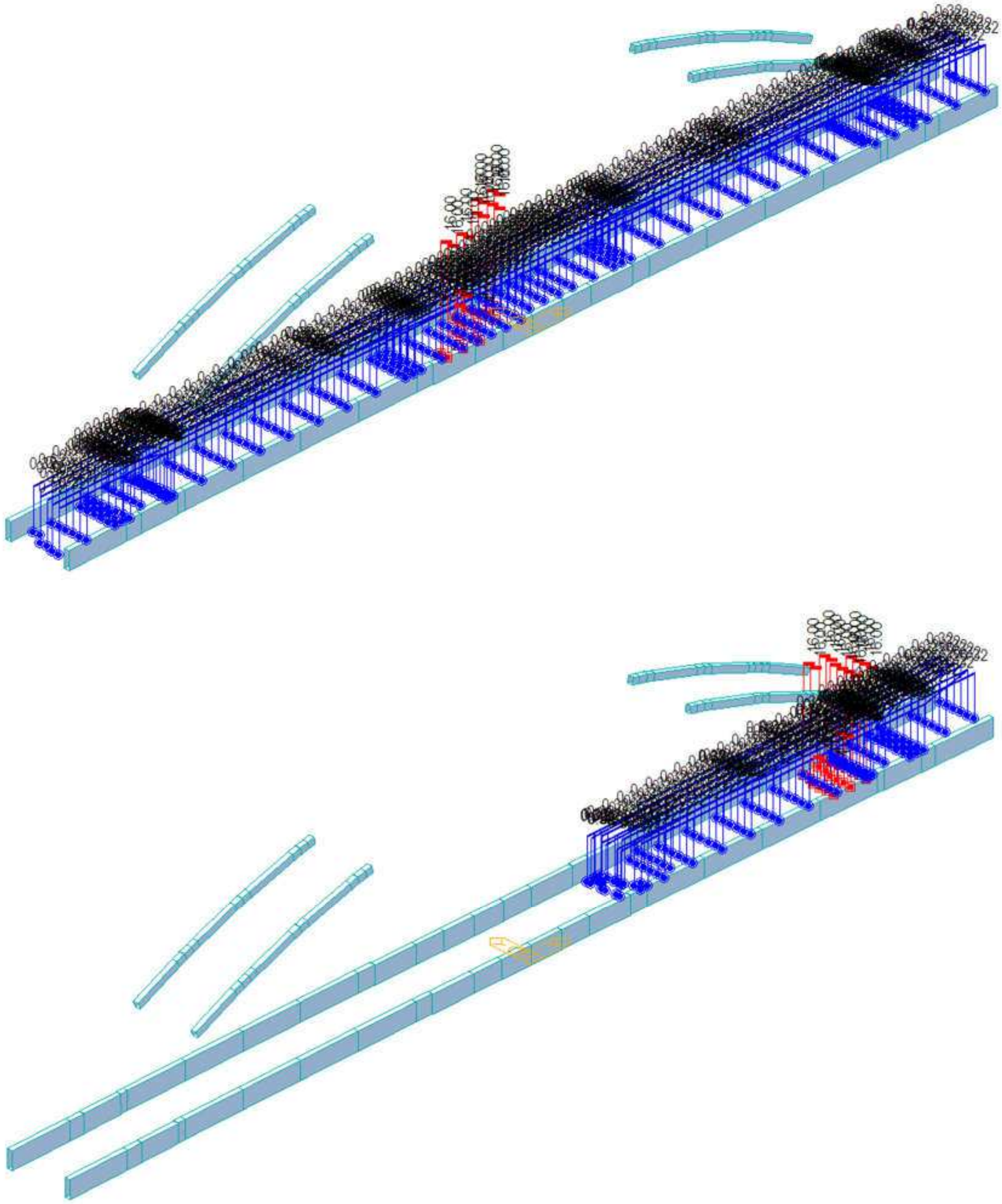

Figure B- 4. Configuration of AASHTO LRFD live load causing maximum compressive force (top) and maximum major bending moment (bottom) in AR 3.

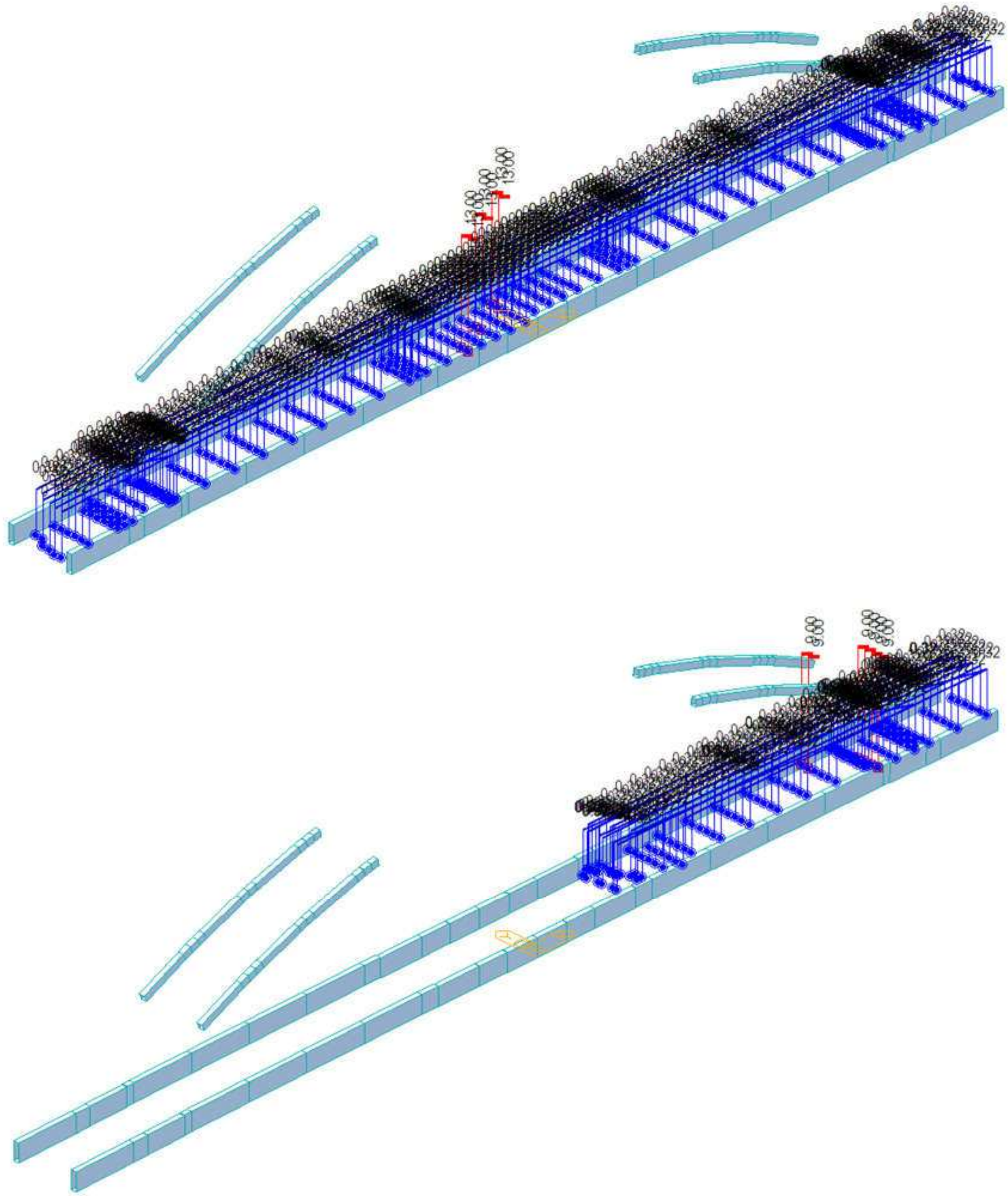

Figure B- 5. Configuration of AASHTO Standard Spec. live load causing maximum compressive force (top) and maximum major bending moment (bottom) in AR 3.

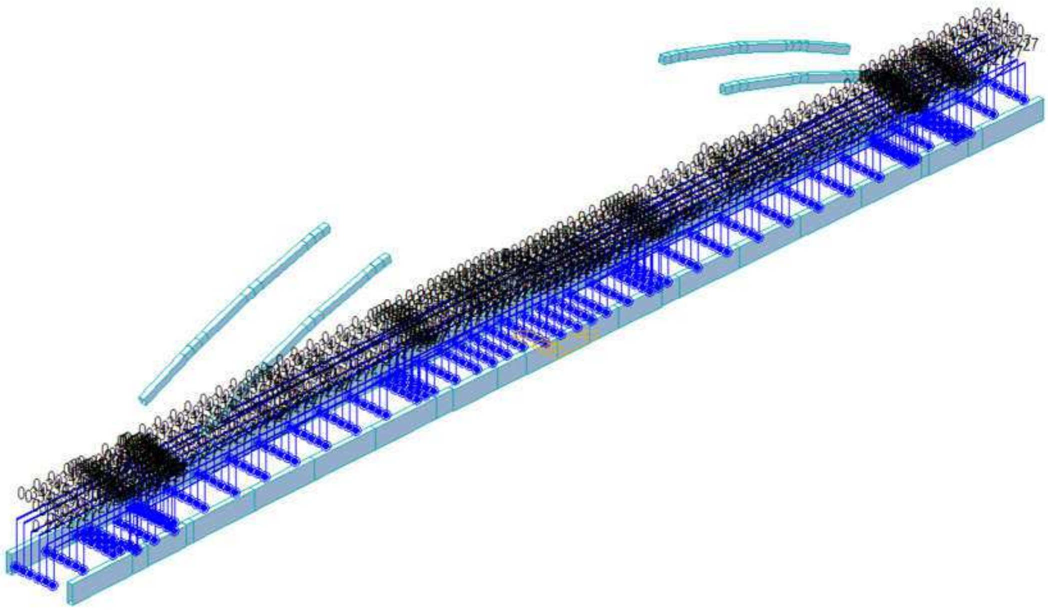

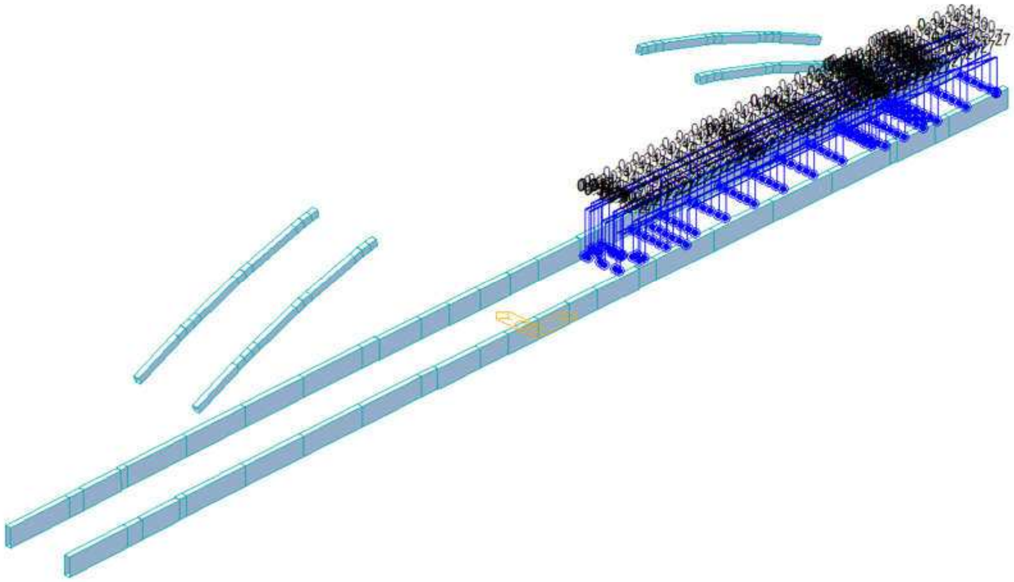

Figure B- 6. Configuration of measured WIM live load causing maximum compressive force (top) and maximum major bending moment (bottom) in AR 3.

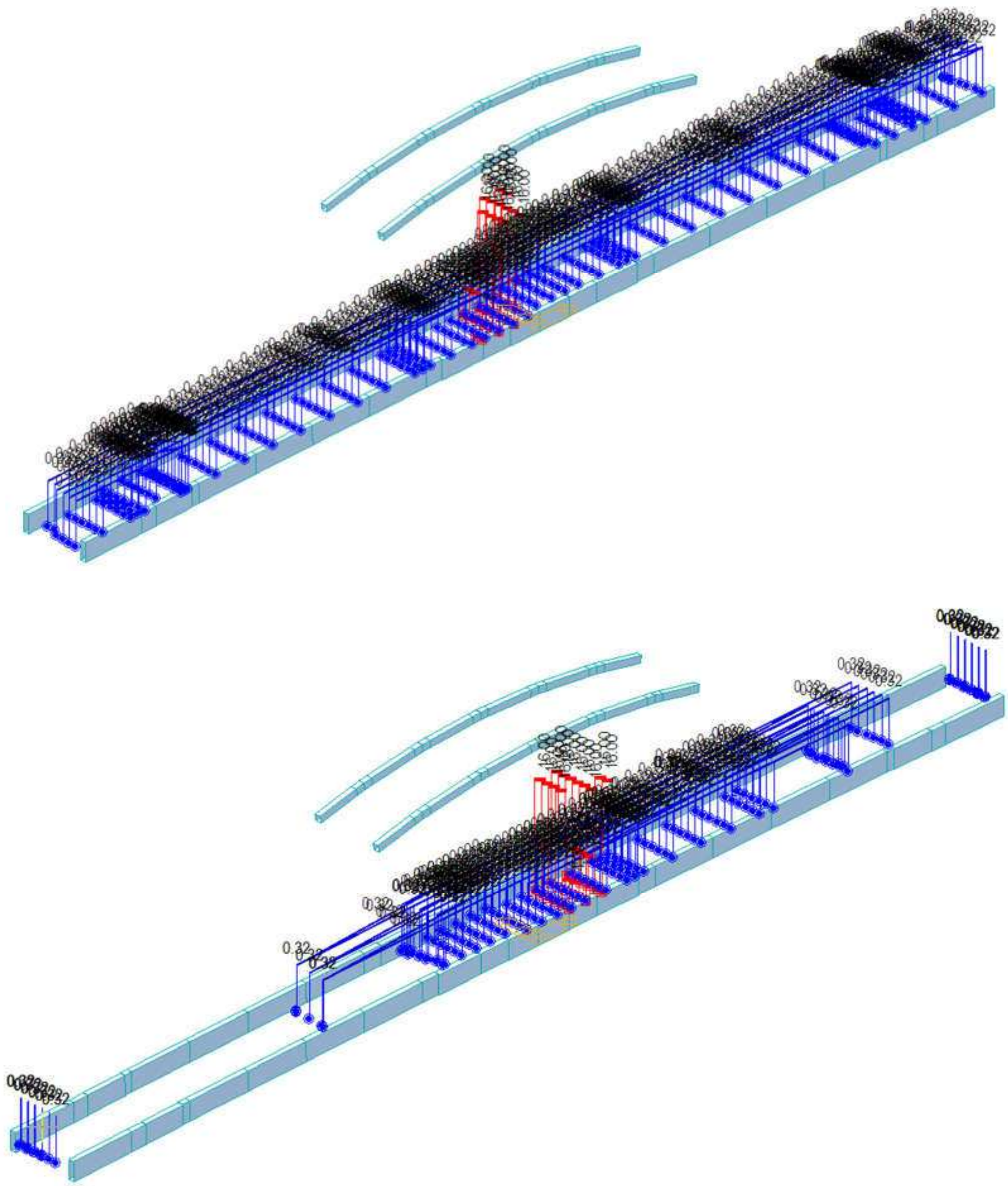

Figure B- 7. Configuration of AASHTO LRFD live load causing maximum compressive force (top) and maximum major bending moment (bottom) in AR 4.

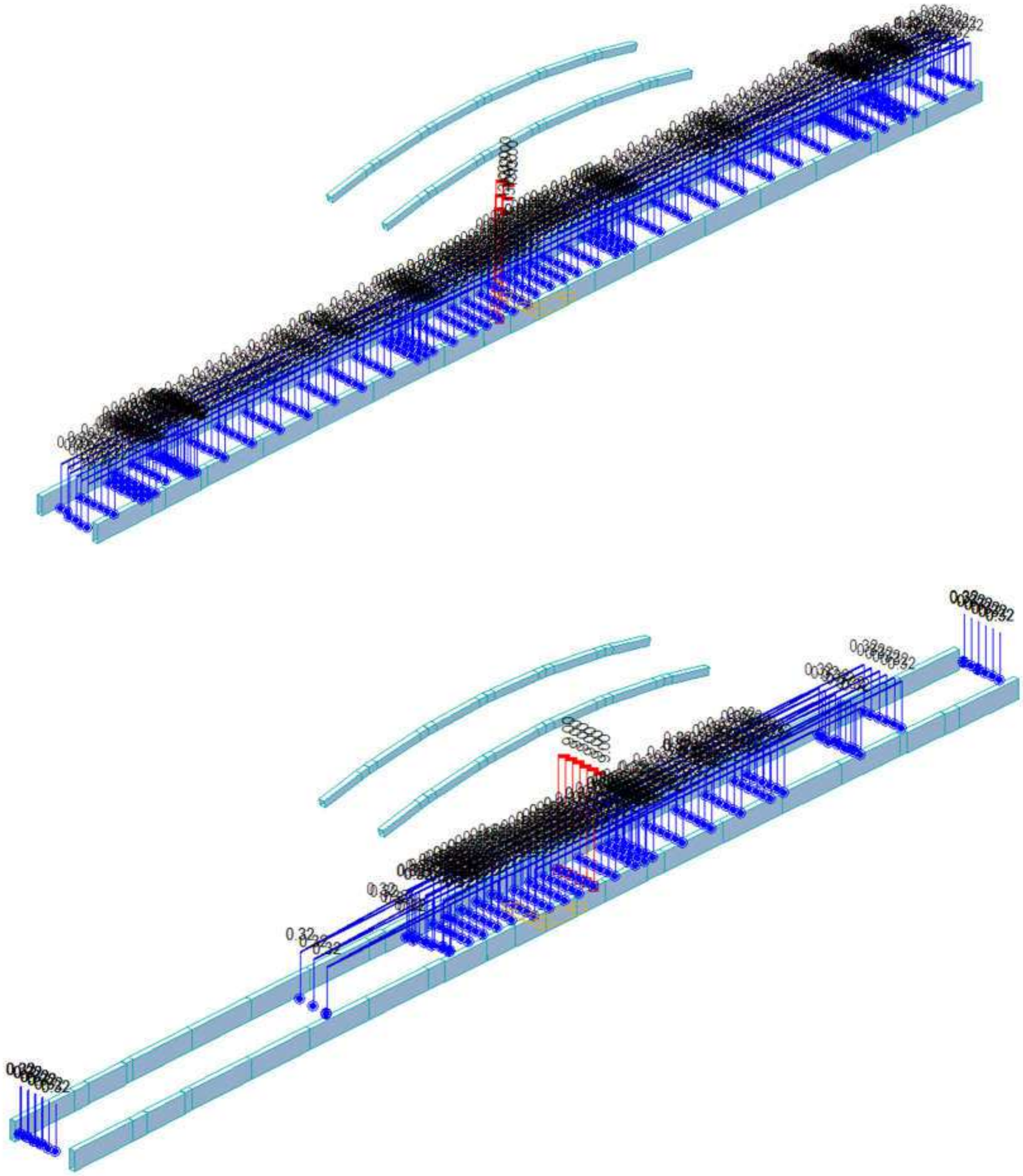

Figure B- 8. Configuration of AASHTO Standard Spec. live load causing maximum compressive force (top) and maximum major bending moment (bottom) in AR 4.

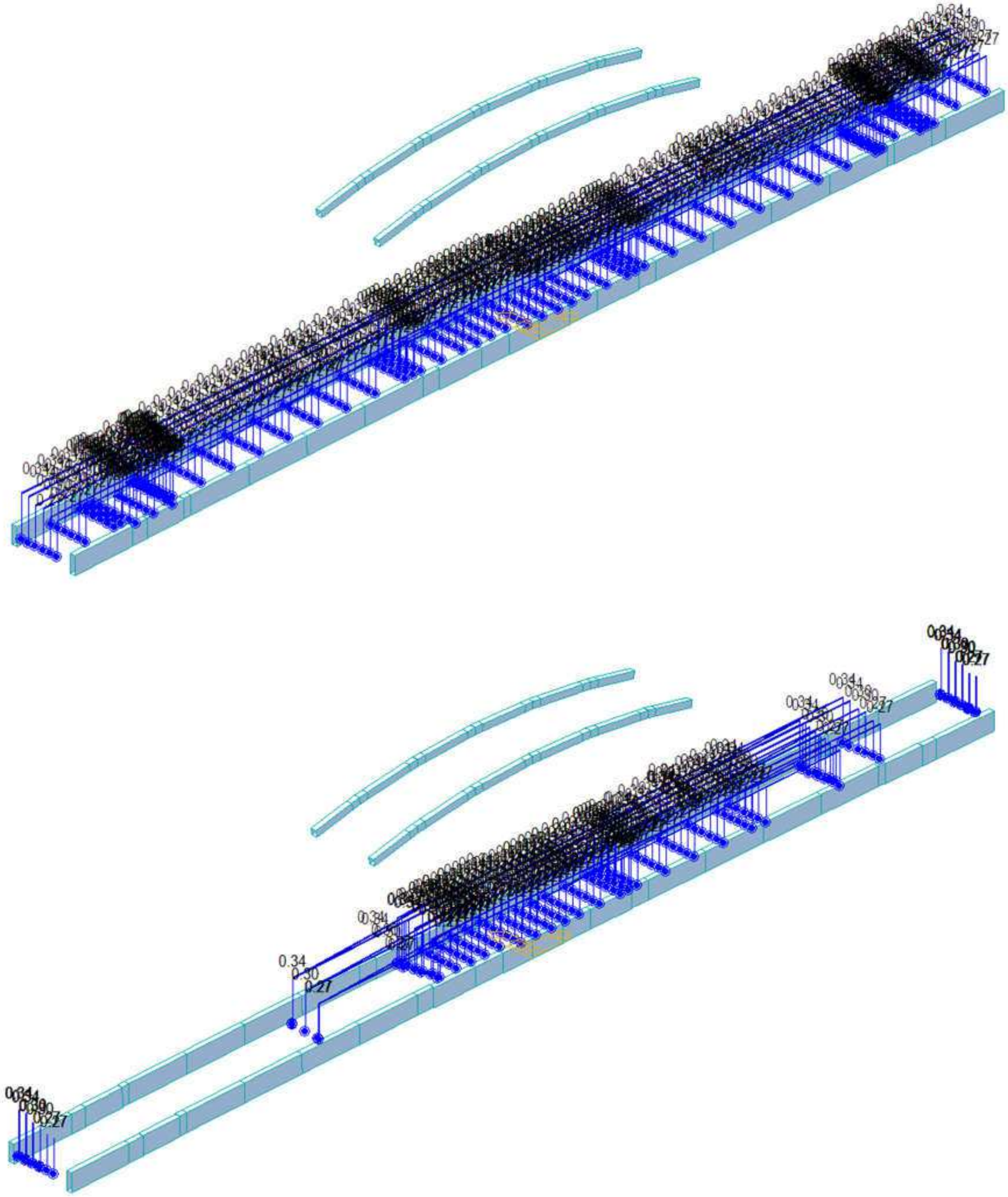

Figure B- 9. Configuration of measured WIM live load causing maximum compressive force (top) and maximum major bending moment (bottom) in AR 4.

APPENDIX C

Table C - 1. Summary of the calculated values of reliability indices.

	WIM		LRFD		STD	
	My	Fx	My	Fx	My	Fx
AR 1	4.56	4.27	3.65	3.25	3.82	3.46
AR 2	4.51	4.03	3.78	3.26	3.94	3.45
AR 3	4.42	4.16	3.85	3.47	4.02	3.62
AR 4	4.36	4.30	3.76	3.73	4.04	3.83
AR 4	4.36	4.30	3.76	3.73	4.04	3.83
AR 3	4.42	4.16	3.85	3.47	4.02	3.62
AR 2	4.51	4.03	3.78	3.26	3.94	3.45
AR 1	4.56	4.27	3.65	3.25	3.82	3.46

Table C - 2. Summary of averaged fractions of mean values of the components of limit state function – load cases with maximum compressive force and maximum major bending moment.

	Fx				My			
	AR 1	AR 2	AR 3	AR 4	AR 1	AR 2	AR 3	AR 4
Pu/Pn	90.6%	90.8%	97.4%	96.3%	68.9%	64.7%	67.3%	72.1%
Muy/Mny	9.2%	9.0%	0.8%	2.7%	30.4%	34.4%	29.6%	27.0%
Muz/Mnz	0.2%	0.2%	1.8%	1.0%	0.7%	1.0%	3.2%	0.9%

Combined axial force - bending moment interaction equations verification according to the AASHTO Standard Specifications for the existing cross sections.

$F_y := 50ksi$ yield strength

$E := 29000ksi$ modulus of elasticity

$t_w := 1.25in$ web thickness

$n := 1..4$

$m := 1..2$

$$t_f := \begin{pmatrix} 2 \\ 1.75 \\ 1.625 \\ 1.5 \end{pmatrix} in$$ flange thicknesses

$$d := \begin{pmatrix} 58 \\ 58 \\ 58 \\ 58 \end{pmatrix} \cdot in$$ height (excluding thickness of the flanges)

$b_f := 48in$ flange width

$$h := d + 2 \cdot t_f = \begin{pmatrix} 62 \\ 61.5 \\ 61.25 \\ 61 \end{pmatrix} \cdot in$$ total height

$$A_{g_n} := \left(t_{f_n} \cdot b_f + t_w \cdot d_n\right) \cdot 2$$

$$A_g = \begin{pmatrix} 337 \\ 313 \\ 301 \\ 289 \end{pmatrix} \cdot in^2$$ gross area

$$S_{y_n} := \frac{b_f \cdot (h_n)^2}{6} - \frac{(b_f - 2 \cdot t_w) \cdot (d_n)^3}{6 \cdot h_n} \qquad S_y = \begin{pmatrix} 6887 \\ 6199 \\ 5856 \\ 5512 \end{pmatrix} \cdot in^3$$ y - section modulus

$$S_{z_n} := \frac{{b_f}^2 \cdot h_n}{6} - \frac{(b_f - 2 \cdot t_w)^3 \cdot d_n}{6 \cdot b_f} \qquad S_z = \begin{pmatrix} 4838 \\ 4646 \\ 4550 \\ 4454 \end{pmatrix} \cdot in^3$$ z - section modulus

$$I_{y_n} := 2 \cdot \left[\frac{b_f \cdot \left(t_{f_n}\right)^3}{12} + b_f \cdot t_{f_n} \cdot \left(\frac{h_n}{2} - \frac{t_w}{2}\right)^2\right] + 2 \cdot \left[\frac{t_w \cdot (d_n)^3}{12}\right] \qquad I_y = \begin{pmatrix} 217859 \\ 193154 \\ 181083 \\ 169198 \end{pmatrix} \cdot in^4$$ y - moment of inertia

$$I_{z_n} := 2 \cdot \left(\frac{t_{f_n} \cdot {b_f}^3}{12}\right) + 2 \cdot \left[\frac{d_n \cdot {t_w}^3}{12} + d_n \cdot t_w \cdot \left(\frac{b_f}{2} - \frac{t_{f_n}}{2}\right)^2\right] \qquad I_z = \begin{pmatrix} 113588 \\ 109816 \\ 107932 \\ 106048 \end{pmatrix} \cdot in^4$$ z - moment of inertia

$$r_{y_n} := \sqrt{\frac{I_{y_n}}{A_{g_n}}} \qquad r_y = \begin{pmatrix} 25.4 \\ 24.8 \\ 24.5 \\ 24.2 \end{pmatrix} \cdot in$$

y radius of gyration

$$r_{z_n} := \sqrt{\frac{I_{z_n}}{A_{g_n}}} \qquad r_z = \begin{pmatrix} 18.4 \\ 18.7 \\ 18.9 \\ 19.2 \end{pmatrix} \cdot in$$

z radius of gyration

$$Z_{y_n} := \left(\frac{h_n}{2}\right)^2 \cdot b_f - \left(\frac{d_n}{2}\right)^2 \cdot \left(b_f - 2 \cdot t_w\right) \qquad Z_y = \begin{pmatrix} 7862 \\ 7121 \\ 6753 \\ 6386 \end{pmatrix} \cdot in^3$$

y - plastic section modulus

$$Z_{z_n} := \left(\frac{b_f}{2}\right)^2 \cdot h_n - \left(\frac{b_f - 2 \cdot t_w}{2}\right)^2 \cdot \left(d_n\right) \qquad Z_z = \begin{pmatrix} 5693 \\ 5405 \\ 5261 \\ 5117 \end{pmatrix} \cdot in^3$$

z - plastic section modulus

Local Buckling CHECK:

$$\frac{b_f}{t_f} = \begin{pmatrix} 24 \\ 27.429 \\ 29.538 \\ 32 \end{pmatrix} \quad \blacksquare \le \blacksquare \quad 1.4 \sqrt{\frac{E}{F_y}} = 33.7$$

Compression flange AISC Manual

Combined Axial Compression and Flexure, calculation according to AASHTO STANDARD Specification:

$$P := \begin{pmatrix} 9621 & 6825 \\ 9621 & 6191 \\ 8989 & 6191 \\ 8315 & 6952 \end{pmatrix} kip$$

From Analysis in Midas Civil -
First column - Max Compressive force case
Second column - Max Major banding moment

$$M_y := \begin{pmatrix} 1422 & 5709 \\ 1422 & 7011 \\ 115 & 7011 \\ 940 & 5550 \end{pmatrix} kip \cdot ft$$

$$M_z := \begin{pmatrix} 9 & 116 \\ 9 & 262 \\ 170 & 262 \\ 84 & 91 \end{pmatrix} kip \cdot ft$$

$l_z := 55ft$ Unbraced Length - z direction

$l_y := 55ft$ Unbraced Length - y direction

$K := 0.75$

$$\frac{K \cdot l_y}{r_y} = \begin{pmatrix} 19.5 \\ 19.9 \\ 20.2 \\ 20.5 \end{pmatrix} \quad \blacksquare \le \blacksquare \quad \sqrt{\frac{2 \cdot \pi^2 \cdot E}{F_y}} = 107$$

(10-154)

$$F_y \cdot A_g = \begin{pmatrix} 16850 \\ 15650 \\ 15050 \\ 14450 \end{pmatrix} \cdot kip$$

$$\frac{K \cdot l_z}{r_z} = \begin{pmatrix} 27 \\ 26.4 \\ 26.1 \\ 25.8 \end{pmatrix}$$

$$A_n := \left(d_n + t_{f_n}\right) \cdot \left(b_f - t_w\right) \qquad A = \begin{pmatrix} 2805 \\ 2793 \\ 2787 \\ 2782 \end{pmatrix} \cdot in^2$$

Area enclosed within the centerlines of the plates comprising the box

$$M_{u.y_n} := F_y \cdot S_{y_n} \cdot \left[1 - \frac{0.064 F_y \cdot S_{y_n} \cdot l_y}{A_n \cdot E} \cdot \left[\frac{2 \cdot \left(\frac{d_n}{t_w} + \frac{b_f}{t_{f_n}} \right)}{l_{y_n}} \right]^{0.5} \right] \qquad M_{u.y} = \begin{pmatrix} 28567 \\ 25716 \\ 24291 \\ 22867 \end{pmatrix} \cdot kip \cdot ft$$

$$M_{u.z_n} := F_y \cdot S_{z_n} \cdot \left[1 - \frac{0.064 F_y \cdot S_{z_n} \cdot l_z}{A_n \cdot E} \cdot \left[\frac{2 \cdot \left(\frac{d_n}{t_w} + \frac{b_f}{t_{f_n}} \right)}{l_{z_n}} \right]^{0.5} \right] \qquad M_{u.z} = \begin{pmatrix} 20069 \\ 19272 \\ 18873 \\ 18475 \end{pmatrix} \cdot kip \cdot ft$$

$$F_{e.y_n} := \frac{E \cdot \pi^2}{\left(\frac{K \cdot l_y}{r_{y_n}} \right)^2} \qquad F_{e.y} = \begin{pmatrix} 755 \\ 721 \\ 703 \\ 684 \end{pmatrix} \cdot ksi$$

(10-157)

$$F_{e.z_n} := \frac{E \cdot \pi^2}{\left(\frac{K \cdot l_z}{r_{z_n}} \right)^2} \qquad F_{e.z} = \begin{pmatrix} 394 \\ 410 \\ 419 \\ 429 \end{pmatrix} \cdot ksi$$

Euler Buckling stress in the plane of bending

$$F_{cr.y_n} := F_y \cdot \left[1 - \frac{F_y}{4 \cdot \pi^2 \cdot E} \cdot \left(\frac{K \cdot l_y}{r_{y_n}} \right)^2 \right] \qquad F_{cr.y} = \begin{pmatrix} 49.2 \\ 49.1 \\ 49.1 \\ 49.1 \end{pmatrix} \cdot ksi$$

buckling stress

(10-151)

$$F_{cr.z_n} := F_y \cdot \left[1 - \frac{F_y}{4 \cdot \pi^2 \cdot E} \cdot \left(\frac{K \cdot l_z}{r_{z_n}} \right)^2 \right] \qquad F_{cr.z} = \begin{pmatrix} 48.4 \\ 48.5 \\ 48.5 \\ 48.5 \end{pmatrix} \cdot ksi$$

$$M_{p.y_n} := F_y \cdot Z_{y_n}$$

$$M_{p.y} = \begin{pmatrix} 32760 \\ 29673 \\ 28139 \\ 26610 \end{pmatrix} \cdot kip \cdot ft$$

y- plastic moment

$$M_{p.z_n} := F_y \cdot Z_{z_n}$$

$$M_{p.z} = \begin{pmatrix} 23722 \\ 22522 \\ 21922 \\ 21322 \end{pmatrix} \cdot kip \cdot ft$$

z- plastic moment

$$InteractionEquation_{1_{n,m}} := \frac{P_{n,m}}{0.85 \cdot A_{g_n} \cdot F_{cr.z_n}} + \frac{M_{y_{n,m}}}{M_{u.y_n} \cdot \left(1 - \frac{P_{n,m}}{A_{g_n} \cdot F_{e.y_n}}\right)} + \frac{M_{z_{n,m}}}{M_{u.z_n} \cdot \left(1 - \frac{P_{n,m}}{A_{g_n} \cdot F_{e.z_n}}\right)} \qquad (10\text{-}155)$$

$$\boxed{InteractionEquation_1 = \begin{pmatrix} 0.75 & 0.70 \\ 0.80 & 0.77 \\ 0.74 & 0.81 \\ 0.75 & 0.84 \end{pmatrix}}$$

$$InteractionEquation_{2_{n,m}} := \frac{P_{n,m}}{0.85 \cdot A_{g_n} \cdot F_{cr.z_n}} + \frac{M_{y_{n,m}}}{M_{p.y_n}} + \frac{M_{z_{n,m}}}{M_{p.z_n}} \qquad (10\text{-}156)$$

$$InteractionEquation_2 = \begin{pmatrix} 0.74 & 0.67 \\ 0.79 & 0.73 \\ 0.74 & 0.76 \\ 0.74 & 0.8 \end{pmatrix}$$

Combined axial force - bending moment interaction equations verification according to the AASHTO LRFD for the existing cross sections.

$F_y := 50ksi$ yield strength $n := 1..4$

$E := 29000ksi$ modulus of elasticity $m := 1..2$

$t_w := 1.25in$ web thickness

$$t_f := \begin{pmatrix} 2 \\ 1.75 \\ 1.625 \\ 1.5 \end{pmatrix} in$$

flange thicknesses

$$d := \begin{pmatrix} 58 \\ 58 \\ 58 \\ 58 \end{pmatrix} \cdot in$$

height (excluding thickness of the flanges)

$b_f := 48in$ flange width

$$h := d + 2 \cdot t_f = \begin{pmatrix} 62 \\ 61.5 \\ 61.25 \\ 61 \end{pmatrix} \cdot in$$

total height

$$A_{g_n} := \left(t_{f_n} \cdot b_f + t_w \cdot d_n\right) \cdot 2$$

$$A_g = \begin{pmatrix} 337 \\ 313 \\ 301 \\ 289 \end{pmatrix} \cdot in^2$$

gross area

$$S_{y_n} := \frac{b_f \cdot (h_n)^2}{6} - \frac{(b_f - 2 \cdot t_w) \cdot (d_n)^3}{6 \cdot h_n} \qquad S_y = \begin{pmatrix} 6887 \\ 6199 \\ 5856 \\ 5512 \end{pmatrix} \cdot in^3$$

y - section modulus

$$S_{z_n} := \frac{b_f^{\,2} \cdot h_n}{6} - \frac{(b_f - 2 \cdot t_w)^3 \cdot d_n}{6 \cdot b_f} \qquad S_z = \begin{pmatrix} 4838 \\ 4646 \\ 4550 \\ 4454 \end{pmatrix} \cdot in^3$$

z - section modulus

$$I_{y_n} := 2 \cdot \left[\frac{b_f \cdot \left(t_{f_n}\right)^3}{12} + b_f \cdot t_{f_n} \cdot \left(\frac{h_n}{2} - \frac{t_w}{2} \right)^2 \right] + 2 \cdot \left[\frac{t_w \cdot (d_n)^3}{12} \right] \qquad I_y = \begin{pmatrix} 217859 \\ 193154 \\ 181083 \\ 169198 \end{pmatrix} \cdot in^4$$

y - moment of inertia

$$I_{z_n} := 2 \cdot \left(\frac{t_{f_n} \cdot b_f^{\,3}}{12} \right) + 2 \cdot \left[\frac{d_n \cdot t_w^{\,3}}{12} + d_n \cdot t_w \cdot \left(\frac{b_f}{2} - \frac{t_{f_n}}{2} \right)^2 \right] \qquad I_z = \begin{pmatrix} 113588 \\ 109816 \\ 107932 \\ 106048 \end{pmatrix} \cdot in^4$$

z - moment of inertia

$$r_{y_n} := \sqrt{\frac{I_{y_n}}{A_{g_n}}} \qquad r_y = \begin{pmatrix} 25.4 \\ 24.8 \\ 24.5 \\ 24.2 \end{pmatrix} \cdot in$$

y radius of gyration

$$r_{z_n} := \sqrt{\frac{I_{z_n}}{A_{g_n}}} \qquad r_z = \begin{pmatrix} 18.4 \\ 18.7 \\ 18.9 \\ 19.2 \end{pmatrix} \cdot in$$

z radius of gyration

$$Z_{y_n} := \left(\frac{h_n}{2}\right)^2 \cdot b_f - \left(\frac{d_n}{2}\right)^2 \cdot \left(b_f - 2 \cdot t_w\right) \qquad Z_y = \begin{pmatrix} 7862 \\ 7121 \\ 6753 \\ 6386 \end{pmatrix} \cdot in^3$$

y - plastic section modulus

$$Z_{z_n} := \left(\frac{b_f}{2}\right)^2 \cdot h_n - \left(\frac{b_f - 2 \cdot t_w}{2}\right)^2 \cdot \left(d_n\right) \qquad Z_z = \begin{pmatrix} 5693 \\ 5405 \\ 5261 \\ 5117 \end{pmatrix} \cdot in^3$$

z - plastic section modulus

Examine Local Buckling:

$$\frac{b_f - 2 \cdot t_w}{t_f} = \begin{pmatrix} 22.75 \\ 26 \\ 28 \\ 30.33 \end{pmatrix} \quad \leq \quad 1.40 \cdot \sqrt{\frac{E}{F_y}} = 33.72 \qquad (6.9.4.2\text{-}1)$$

local buckling is avoided

Combined Axial Compression and Flexure, calculation according to AASHTO LRFD:

$$P_e := \begin{pmatrix} 25782 \\ 25650 \\ 23951 \\ 22153 \end{pmatrix} kip$$

Elastic critical buckling resistance — From Buckling Analysis in Midas Civil Model

$Q := 1.0$ — Slender Element reduction factor

$$P_0 := Q \cdot F_y \cdot A_g = \begin{pmatrix} 16850 \\ 15650 \\ 15050 \\ 14450 \end{pmatrix} \cdot kip$$

Equivalent nominal yield resistance

Determination of P_n (nominal compressive resistance):

$$\frac{P_e}{P_0} = \begin{pmatrix} 1.53 \\ 1.639 \\ 1.591 \\ 1.533 \end{pmatrix}$$

If $\dfrac{P_e}{P_0} \le 0.44$ $\quad P_n := 0.877 \cdot P_e = \begin{pmatrix} 22611 \\ 22495 \\ 21005 \\ 19428 \end{pmatrix} \cdot kip$ (6.9.4.1.1-1)

If $\dfrac{P_e}{P_0} > 0.44$ $\quad P_{n_n} := \left[0.658^{\left(\frac{P_{0_n}}{P_{e_n}} \right)} \right] \cdot P_{0_n}$ $\quad P_n = \begin{pmatrix} 12817 \\ 12123 \\ 11570 \\ 10998 \end{pmatrix} \cdot kip$ (6.9.4.1.1-2)

$\phi_c := 0.9$ Resistance factor for compression (6.5.4.2)

$P_r := \phi_c \cdot P_n = \begin{pmatrix} 11536 \\ 10911 \\ 10413 \\ 9898 \end{pmatrix} \cdot kip$ Factored resistance of components in compression (6.9.2.1-1)

$P_u := \begin{pmatrix} 8434 & 6259 \\ 8434 & 5819 \\ 7886 & 5819 \\ 7285 & 6297 \end{pmatrix} kip$

From Analysis in Midas Civil -
First column - Max Compressive force case
Second column - Max Major banding moment

$M_{uy} := \begin{pmatrix} 1143 & 5122 \\ 1143 & 6299 \\ 224 & 6299 \\ 599 & 4818 \end{pmatrix} kip \cdot ft$

$M_{uz} := \begin{pmatrix} 12 & 114 \\ 12 & 197 \\ 150 & 169 \\ 76 & 85 \end{pmatrix} kip \cdot ft$

$\phi_f := 1.0$ Resistance factor for flexure (6.5.4.2)

$l_z := 55ft$ Unbraced Length - z direction

$l_y := 55ft$ Unbraced Length - y direction

$A_n := \left(d_n + t_{f_n}\right) \cdot \left(b_f - t_w\right)$ $\quad A = \begin{pmatrix} 2805 \\ 2793 \\ 2787 \\ 2782 \end{pmatrix} \cdot in^2$ Area enclosed within the centerlines of the plates comprising the box

$$M_{ny_n} := F_y \cdot S_{y_n} \cdot \left[1 - \frac{0.064 F_y \cdot S_{y_n} \cdot l_y}{A_n \cdot E} \cdot \left[\frac{2 \cdot \left(\frac{d_n}{t_w} + \frac{b_f}{t_{f_n}} \right)}{l_{y_n}} \right]^{0.5} \right] \qquad M_{ny} = \begin{pmatrix} 28567 \\ 25716 \\ 24291 \\ 22867 \end{pmatrix} \cdot kip \cdot ft \qquad M_{ry} := \phi_f \cdot M_{ny}$$

(6.12.2.2.2-1)

$$M_{nz_n} := F_y \cdot S_{z_n} \cdot \left[1 - \frac{0.064 F_y \cdot S_{z_n} \cdot l_z}{A_n \cdot E} \cdot \left[\frac{2 \cdot \left(\frac{d_n}{t_w} + \frac{b_f}{t_{f_n}} \right)}{l_{z_n}} \right]^{0.5} \right] \qquad M_{nz} = \begin{pmatrix} 20069 \\ 19272 \\ 18873 \\ 18475 \end{pmatrix} \cdot kip \cdot ft \qquad M_{rz} := \phi_f \cdot M_{nz}$$

$$M_{p.y_n} := F_y \cdot Z_{y_n} \qquad M_{p.y} = \begin{pmatrix} 32760 \\ 29673 \\ 28139 \\ 26610 \end{pmatrix} \cdot kip \cdot ft$$

y- plastic moment

$$M_{p.z_n} := F_y \cdot Z_{z_n} \qquad M_{p.z} = \begin{pmatrix} 23722 \\ 22522 \\ 21922 \\ 21322 \end{pmatrix} \cdot kip \cdot ft$$

z- plastic moment

$$ratio_{n,m} := \frac{P_{u_{n,m}}}{P_{r_n}} \qquad ratio = \begin{pmatrix} 0.731 & 0.543 \\ 0.773 & 0.533 \\ 0.757 & 0.559 \\ 0.736 & 0.636 \end{pmatrix}$$

If $\frac{P_u}{P_r} < 0.2$ $\quad InteractionEquation_{1_{n,m}} := \frac{P_{u_{n,m}}}{2.0\,P_{r_n}} + \left(\frac{M_{uz_{n,m}}}{M_{rz_n}} + \frac{M_{uz_{n,m}}}{M_{ry_n}} \right)$ $\blacksquare \le 1.0$ CHECK (6.9.2.2-1)

$$InteractionEquation_1 = \begin{pmatrix} 0.37 & 0.28 \\ 0.39 & 0.28 \\ 0.39 & 0.3 \\ 0.38 & 0.33 \end{pmatrix}$$

If $\frac{P_u}{P_r} \ge 0.2$

$InteractionEquation_{2_{n,m}} := \frac{P_{u_{n,m}}}{P_{r_n}} + \frac{8.0}{9.0} \left(\frac{M_{uz_{n,m}}}{M_{rz_n}} + \frac{M_{uy_{n,m}}}{M_{ry_n}} \right)$ $\blacksquare \le 1.0$ CHECK (6.9.2.2-2)

$$\boxed{InteractionEquation_2 = \begin{pmatrix} 0.77 & 0.71 \\ 0.81 & 0.76 \\ 0.77 & 0.80 \\ 0.76 & 0.83 \end{pmatrix}}$$

Combined axial force - bending moment interaction equations for determination of the cross sections according to AASHTO Standard Specifications.

$F_y := 50ksi$ yield strength $n := 1..4$

$E := 29000ksi$ modulus of elasticity $m := 1..2$

$t_w := 1in$ web thickness

$$t_f := \begin{pmatrix} 1.75 \\ 1.75 \\ 1.5 \\ 1.5 \end{pmatrix} in$$ flange thicknesses

$$d := \begin{pmatrix} 48 \\ 48 \\ 55 \\ 54 \end{pmatrix} \cdot in$$ height (excluding thickness of the flanges)

$b_f := 46in$ flange width

$$h := d + 2 \cdot t_f = \begin{pmatrix} 51.5 \\ 51.5 \\ 58 \\ 57 \end{pmatrix} \cdot in$$ total height

$$A_{g_n} := \left(t_{f_n} \cdot b_f + t_w \cdot d_n\right) \cdot 2$$

$$A_g = \begin{pmatrix} 257 \\ 257 \\ 248 \\ 246 \end{pmatrix} \cdot in^2$$ gross area

$$S_{y_n} := \frac{b_f \cdot (h_n)^2}{6} - \frac{\left(b_f - 2 \cdot t_w\right) \cdot (d_n)^3}{6 \cdot h_n} \qquad S_y = \begin{pmatrix} 4586 \\ 4586 \\ 4755 \\ 4650 \end{pmatrix} \cdot in^3$$ y - section modulus

$$S_{z_n} := \frac{b_f^{\,2} \cdot h_n}{6} - \frac{\left(b_f - 2 \cdot t_w\right)^3 \cdot d_n}{6 \cdot b_f} \qquad S_z = \begin{pmatrix} 3348 \\ 3348 \\ 3480 \\ 3436 \end{pmatrix} \cdot in^3$$ z - section modulus

$$I_{y_n} := 2 \cdot \left[\frac{b_f \cdot \left(t_{f_n}\right)^3}{12} + b_f \cdot t_{f_n} \cdot \left(\frac{h_n}{2} - \frac{t_w}{2}\right)^2\right] + 2 \cdot \left[\frac{t_w \cdot (d_n)^3}{12}\right] \qquad I_y = \begin{pmatrix} 121121 \\ 121121 \\ 139846 \\ 134462 \end{pmatrix} \cdot in^4$$ y - moment of inertia

$$I_{z_n} := 2 \cdot \left(\frac{t_{f_n} \cdot b_f^{\,3}}{12}\right) + 2 \cdot \left[\frac{d_n \cdot t_w^{\,3}}{12} + d_n \cdot t_w \cdot \left(\frac{b_f}{2} - \frac{t_{f_n}}{2}\right)^2\right] \qquad I_z = \begin{pmatrix} 75391 \\ 75391 \\ 78800 \\ 77810 \end{pmatrix} \cdot in^4$$ z - moment of inertia

$$r_{y_n} := \sqrt{\frac{I_{y_n}}{A_{g_n}}} \qquad r_y = \begin{pmatrix} 21.7 \\ 21.7 \\ 23.7 \\ 23.4 \end{pmatrix} \cdot in$$

y radius of gyration

$$r_{z_n} := \sqrt{\frac{I_{z_n}}{A_{g_n}}} \qquad r_z = \begin{pmatrix} 17.1 \\ 17.1 \\ 17.8 \\ 17.8 \end{pmatrix} \cdot in$$

z radius of gyration

$$Z_{y_n} := \left(\frac{h_n}{2}\right)^2 \cdot b_f - \left(\frac{d_n}{2}\right)^2 \cdot \left(b_f - 2 \cdot t_w\right) \qquad Z_y = \begin{pmatrix} 5157 \\ 5157 \\ 5411 \\ 5287 \end{pmatrix} \cdot in^3$$

y - plastic section modulus

$$Z_{z_n} := \left(\frac{b_f}{2}\right)^2 \cdot h_n - \left(\frac{b_f - 2 \cdot t_w}{2}\right)^2 \cdot \left(d_n\right) \qquad Z_z = \begin{pmatrix} 4011 \\ 4011 \\ 4062 \\ 4017 \end{pmatrix} \cdot in^3$$

z - plastic section modulus

Local Buckling CHECK:

$$\frac{b_f}{t_f} = \begin{pmatrix} 26.286 \\ 26.286 \\ 30.667 \\ 30.667 \end{pmatrix} \quad \le \quad 1.4\sqrt{\frac{E}{F_y}} = 33.7$$

Compression flange AISC Manual

Combined Axial Compression and Flexure, calculation according to AASHTO STANDARD Specification:

$$P := \begin{pmatrix} 9621 & 6825 \\ 9621 & 6191 \\ 8989 & 6191 \\ 8315 & 6952 \end{pmatrix} kip$$

From Analysis in Midas Civil -
First column - Max Compressive force case
Second column - Max Major banding moment

$$M_y := \begin{pmatrix} 1422 & 5709 \\ 1422 & 7011 \\ 115 & 7011 \\ 940 & 5550 \end{pmatrix} kip \cdot ft$$

$$M_z := \begin{pmatrix} 9 & 116 \\ 9 & 262 \\ 170 & 262 \\ 84 & 91 \end{pmatrix} kip \cdot ft$$

$l_z := 55ft$ Unbraced Length - z direction

$l_y := 55ft$ Unbraced Length - y direction

$K := 0.75$

$$\frac{K \cdot l_y}{r_y} = \begin{pmatrix} 22.8 \\ 22.8 \\ 20.8 \\ 21.2 \end{pmatrix} \quad \blacksquare \le \blacksquare \quad \sqrt{\frac{2 \cdot \pi^2 \cdot E}{F_y}} = 107$$

(10-154)

$$F_y \cdot A_g = \begin{pmatrix} 12850 \\ 12850 \\ 12400 \\ 12300 \end{pmatrix} \cdot kip$$

$$\frac{K \cdot l_z}{r_z} = \begin{pmatrix} 28.9 \\ 28.9 \\ 27.8 \\ 27.8 \end{pmatrix}$$

$$A_n := \left(d_n + t_{f_n}\right) \cdot \left(b_f - t_w\right) \qquad A = \begin{pmatrix} 2239 \\ 2239 \\ 2543 \\ 2497 \end{pmatrix} \cdot in^2$$

Area enclosed within the centerlines of the plates comprising the box

$$M_{u.y_n} := F_y \cdot S_{y_n} \cdot \left[1 - \frac{0.064 F_y \cdot S_{y_n} \cdot l_y}{A_n \cdot E} \cdot \left[\frac{2 \cdot \left(\frac{d_n}{t_w} + \frac{b_f}{t_{f_n}}\right)}{l_{y_n}}\right]^{0.5}\right] \qquad M_{u.y} = \begin{pmatrix} 19009 \\ 19009 \\ 19717 \\ 19284 \end{pmatrix} \cdot kip \cdot ft$$

$$M_{u.z_n} := F_y \cdot S_{z_n} \cdot \left[1 - \frac{0.064 F_y \cdot S_{z_n} \cdot l_z}{A_n \cdot E} \cdot \left[\frac{2 \cdot \left(\frac{d_n}{t_w} + \frac{b_f}{t_{f_n}}\right)}{l_{z_n}}\right]^{0.5}\right] \qquad M_{u.z} = \begin{pmatrix} 13881 \\ 13881 \\ 14431 \\ 14248 \end{pmatrix} \cdot kip \cdot ft$$

$$F_{e.y_n} := \frac{E \cdot \pi^2}{\left(\frac{K \cdot l_y}{r_{y_n}}\right)^2} \qquad F_{e.y} = \begin{pmatrix} 551 \\ 551 \\ 659 \\ 638 \end{pmatrix} \cdot ksi$$

(10-157)

$$F_{e.z_n} := \frac{E \cdot \pi^2}{\left(\frac{K \cdot l_z}{r_{z_n}}\right)^2} \qquad F_{e.z} = \begin{pmatrix} 343 \\ 343 \\ 371 \\ 369 \end{pmatrix} \cdot ksi$$

Euler Buckling stress in the plane of bending

$$F_{cr.y_n} := F_y \cdot \left[1 - \frac{F_y}{4 \cdot \pi^2 \cdot E} \cdot \left(\frac{K \cdot l_y}{r_{y_n}}\right)^2\right] \qquad F_{cr.y} = \begin{pmatrix} 48.9 \\ 48.9 \\ 49.1 \\ 49 \end{pmatrix} \cdot ksi$$

buckling stress

(10-151)

$$F_{cr.z_n} := F_y \cdot \left[1 - \frac{F_y}{4 \cdot \pi^2 \cdot E} \cdot \left(\frac{K \cdot l_z}{r_{z_n}}\right)^2\right] \qquad F_{cr.z} = \begin{pmatrix} 48.2 \\ 48.2 \\ 48.3 \\ 48.3 \end{pmatrix} \cdot ksi$$

$$M_{p.y_n} := F_y \cdot Z_{y_n}$$

$$M_{p.y} = \begin{pmatrix} 21487 \\ 21487 \\ 22546 \\ 22031 \end{pmatrix} \cdot kip \cdot ft$$

y- plastic moment

$$M_{p.z_n} := F_y \cdot Z_{z_n}$$

$$M_{p.z} = \begin{pmatrix} 16715 \\ 16715 \\ 16925 \\ 16738 \end{pmatrix} \cdot kip \cdot ft$$

z- plastic moment

$$InteractionEquation_{1_{n,m}} := \frac{P_{n,m}}{0.85 \cdot A_{g_n} \cdot F_{cr.z_n}} + \frac{M_{y_{n,m}}}{M_{u.y_n} \cdot \left(1 - \frac{P_{n,m}}{A_{g_n} \cdot F_{e.y_n}}\right)} + \frac{M_{z_{n,m}}}{M_{u.z_n} \cdot \left(1 - \frac{P_{n,m}}{A_{g_n} \cdot F_{e.z_n}}\right)} \qquad (10\text{-}155)$$

$$\boxed{InteractionEquation_1 = \begin{pmatrix} 1.00 & 0.97 \\ 1.00 & 0.99 \\ 0.90 & 1.00 \\ 0.88 & 1.00 \end{pmatrix}}$$

$$InteractionEquation_{2_{n,m}} := \frac{P_{n,m}}{0.85 \cdot A_{g_n} \cdot F_{cr.z_n}} + \frac{M_{y_{n,m}}}{M_{p.y_n}} + \frac{M_{z_{n,m}}}{M_{p.z_n}} \qquad (10\text{-}156)$$

$$InteractionEquation_2 = \begin{pmatrix} 0.98 & 0.92 \\ 0.98 & 0.93 \\ 0.90 & 0.93 \\ 0.87 & 0.95 \end{pmatrix}$$

Combined axial force - bending moment interaction equations for determination of the cross sections according to AASHTO LRFD.

$F_y := 50ksi$ yield strength $n := 1 .. 4$

$E := 29000ksi$ modulus of elasticity $m := 1 .. 2$

$t_w := 1in$ web thickness

$t_f := \begin{pmatrix} 1.625 \\ 1.625 \\ 1.5 \\ 1.5 \end{pmatrix} in$ flange thicknesses

$d := \begin{pmatrix} 50 \\ 50 \\ 52 \\ 51 \end{pmatrix} \cdot in$ height (excluding thickness of the flanges)

$b_f := 44in$ flange width

$h := d + 2 \cdot t_f = \begin{pmatrix} 53.25 \\ 53.25 \\ 55 \\ 54 \end{pmatrix} \cdot in$ total height

$A_{g_n} := \left(t_{f_n} \cdot b_f + t_w \cdot d_n\right) \cdot 2$

$A_g = \begin{pmatrix} 243 \\ 243 \\ 236 \\ 234 \end{pmatrix} \cdot in^2$ gross area

$S_{y_n} := \dfrac{b_f \cdot (h_n)^2}{6} - \dfrac{(b_f - 2 \cdot t_w) \cdot (d_n)^3}{6 \cdot h_n}$ $S_y = \begin{pmatrix} 4362 \\ 4362 \\ 4288 \\ 4189 \end{pmatrix} \cdot in^3$ y - section modulus

$S_{z_n} := \dfrac{b_f^{\,2} \cdot h_n}{6} - \dfrac{(b_f - 2 \cdot t_w)^3 \cdot d_n}{6 \cdot b_f}$ $S_z = \begin{pmatrix} 3150 \\ 3150 \\ 3154 \\ 3112 \end{pmatrix} \cdot in^3$ z - section modulus

$I_{y_n} := 2 \cdot \left[\dfrac{b_f \cdot \left(t_{f_n}\right)^3}{12} + b_f \cdot t_{f_n} \cdot \left(\dfrac{h_n}{2} - \dfrac{t_w}{2} \right)^2 \right] + 2 \cdot \left[\dfrac{t_w \cdot (d_n)^3}{12} \right]$ $I_y = \begin{pmatrix} 118465 \\ 118465 \\ 119687 \\ 114830 \end{pmatrix} \cdot in^4$ y - moment of inertia

$I_{z_n} := 2 \cdot \left(\dfrac{t_{f_n} \cdot b_f^{\,3}}{12} \right) + 2 \cdot \left[\dfrac{d_n \cdot t_w^{\,3}}{12} + d_n \cdot t_w \cdot \left(\dfrac{b_f}{2} - \dfrac{t_{f_n}}{2} \right)^2 \right]$ $I_z = \begin{pmatrix} 67970 \\ 67970 \\ 68267 \\ 67364 \end{pmatrix} \cdot in^4$ z - moment of inertia

$$r_{y_n} := \sqrt{\frac{I_{y_n}}{A_{g_n}}} \qquad r_y = \begin{pmatrix} 22.1 \\ 22.1 \\ 22.5 \\ 22.2 \end{pmatrix} \cdot in$$

y radius of gyration

$$r_{z_n} := \sqrt{\frac{I_{z_n}}{A_{g_n}}} \qquad r_z = \begin{pmatrix} 16.7 \\ 16.7 \\ 17 \\ 17 \end{pmatrix} \cdot in$$

z radius of gyration

$$Z_{y_n} := \left(\frac{h_n}{2}\right)^2 \cdot b_f - \left(\frac{d_n}{2}\right)^2 \cdot \left(b_f - 2 \cdot t_w\right) \qquad Z_y = \begin{pmatrix} 4941 \\ 4941 \\ 4883 \\ 4766 \end{pmatrix} \cdot in^3$$

y - plastic section modulus

$$Z_{z_n} := \left(\frac{b_f}{2}\right)^2 \cdot h_n - \left(\frac{b_f - 2 \cdot t_w}{2}\right)^2 \cdot \left(d_n\right) \qquad Z_z = \begin{pmatrix} 3723 \\ 3723 \\ 3688 \\ 3645 \end{pmatrix} \cdot in^3$$

z - plastic section modulus

Examine Local Buckling:

$$\frac{b_f - 2 \cdot t_w}{t_f} = \begin{pmatrix} 25.85 \\ 25.85 \\ 28 \\ 28 \end{pmatrix} \leq 1.40 \cdot \sqrt{\frac{E}{F_y}} = 33.72 \qquad (6.9.4.2\text{-}1)$$

local buckling is avoided

Combined Axial Compression and Flexure, calculation according to AASHTO LRFD:

$$P_e := \begin{pmatrix} 25148 \\ 25019 \\ 23372 \\ 21600 \end{pmatrix} kip$$

Elastic critical buckling resistance — From Buckling Analysis in Midas Civil Model

$Q := 1.0$ — Slender Element reduction factor

$$P_0 := Q \cdot F_y \cdot A_g = \begin{pmatrix} 12150 \\ 12150 \\ 11800 \\ 11700 \end{pmatrix} \cdot kip$$

Equivalent nominal yield resistance

Determination of P_n (nominal compressive resistance):

$$\frac{P_e}{P_0} = \begin{pmatrix} 2.07 \\ 2.059 \\ 1.981 \\ 1.846 \end{pmatrix}$$

If $\frac{P_e}{P_0} \le 0.44$ $\quad P_n := 0.877 \cdot P_e = \begin{pmatrix} 22055 \\ 21942 \\ 20497 \\ 18943 \end{pmatrix} \cdot kip$ (6.9.4.1.1-1)

If $\frac{P_e}{P_0} > 0.44$ $\quad P_{n_n} := \left[0.658^{\left(\frac{P_{0_n}}{P_{e_n}}\right)} \right] \cdot P_{0_n}$ $\quad P_n = \begin{pmatrix} 9926 \\ 9915 \\ 9552 \\ 9327 \end{pmatrix} \cdot kip$ (6.9.4.1.1-2)

$\phi_c := 0.9$ Resistance factor for compression (6.5.4.2)

$P_r := \phi_c \cdot P_n = \begin{pmatrix} 8933 \\ 8924 \\ 8597 \\ 8394 \end{pmatrix} \cdot kip$ Factored resistance of components in compression (6.9.2.1-1)

$P_u := \begin{pmatrix} 8434 & 6259 \\ 8434 & 5819 \\ 7886 & 5819 \\ 7285 & 6297 \end{pmatrix} kip$

From Analysis in Midas Civil -
First column - Max Compressive force case
Second column - Max Major banding moment

$M_{uy} := \begin{pmatrix} 1143 & 5122 \\ 1143 & 6299 \\ 224 & 6299 \\ 599 & 4818 \end{pmatrix} kip \cdot ft$

$M_{uz} := \begin{pmatrix} 12 & 114 \\ 12 & 197 \\ 150 & 169 \\ 76 & 85 \end{pmatrix} kip \cdot ft$

$\phi_f := 1.0$ Resistance factor for flexure (6.5.4.2)

$l_z := 55ft$ Unbraced Length - z direction

$l_y := 55ft$ Unbraced Length - y direction

$A_n := \left(d_n + t_{f_n}\right) \cdot \left(b_f - t_w\right)$ $\quad A = \begin{pmatrix} 2220 \\ 2220 \\ 2300 \\ 2257 \end{pmatrix} \cdot in^2$ Area enclosed within the centerlines of the plates comprising the box

$$M_{ny_n} := F_y \cdot S_{y_n} \cdot \left[1 - \frac{0.064 F_y \cdot S_{y_n} \cdot l_y}{A_n \cdot E} \cdot \left[\frac{2 \cdot \left(\frac{d_n}{t_w} + \frac{b_f}{t_{f_n}} \right)}{l_{y_n}} \right]^{0.5} \right] \qquad M_{ny} = \begin{pmatrix} 18082 \\ 18082 \\ 17776 \\ 17364 \end{pmatrix} \cdot kip \cdot ft \qquad M_{ry} := \phi_f \cdot M_{ny}$$

(6.12.2.2.2-1)

$$M_{nz_n} := F_y \cdot S_{z_n} \cdot \left[1 - \frac{0.064 F_y \cdot S_{z_n} \cdot l_z}{A_n \cdot E} \cdot \left[\frac{2 \cdot \left(\frac{d_n}{t_w} + \frac{b_f}{t_{f_n}} \right)}{l_{z_n}} \right]^{0.5} \right] \qquad M_{nz} = \begin{pmatrix} 13061 \\ 13061 \\ 13076 \\ 12901 \end{pmatrix} \cdot kip \cdot ft \qquad M_{rz} := \phi_f \cdot M_{nz}$$

$$M_{p.y_n} := F_y \cdot Z_{y_n} \qquad M_{p.y} = \begin{pmatrix} 20588 \\ 20588 \\ 20346 \\ 19856 \end{pmatrix} \cdot kip \cdot ft$$

y- plastic moment

$m := 1 .. 2$

$$M_{p.z_n} := F_y \cdot Z_{z_n} \qquad M_{p.z} = \begin{pmatrix} 15512 \\ 15512 \\ 15367 \\ 15187 \end{pmatrix} \cdot kip \cdot ft$$

z- plastic moment

$$ratio_{n,m} := \frac{P_{u_{n,m}}}{P_{r_n}} \qquad ratio = \begin{pmatrix} 0.944 & 0.701 \\ 0.945 & 0.652 \\ 0.917 & 0.677 \\ 0.868 & 0.75 \end{pmatrix}$$

If $\frac{P_u}{P_r} < 0.2$ $\quad InteractionEquation1_{n,m} := \frac{P_{u_{n,m}}}{2.0 P_{r_n}} + \left(\frac{M_{uz_{n,m}}}{M_{rz_n}} + \frac{M_{uz_{n,m}}}{M_{ry_n}} \right)$ $\quad \le 1.0$ CHECK (6.9.2.2-1)

$$InteractionEquation1 = \begin{pmatrix} 0.47 & 0.37 \\ 0.47 & 0.35 \\ 0.48 & 0.36 \\ 0.44 & 0.39 \end{pmatrix}$$

If $\frac{P_u}{P_r} \ge 0.2$

$InteractionEquation2_{n,m} := \frac{P_{u_{n,m}}}{P_{r_n}} + \frac{8.0}{9.0} \left(\frac{M_{uz_{n,m}}}{M_{rz_n}} + \frac{M_{uy_{n,m}}}{M_{ry_n}} \right)$ $\quad \le 1.0$ CHECK (6.9.2.2-2)

$$\boxed{InteractionEquation2 = \begin{pmatrix} 1.00 & 0.96 \\ 1.00 & 0.98 \\ 0.94 & 1.00 \\ 0.90 & 1.00 \end{pmatrix}}$$

System Reliability calculations for the existing cross sections.

Dominating effect - Major bending moment:

$$\beta_M := \begin{pmatrix} 4.56 \\ 4.51 \\ 4.42 \\ 4.36 \\ 4.36 \\ 4.42 \\ 4.51 \\ 4.56 \end{pmatrix}$$

Reliability index for all segments of the arch

$mean(\beta_M) = 4.46$

$min(\beta_M) = 4.36$

$$p_{fM} := cnorm(-\beta_M) = \begin{pmatrix} 2.56 \times 10^{-6} \\ 3.24 \times 10^{-6} \\ 4.94 \times 10^{-6} \\ 6.5 \times 10^{-6} \\ 6.5 \times 10^{-6} \\ 4.94 \times 10^{-6} \\ 3.24 \times 10^{-6} \\ 2.56 \times 10^{-6} \end{pmatrix}$$

Probabilites of failure for all segments of the arch

Probability of failure for the arch, full correlation:

$max(p_{fM}) = 6.5 \times 10^{-6}$ Lower Bound

Probability of failure for the arch, no correlation:

Upper Bound

$$1 - \left(1 - p_{fM_1}\right)\left(1 - p_{fM_2}\right)\cdot\left(1 - p_{fM_3}\right)\cdot\left(1 - p_{fM_4}\right)\cdot\left(1 - p_{fM_5}\right)\cdot\left(1 - p_{fM_6}\right)\left(1 - p_{fM_7}\right)\cdot\left(1 - p_{fM_8}\right) = 3.45 \times 10^{-5}$$

$$\rho := \begin{pmatrix} 0.0 \\ 0.2 \\ 0.4 \\ 0.6 \\ 0.8 \\ 0.99 \end{pmatrix}$$

$\beta_{eM.WIM} := mean(\beta_M)$ $n := 8$

$\beta_{eM} := \beta_{eM.WIM}$

$$P_{fM_1} := 1 - \int_{-\infty}^{\infty} \left(cnorm\left(\frac{\beta_{eM} + t\cdot\sqrt{\rho_1}}{\sqrt{1-\rho_1}} \right)^n \right) dnorm(t, 0, 1)\ dt = 3.2 \times 10^{-5}$$

$$P_{fM_2} := 1 - \int_{-\infty}^{\infty} \left(cnorm\left(\frac{\beta_{eM} + t\cdot\sqrt{\rho_2}}{\sqrt{1-\rho_2}} \right)^n \right) dnorm(t, 0, 1)\ dt = 3.2 \times 10^{-5}$$

$$P_{fM_3} := 1 - \int_{-\infty}^{\infty} \left(cnorm\left(\frac{\beta_{eM} + t\cdot\sqrt{\rho_3}}{\sqrt{1-\rho_3}} \right)^n \right) dnorm(t, 0, 1)\ dt = 3.2 \times 10^{-5}$$

$$P_{fM_4} := 1 - \int_{-\infty}^{\infty} \left(cnorm\left(\frac{\beta_{eM} + t\cdot\sqrt{\rho_4}}{\sqrt{1-\rho_4}} \right)^n \right) dnorm(t, 0, 1)\ dt = 3.1 \times 10^{-5}$$

$$P_{fM_5} := 1 - \int_{-\infty}^{\infty} \left(cnorm\left(\frac{\beta_{eM} + t\cdot\sqrt{\rho_5}}{\sqrt{1-\rho_5}} \right)^n \right) dnorm(t, 0, 1)\ dt = 2.4 \times 10^{-5}$$

$$P_{fM_6} := 1 - \int_{-\infty}^{\infty} \left(cnorm\left(\frac{\beta_{eM} + t\cdot\sqrt{\rho_6}}{\sqrt{1-\rho_6}} \right)^n \right) dnorm(t, 0, 1)\ dt = 5.2 \times 10^{-6}$$

$$P_{fsysM.WIM} := \begin{pmatrix} P_{fM_1} \\ P_{fM_2} \\ P_{fM_3} \\ P_{fM_4} \\ P_{fM_5} \\ P_{fM_6} \end{pmatrix} = \begin{pmatrix} 3.2 \times 10^{-5} \\ 3.2 \times 10^{-5} \\ 3.2 \times 10^{-5} \\ 3.1 \times 10^{-5} \\ 2.4 \times 10^{-5} \\ 5.2 \times 10^{-6} \end{pmatrix} \quad \beta sysM_{WIM} := -qnorm\left(P_{fsysM.WIM}, 0, 1\right) = \begin{pmatrix} 3.99 \\ 3.99 \\ 4.00 \\ 4.01 \\ 4.06 \\ 4.41 \end{pmatrix}$$

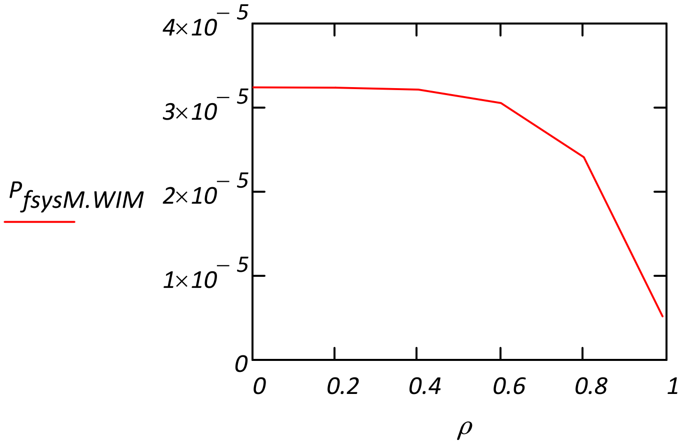

4×10⁻⁵
3×10⁻⁵
2×10⁻⁵
1×10⁻⁵
0
PfsysM.WIM
0
0.2
0.4
0.6
0.8
1
ρ

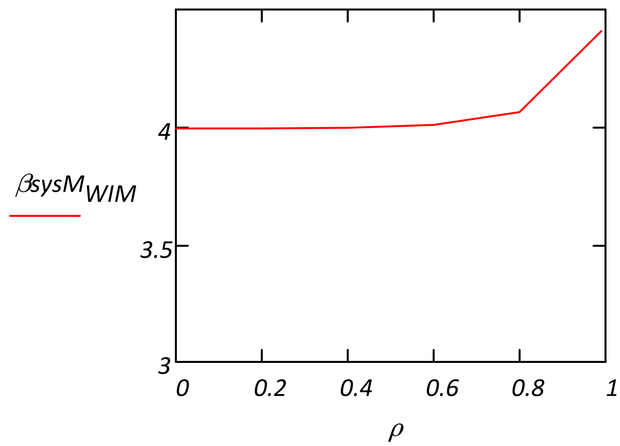

4
3.5
3
βsysMWIM
0
0.2
0.4
0.6
0.8
1
ρ

Dominating effect - Compressive force

$$\beta_P := \begin{pmatrix} 4.27 \\ 4.03 \\ 4.16 \\ 4.30 \\ 4.30 \\ 4.16 \\ 4.03 \\ 4.27 \end{pmatrix}$$

Reliability index for all segments of the arch

$mean(\beta_P) = 4.19$

$min(\beta_P) = 4.03$

$$p_{fP} := cnorm(-\beta_P) = \begin{pmatrix} 9.77 \times 10^{-6} \\ 2.79 \times 10^{-5} \\ 1.59 \times 10^{-5} \\ 8.54 \times 10^{-6} \\ 8.54 \times 10^{-6} \\ 1.59 \times 10^{-5} \\ 2.79 \times 10^{-5} \\ 9.77 \times 10^{-6} \end{pmatrix}$$

Probabilites of failure for all segments of the arch

Probability of failure for the arch, full correlation:

$max(p_{fP}) = 2.8 \times 10^{-5}$ Lower Bound

Probability of failure for the arch, no correlation:

Upper Bound

$$1 - \left(1 - p_{fP_1}\right)\left(1 - p_{fP_2}\right)\cdot\left(1 - p_{fP_3}\right)\cdot\left(1 - p_{fP_4}\right)\cdot\left(1 - p_{fP_5}\right)\cdot\left(1 - p_{fP_6}\right)\left(1 - p_{fP_7}\right)\cdot\left(1 - p_{fP_8}\right) = 1.24 \times 10^{-4}$$

$$\rho := \begin{pmatrix} 0.0 \\ 0.2 \\ 0.4 \\ 0.6 \\ 0.8 \\ 0.99 \end{pmatrix}$$

$\beta_{eP.WIM} := mean(\beta_P)$ $n := 8$

$\beta_{eP} := \beta_{eP.WIM}$

$$P_{fP_1} := 1 - \int_{-\infty}^{\infty} \left(cnorm\left(\frac{\beta_{eP} + t \cdot \sqrt{\rho_1}}{\sqrt{1 - \rho_1}} \right)^n \right) dnorm(t, 0, 1)\ dt = 1.1 \times 10^{-4}$$

$$P_{fP_2} := 1 - \int_{-\infty}^{\infty} \left(cnorm\left(\frac{\beta_{eP} + t \cdot \sqrt{\rho_2}}{\sqrt{1 - \rho_2}} \right)^n \right) dnorm(t, 0, 1)\ dt = 1.1 \times 10^{-4}$$

$$P_{fP_3} := 1 - \int_{-\infty}^{\infty} \left(cnorm\left(\frac{\beta_{eP} + t \cdot \sqrt{\rho_3}}{\sqrt{1 - \rho_3}} \right)^n \right) dnorm(t, 0, 1)\ dt = 1.1 \times 10^{-4}$$

$$P_{fP_4} := 1 - \int_{-\infty}^{\infty} \left(cnorm\left(\frac{\beta_{eP} + t \cdot \sqrt{\rho_4}}{\sqrt{1 - \rho_4}} \right)^n \right) dnorm(t, 0, 1)\ dt = 1 \times 10^{-4}$$

$$P_{fP_5} := 1 - \int_{-\infty}^{\infty} \left(cnorm\left(\frac{\beta_{eP} + t \cdot \sqrt{\rho_5}}{\sqrt{1 - \rho_5}} \right)^n \right) dnorm(t, 0, 1)\ dt = 8 \times 10^{-5}$$

$$P_{fP_6} := 1 - \int_{-\infty}^{\infty} \left(cnorm\left(\frac{\beta_{eP} + t \cdot \sqrt{\rho_6}}{\sqrt{1 - \rho_6}} \right)^n \right) dnorm(t, 0, 1)\ dt = 2 \times 10^{-5}$$

$$P_{fsysP.WIM} := \begin{pmatrix} P_{fP_1} \\ P_{fP_2} \\ P_{fP_3} \\ P_{fP_4} \\ P_{fP_5} \\ P_{fP_6} \end{pmatrix} = \begin{pmatrix} 1.1 \times 10^{-4} \\ 1.1 \times 10^{-4} \\ 1.1 \times 10^{-4} \\ 1.0 \times 10^{-4} \\ 8.0 \times 10^{-5} \\ 2.0 \times 10^{-5} \end{pmatrix} \qquad \beta sysP_{WIM} := -qnorm\left(P_{fsysP.WIM}, 0, 1\right) = \begin{pmatrix} 3.69 \\ 3.69 \\ 3.69 \\ 3.71 \\ 3.78 \\ 4.11 \end{pmatrix}$$

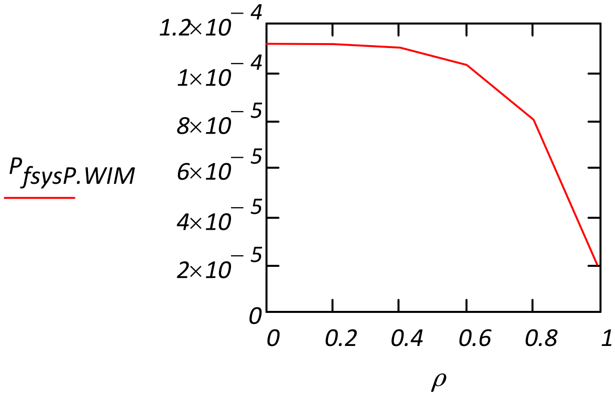
$P_{fsysP.WIM}$
1.2×10^{-4}
1×10^{-4}
8×10^{-5}
6×10^{-5}
4×10^{-5}
2×10^{-5}
0
0 0.2 0.4 0.6 0.8 1
ρ

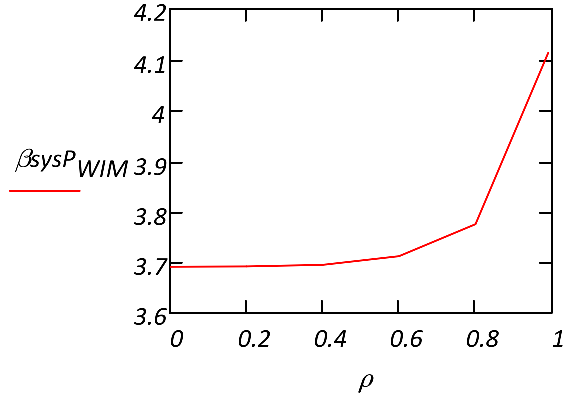
$\beta sysP_{WIM}$
4.2
4.1
4
3.9
3.8
3.7
3.6
0 0.2 0.4 0.6 0.8 1
ρ

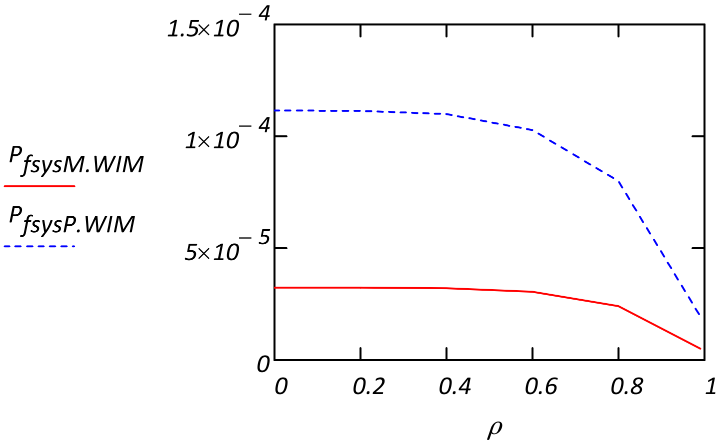
$P_{fsysM.WIM}$
$P_{fsysP.WIM}$
1.5×10^{-4}
1×10^{-4}
5×10^{-5}
0
0 0.2 0.4 0.6 0.8 1
ρ

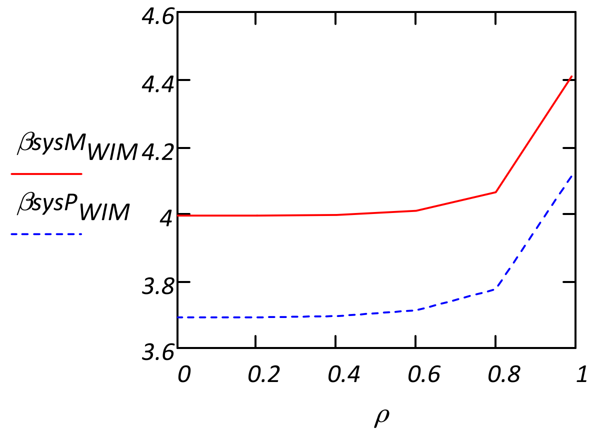
$\beta sysM_{WIM}$
$\beta sysP_{WIM}$
4.6
4.4
4.2
4
3.8
3.6
0 0.2 0.4 0.6 0.8 1
ρ

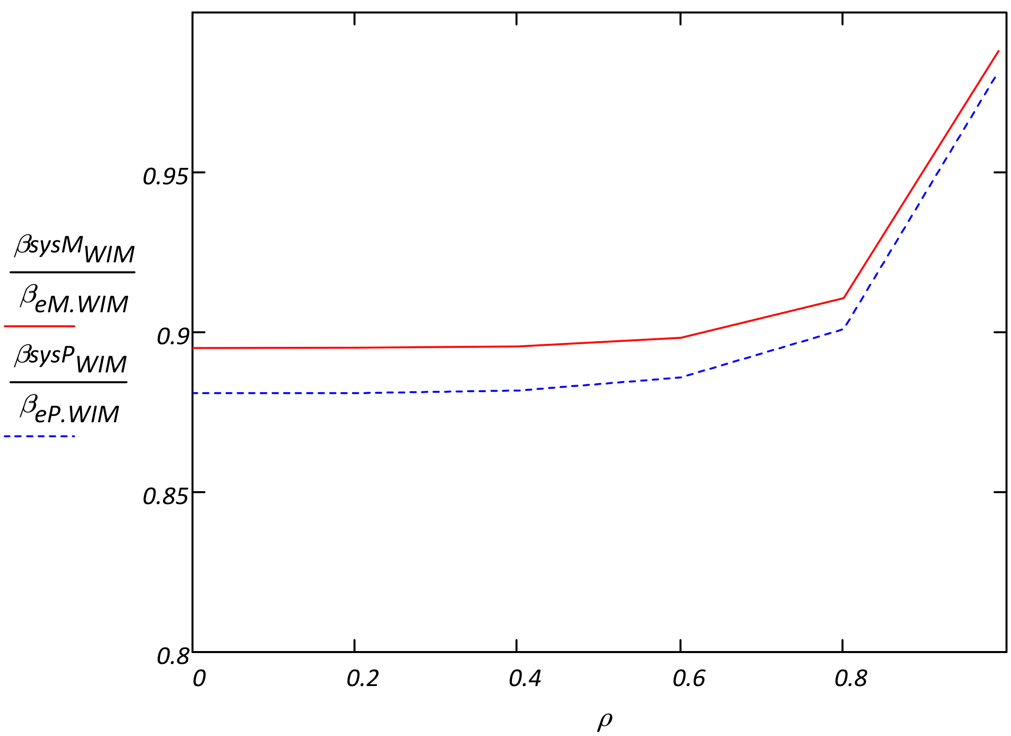
$\frac{\beta sysM_{WIM}}{\beta_{eM.WIM}}$
$\frac{\beta sysP_{WIM}}{\beta_{eP.WIM}}$
0.95
0.9
0.85
0.8
0 0.2 0.4 0.6 0.8
ρ

System Reliability calculations for the cross sections determined according to AASHTO Standard Specifications.

Dominating effect - Major bending moment:

$$\beta_M := \begin{pmatrix} 3.82 \\ 3.94 \\ 4.02 \\ 4.04 \\ 4.04 \\ 4.02 \\ 3.94 \\ 3.82 \end{pmatrix}$$

Reliability index for all segments of the arch

$$mean(\beta_M) = 3.955$$

$$min(\beta_M) = 3.82$$

$$p_{fM} := cnorm(-\beta_M) = \begin{pmatrix} 6.67 \times 10^{-5} \\ 4.07 \times 10^{-5} \\ 2.91 \times 10^{-5} \\ 2.67 \times 10^{-5} \\ 2.67 \times 10^{-5} \\ 2.91 \times 10^{-5} \\ 4.07 \times 10^{-5} \\ 6.67 \times 10^{-5} \end{pmatrix}$$

Probabilites of failure for all segments of the arch

Probability of failure for the arch, full correlation:

$$max(p_{fM}) = 6.673 \times 10^{-5}$$

Lower Bound

Probability of failure for the arch, no correlation:

$$1 - \left(1 - p_{fM_1}\right)\left(1 - p_{fM_2}\right)\cdot\left(1 - p_{fM_3}\right)\cdot\left(1 - p_{fM_4}\right)\cdot\left(1 - p_{fM_5}\right)\cdot\left(1 - p_{fM_6}\right)\left(1 - p_{fM_7}\right)\cdot\left(1 - p_{fM_8}\right) = 3.27 \times 10^{-4}$$

Upper Bound

$$\rho := \begin{pmatrix} 0.0 \\ 0.2 \\ 0.4 \\ 0.6 \\ 0.8 \\ 0.99 \end{pmatrix}$$

$\beta_{eM.STD} := mean(\beta_M)$ $\quad n := 8$

$\beta_{eM} := \beta_{eM.STD}$ $\quad \beta_{eM.STD} = 3.955$

$$P_{fM_1} := 1 - \int_{-\infty}^{\infty} \left(cnorm\left(\frac{\beta_{eM} + t \cdot \sqrt{\rho_1}}{\sqrt{1 - \rho_1}} \right)^n \right) dnorm(t, 0, 1)\, dt = 3.1 \times 10^{-4}$$

$$P_{fM_2} := 1 - \int_{-\infty}^{\infty} \left(cnorm\left(\frac{\beta_{eM} + t \cdot \sqrt{\rho_2}}{\sqrt{1 - \rho_2}} \right)^n \right) dnorm(t, 0, 1)\, dt = 3.1 \times 10^{-4}$$

$$P_{fM_3} := 1 - \int_{-\infty}^{\infty} \left(cnorm\left(\frac{\beta_{eM} + t \cdot \sqrt{\rho_3}}{\sqrt{1 - \rho_3}} \right)^n \right) dnorm(t, 0, 1)\, dt = 3 \times 10^{-4}$$

$$P_{fM_4} := 1 - \int_{-\infty}^{\infty} \left(cnorm\left(\frac{\beta_{eM} + t \cdot \sqrt{\rho_4}}{\sqrt{1 - \rho_4}} \right)^n \right) dnorm(t, 0, 1)\, dt = 2.8 \times 10^{-4}$$

$$P_{fM_5} := 1 - \int_{-\infty}^{\infty} \left(cnorm\left(\frac{\beta_{eM} + t \cdot \sqrt{\rho_5}}{\sqrt{1 - \rho_5}} \right)^n \right) dnorm(t, 0, 1)\, dt = 2.1 \times 10^{-4}$$

$$P_{fM_6} := 1 - \int_{-\infty}^{\infty} \left(cnorm\left(\frac{\beta_{eM} + t \cdot \sqrt{\rho_6}}{\sqrt{1 - \rho_6}} \right)^n \right) dnorm(t, 0, 1)\, dt = 6.6 \times 10^{-5}$$

$$P_{fsysM} := \begin{pmatrix} P_{fM_1} \\ P_{fM_2} \\ P_{fM_3} \\ P_{fM_4} \\ P_{fM_5} \\ P_{fM_6} \end{pmatrix} = \begin{pmatrix} 3.1 \times 10^{-4} \\ 3.1 \times 10^{-4} \\ 3 \times 10^{-4} \\ 2.8 \times 10^{-4} \\ 2.1 \times 10^{-4} \\ 6.6 \times 10^{-5} \end{pmatrix} \qquad \beta sysM := -qnorm\left(P_{fsysM}, 0, 1\right) = \begin{pmatrix} 3.43 \\ 3.43 \\ 3.43 \\ 3.45 \\ 3.53 \\ 3.82 \end{pmatrix}$$

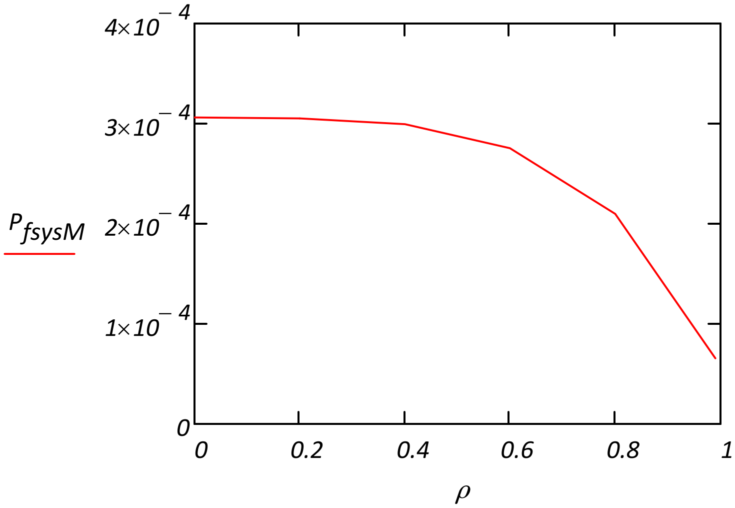

P_{fsysM}
4×10^{-4}
3×10^{-4}
2×10^{-4}
1×10^{-4}
0
0
0.2
0.4
0.6
0.8
1
ρ

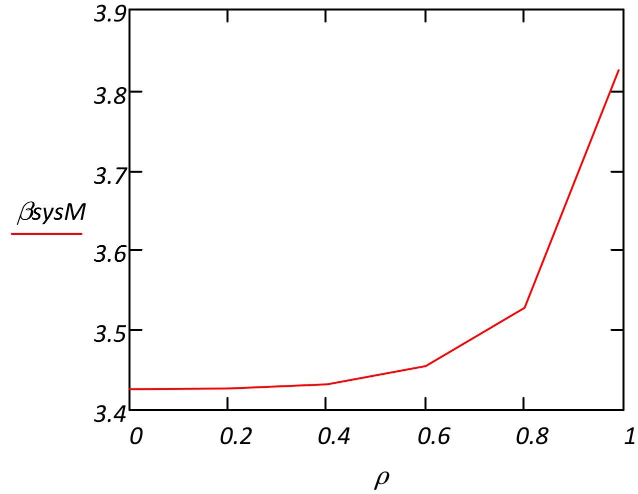

$\beta sysM$
3.9
3.8
3.7
3.6
3.5
3.4
0
0.2
0.4
0.6
0.8
1
ρ

Dominating effect - Compressive force

$$\beta_P := \begin{pmatrix} 3.46 \\ 3.45 \\ 3.62 \\ 3.83 \\ 3.83 \\ 3.62 \\ 3.45 \\ 3.46 \end{pmatrix}$$

Reliability index for all segments of the arch

$mean(\beta_P) = 3.59$

$min(\beta_P) = 3.45$

$$p_{fP} := cnorm(-\beta_P) = \begin{pmatrix} 2.7 \times 10^{-4} \\ 2.8 \times 10^{-4} \\ 1.47 \times 10^{-4} \\ 6.41 \times 10^{-5} \\ 6.41 \times 10^{-5} \\ 1.47 \times 10^{-4} \\ 2.8 \times 10^{-4} \\ 2.7 \times 10^{-4} \end{pmatrix}$$

Probabilites of failure for all segments of the arch

Probability of failure for the arch, full correlation:

$$max(p_{fP}) = 2.803 \times 10^{-4}$$

Lower Bound

Probability of failure for the arch, no correlation:

$$1 - \left(1 - p_{fP_1}\right)\left(1 - p_{fP_2}\right)\cdot\left(1 - p_{fP_3}\right)\cdot\left(1 - p_{fP_4}\right)\cdot\left(1 - p_{fP_5}\right)\cdot\left(1 - p_{fP_6}\right)\left(1 - p_{fP_7}\right)\cdot\left(1 - p_{fP_8}\right) = 1.52 \times 10^{-3}$$

Upper Bound

$$\rho := \begin{pmatrix} 0.0 \\ 0.2 \\ 0.4 \\ 0.6 \\ 0.8 \\ 0.99 \end{pmatrix}$$

$\beta_{eP.STD} := mean\left(, n := 8 \right.$

$\beta_{eP.STD} = 3.59$

$\beta_{eP} := \beta_{eP.STD}$

$$P_{fP_1} := 1 - \int_{-\infty}^{\infty} \left(cnorm\left(\frac{\beta_{eP} + t \cdot \sqrt{\rho_1}}{\sqrt{1-\rho_1}} \right)^n \right) dnorm(t, 0, 1)\ dt = 1.3 \times 10^{-3}$$

$$P_{fP_2} := 1 - \int_{-\infty}^{\infty} \left(cnorm\left(\frac{\beta_{eP} + t \cdot \sqrt{\rho_2}}{\sqrt{1-\rho_2}} \right)^n \right) dnorm(t, 0, 1)\ dt = 1.3 \times 10^{-3}$$

$$P_{fP_3} := 1 - \int_{-\infty}^{\infty} \left(cnorm\left(\frac{\beta_{eP} + t \cdot \sqrt{\rho_3}}{\sqrt{1-\rho_3}} \right)^n \right) dnorm(t, 0, 1)\ dt = 1.3 \times 10^{-3}$$

$$P_{fP_4} := 1 - \int_{-\infty}^{\infty} \left(cnorm\left(\frac{\beta_{eP} + t \cdot \sqrt{\rho_4}}{\sqrt{1-\rho_4}} \right)^n \right) dnorm(t, 0, 1)\ dt = 1.1 \times 10^{-3}$$

$$P_{fP_5} := 1 - \int_{-\infty}^{\infty} \left(cnorm\left(\frac{\beta_{eP} + t \cdot \sqrt{\rho_5}}{\sqrt{1-\rho_5}} \right)^n \right) dnorm(t, 0, 1)\ dt = 8.4 \times 10^{-4}$$

$$P_{fP_6} := 1 - \int_{-\infty}^{\infty} \left(cnorm\left(\frac{\beta_{eP} + t \cdot \sqrt{\rho_6}}{\sqrt{1-\rho_6}} \right)^n \right) dnorm(t, 0, 1)\ dt = 2.7 \times 10^{-4}$$

$$P_{fsysP} := \begin{pmatrix} P_{fP_1} \\ P_{fP_2} \\ P_{fP_3} \\ P_{fP_4} \\ P_{fP_5} \\ P_{fP_6} \end{pmatrix} = \begin{pmatrix} 1.3 \times 10^{-3} \\ 1.3 \times 10^{-3} \\ 1.3 \times 10^{-3} \\ 1.1 \times 10^{-3} \\ 8.4 \times 10^{-4} \\ 2.7 \times 10^{-4} \end{pmatrix} \qquad \beta sysP := -qnorm\left(P_{fsysP}, 0, 1\right) = \begin{pmatrix} 3.01 \\ 3.01 \\ 3.02 \\ 3.05 \\ 3.14 \\ 3.46 \end{pmatrix}$$

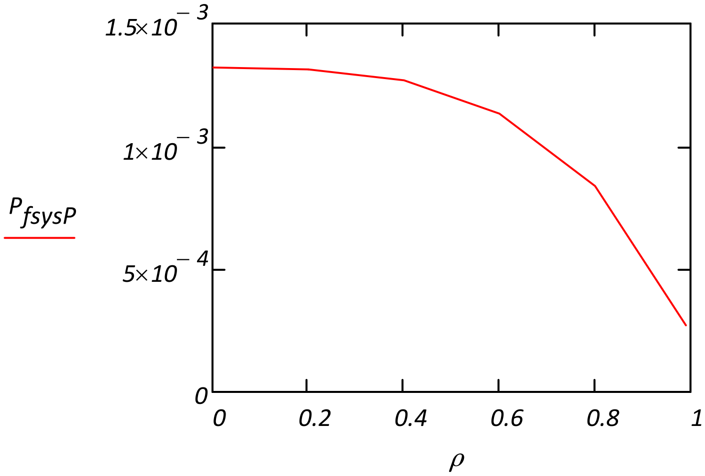
1.5×10⁻³
1×10⁻³
5×10⁻⁴
0
0
0.2
0.4
0.6
0.8
1
ρ
PfsysP

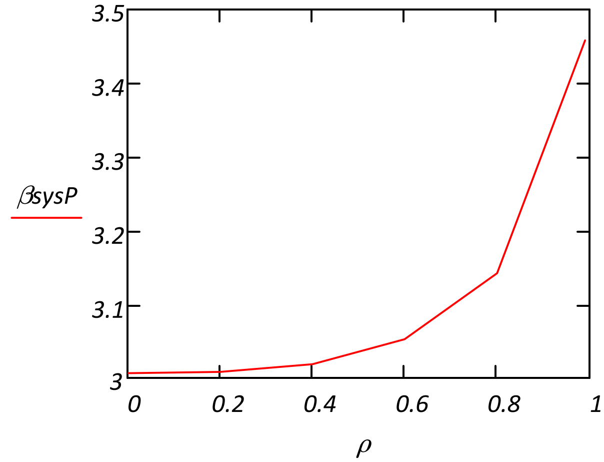
3.5
3.4
3.3
3.2
3.1
3
0
0.2
0.4
0.6
0.8
1
ρ
βsysP

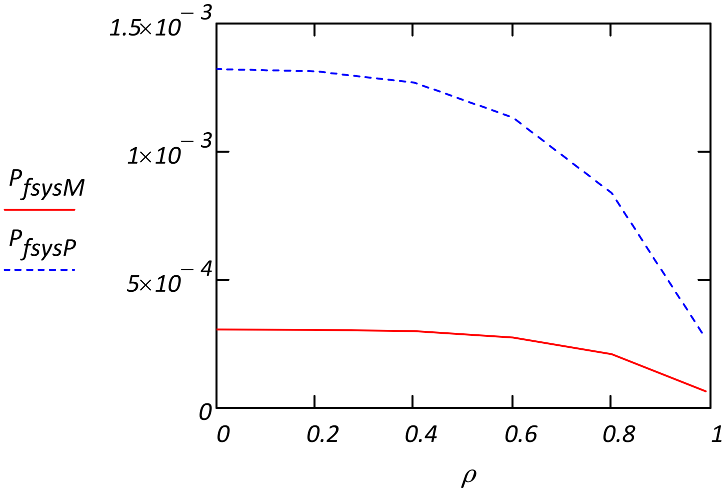
1.5×10⁻³
1×10⁻³
5×10⁻⁴
0
0
0.2
0.4
0.6
0.8
1
ρ
PfsysM
PfsysP

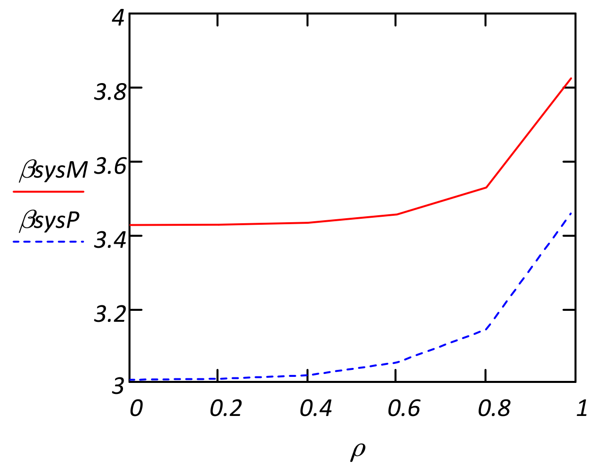
4
3.8
3.6
3.4
3.2
3
0
0.2
0.4
0.6
0.8
1
ρ
βsysM
βsysP

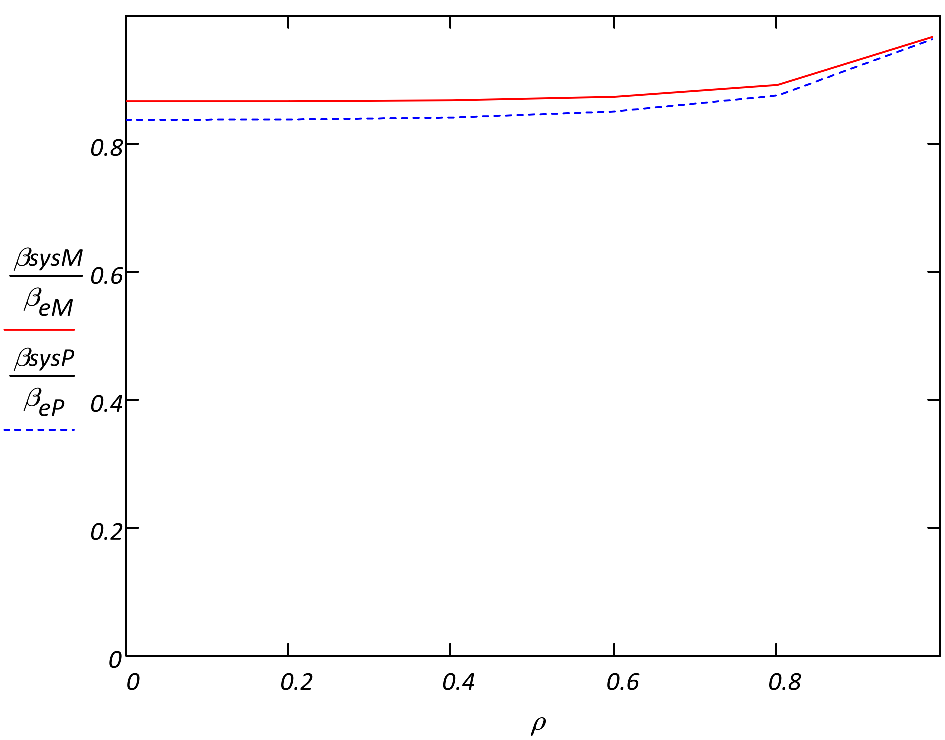
0.8
0.6
0.4
0.2
0
0
0.2
0.4
0.6
0.8
ρ
βsysM / βeM
βsysP / βeP

System Reliability calculations for the cross sections determined according to AASHTO LRFD.

Dominating effect - Major bending moment:

Reliability index for all segments of the arch

$$\beta_M := \begin{pmatrix} 3.65 \\ 3.78 \\ 3.85 \\ 3.76 \\ 3.76 \\ 3.85 \\ 3.78 \\ 3.65 \end{pmatrix} \qquad mean(\beta_M) = 3.76 \qquad min(\beta_M) = 3.65$$

Probabilites of failure for all segments of the arch

$$p_{fM} := cnorm(-\beta_M) = \begin{pmatrix} 1.31 \times 10^{-4} \\ 7.84 \times 10^{-5} \\ 5.91 \times 10^{-5} \\ 8.5 \times 10^{-5} \\ 8.5 \times 10^{-5} \\ 5.91 \times 10^{-5} \\ 7.84 \times 10^{-5} \\ 1.31 \times 10^{-4} \end{pmatrix}$$

Probability of failure for the arch, full correlation:

$$max(p_{fM}) = 1.3 \times 10^{-4}$$ Lower Bound

Probability of failure for the arch, no correlation:

$$1 - \left(1 - p_{fM_1}\right)\left(1 - p_{fM_2}\right)\cdot\left(1 - p_{fM_3}\right)\cdot\left(1 - p_{fM_4}\right)\cdot\left(1 - p_{fM_5}\right)\cdot\left(1 - p_{fM_6}\right)\left(1 - p_{fM_7}\right)\cdot\left(1 - p_{fM_8}\right) = 7.07 \times 10^{-4}$$

Upper Bound

$$\rho := \begin{pmatrix} 0.0 \\ 0.2 \\ 0.4 \\ 0.6 \\ 0.8 \\ 0.99 \end{pmatrix}$$

$$\beta_{eM.LRFD} := mean(\beta_M) \qquad n := 8$$

$$\beta_{eM} := \beta_{eM.LRFD}$$

$$P_{fM_1} := 1 - \int_{-\infty}^{\infty} \left(cnorm\left(\frac{\beta_{eM} + t\cdot\sqrt{\rho_1}}{\sqrt{1-\rho_1}}\right)^n \right) dnorm(t,0,1)\ dt = 6.8 \times 10^{-4}$$

$$P_{fM_2} := 1 - \int_{-\infty}^{\infty} \left(cnorm\left(\frac{\beta_{eM} + t\cdot\sqrt{\rho_2}}{\sqrt{1-\rho_2}}\right)^n \right) dnorm(t,0,1)\ dt = 6.8 \times 10^{-4}$$

$$P_{fM_3} := 1 - \int_{-\infty}^{\infty} \left(cnorm\left(\frac{\beta_{eM} + t\cdot\sqrt{\rho_3}}{\sqrt{1-\rho_3}}\right)^n \right) dnorm(t,0,1)\ dt = 6.6 \times 10^{-4}$$

$$P_{fM_4} := 1 - \int_{-\infty}^{\infty} \left(cnorm\left(\frac{\beta_{eM} + t\cdot\sqrt{\rho_4}}{\sqrt{1-\rho_4}}\right)^n \right) dnorm(t,0,1)\ dt = 6 \times 10^{-4}$$

$$P_{fM_5} := 1 - \int_{-\infty}^{\infty} \left(cnorm\left(\frac{\beta_{eM} + t\cdot\sqrt{\rho_5}}{\sqrt{1-\rho_5}}\right)^n \right) dnorm(t,0,1)\ dt = 4.5 \times 10^{-4}$$

$$P_{fM_6} := 1 - \int_{-\infty}^{\infty} \left(cnorm\left(\frac{\beta_{eM} + t\cdot\sqrt{\rho_6}}{\sqrt{1-\rho_6}}\right)^n \right) dnorm(t,0,1)\ dt = 1.2 \times 10^{-4}$$

$$P_{fsysM} := \begin{pmatrix} P_{fM_1} \\ P_{fM_2} \\ P_{fM_3} \\ P_{fM_4} \\ P_{fM_5} \\ P_{fM_6} \end{pmatrix} = \begin{pmatrix} 6.8 \times 10^{-4} \\ 6.8 \times 10^{-4} \\ 6.6 \times 10^{-4} \\ 6 \times 10^{-4} \\ 4.5 \times 10^{-4} \\ 1.2 \times 10^{-4} \end{pmatrix} \qquad \beta sysM := -qnorm\left(P_{fsysM}, 0, 1\right) = \begin{pmatrix} 3.2 \\ 3.2 \\ 3.21 \\ 3.24 \\ 3.32 \\ 3.67 \end{pmatrix}$$

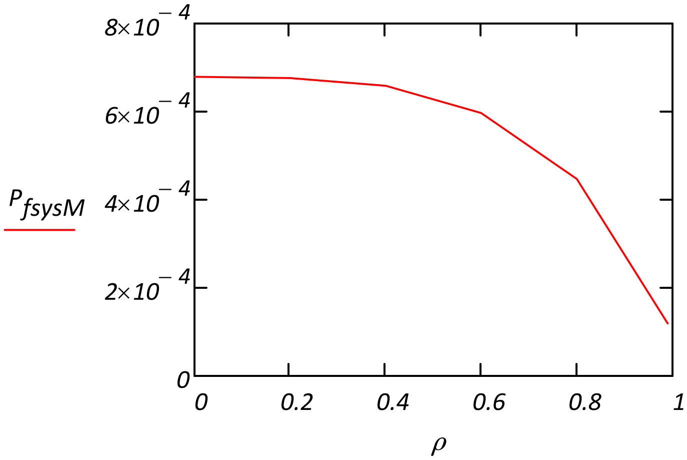

8×10^− 4
6×10^− 4
4×10^− 4
2×10^− 4
0
P_fsysM
0
0.2
0.4
0.6
0.8
1
ρ

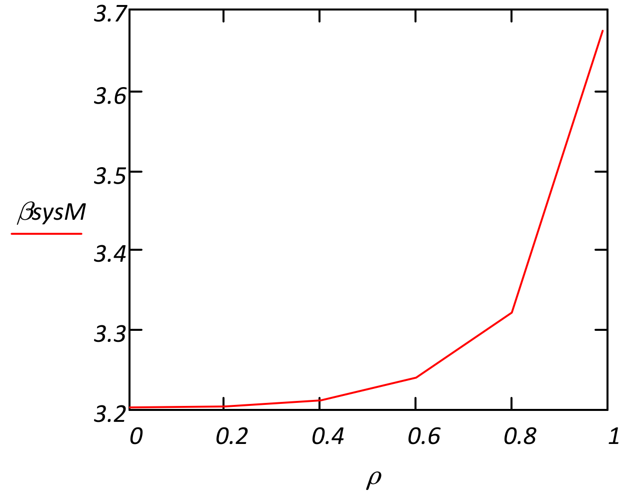

3.7
3.6
3.5
3.4
3.3
3.2
βsysM
0
0.2
0.4
0.6
0.8
1
ρ

Dominating effect - Compressive force

$$\beta_P := \begin{pmatrix} 3.25 \\ 3.26 \\ 3.47 \\ 3.73 \\ 3.73 \\ 3.47 \\ 3.26 \\ 3.25 \end{pmatrix}$$

Reliability index for all segments of the arch

$$mean(\beta_P) = 3.428$$

$$min(\beta_P) = 3.25$$

$$p_{fP} := cnorm(-\beta_P) = \begin{pmatrix} 5.77 \times 10^{-4} \\ 5.57 \times 10^{-4} \\ 2.6 \times 10^{-4} \\ 9.57 \times 10^{-5} \\ 9.57 \times 10^{-5} \\ 2.6 \times 10^{-4} \\ 5.57 \times 10^{-4} \\ 5.77 \times 10^{-4} \end{pmatrix}$$

Probabilites of failure for all segments of the arch

Probability of failure for the arch, full correlation:

$$max(p_{fP}) = 5.8 \times 10^{-4}$$

Lower Bound

Probability of failure for the arch, no correlation:

$$1 - \left(1 - p_{fP_1}\right)\left(1 - p_{fP_2}\right)\cdot\left(1 - p_{fP_3}\right)\cdot\left(1 - p_{fP_4}\right)\cdot\left(1 - p_{fP_5}\right)\cdot\left(1 - p_{fP_6}\right)\left(1 - p_{fP_7}\right)\cdot\left(1 - p_{fP_8}\right) = 2.98 \times 10^{-3}$$

Upper Bound

$$\rho := \begin{pmatrix} 0.0 \\ 0.2 \\ 0.4 \\ 0.6 \\ 0.8 \\ 0.99 \end{pmatrix}$$

$$\beta_{eP.LRFD} := mean(\beta_P) \qquad n := 8$$

$$\beta_{eP} := \beta_{eP.LRFD}$$

$$P_{fP_1} := 1 - \int_{-\infty}^{\infty} \left(cnorm\left(\frac{\beta_{eP} + t \cdot \sqrt{\rho_1}}{\sqrt{1 - \rho_1}} \right)^n \right) dnorm(t, 0, 1)\ dt = 2.4 \times 10^{-3}$$

$$P_{fP_2} := 1 - \int_{-\infty}^{\infty} \left(cnorm\left(\frac{\beta_{eP} + t \cdot \sqrt{\rho_2}}{\sqrt{1 - \rho_2}} \right)^n \right) dnorm(t, 0, 1)\ dt = 2.4 \times 10^{-3}$$

$$P_{fP_3} := 1 - \int_{-\infty}^{\infty} \left(cnorm\left(\frac{\beta_{eP} + t \cdot \sqrt{\rho_3}}{\sqrt{1 - \rho_3}} \right)^n \right) dnorm(t, 0, 1)\ dt = 2.3 \times 10^{-3}$$

$$P_{fP_4} := 1 - \int_{-\infty}^{\infty} \left(cnorm\left(\frac{\beta_{eP} + t \cdot \sqrt{\rho_4}}{\sqrt{1 - \rho_4}} \right)^n \right) dnorm(t, 0, 1)\ dt = 2 \times 10^{-3}$$

$$P_{fP_5} := 1 - \int_{-\infty}^{\infty} \left(cnorm\left(\frac{\beta_{eP} + t \cdot \sqrt{\rho_5}}{\sqrt{1 - \rho_5}} \right)^n \right) dnorm(t, 0, 1)\ dt = 1.5 \times 10^{-3}$$

$$P_{fP_6} := 1 - \int_{-\infty}^{\infty} \left(cnorm\left(\frac{\beta_{eP} + t \cdot \sqrt{\rho_6}}{\sqrt{1 - \rho_6}} \right)^n \right) dnorm(t, 0, 1)\ dt = 4.7 \times 10^{-4}$$

$$P_{fsysP} := \begin{pmatrix} P_{fP_1} \\ P_{fP_2} \\ P_{fP_3} \\ P_{fP_4} \\ P_{fP_5} \\ P_{fP_6} \end{pmatrix} = \begin{pmatrix} 2.4 \times 10^{-3} \\ 2.4 \times 10^{-3} \\ 2.3 \times 10^{-3} \\ 2 \times 10^{-3} \\ 1.5 \times 10^{-3} \\ 4.7 \times 10^{-4} \end{pmatrix} \qquad \beta sysP := -qnorm\left(P_{fsysP}, 0, 1\right) = \begin{pmatrix} 2.82 \\ 2.82 \\ 2.83 \\ 2.87 \\ 2.97 \\ 3.31 \end{pmatrix}$$

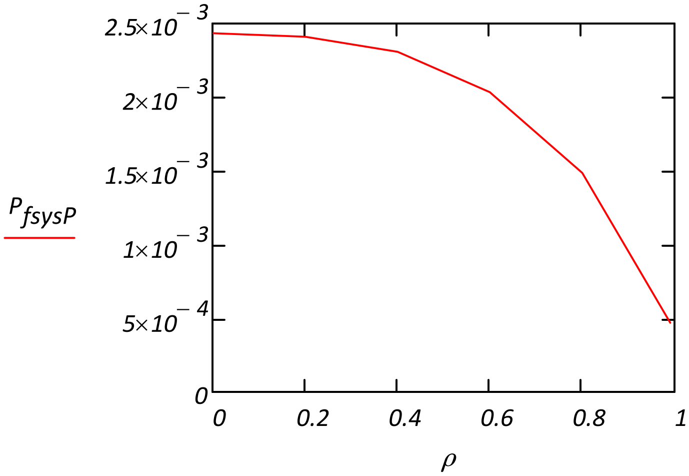

2.5×10^{-3}
2×10^{-3}
1.5×10^{-3}
1×10^{-3}
5×10^{-4}
0
P_{fsysP}
0 0.2 0.4 0.6 0.8 1
ρ

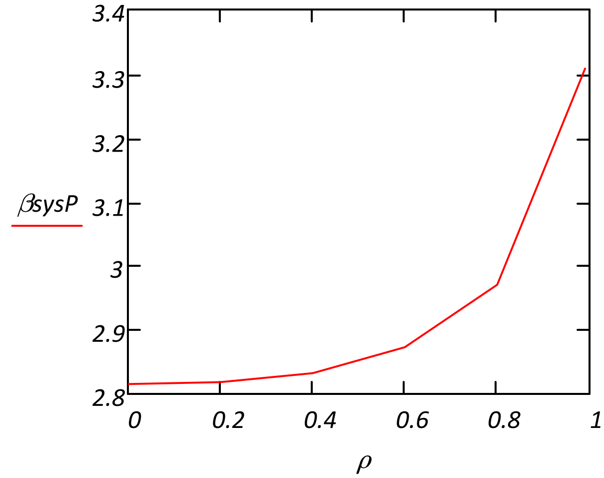

3.4
3.3
3.2
3.1
3
2.9
2.8
$\beta sysP$
0 0.2 0.4 0.6 0.8 1
ρ

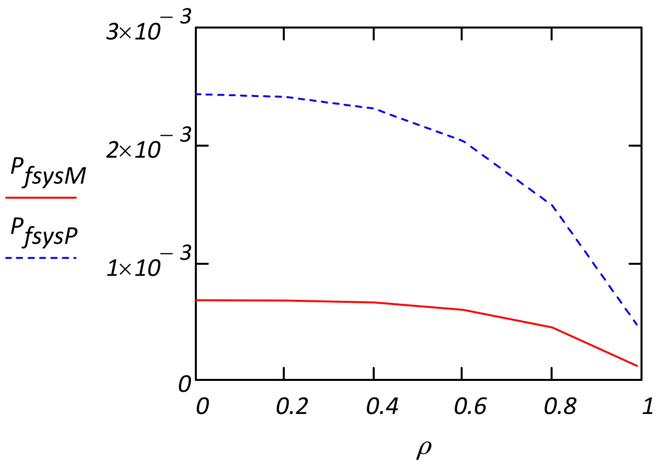

3×10^{-3}
2×10^{-3}
1×10^{-3}
0
P_{fsysM}
P_{fsysP}
0 0.2 0.4 0.6 0.8 1
ρ

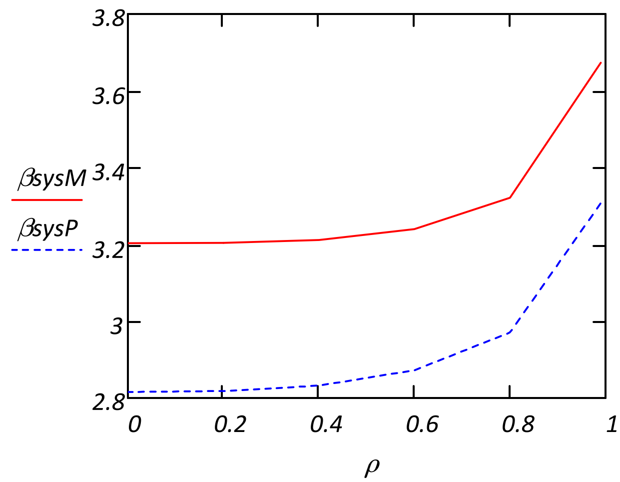

3.8
3.6
3.4
3.2
3
2.8
$\beta sysM$
$\beta sysP$
0 0.2 0.4 0.6 0.8 1
ρ

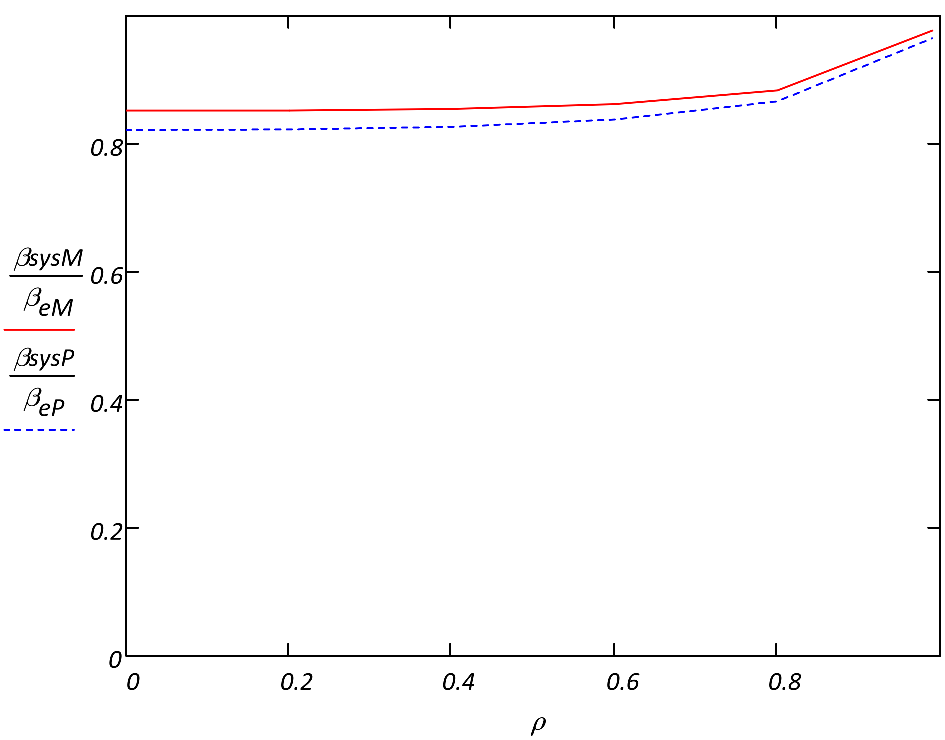

0.8
0.6
0.4
0.2
0
$\frac{\beta sysM}{\beta_{eM}}$
$\frac{\beta sysP}{\beta_{eP}}$
0 0.2 0.4 0.6 0.8
ρ